WOLF CREEK
NUCLEAR OPERATING CORPORATION

Karl A. (Tony) Harris
Manager Regulatory Affairs

APR 18 2003

RA 03-0059

U. S. Nuclear Regulatory Commission
ATTN: Document Control Desk
Washington, DC 20555

Subject: Docket No. 50-482: Submittal of Wolf Creek Nuclear Operating Corporation Evaluation of Stress Corrosion Cracking for Component Cooling Water System Piping

Gentlemen:

Enclosed are three reports evaluating corrosion assisted cracking of several samples of piping that were removed from Wolf Creek Generating Station (WCGS). Enclosure I is an EPRI report titled "Wolf Creek Nuclear Operating Corporation Pipe Evaluation." Enclosure II is an EPRI report titled "Evaluation of NDE of CCW Piping at Wolf Creek Generating Station." Enclosure III is a report by Roger W. Staehle titled "Assessment of Stress Corrosion Cracking (SCC) in the Component Cooling Water System (CCW) of the Wolf Creek Pressurized Water Reactor (WCNOC)."

There are no commitments contained in this correspondence. If you have any questions concerning this matter, please contact me at (620) 364-4038, or Ms. Jennifer Yunk at (620) 364-4272.

Very truly yours,

Ruth A Kewing for

Karl A. (Tony) Harris

A001

KAH/rlg

Enclosures: I – EPRI Report: Wolf Creek Nuclear Operating Corporation Pipe Evaluation
II – EPRI Report: Evaluation of NDE of CCW Piping at Wolf Creek Generating Station
III – Roger W. Staehle Report

cc: J. N. Donohew (NRC), w/e
Senior Resident Inspector (NRC), w/o

Final Report

ASSESSMENT OF STRESS CORROSION CRACKING (SCC) IN THE COMPONENT COOLING WATER SYSTEM (CCW) OF THE WOLF CREEK PRESSURIZED WATER REACTOR (WCNOC)

Prepared by

Roger W. Staehle
Staehle Consulting

22 Red Fox Road
North Oaks, Minnesota
55127
USA

651 482 9493 (direct)
651 484 5735 (telefax)

rwstaehle@rwstaehle.com
www.staehleconsulting.com

WCNOC Purchase order 0718047/0 dated 06/04/02

03/04/10

POWERING PROGRESS THROUGH
SCIENCE AND TECHNOLOGY

EPRI

August 23, 2002

Mr. Stan Walker
EPRI –NDEC

Subject: Wolf Creek Nuclear Operating Corporation Pipe Evaluation

Stan,

As received photos were taken to document where the indications were observed during the ultrasonic examination. The areas drawn on the components served as the basis for sectioning and metallographic sample removal. As shown in the Sectioning and Visual Examination section of the report, inside surface photos were taken to show the condition of the inside of the pipe. The components were sectioned, placed together in the original orientation, and photographed to document how the metallographic samples were removed.

Figures 12 thru 32 contain metallographic photos taken to investigate possible sources of ultrasonic indications. As a result of the examination, I have included a list of general observations limited to what could be surmised via metallographic inspection. The observations are only representative of sectioning and viewing samples in the general location where indications were thought to exist. No exploratory metallography was conducted to try and search for indications around the circumference other than the initial polished section.

1. All samples indicate corrosive attack.
2. Sample C-7 has micro-cracks from corrosive attack present in the weld heat affected zone, observed in the cross-sectional view of the weld.
3. A longitudinal cross section of sample C-7 does not show evidence of any axial cracking when approximately 3 inches of the circumference was examined, however corrosive attack was evident.
4. The deposit on the inside surface beyond the counterbore area is intermittent on the various samples investigated.
5. The deposit was either completely missing or disrupted along the counterbore area, more than likely due to flow changes associated with the transition.
6. The deposit was extremely heavy on C-7.
7. Sample C-26 contained a defect from the fabrication of the pipe (scab) that may have been responsible for causing an ultrasonic indication to occur.
8. The indication observed on D-42A is a result of insufficient material being removed during the machining to fully eliminate the prior surface conditions.

1300 W.T. Harris Blvd., Charlotte, NC 28262
704 547 6100 • 704 547 6109 FAX

To more accurately assess the cause of this type of attack, further examinations, i.e. SEM, metallographic, microhardness, base metal chemistry, weld metal chemistry, and detailed weld procedure specification information would be needed. Information could be available which may serve to help mitigate the reoccurrence of this phenomenon.

The RRAC has initial indication that SCC of low alloy steel and / or low carbon steels of this type are becoming more prevalent and investigation as to the mechanism associated with the initiation and propagation of corrosion assisted cracking is needed.

If I can be of further assistance with this issue please let me know. We have the capability of performing a detailed failure analysis if needed.

Report Submitted By

Andy McGehee, P.E.
Manager - Materials Engineering

EPRI RRAC
1300 Harris Blvd
Charlotte, NC 28262
(704) 547-6126 P#
(704) 547-6109 F#
amcgehee@epri.com

INTRODUCTION

Four sections of pipe Identified as C-26, C-6, C-7, and D-42A were submitted for metallographic inspection and photographed in the as-received condition as shown in Figures 1 through 4, respectively. The purpose of the inspection was to visually confirm indications detected during ultrasonic examination.

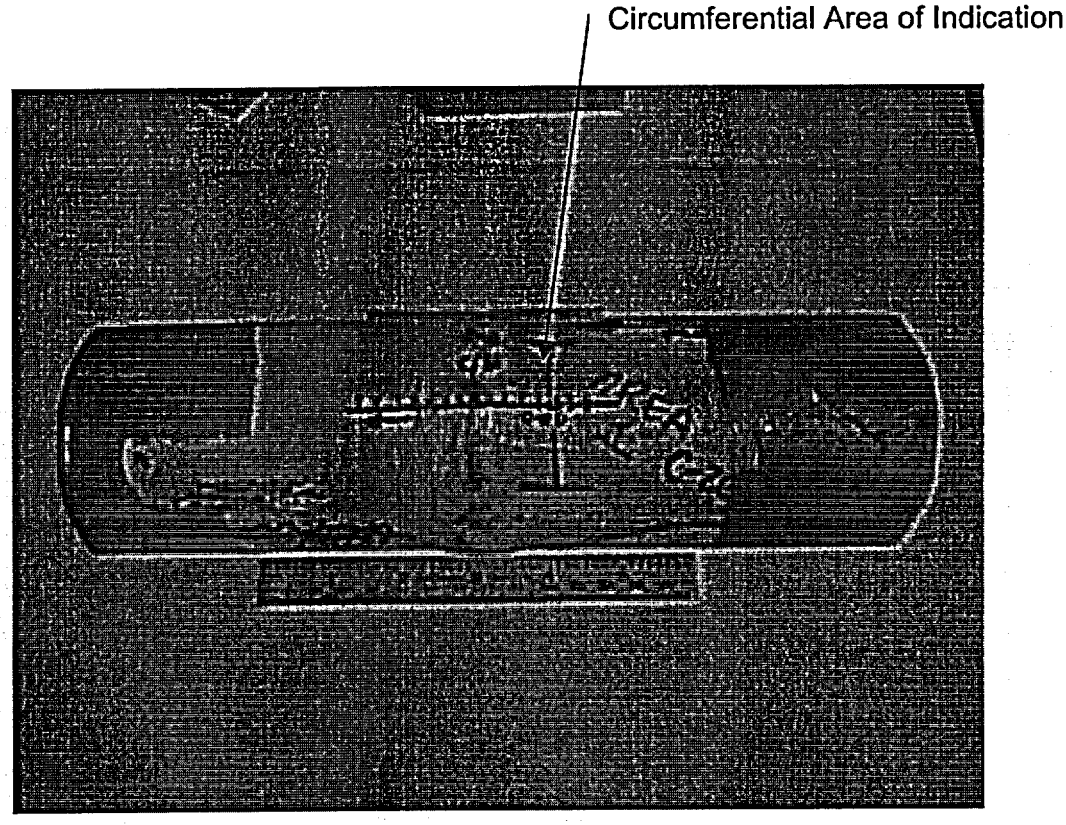

FIGURE 1: Photo of the as-received pipe section identified as C-26.

Circumferential Area of Indication

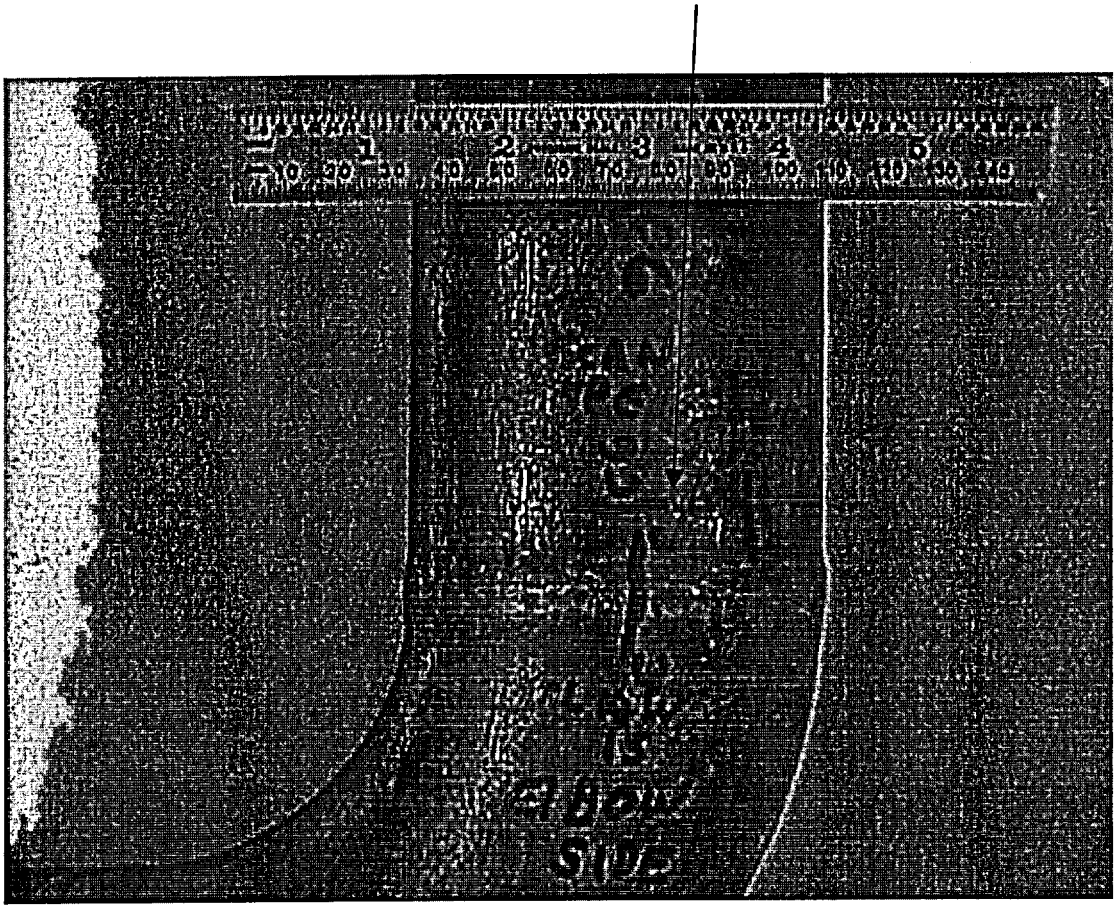

FIGURE 2: Photo of the as-received pipe to elbow section identified as C-6.

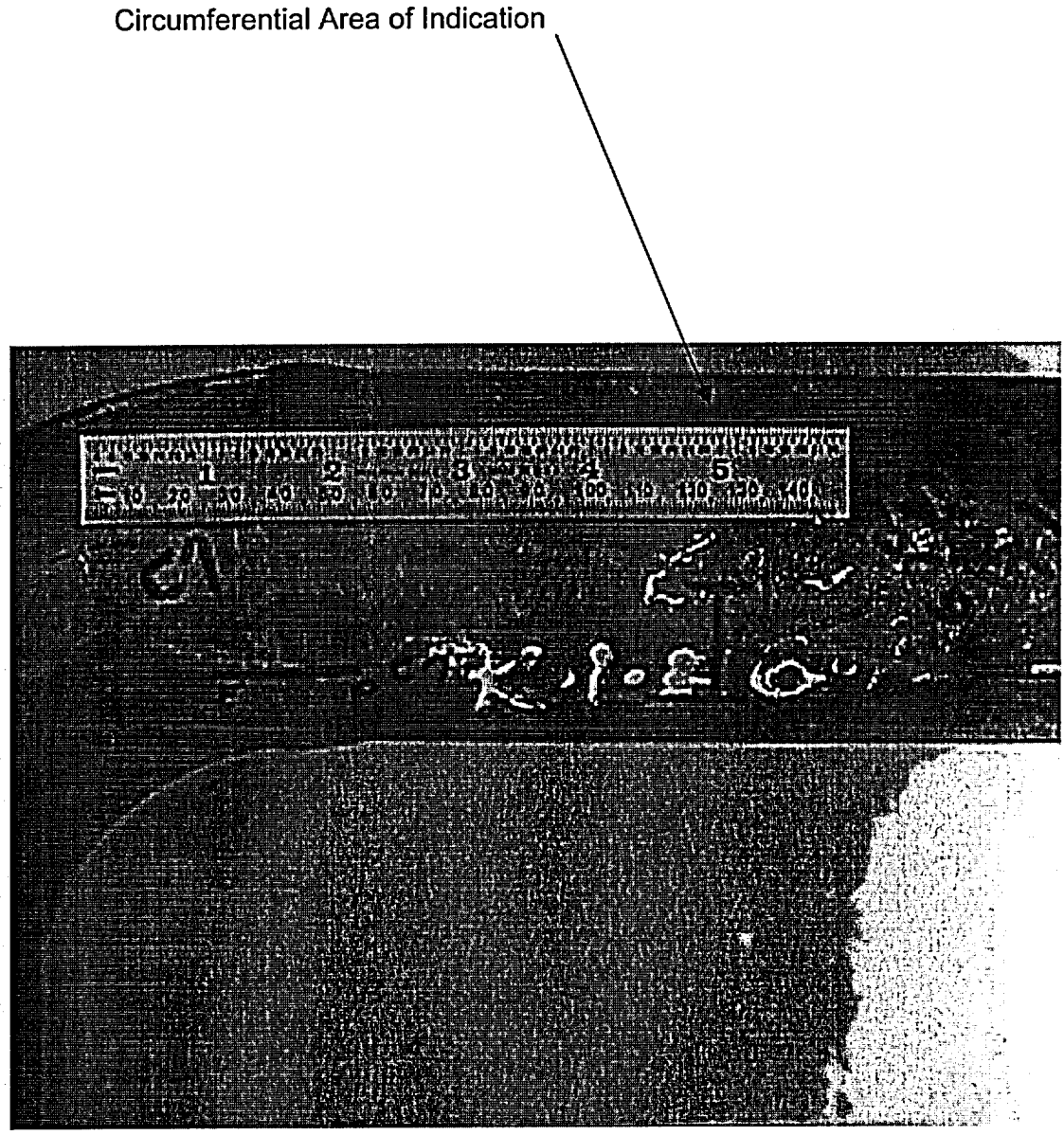

FIGURE 3: Photo of the as-received pipe to elbow section identified as C-7.

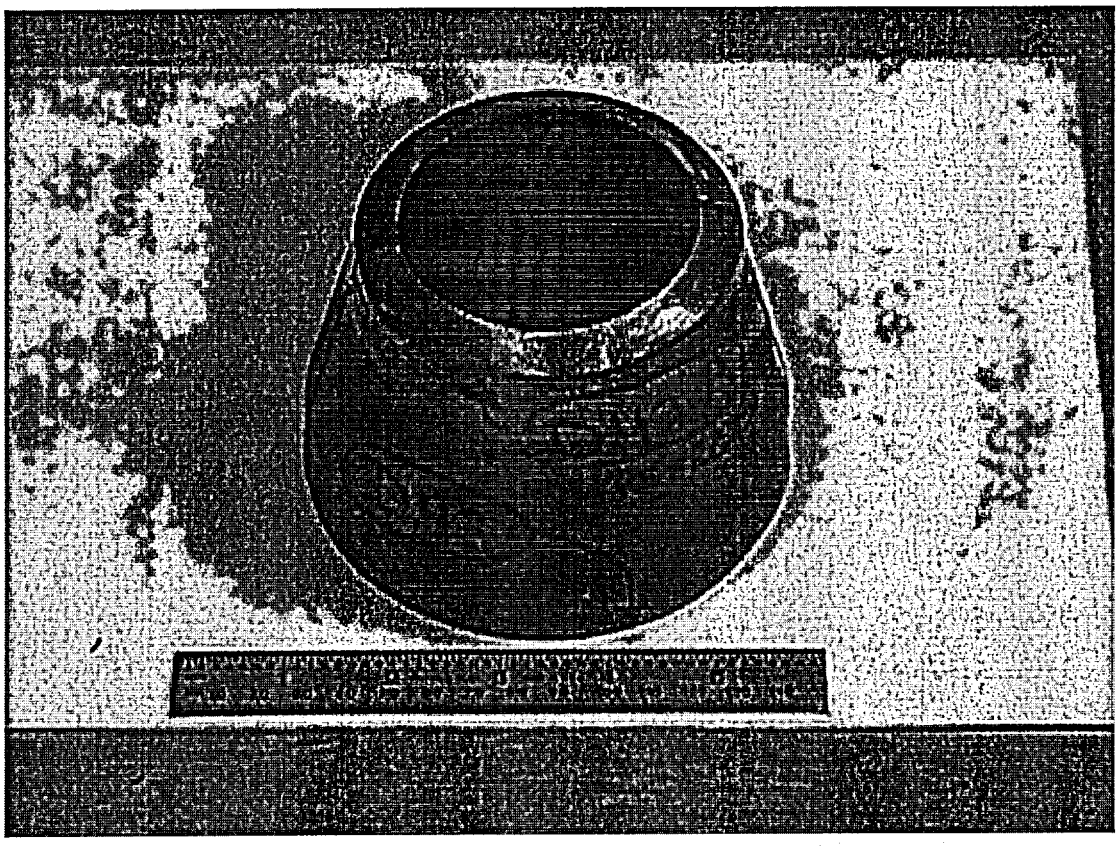

FIGURE 4: Photo of the as-received reducer identified as D-42A.

Sectioning & Visual Examination

Initial cuts were made so that the inside surface of each component could be photographed. Sectioning for sample removal was conducted so that cross sections of the weld and counterbore of the adjoining pipe and elbow sections could be examined. Each component is assessed separately below.

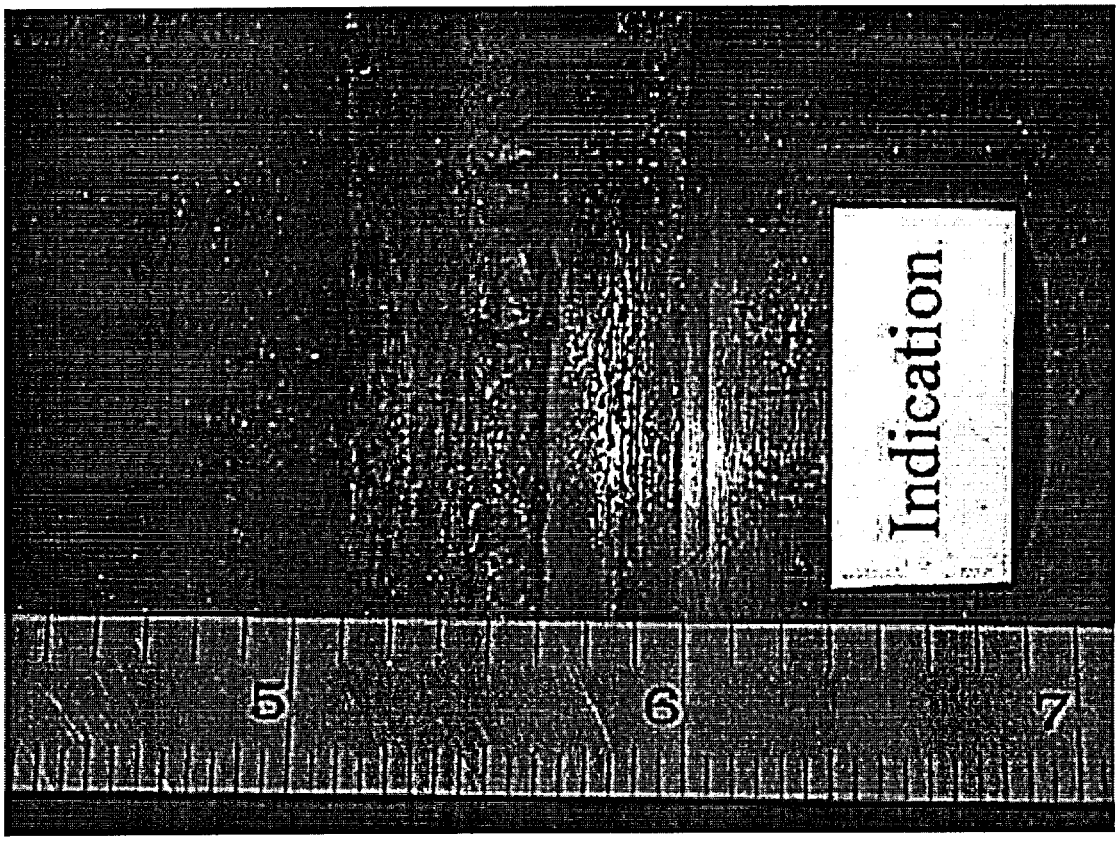

FIGURE 5: Photo showing the inside surface of C-26 in the area where the ultrasonic indication was detected.

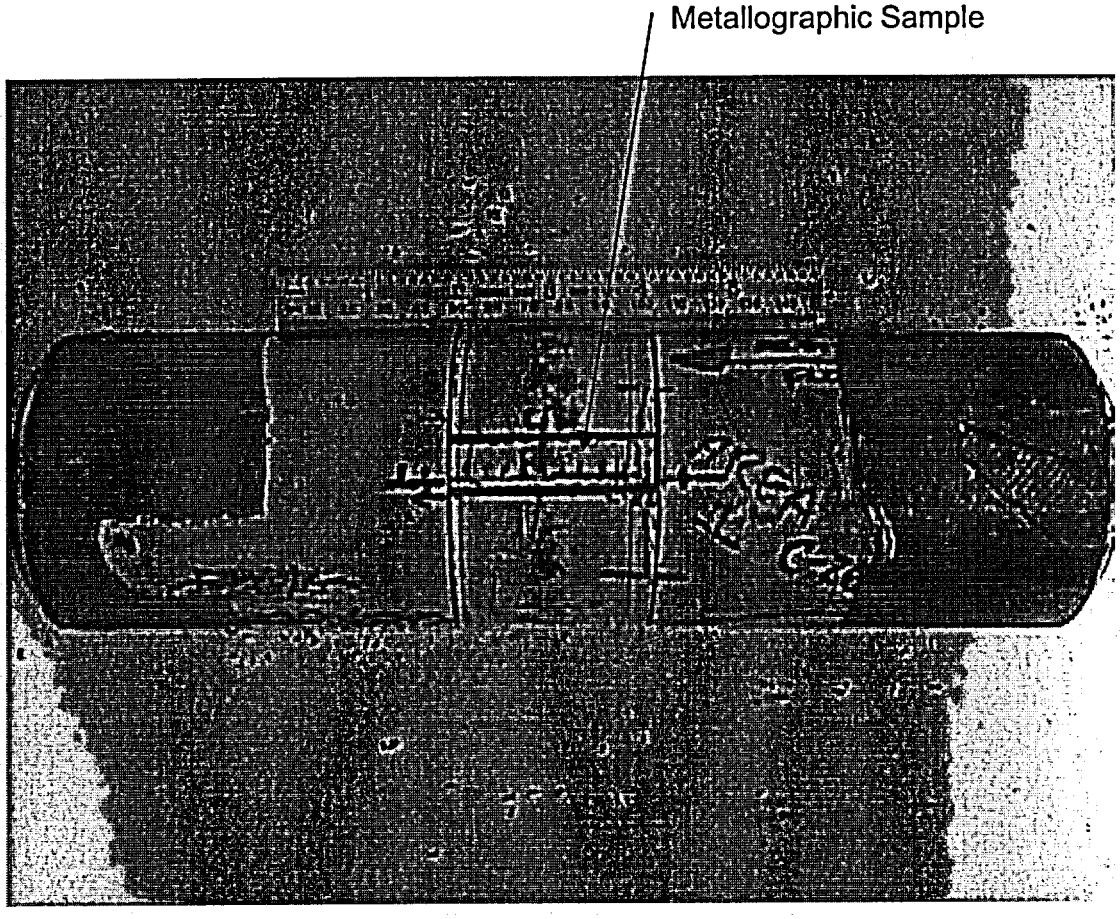

FIGURE 6: Photo showing sample removal from C-26 for metallographic preparation.

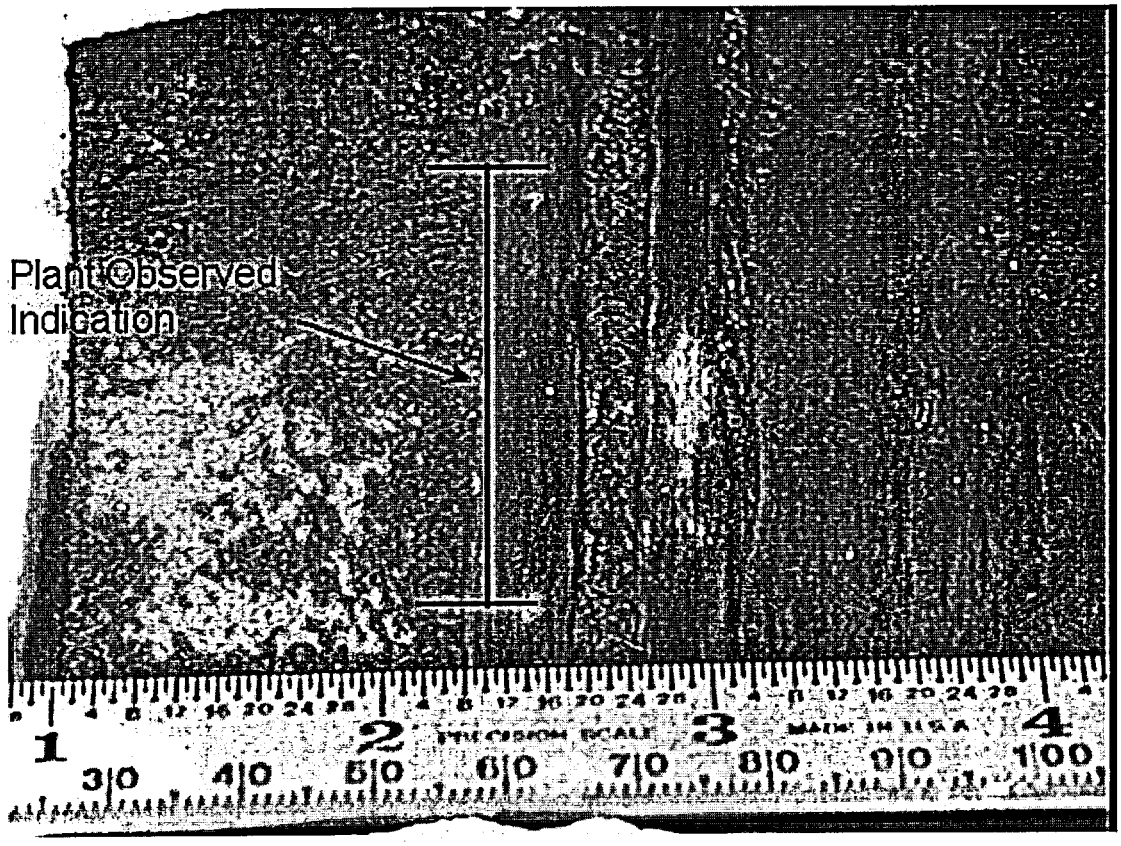

FIGURE 7: Photo showing the inside surface of C-6 where the ultrasonic indication was detected.

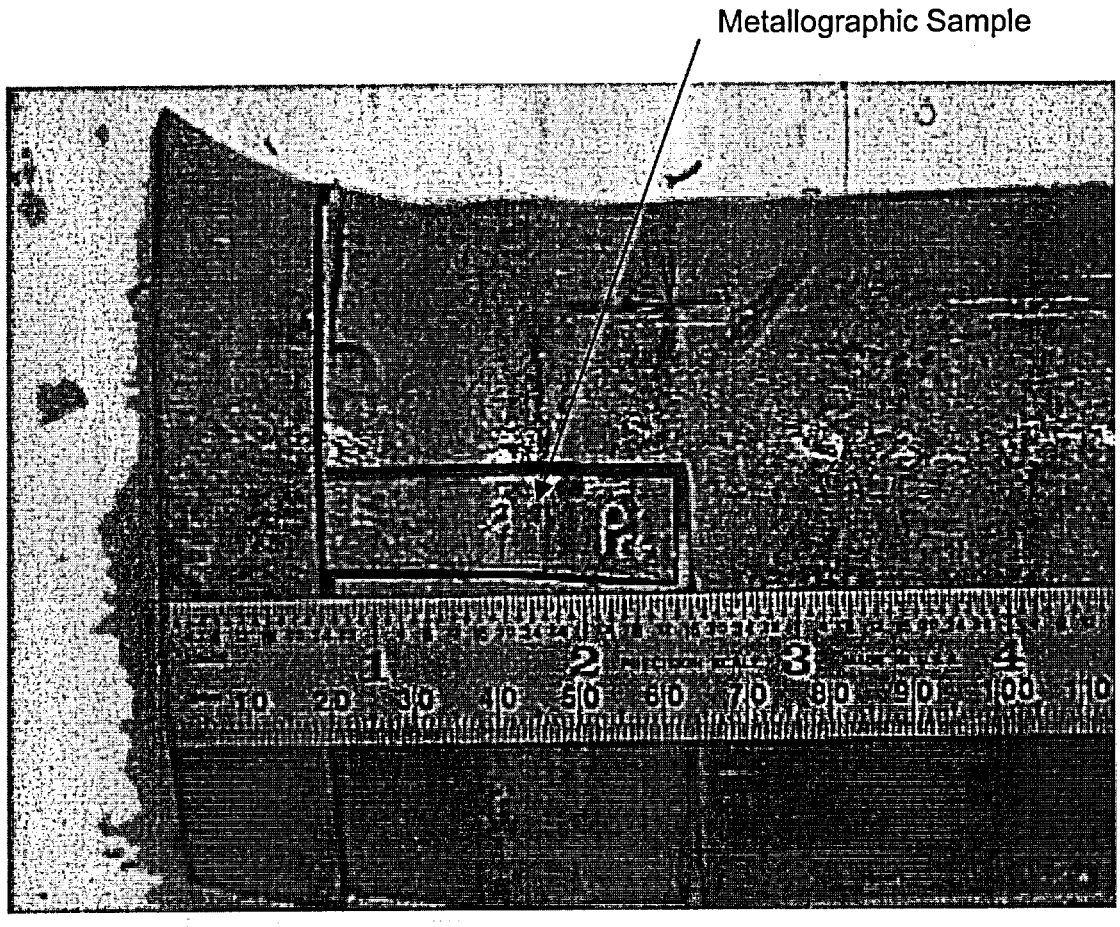

FIGURE 8: Photo showing sample removal from C-6 for metallographic preparation.

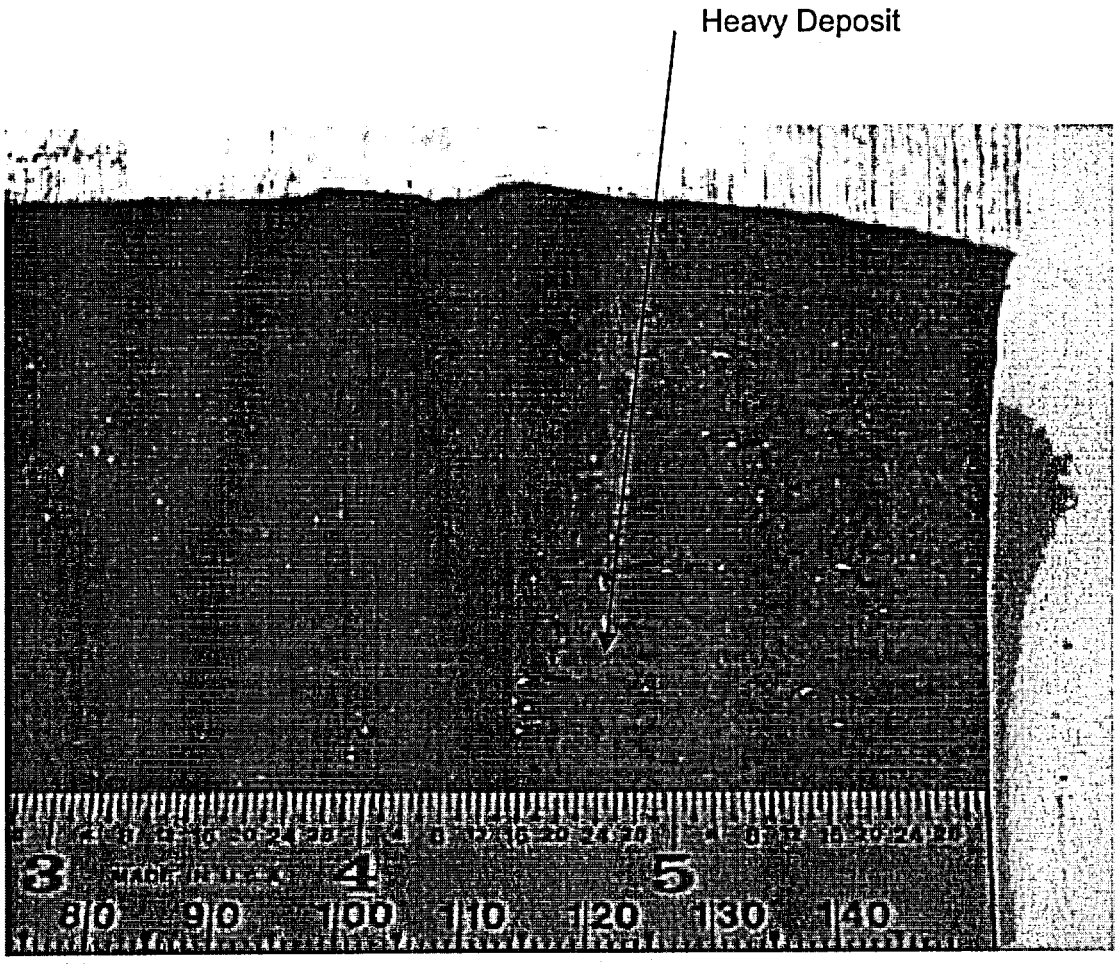

FIGURE 9: Photo showing inside surface of C-7 and deposits where an indication occurred.

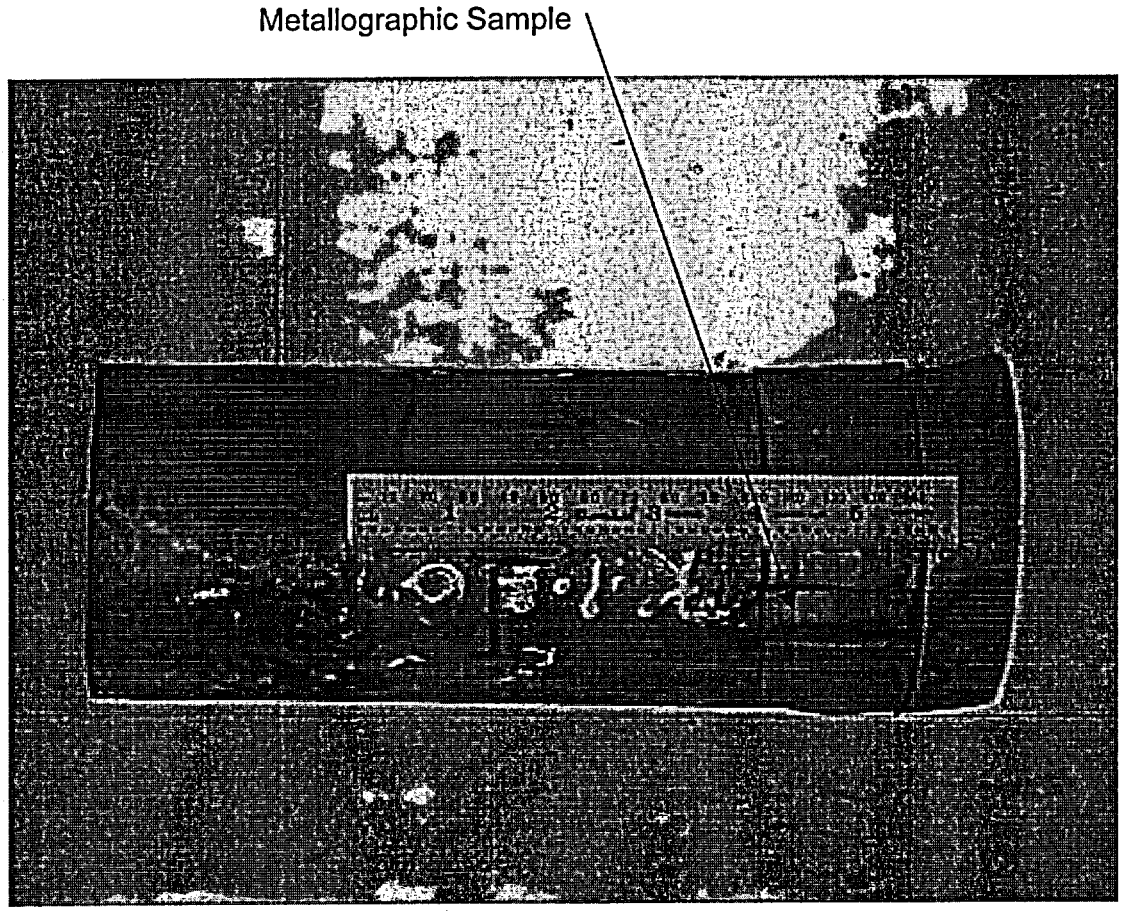

FIGURE 10: Photo showing sample removal from C-7 for metallographic preparation.

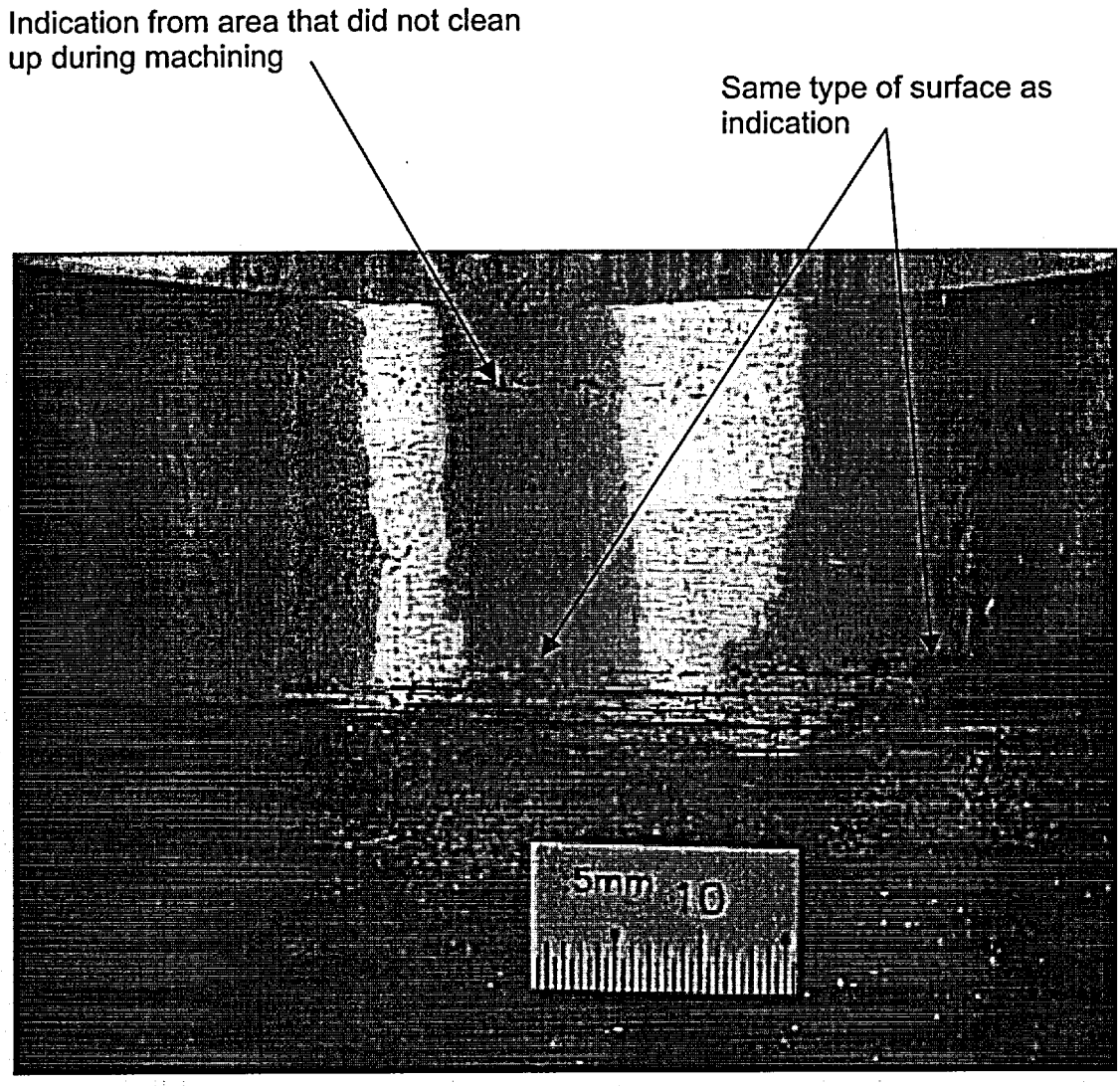

FIGURE 11: Photo showing area with an ultrasonic indication in D-42A near the bevel of the reducer on the inside surface.

METALLOGRAPHIC INSPECTION

Macros of each weldment cross section were taken to show the counterbore geometry and weld macrostructure for each sample. Metallographic inspection of the components was conducted to examine the microstructure of the individual components. Particular attention was given to the inside surface areas where stress corrosion cracking would initiate in order to identify any locations of possible features responsible for ultrasonic indications.

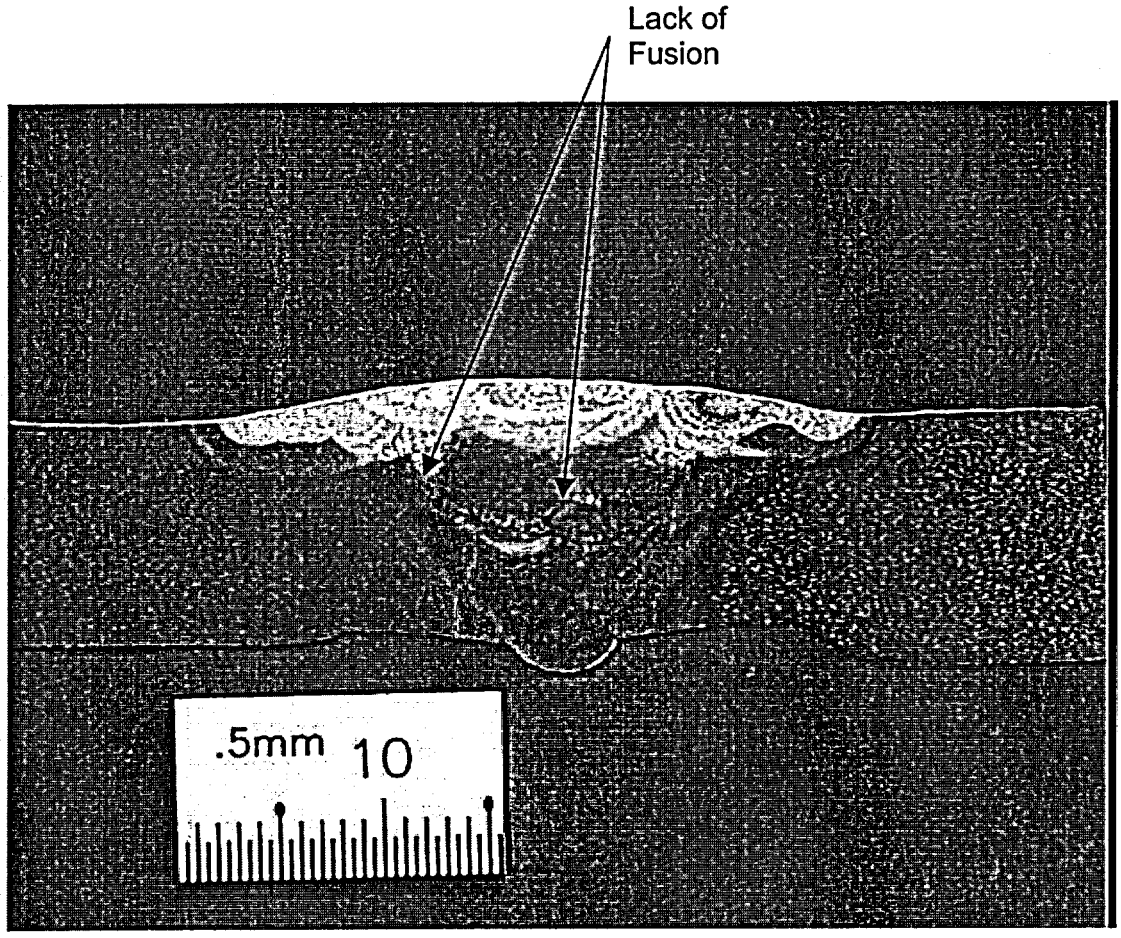

FIGURE 12: Macrograph showing weld cross section and counterbore geometry of C-26.

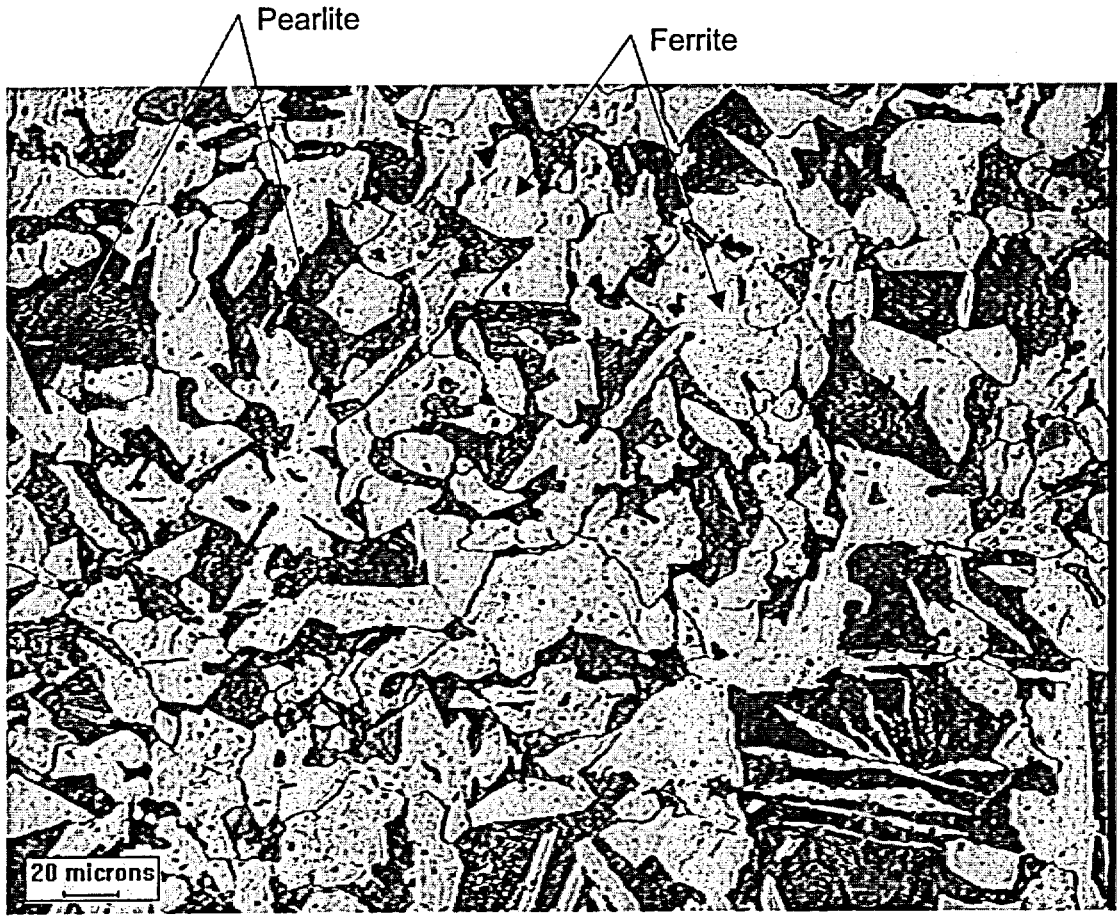

FIGURE 13: Photomicrograph of C-26 showing microstructure consisting of pearlite and ferrite, which was typical of all unaffected pipe base metal components. 3% Nital etch. 200X

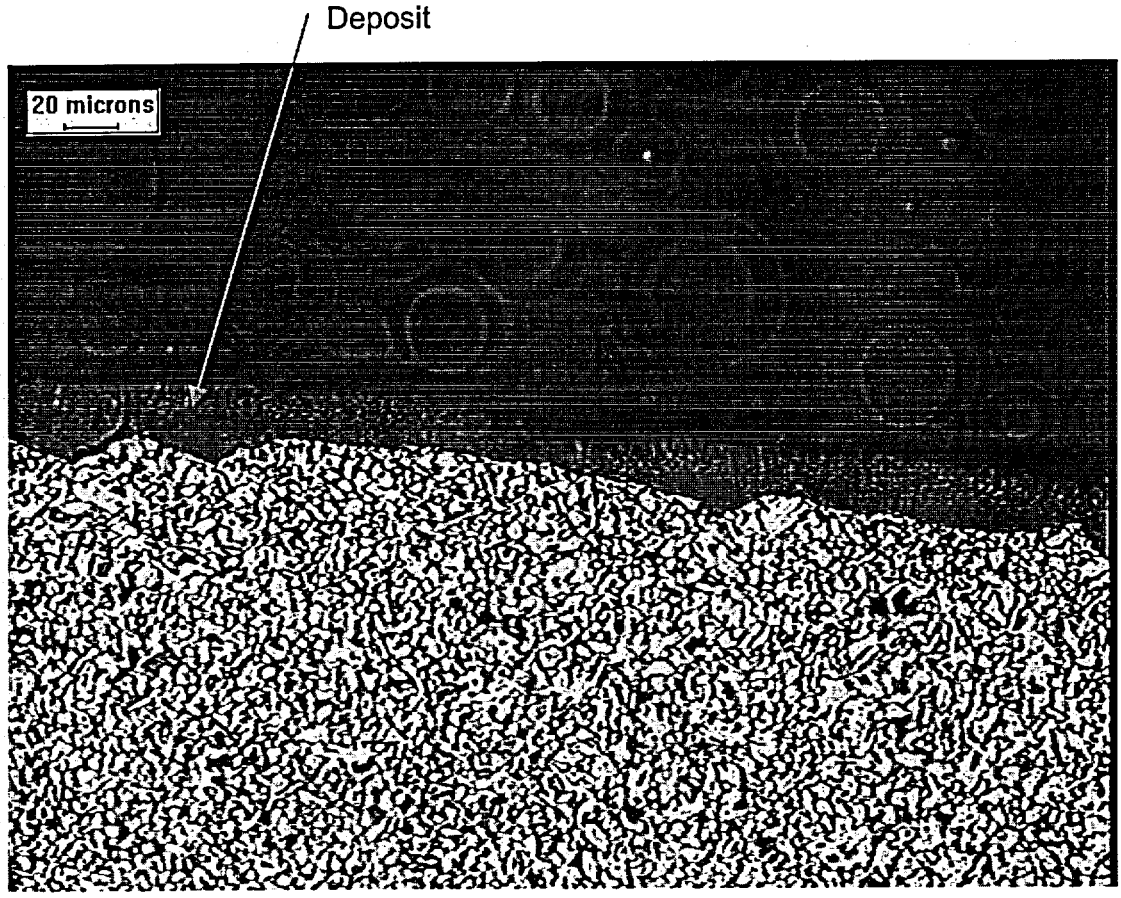

FIGURE 14: Fine grained HAZ microstructure of C-26 with molybdate or corrosion deposit on the surface. 3% Nital etch. 200X

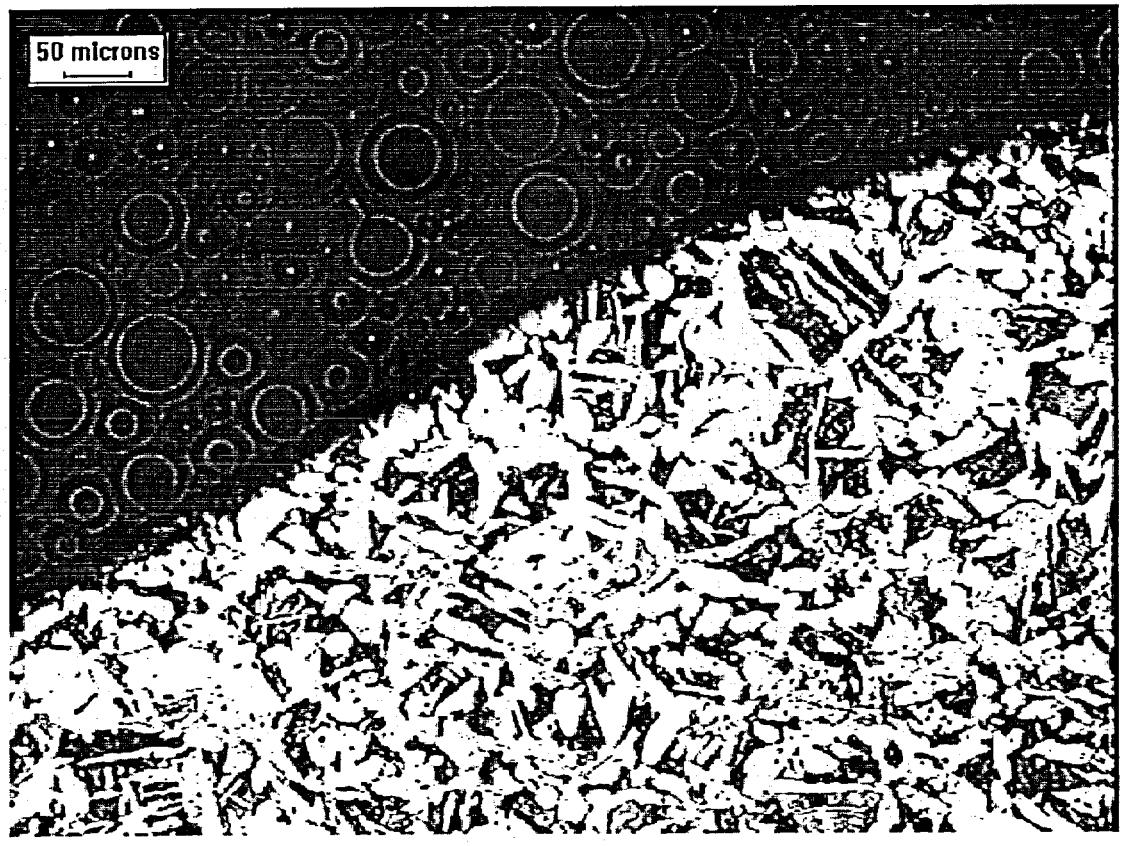

FIGURE 15: Microstructure along counterbore of indication side of weldment C-26. 3% Nital etch. 100X

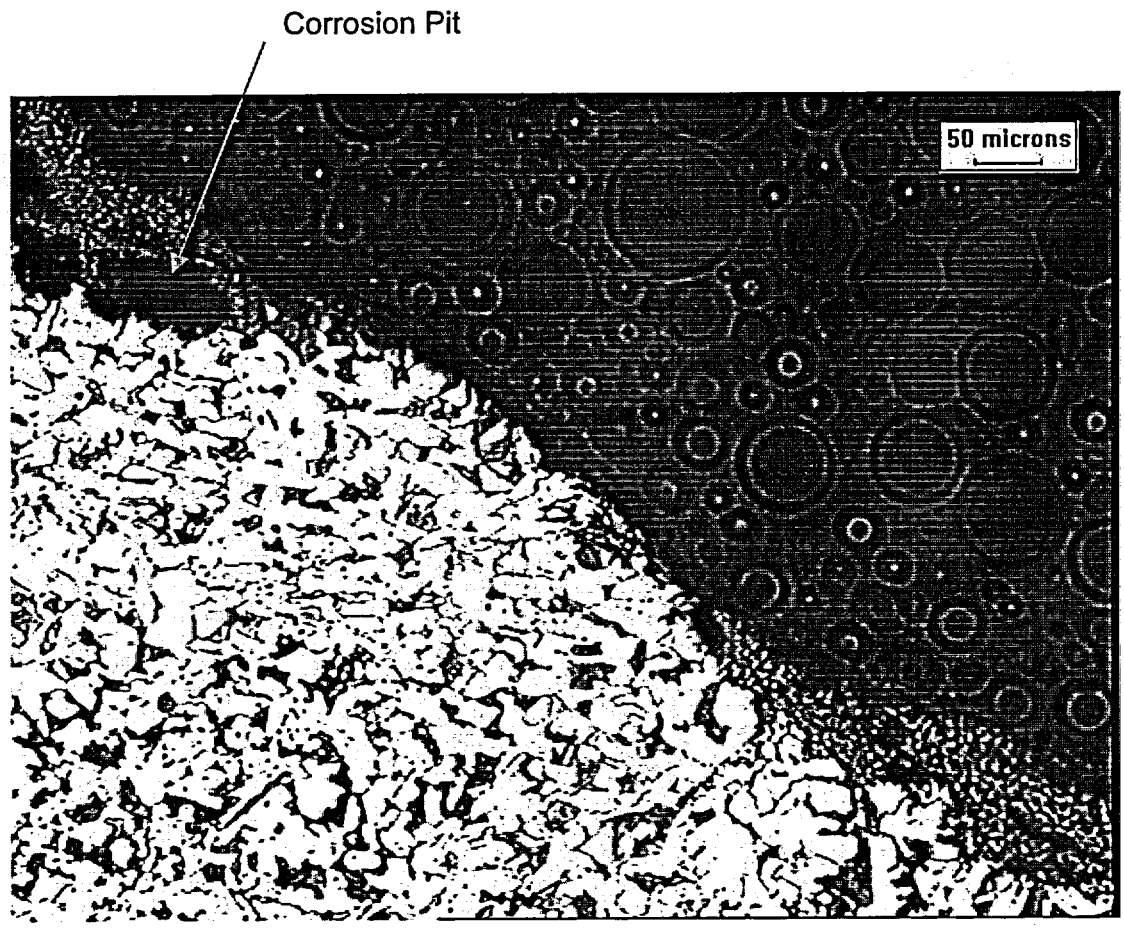

FIGURE 16: Micrograph of opposite C-26 counterbore.3% Nital etch. 100X

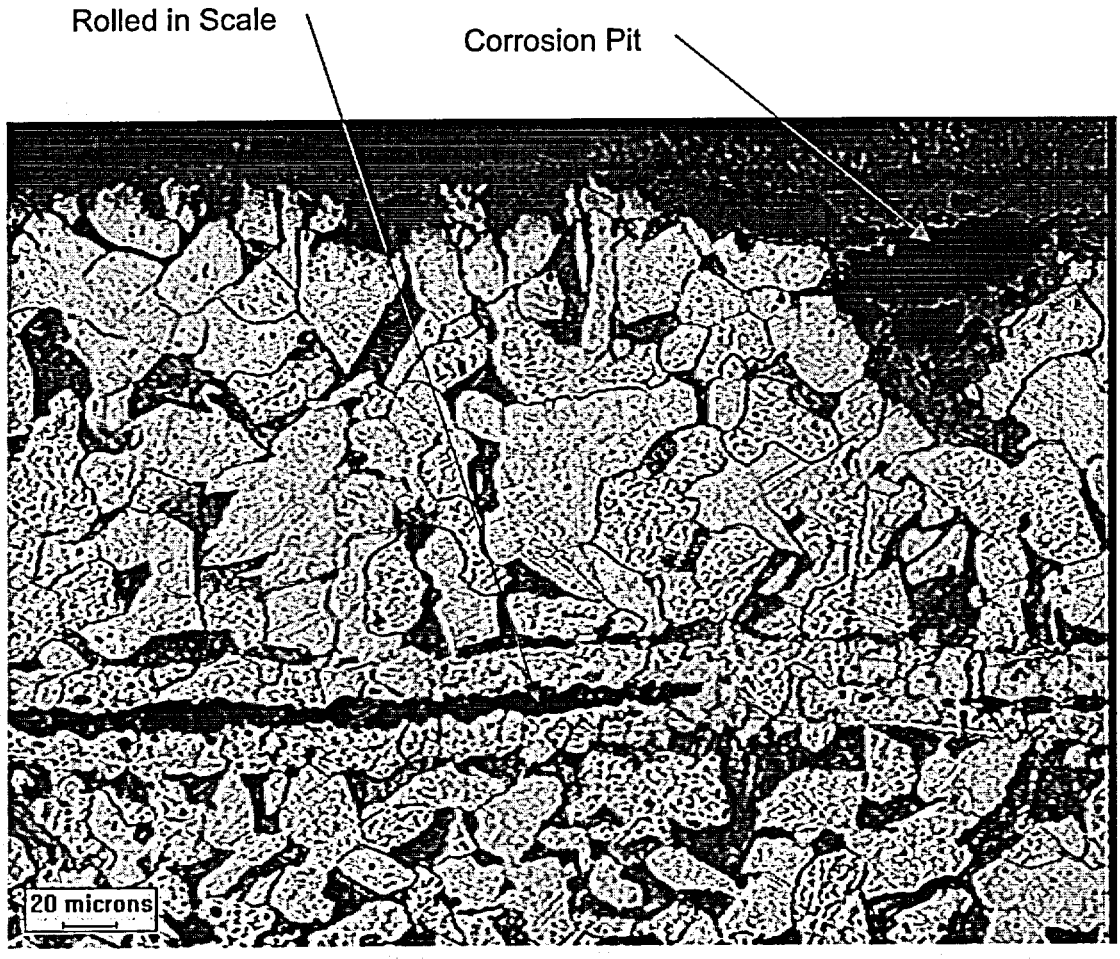

FIGURE 17: Micrograph of rolled in defect during manufacturing of pipe in C-26. 3% Nital etch. 200X

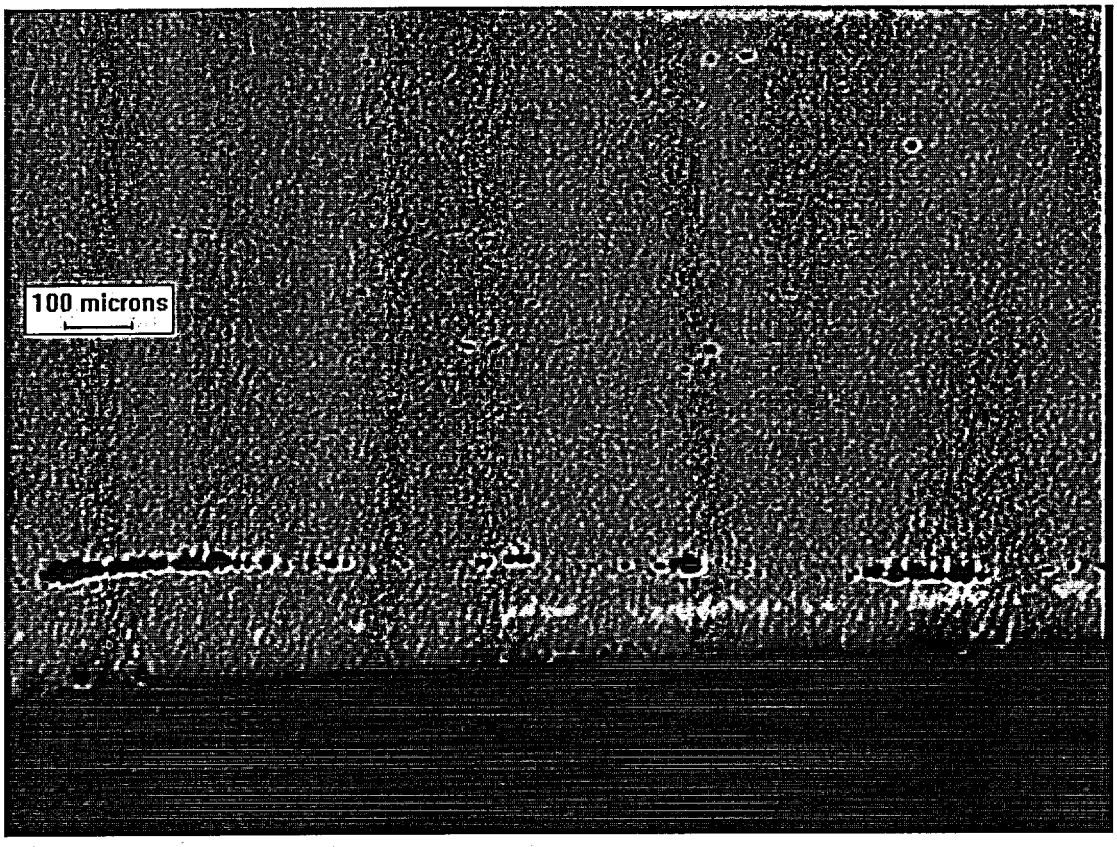

FIGURE 18: Same as Figure 17 but unetched showing rolled in scale. 50X

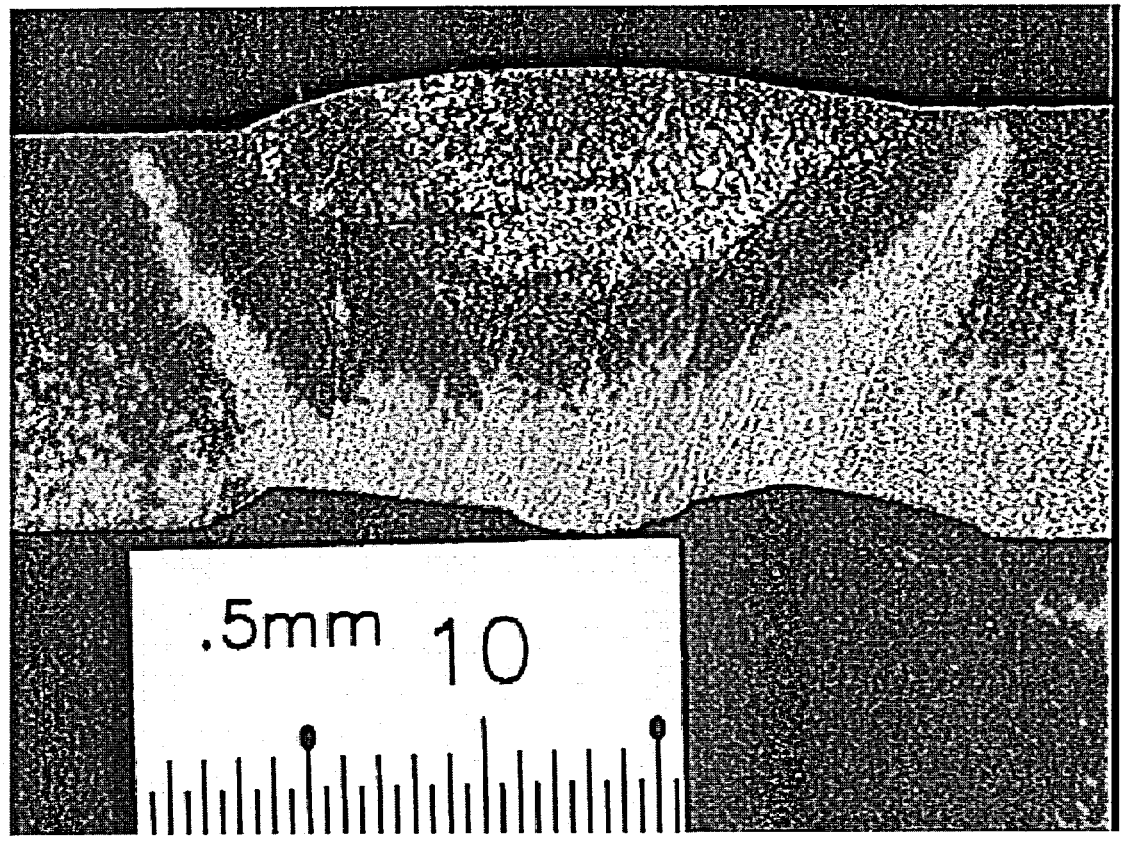

FIGURE 19: Macrograph showing weld cross section and counterbore geometry for C-6.

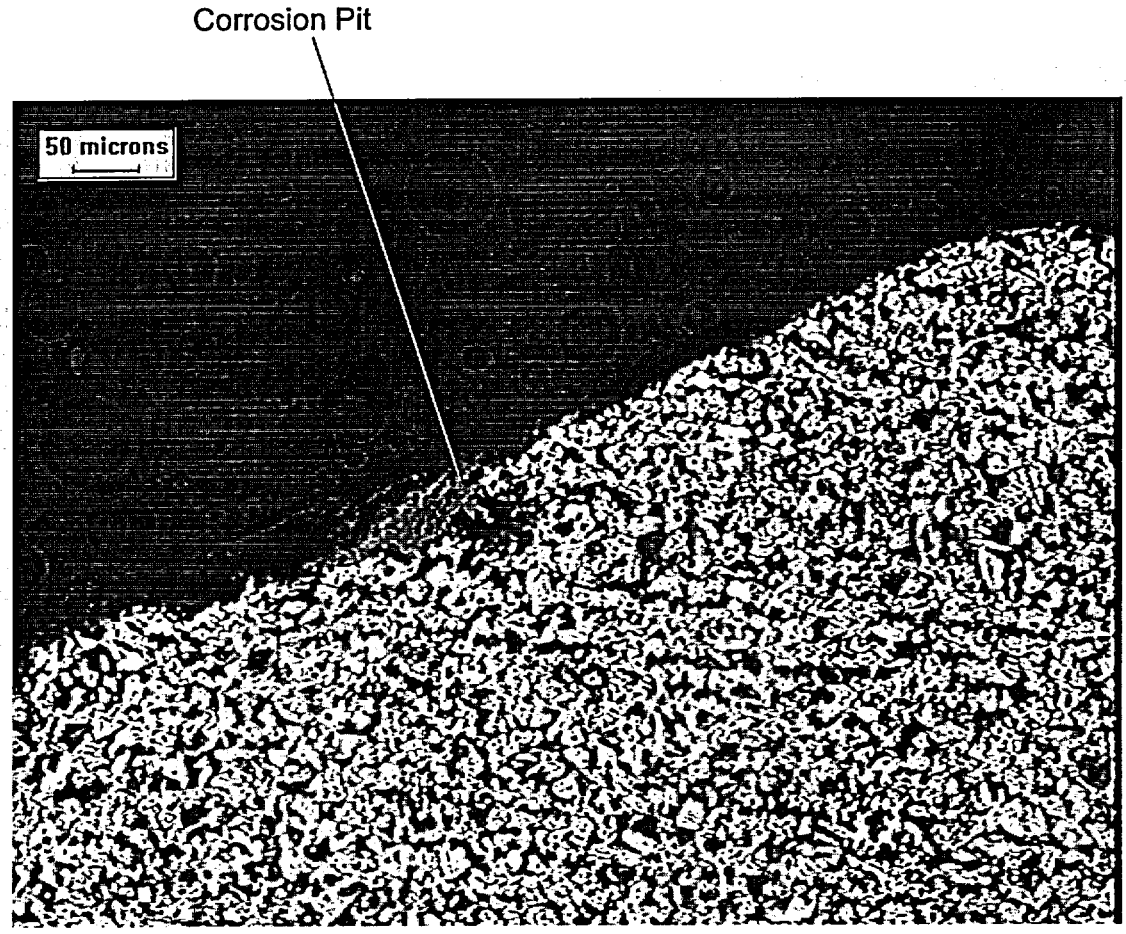

FIGURE 20: Micrograph of C-6 elbow counterbore. 3% Nital etch. 100X

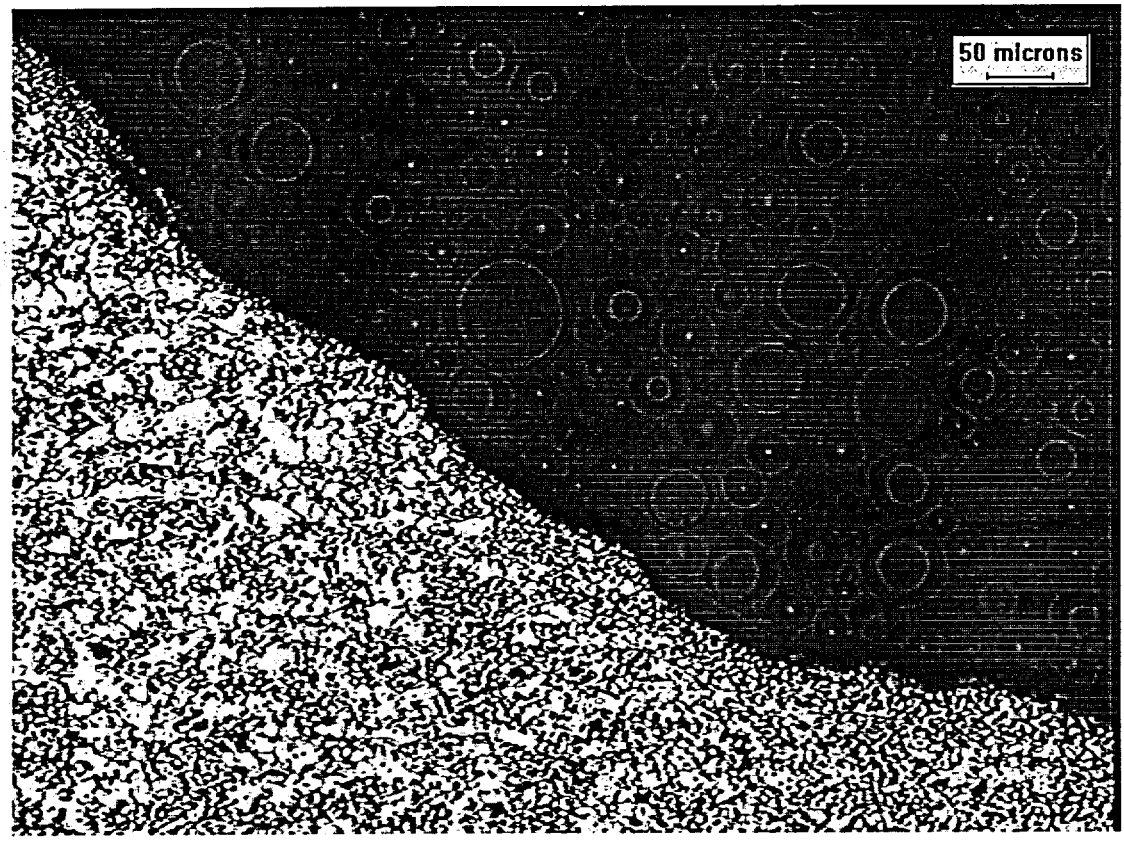

FIGURE 21: Micrograph of C-6 pipe counterbore. 3% Nital etch. 100X

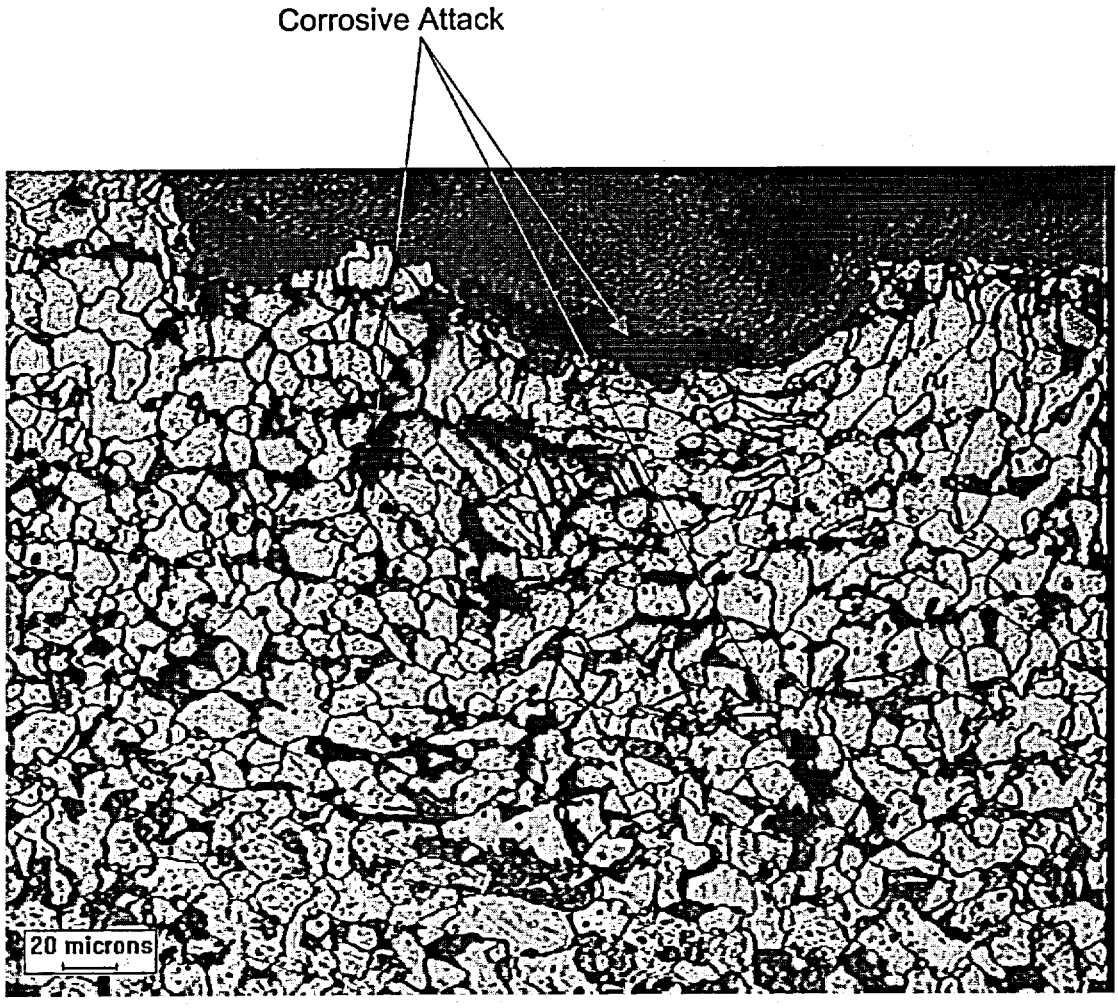

FIGURE 22: Micrograph of C-6 elbow inside surface showing pitting and corrosive attack. 3% Nital etch. 200X

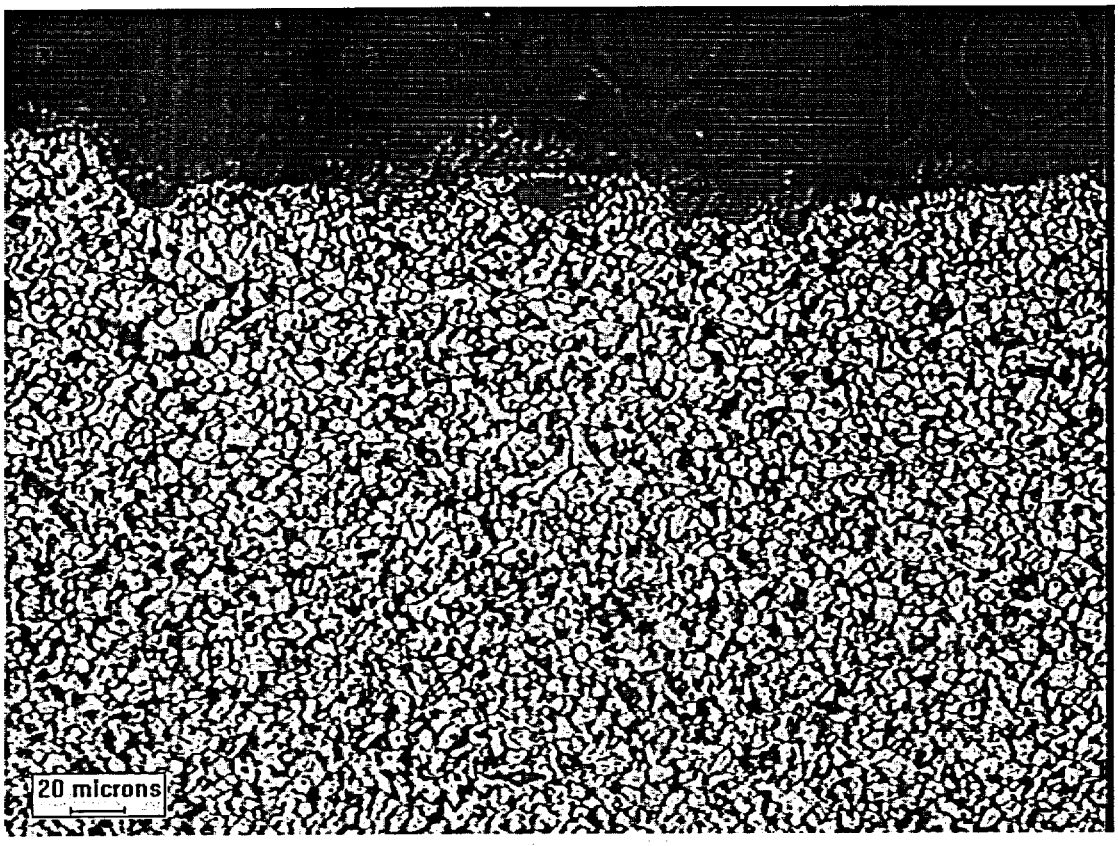

FIGURE 23: Micrograph of C-6 elbow HAZ. 3% Nital etch. 200X

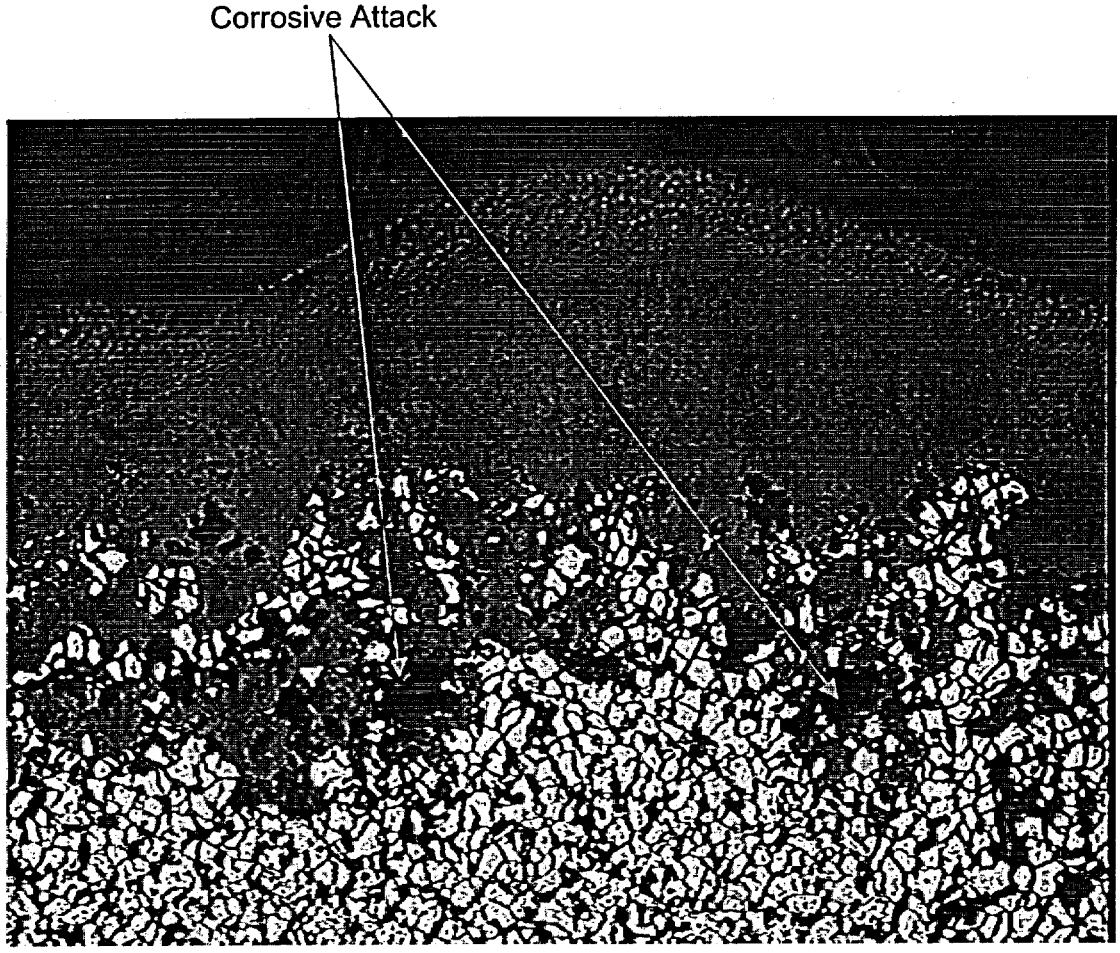

FIGURE 24: Micrograph of C-6 weld root showing corrosive attack on the weld reinforcement. 3% Nital etch. 200X

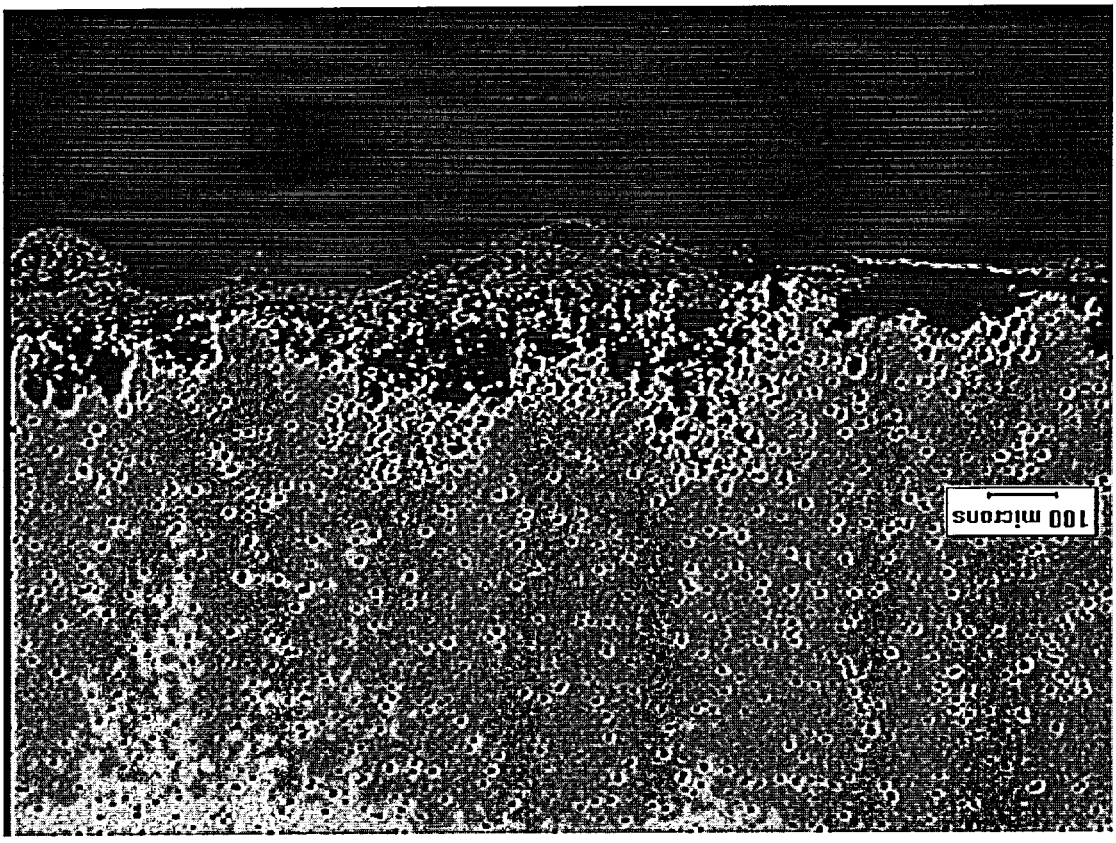

FIGURE 25: Same As Figure 24 in the unetched condition. 50X.

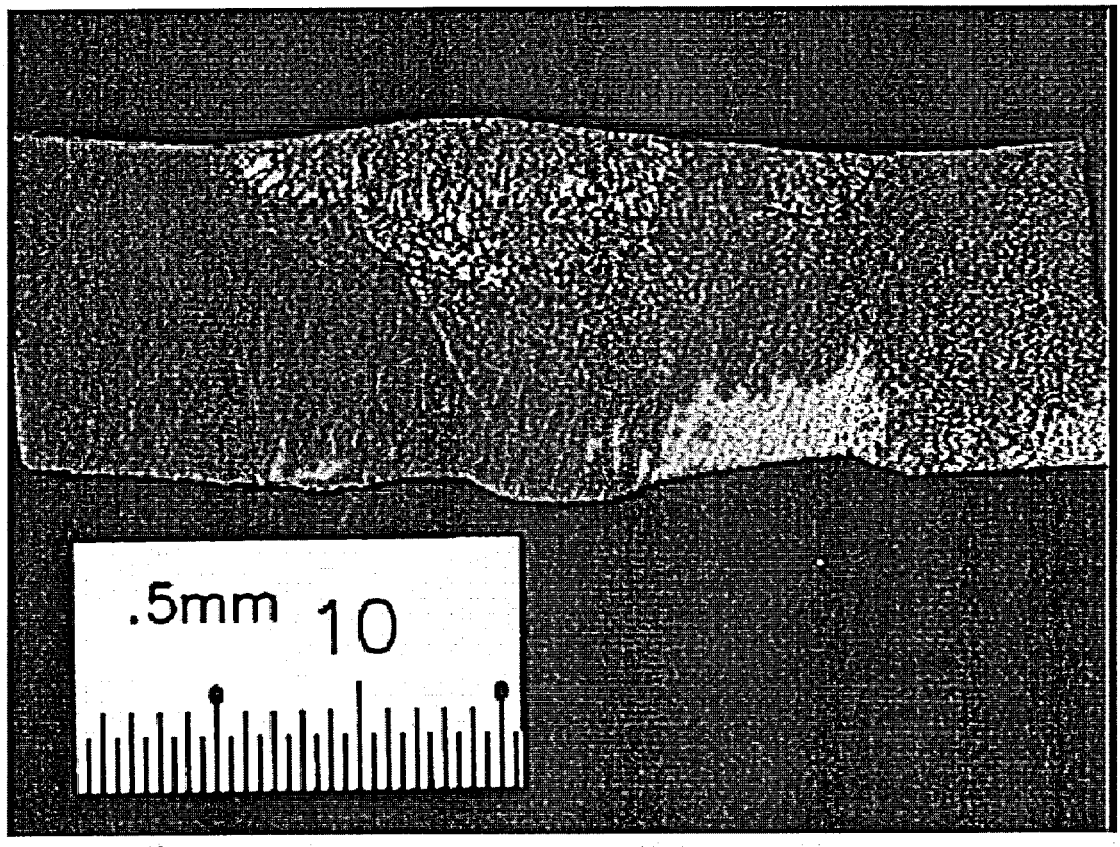

FIGURE 26: Macrograph showing C-7 weld cross section and counterbore geometry.

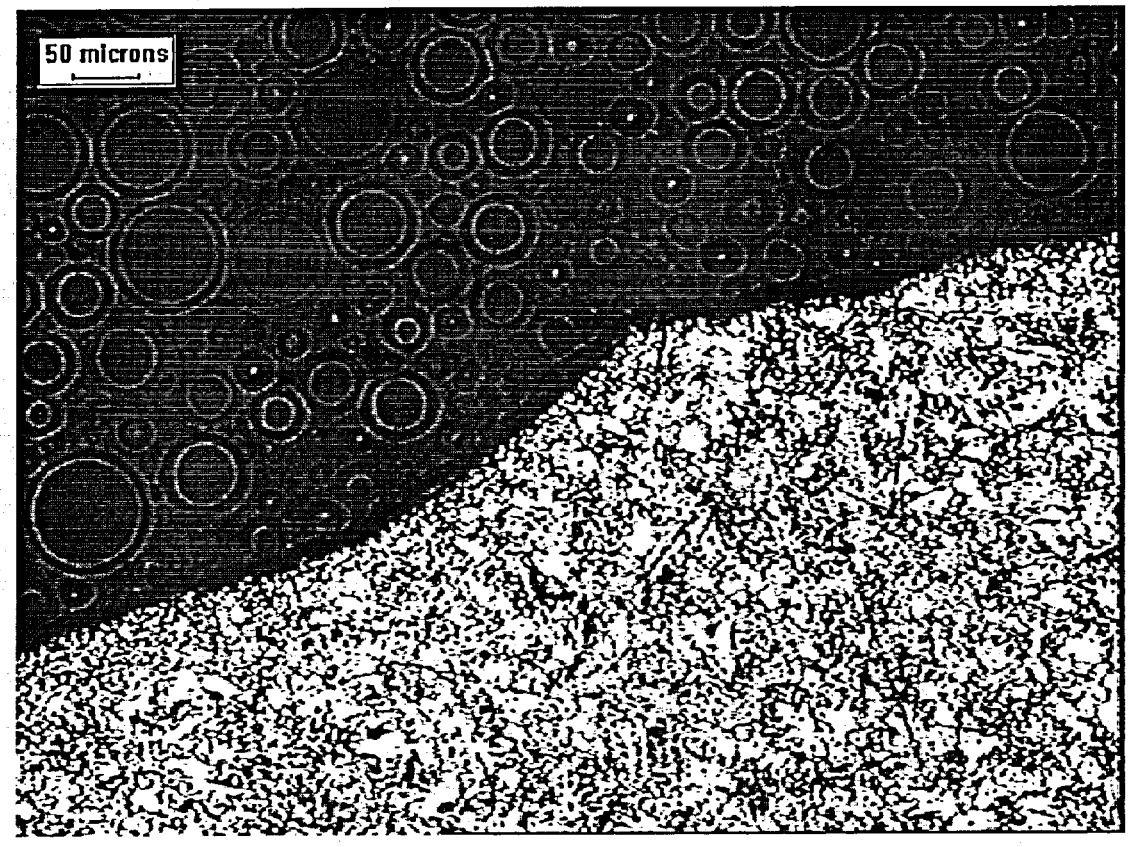

FIGURE 27: Micrograph of C-7 pipe counterbore. 3% Nital etch. 100X

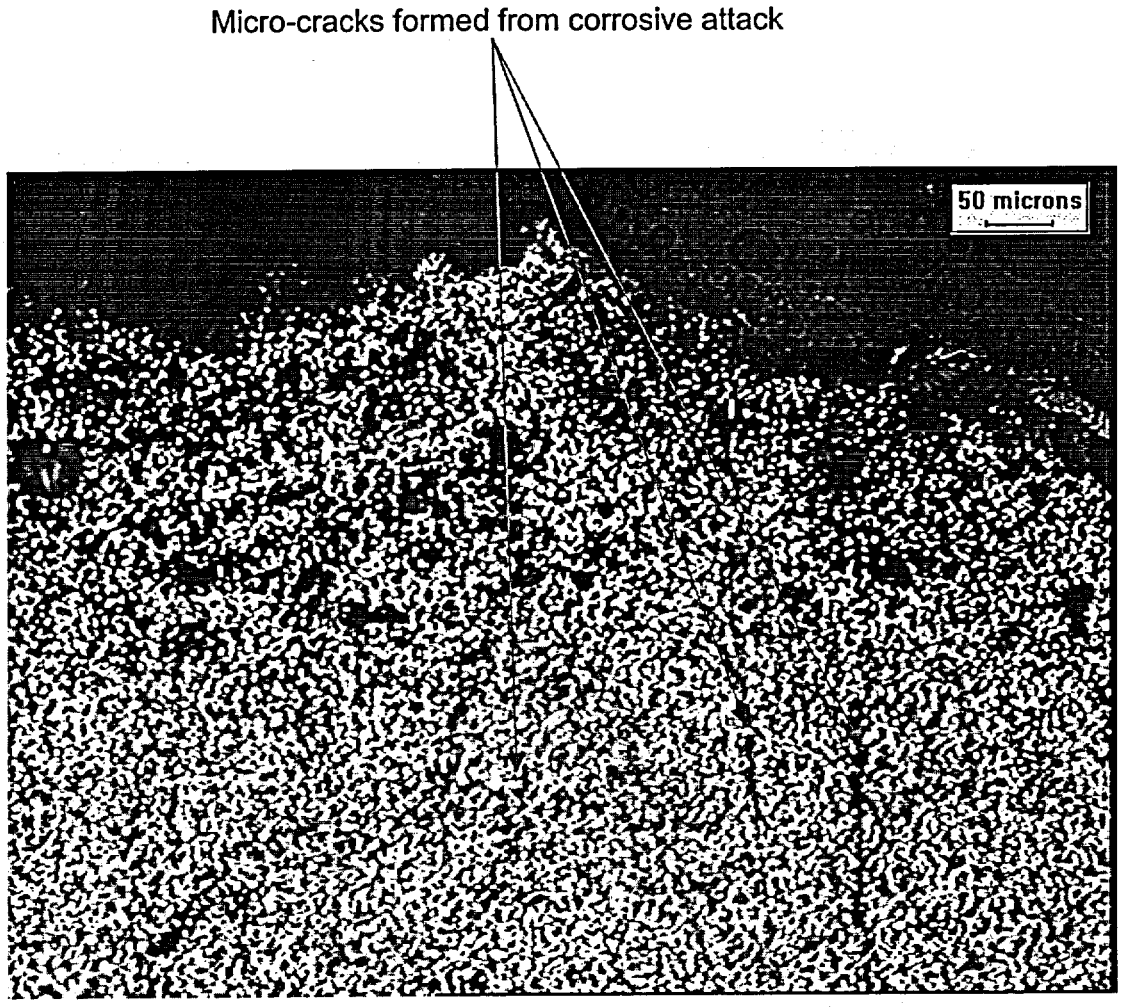

FIGURE 28: Micrograph of the beginning of SCC in the HAZ of C-7. 3%Nital etch. 100X

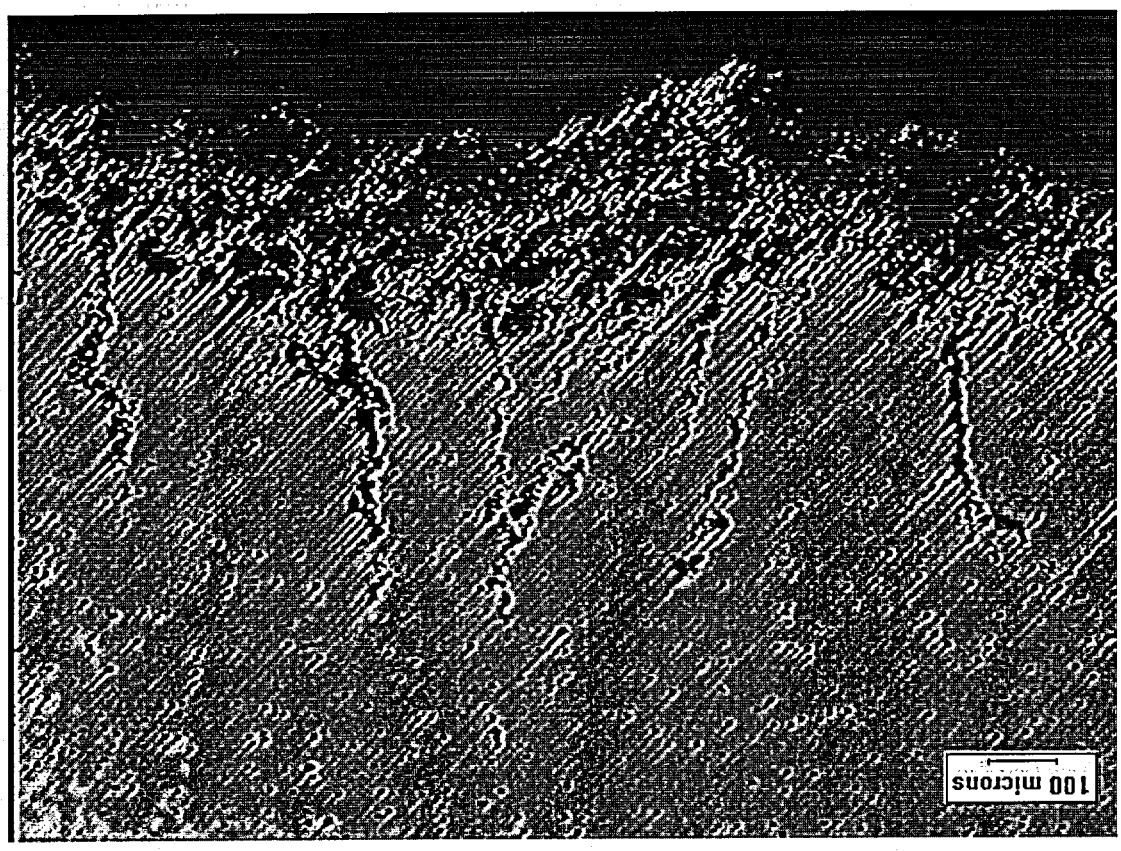

FIGURE 29: Same micrograph as Figure 28 but in the unetched condition showing corrosive attack path. 50X

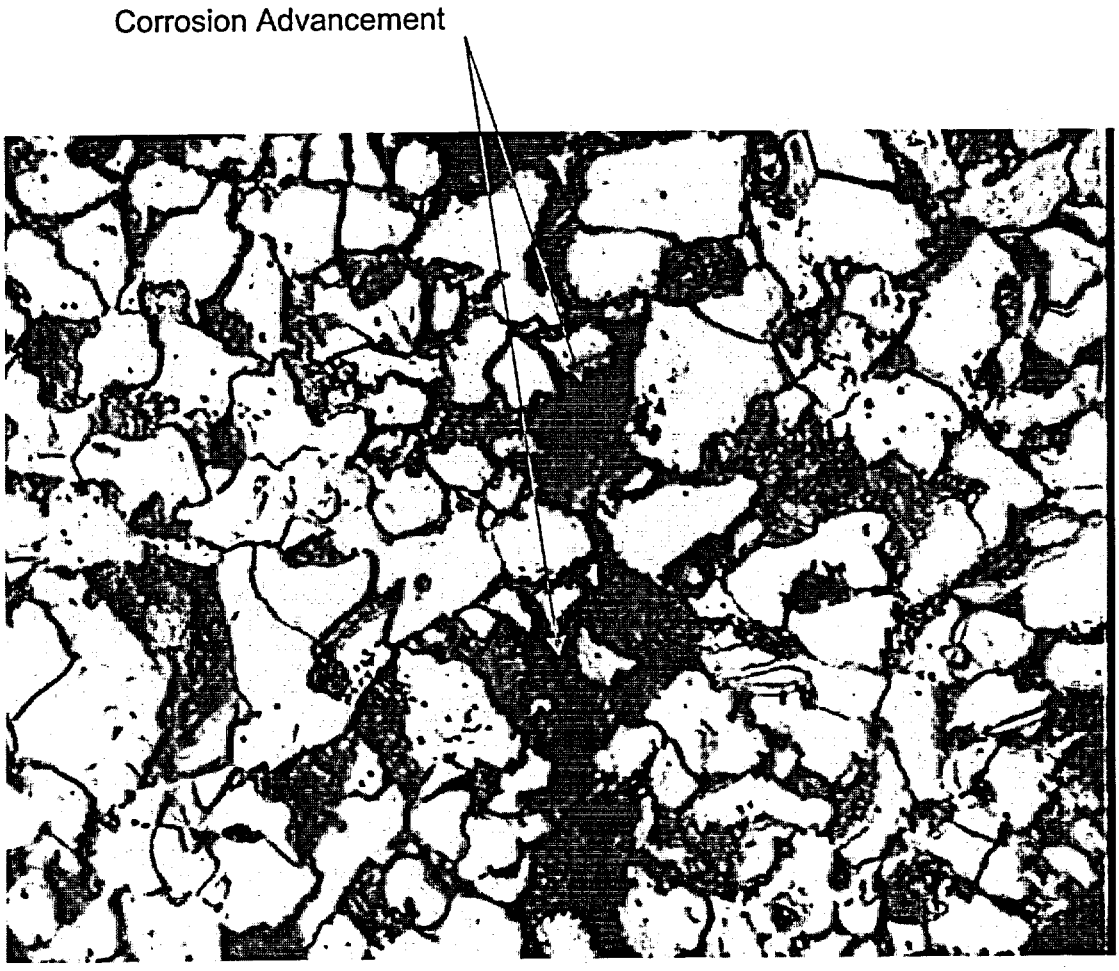

FIGURE 30: Micrograph showing corrosive attack at grain boundaries in C-7. 3% Nital etch. 1000X.

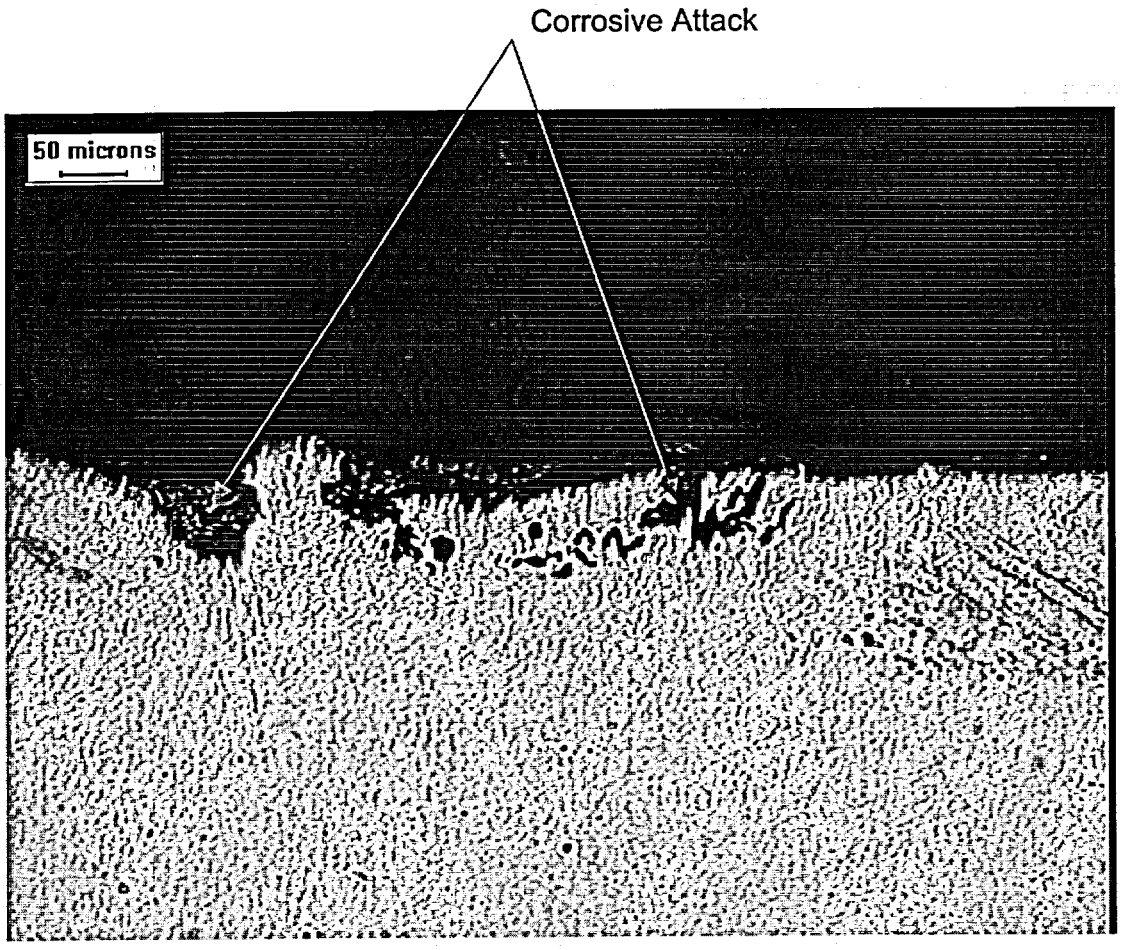

FIGURE 31: Micrograph directly adjacent to the weld root of a longitudinal cross section of C-7 showing some corrosive attack. Unetched. 100X

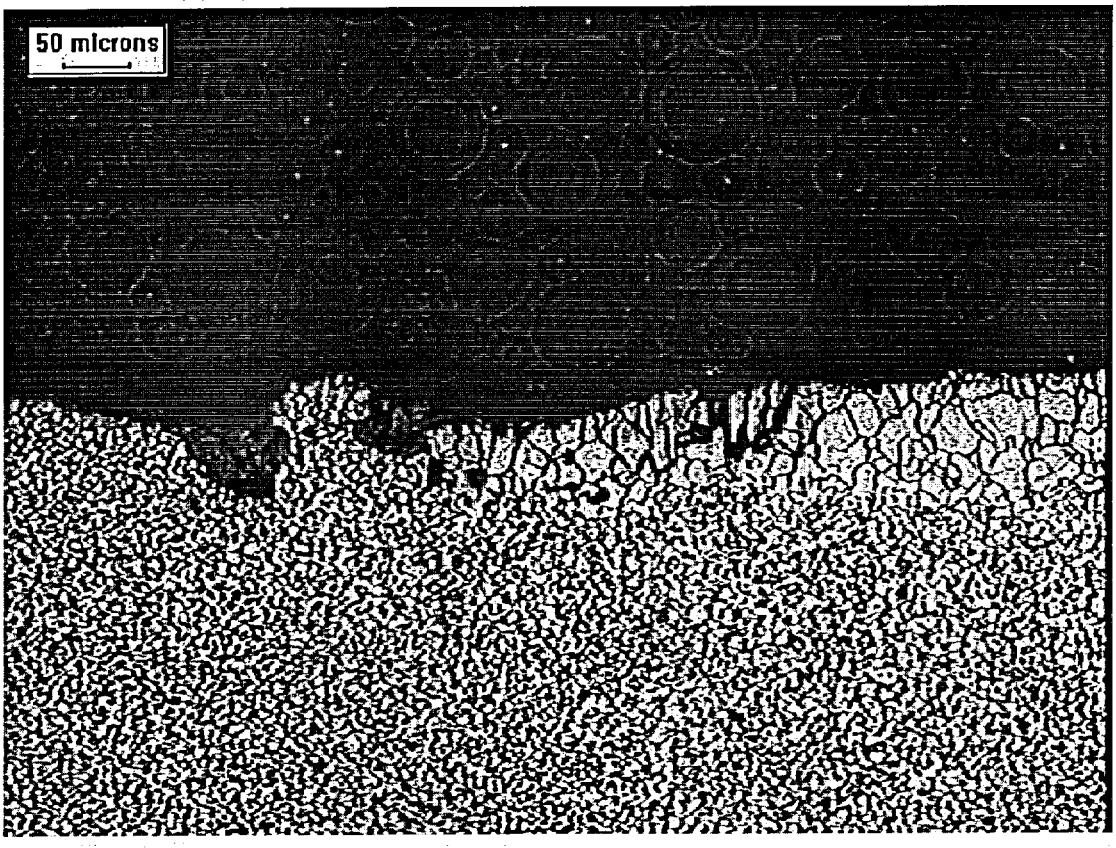

FIGURE 32: Same area as Figure 31 but etched to reveal grain structure. 3% Nital etch. 100X

ELECTRIFY THE WORLD

EPRI

August 29, 2002

Mr. John F. Hall
NDE Coordinator
Wolf Creek Nuclear Operating Corporation
1550 Oxen Lane NE
Burlington, KS 66801-0411

Dear Fred:

At your request, the EPRI NDE Center provided assistance to the Wolf Creek Generating Station with a critique of the ultrasonic examination methodology that was used for examination of 3-inch diameter, ASME Section XI Code Class 3, carbon steel, component cooling water (CCW) piping which was examined during the last two refueling outages.

The attached NDE and metallurgical reports document the results of the EPRI evaluation on four welds that you sent to Charlotte. As per your instructions, this evaluation was performed under the Subscriber Requested Assistance program at the NDE Center.

If you have questions or if we can be of further assistance, please do not hesitate to call.

Sincerely,

Stan Walker

Stan M. Walker
Project Manager

SW/rg

cc: Frank Ammirato
Bob Woehl, Palo Alto
Mike Sherwin, WCNOC
Guenter Grell, WCNOC
Bob Kokoska, Ameren
Gordon Forster, Ameren

CHARLOTTE OFFICE
1300 W.T. Harris Blvd | Charlotte NC 28262-8550 USA | 704.547.6100 | Fax 704.547.6168
CORPORATE HEADQUARTERS
3412 Hillview Avenue | Palo Alto CA 94304-1395 USA | 650.855.2000 | Customer Service 800.313.3774 | www.epri.com

Evaluation of NDE of CCW Piping at Wolf Creek Generating Station

Stan Walker
EPRI NDE Center

August 29, 2002

The EPRI Nondestructive Evaluation (NDE) Center was requested by Wolf Creek Nuclear Operating Corporation (WCNOC) to assist the Wolf Creek Generating Station (WCGS) with a critique of the ultrasonic examination methodology that was used for examination of 3-inch diameter, ASME Section XI Code Class 3, carbon steel, component cooling water (CCW) piping.

The assistance was provided to WCNOC under the Subscriber Requested Assistance (SRA) program within the EPRI NDE Center.

Background

According to the NDE examiners at WCGS, many of the weld joints examined during R10, R11 and R12 exhibited a classic crack signal as would be obtained from stress corrosion cracking (SCC) during the examination. After selected piping sections in the CCW system examined during R12 were removed, several welds were sent to Atomic Energy Canada Limited (AECL) for failure analysis. While performing the failure analysis, it was determined that significant cracking was not present, but very shallow cracking representative of early stages of intergranular attack was apparent. These early stages of cracking were on the order of 0.020 – 0.040 inch deep and were not expected to produce the type of ultrasonic signals that were observed during the inservice examination. Extensive cracking like that confirmed in R10 and R11 was not identified.

Requested Assistance

Due to the results reported in the hardware failure analysis report from AECL, WCNOC requested that the EPRI NDE Center evaluate several of these weld joints with ultrasound and then perform a metallographic examination to determine the source of the ultrasonic signals. A critique of the examination methodology employed for the CCW welds was also requested.

As defined by WCNOC, the deliverables for the NDE Center assistance are as follows:

1. Evaluation of techniques and procedures utilized in the detection and sizing of CCW welds during R12,
2. Determination of the origin of identified flaw signals in CCW weld specimens, and
3. Recommendation(s) for improvement in future CCW ultrasonic examinations.

Trip to Wolf Creek

An EPRI NDE Center staff member traveled to the WCGS site to discuss the examination history with the ultrasonic examiners and to witness the examination protocol that was utilized during R11 and R12.

During the site visit, WCGS ultrasonic examiners demonstrated the ultrasonic calibration to the EPRI staff member, showed verification of ultrasonic signals from welds which had been removed from service during previous outages and contained known cracking, and then performed a re-examination of one of the recently removed welds. Four welds that had been rejected based on ultrasonic examination during R12 were then selected by WCGS and the areas containing ultrasonic indications indicative of cracking were identified.

Based on the onsite demonstrations, it was evident that the ultrasonic examinations performed on the CCW piping system were optimized through:

1. The use of experienced NDE personnel who had previously observed ultrasonic indications from various crack types
2. The use of appropriate calibration and scanning procedures as detailed in the examination procedure WCNOC QCP 20-504, "Ultrasonic Examination for Flaw Detection" and the WCNOC Work Orders 02-234807-024, 02-234913-000, 02-234914-000, and 02-235265-001.
3. Operator familiarization with ultrasonic signals on known cracks
4. The availability of previous root cause analysis reports showing the type of cracking that should be expected in the CCW piping system

While witnessing the onsite examination of weld C-26, the following practices were observed that are also included in the Performance Demonstration Initiative (PDI) Generic Procedure for ultrasonic examination of ferritic steel welds:

1. The size, frequency, and mode of propagation of the search units were appropriate for the piping being examined and the damage mechanism expected.
2. Multiple beam angles were used in order to obtain coverage of the examination area with wide weld crowns left in the as-welded condition.
3. Confirmation of indications was obtained through the weld.
4. Ultrasonic indications were observed in susceptible locations.
5. Echodynamic travel was monitored to help discriminate flaws from geometric conditions.
6. Examiners looked for inconsistent ultrasonic instrument timebase positions when scanning along the indication length, representative of typical cracking conditions.
7. Examiners observed evidence of flaw tips associated with the reflection indications, typical of that obtained with very shallow cracks.
8. The reported ultrasonic indications lay in close proximity to geometrical reflectors, but were distinguishable from the geometry indications.

The following discrepancies from the examination procedure (WCNOC QCP 20-504, "Ultrasonic Examination for Flaw Detection") were also observed:

1. Many of the welds had very wide weld crowns, in the as-welded condition. PDI recommends external surface conditioning when the width of the weld is more than three times the wall thickness.
2. Component external and internal contours were not obtained.
3. Beam plots were not made, which could have provided evidence that the indications from each side of the weld were not, indeed, related to the same reflector.
4. Measurements of search unit position and indication parameters were not always recorded.

Additionally, it was noted that the examination procedure (WCNOC QCP 20-504, "Ultrasonic Examination for Flaw Detection") did not contain descriptive flaw discrimination methodology such as:

1. Observe of comparable or higher amplitude signals when using higher beam angles, which would be indicative of substantial cracking.

Interviews with examination personnel found that examinations were performed under the time constraints of a short plant outage window. These tight time constraints may have prevented making beam plots and search unit position measurements for some of the examinations.

Examiners should ensure that indications are evaluated at reference sensitivity. Occasionally, a tendency to increase the instrument gain in order to evaluate early stages of damage (e.g. corrosive attack) can lead to too high sensitivity; thus resulting in rejection of welds without actual macro-cracking.

Flaw Depth Sizing

Flaw depth sizing would be ineffective if performed on these particular welds due to the wide weld crowns, left in the as-welded condition. The PDI procedures state that weld crowns must be ground flush with the base metal in order to perform accurate depth sizing.

If the weld crowns had been ground flush with the base metal and qualified depth sizing procedures utilized, it is expected that flaw depths could be measured to the nearest 0.050 inch, as demonstrated through the PDI program for qualified procedures and personnel. Without removal of weld crowns, accurate flaw sizing is not possible.

Industry Experiences

The utility industry has several experiences with examinations either missing cracks or calling cracks where none existed. The EPRI staff member providing this assistance to WCNOC has experience with three of these occurrences. In order to answer the question from WCNOC concerning relevance of these other experiences, they are described below.

Examination for Creep Cracking. In one instance, a fossil plant utilized examiners who were qualified to detect intergranular stress corrosion cracking (IGSCC) in boiling water reactor piping to examine chrome-moly pipe for creep damage. At that plant, several welds were called cracked and boat samples were removed. The samples revealed no cracking at all. The plant later removed boat samples in several welds that were reported to be void of cracking and observed creep cracking in each of those samples. The examination results were incorrect in all cases.

The failure in the examinations was attributed to the utilization of examiners that only had experience with detection of IGSCC in stainless steel piping, rather than examiners that were familiar with the creep cracking mechanism.

Examination for Thermal Fatigue Cracking. In another case, examiners with experience in detection of IGSCC were utilized at a nuclear plant for detection of thermal fatigue cracking in carbon steel piping. As in the case with creep cracking, these examiners had no prior experience with the anticipated damage mechanism and completely missed the nearly through wall thermal fatigue cracking.

Examination of Piping with Backing Rings. The third example is related to examination of CCW piping. In this case, the examiners were not aware that backing rings had been used during fabrication of the welds. Because they were not aware of the presence of backing rings, and did not have experience with the ultrasonic indications that are associated with backing rings, welds were called cracked that were not flawed.

Relevance to Wolf Creek. It is felt that none of the above mentioned scenarios are applicable to the current situation at WCGS. This is because the examiners at WCGS:

1. Were experienced with SCC in carbon steel pipe,
2. Had the opportunity to examine examples of similar cracks in similar thickness carbon steel pipes,
3. Were aware of the welding procedures used and weld joint configurations since they had obtained internal configuration data from the weld joints that had been removed from service in R10 and R11, and
4. Noted during the examinations that weld backing rings were not present and that the pipes had been counterbored prior to welding.

Results of EPRI Metallography

After the four welds arrived at the EPRI offices in Charlotte and ultrasonic evaluations were performed, the samples were transmitted to the metallography lab for evaluation. Photographs were taken of the as-received samples to document the condition of the pipe and the locations where the indications were observed during the onsite and laboratory ultrasonic examinations. The areas drawn on the components served as the basis for sectioning and metallographic sample removal. As shown in the attached metallographic report, photos were taken of the inside surfaces to show the condition of the pipes. The components were sectioned, placed together in the original orientation, and photographed to document how the metallographic samples were removed.

As a result of the examination, a list of general observations limited to what could be surmised via metallographic inspection were compiled. The observations are only representative of sectioning and viewing samples in the general location where indications were thought to exist. No exploratory metallography was conducted to search for indications around the circumference other than the initial polished section.

1. All samples indicate corrosive attack.
2. None of the samples contain significant levels of SCC.
3. Sample C-7 contains micro-cracks due to corrosive attack.
4. The deposit on the inside surface beyond the counterbore area is intermittent on the various samples investigated.
5. The deposit was either completely missing or disrupted along the counterbore area, most likely due to product flow changes associated with the thickness transition.
6. The deposit was extremely heavy on sample C-7.
7. Sample C-26 contained a defect from the fabrication of the pipe that may have been responsible for causing an ultrasonic indication.
8. The indication observed visually and ultrasonically on sample D-42A is a result of insufficient material removal during fabrication and fitup machining.

Probable Source of Ultrasonic Indications

Based on the metallographic report, each of the samples contains corrosive attack, but none contained significant SCC. As an attempt to determine the source of the ultrasonic indications that had been classified as SCC, the following theories are proposed.

The indication in the reducer (D-42A) has been attributed to inadequate machining of the inside surface of the reducer. A small line was present on the inside surface that precisely matched the location of the ultrasonic indication. A slightly deeper machining would have removed the anomaly.

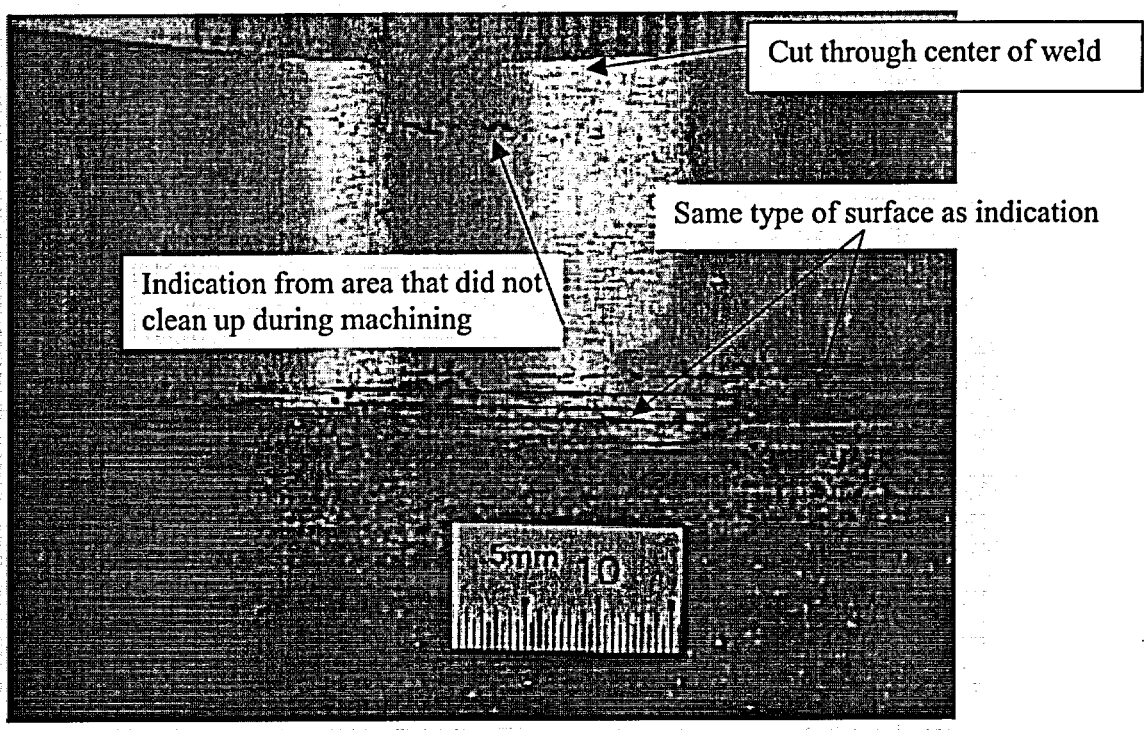

Photo showing area with an ultrasonic indication in D-42A near the bevel of the reducer on the inside surface

The indication in the pipe-to-pipe weld (C-26) is associated with a counterbore that had been cut at two different angles (resulting in a compound counterbore) for the duration of the circumferential extent of the ultrasonic indication. Rather large areas of interbead lack of fusion were also present in the weld. It is felt that the examiners had a tendency to associate the reflections from the lack of fusion with upper extremities of an inside surface crack, and the reflections from the double counterbore with an initiation point for an inside surface crack. Because the counterbore contained two distinct cuts, it is likely that the two cuts were assumed to be a crack signal and a counterbore signal occurring simultaneously. Accurate cross-sectional plotting of the weld and ultrasonic search unit locations should have shown that separate reflectors were being observed, rather than one large reflector (crack).

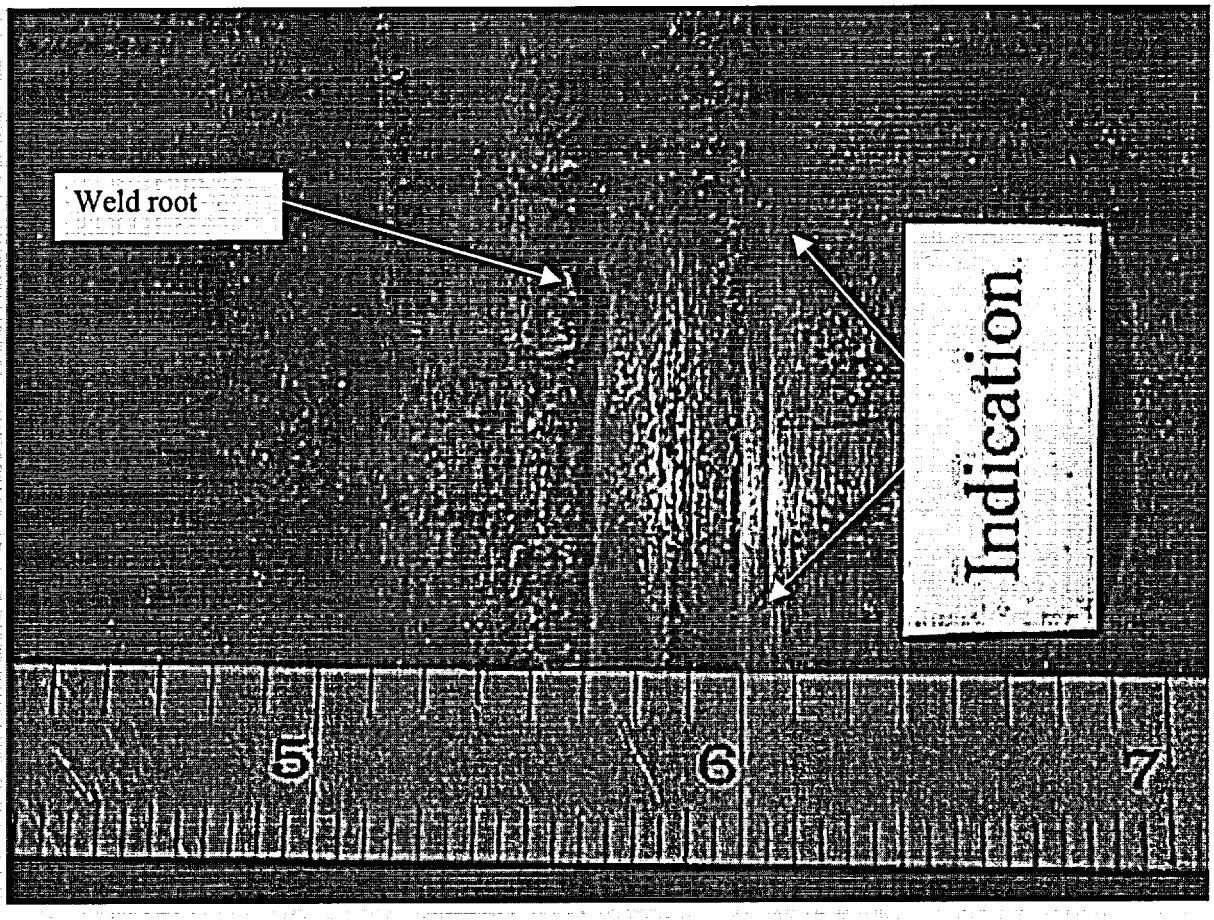

Photo showing the inside surface of C-26 (with a double counterbore) in the area where the ultrasonic indication was detected

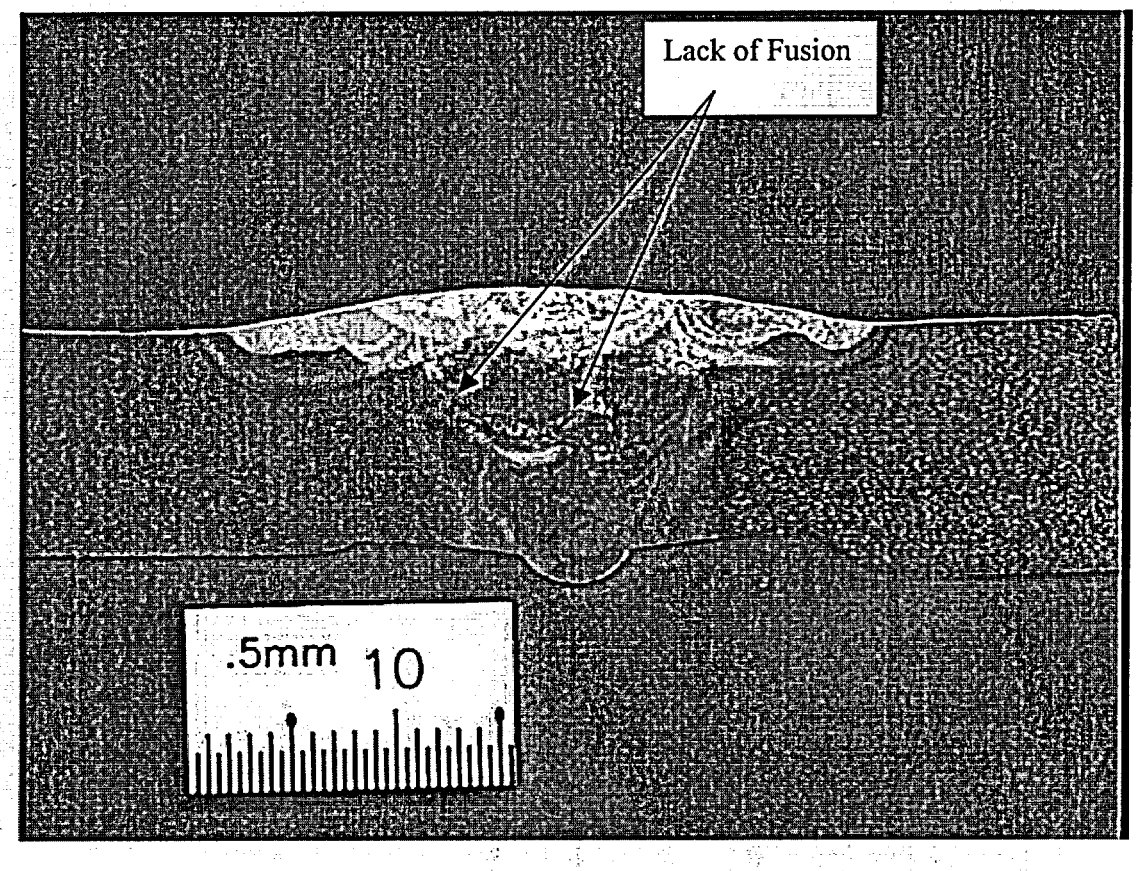

Macrograph showing weld cross section and counterbore geometry of C-26

The indications in the pipe-to-elbow welds (C-6 and C-7) were very weak in amplitude and were not observed from both sides of the weld. Additionally, the use of higher beam angles did not result in comparable or higher amplitude signals. It is surmised that these indications are related to the early stages of SCC or corrosive attack. The calibration notches in the basic calibration block are 10% of wall thickness, or 0.042 inch deep. This places the small SCC at about the same size as the calibration reflectors. This reflector size is something that should be detectable, but should have been determined to be insignificant with proper ultrasonic examination procedure discrimination techniques.

Recommendations for Examination Procedure Improvements

The ultrasonic examination procedure could be improved by incorporating the following requirement:

1. Discrimination methodology such that the results from scanning through the weld and the use of higher beam angles becomes part of the process of determination of reflector characterization.

The ultrasonic examination procedure contained the following requirements, but they were not always implemented due to the time constraints of the plant outage:

1. Weld crowns should be ground smooth to the pipe base metal surface,
2. Recording of each indication and accurate plotting on a cross-sectional drawing of the actual component thickness, and
3. Evaluation of reflectors at the calibration sensitivity.

Consistent implementation of all procedure requirements is necessary in order to obtain accurate examination results.

Conclusions

Ultrasonic and metallographic examination of four CCW welds removed from service at WCGS in 2002 resulted in the presence of corrosive attack with some micro-cracking, but no significant levels of SCC.

For two of the welds (C-26 and D-42A), geometrical conditions were found that could have resulted in the type of ultrasonic indications identified at WCGS. Adjacent to one of these welds, the counterbore was cut at a second angle – potentially creating an ultrasonic indication that resembled a crack in close proximity to counterbore. In the base metal, adjacent to the other weld, machining of the inside surface was partially accomplished – resulting in a fine groove that would resemble a crack from ultrasonic examination. The conditions on the inside surface of these two samples closely resemble cracking when examined ultrasonically.

The other two welds (C-6 and C-7) contained minor corrosive attack, with micro-cracking on the inside surface which should be distinguishable from cracking.

While experienced, competent NDE examiners had performed the examinations with appropriate NDE procedures, some discrepancies were noted. The NDE procedure was not strictly followed with respect to the removal of external weld reinforcement, acquisition of internal and external surface contours, recording of indication location, or plotting of indications on a cross-sectional drawing of the component.

In addition to strict adherence to the NDE procedure, it is felt that procedural enhancements could be made by the inclusion of flaw discrimination techniques. This flaw discrimination methodology could include criteria such as observing that flaw amplitude should remain at similar amplitude, or increased amplitude, when higher angle search units are applied.

Final Report

ASSESSMENT OF STRESS CORROSION CRACKING (SCC) IN THE COMPONENT COOLING WATER SYSTEM (CCW) OF THE WOLF CREEK PRESSURIZED WATER REACTOR (WCNOC)

Prepared by

Roger W. Staehle
Staehle Consulting

22 Red Fox Road
North Oaks, Minnesota
55127
USA

651 482 9493 (direct)
651 484 5735 (telefax)

rwstaehle@rwstaehle.com
www.staehleconsulting.com

WCNOC Purchase order 0718047/0 dated 06/04/02

03/04/10

Abstract

Stress corrosion cracking (SCC) has occurred in the component cooling water (CCW) system of the WCNOC PWR power plant near Burlington, Kansas after the plant started commercial operation in September 1985. This plant is rated at 1235 MW_e. This SCC first occurred in the CCW system in 1994. SCC in several other locations occurred in 2000; and, since then, other SCC has been detected by NDE (UT).

The purpose of this report is to determine why this SCC occurred, to what extent it could occur in the near future, and what remedial actions should be taken. In preparing this report the following were utilized: previous reports on the subject starting in 1995, laboratory investigations undertaken in support of this report, a survey of domestic and foreign experience, and data in the published technical literature.

It was determined in this study that the SCC did not result from defects in materials, design, nor operation. It is also noted that the water chemistry used at WCNOC is one of several used as standard practice throughout the utility industry as well as other industries. The SCC resulted mainly from a combination of high residual stresses at welds and dissolved oxygen in the coolant. Other possible contributions from slightly low concentrations of molybdate, the presence of tolyltriazole, and slightly low pH could be important but are probably not critical. The data from SCC in the CCW system at WCNOC are consistent with those obtained at higher temperatures in oxygenated environments.

Two remedial approaches are identified: (a) keeping the same general molybdate-oxygen-tolyltriazole but with post weld heat treatment (PWHT) and some adjustments in the concentration of molybdate and pH; (b) changing to a hydrazine-amine low oxygen water chemistry also with PWHT. Additional experimental work is proposed to assess possible problems with proposed changes.

Table of Contents

1.0 Summary and Conclusions

The Wolf Creek plant started commercial power production in September 1985. In 1994 the first evidence of stress corrosion cracking (SCC) was observed in the CCW system in piping operating at about 150°F. This incident was investigated, and the results are described in a report in 1995 by Dominion Engineering.[1] Subsequently, leaks due to SCC were observed in 2000 also in piping operating at about 150°F. These were investigated and reported on by Altran Corporation in a series of reports from 2000 to 2001.[2,3,4,5,6] The locations of these SCC are shown in Figure 3.1 Subsequently, in 2002 NDE (UT) investigations by WCNOC personnel identified SCC in the schedule 160 and 120, 3" and 4" diameter, respectively, pipes operating in the range of about 90°F. These observations were surprising in view of the lower temperature. At that point I was asked by WCNOC to investigate the overall problem of SCC in the CCW system and to determine why this SCC was occurring over the range of temperatures in the CCW system. I was also asked to recommend remedial actions.

My investigation was aided by experimental work conducted at the Atomic Energy of Canada Ltd. under WCNOC purchase order 0718049 Rev. 1 dated 02-06-17 who conducted chemical and metallographic analyses as described in Sections 4.0 and 5.0 respectively, and by Dr. Brenda Little under WCNOC purchase order 0718194 dated 02-06-20, who characterized microbial and fungal activity as described in Section 4.5 and Appendix 1.0. Brief backgrounds of the principal investigator at AECL, M. Wright, and Brenda Little are attached in the Appendices. Additional assessments were prepared by Turner, a consultant to WCNOC,[7] who analyzed the Altran work and by the NRC,[8] which conducted chemical analyses and metallography on specimens similar to those examined by AECL. WCNOC and I analyzed the practice of other domestic and international utilities, as reported in Section 6.0. Also, I analyzed the relevant published literature as well as the reports by previous investigations. The results of this analysis are contained in Sections 7.0 and 8.0.

This assessment required that several subjects be investigated in detail in order to reach reliable conclusions. The information necessary to formulate reliable conclusions had not been reviewed before and substantial work was required in order to analyze these data. For example,

1. SCC of mild steel such as used in the temperature range of the CCW system is not often observed, and specific data in the relevant range of temperature can only be obtained by extrapolating data for the rate of SCC from higher temperatures. The data obtained to support and analyze such extrapolations is shown in Figures 7.31 through 7.42. The result of these extrapolations is shown in Figure 8.1 where the rate of SCC in the CCW system is shown to be consistent with data at higher temperatures.

2. The molybdate inhibitor used by WCNOC in the CCW system is used by other utilities to minimize corrosion in water cooled systems as shown in Tables 6.1, 6.2 and 6.3. However, the optimum composition and pH for the CCW system application are not so clear and there are some ambiguities. Also, there are few direct data concerning the

effect of molybdates on SCC. The data on molybdates obtained to support the interpretations and recommendations are given in Figures 7.16 through 7.30.

3. The saturated oxygen used in the CCW system is considered most likely to be the critical environmental species in promoting the SCC. The role of oxygen in producing SCC of mild steels is supported in Figures 7.11 through 7.15 as well as in Figures 7.32, 7.35, 7.36, 7.39, 7.40, 7.41, and 7.42.

4. The occurrence of SCC is greatly affected by its statistical distribution but relevant data are difficult to locate. Possible patterns of statistical distribution are supported in Figures 7.6 and 7.8.

5. The effects of stress on the SCC of mild steel in both the initiation and propagation stages in the temperature range of interest are not readily available, but some data are shown in Figures 7.49 through 7.53. Further, there is no credible means for separating the times required, respectively, for the initiation and propagation phases.

As a result of my investigations, I have concluded the following:

1. There were no defects in materials, fabrication, design, nor operation that led to the perforations by the SCC. This is based on the metallographic examinations from the work of Altran,[2,3,4,5,6] NRC[8] and AECL.[9] The SA106BGr.B alloy material used in the CCW system is commonly used throughout the industry as indicated in Tables 6.1 and 6.3, and chemical analyses of the pipe and welds in Table 3.1 show no unusual species or concentrations. There were no spurious chemicals observed in the detailed analysis of the water in the CCW system nor in the chemical use for the molybdate additive as shown in Table 4.5 of Section 4.0. Further, there were no aggressive microbes nor fungi that could produce aggressive corrosion as noted in Appendix 1.0 and Section 4.5.

2. There is no evidence that the SCC in the CCW system was accidental as might result from a chemical incursion. The growth of SCC most likely persisted over a long time. Further, a new weld installed in 1994 also sustained significant SCC. Also, only molybdate was observed significantly in the SCC. No other species were observed to be significant in measurements by the NRC, Altran and AECL.

3. The choice of the molybdate-tolyltriazole-oxygenated water chemistry used in the CCW system was consistent with industry practice as shown in Tables 6.1, 6.2 and 6.3, with EPRI guidelines in EPRI TR 107396 "Closed Cooling Water Chemistry Guideline,"[10] and with findings of experimental investigations reported in the published literature in Figures 7.16 through 7.30. However, this water chemistry has been optimized only for minimizing general corrosion and not for SCC. Molybdates are regarded broadly as being as effective as chromates in minimizing general corrosion.[11,12]

4. The SCC occurred by a submode of SCC known as high potential SCC (HPSCC). This SCC observed in the CCW system can be related to this submode via the high (generally saturated at room temperature (RT)) oxygen present in the CCW system coolant. The occurrence of this submode and its relationship to data at higher temperatures are described in Section 8.2 and are shown specifically in Figure 8.1, which is the basis for predicting performance. The background for these predictions is given in Section 8.1. HPSCC does not require molybdate to produce SCC; if anything, molybdate is expected to inhibit such SCC. Further, SCC has occurred at three other plants and is summarized by the 1995 DEI report in their Table 1; this table is reproduced here as Table 6.4. While the analysis by DEI suggested that these occurrences of SCC could most likely result from the oxidation of the nitrite inhibitor to nitrate in which SCC occurs, as shown in Figure 7.15, this explanation is not likely. It is more credible that such SCC occurs also via HPSCC owing to the high open circuit potential of the nitrates and nitrites although such potentials have not been verified. However, when such data are included with those from WCNOC, the HPSCC in the CCW system begins to appear more broadly distributed. In view of the correlation of the CCW system data with higher temperature data, the SCC that occurred at WCNOC is consistent with other HPSCC data.

5. In early-2002 (RF 12), it appeared that SCC was occurring at lower temperatures, in the 80-100°F range, and intermittent penetrations of up to 90% through wall and 360° in circumference had been identified by NDE (UT). When specimens from these locations were subjected to metallographic examination at AECL, no significant SCC was found in the circumferential direction; however, SCC in the longitudinal direction was found to a depth of about 1.2 mm (0.047" compared to the wall thickness of 0.438") as shown in Figures 5.11-5.13. After analyzing the NDE (UT), it appeared that erroneous indications of extensive SCC had resulted, most likely, from weld discontinuities. WCNOC has since reviewed its procedures for NDE (UT) with EPRI.

6. The HPSCC occurred in the weld metal, the heat affected zone (HAZ), and in the pipe matrix. Thus, it is independent of the metallurgical structure. The morphology of the SCC is intergranular in these three structures.

7. The initiation of the HPSCC is characterized by intergranular corrosion (IGC) at the inner surface as illustrated in Figures 5.4 and 5.5. However, while such IGC does not usually depend on stress, this IGC seems to have occurred mainly at locations where SCC sometimes initiated. This may be related to undercutting of the welds and local stresses, but this is not clear. There appears to be no significant IGC on the pipe surface away from the weld although this possibility has not been adequately investigated. In this region of IGC at the sites of SCC initiation, some localized corrosion of the microstructural element, "pearlite," was observed both by NRC[8] and by Altran.[2,3,4,5,6] This observation is not significant to the initiation or propagation of SCC.

8. The data in Figures 7.16 through 7.30 indicate that 500 ppm is the optimum value for the molybdate. These data also indicate the optimum pH for this molybdate is about

9.0. There are data which show that molybdate tends to inhibit SCC in Figures 7.24, 7.25, 7.26, 7.28.

9. There are some data from Holroyd[13] in Figure 7.27 and the associated discussion showing that molybdate in the range of pH 4-5 produces SCC in mild steels. However, this is in the range of pH where the oxide film on mild steel in molybdate environments is not sufficiently protective, and SCC should be expected. However, above about pH 6 the oxide film is quite protective in molybdate solutions and SCC due to molybdate would not be expected. Also, the range of potential in which this SCC occurred in Holroyd's experiments is below that expected in the aerated condition of the CCW system. Finally, the concentration of molybdate and the pH of the Holroyd work were significantly higher and lower, respectively, compared to those in the CCW system application.

10. The AECL work showed that molybdenum occurs inside advancing SCC as deep as the tip of the advancing SCC. This is expected since the concentration of molybdate is relatively high and since molybdate is a negatively charged ion which, in the presence of a highly oxidizing environment, should migrate to the crack tip.

11. In addition to the oxygen, the other main factor in producing HPSCC are high residual stresses, which are associated with welding. These stresses not only affected the occurrence of SCC but also determined whether, for the different pipe geometries, the SCC would be longitudinal or circumferential. Without these stresses, the SCC would be greatly reduced if not negligible. These stresses can be most efficiently reduced by "post weld heat treatment"(PWHT). The data from other plants shown in Tables 6.1 and 6.3 of Section 6.0 indicate that PWHT is not widely used. It should be noted that the ASME code does not require PWHT for this size and wall thickness of pipe.

12. A detailed procedure for predicting the future evolution of SCC in the CCW system, assuming no PWHT, is described in Section 8.2.2. If the present water chemistry and residual stresses are not changed, HPSCC can be expected in most welds in the 150°F range of temperatures in pipes according to a statistical distribution such as the ones shown in Figures 7.6 and 7.7. For pipes operating at lower temperatures in the range of 80-100°F, the mean rate of SCC will proceed at about 2.5×10^{-12} ms^{-1} and would perforate the 0.438" wall of a 4" schedule 120 pipe in about 142 years. If conservatisms in rate (factor of two) and in acceptable depth (half depth) are taken, a reasonable lower bound of life would be about 40 years if the SCC started from the inside surface.

13. Developing a detailed procedure for prediction is confounded by the relative durations associated with the initiation and propagation stages as identified in Figures 7.5 and 7.43. Typically, the stage of initiation might occupy half to two thirds of the time to perforation. This means that a propagation rate, determined from the literature, should relate to the remainder. This implies that data from the literature that is unique to propagation such as that in Figure 8.1 should relate only to

propagation steps of the SCC in the CCW system. However, there is no way to separate the times of the initiation and propagation stages, and it is assumed in this study that the SCC progressed more or less linearly from the time operation of the plant started. This is a less conservative assumption; and more conservative estimates of times-to-failure based on already existing SCC should consider rates about twice as high as those given for the CCW system in Figure 8.1.

14. An important problem in predicting performance of the CCW system is associated with the circumferential SCC observed in the 6" pipes operating at about 150°F. Here, the metallographic examinations by Altran,[2,3,4,5,6] are identified in Table 5.1 and Figure 3.1, showed that some specimens examined sustained circumferential SCC. However, this examination did not determine the circumferential extent on any one pipe nor did it systematically evaluate all pipes that were supplied by WCNOC. This piping was examined by WCNOC before sending it to Altran using NDE (UT); SCC was determined to occur intermittently around the circumference, and the depths of penetration were determined to be intermittent; however, these results were not confirmed by systematic metallography. Further, the stage of IGC initiation at the inside surfaces was observed in all samples examined by NRC, Altran and AECL. These results imply that the initiation stage could be uniform around the circumferences of the pipes. With these limited data it can only be assumed that the SCC could be fully circumferential as illustrated in Figures 7.46, 7.47 and 7.48. In the crack propagation stage, the rate of propagation is generally independent of stress in the plateau region of the V-K curve as shown in Figure 7.46. In the event of using PWHT the K of existing SCC may not leave the plateau range of the V-K characteristic. Thus, a worst case here could be an extensive circumferential crack of the pipe in a break before leak (BBL) mode even with the application of PWHT as shown in Figure 7.48.

15. There are two options for minimizing or preventing future HPSCC as described in Section 9.1:

    a. Retaining molybdate water chemistry: mainly, optimize the molybdate according to the discussion in Section 7.3.3, leave the oxygen, raise the pH, reduce residual stresses in welds by PWHT as noted in Figure 7.48, and improve NDE (UT). This approach can be expected to mitigate but not eliminate the HPSCC. While new SCC may not initiate, existing SCC may not be affected by PWHT if the resulting K remains in the plateau regions of the V-K curve.

    b. Change the water chemistry: mainly, use a low oxygen and hydrazine treatment, raise the pH with an amine, lower residual stresses, improve NDE (UT). This approach will prevent the HPSCC, including that which is now propagating. Using this treatment may affect other components, especially those with copper-base alloys, and such implications would need to be evaluated.

16. In order to qualify the actions recommended for minimizing/preventing HPSCC, some work should be undertaken as described in Section 9.2:

a. The PWHT should be evaluated to assure that the resulting metallurgy is not more prone to SCC than the present condition.

b. The PWHT procedure should be evaluated to assure that the stresses are adequately relieved when the PWHT is performed according to the ASME code.

c. The use of tolyltriazole should be investigated to assess its importance to accelerating SCC.

d. The effectiveness of the hydrazine treatment should be evaluated with respect to eliminating SCC.

e. The water should be evaluated periodically for microbes and fungi. Plans for using a suitable biocide should be available.

f. The change of pH should be evaluated to assure that it reduces SCC.

g. Future metallography of pipes containing NDE indications should include assessments of both circumferential and longitudinal directions, the presence of a shear lip should be determined, and details of the initiation sites should be compared with corrosion away from the initiating location.

2.0 Introduction

The objective of this report is to assess the stress corrosion cracking (SCC) that has been observed in the "component cooling water" (CCW) system of the Wolf Creek Nuclear Operating Corporation (WCNOC) pressurized water reactor (PWR) during the period of its starting commercial operation in 1985 until the present. The principal parts of this objective are to assess the remaining useful life of the present CCW system piping and to recommend changes where SCC has perforated or is expected to perforate in the future.

My work was undertaken under purchase order 0718047/0 dated 06/04/02 from WCNOC. Additional work under my technical direction was undertaken by the Atomic Energy of Canada Ltd. (AECL) under contract to WCNOC and by Dr. Brenda Little, an independent consultant. AECL conducted work on metallography, fractography, and chemical analysis. Dr. Little conducted work on microbiological corrosion. AECL was involved because their laboratory has extensive experience with the stress corrosion cracking (SCC) of carbon steel and is currently the most qualified of the nuclear laboratories in North America. Dr. Little was involved because she is recognized as one of the premier experts in the world on microbial influences on corrosion. My curriculum vitae, that of Dr. Wright of AECL, and that of Dr. Little are attached as Appendices 2, 3 and 4.

A major reason for my involvement was the observations that the occurrences of SCC appeared to be increasing in lower temperature piping in the CCW system:

1. SCC was first observed to perforate the walls of 6" schedule 40, 150°F, piping in the CCW system in 1994 as noted in Figure 3.1 and Table 5.1.

2. Perforation of this 6" schedule 40 piping was again observed in 2000.

3. In 2002, extensive SCC had been determined by NDE (UT) to exist in many welds of the lower temperature, about 100°F, 3" and 4" schedule 160 and 120 piping, respectively. Some of the NDE (UT) signals indicated a 360° intermittent circumferential extent and intermittently up to 90% penetrated. However, such extensive occurrences were later shown to be erroneous, as discussed in Section 5.0.

In conducting my work for WCNOC I have been involved in the following:

1. Preparing protocols and reviewing, including by visits, the work at AECL.

2. Preparing protocols and reviewing the work of Dr. Little.

3. Participating in work on behalf of WCNOC with the Nuclear Regulatory Commission (NRC) in their oversight role.

4. Obtaining information from other utilities, both domestic and international, concerning their experiences with water treatment, materials, and corrosion experience with CCW systems.

5. Obtaining and analyzing relevant technical literature.

6. Analyzing existing data together with the experimental work by AECL and Dr. Little and developing: an explanation for the occurrence of the SCC (Section 7.0); a prediction for the current life of piping in the CCW system (Section 8.0); recommendations for remedial actions (Section 9.0).

My work involved the following visits and trips:

1. I was first contacted by Dr. Art Turner on 02-04-10, a consultant for WCNOC, to determine my interest in investigating SCC that was occurring in the CCW system.

2. I first met with WCNOC personnel on 02-05-15 at their offices in Burlington, Kansas. Based on this meeting I proposed a plan of work dated 02-05-17. During this first trip to WCNOC I was provided with background of the SCC and the CCW system.

3. I participated in a meeting with WCNOC and NRC 02-06-11 at Burlington.

4. I visited AECL on 02-06-13 to describe the necessary work and to arrange for contracts together with WCNOC personnel.

5. I visited WCNOC with Dr. Little on 02-07-02 to take samples for microbial and fungal examination.

6. I visited AECL on 02-07-09 with WCNOC personnel to compare the metallography of SCC with NDE (UT) indications.

Prior to and during my involvement, work to understand the SCC in the CCW system at WCNOC had been conducted by:

1. References in Appendix B of the 1995 DEI report: Reports by Reischmann et al. and by Agle.[14,15,16] These concerned SCC of 6" piping and elbows located downstream of the letdown heat exchanger.

2. Dominion Engineering (DEI) issued a report "Review of McGuire and Wolf Creek Component Cooling Water System Cracking" in May 1995. This report reviewed information from the WCNOC failures and from SCC in similar systems in other plants. They also reviewed and assessed the relevance of published literature.[1]

3. Altran issued a series of reports:

   a. "Failure Analysis of Cracked Welds in Component Cooling Water Piping," Technical Report No. 00617-TR-001, Rev. 0, Vol. 1/1, August, 2000.[2]

   b. "Failure Analysis of Cracked Component Cooling Water System Welds," Technical Report No. 00628-TR-001, Rev. 0, Vol. 1/1, February 2001.[3]

c. "Root Cause Investigation of CCWS System Weld Cracking," Technical Report No. 00628-TR-002, Rev. 0, Vol. 1/1, April 2001.[4]

d. "Failure Analysis of Cracked Component Cooling Water System Welds," Technical Report No. 00628-TR-001, Rev. 1, Vol. 1/1, May 2001.[5]

e. "Root Cause Investigation of CCWS System Weld Cracking," Technical Report No. 0068-TR-002, Rev. 1, Vol. 1/2, June 2001.[6]

These reported on metallographic examinations, water chemistry, and information in the technical literature.

4. "Stress Corrosion Cracking of Component Cooling Water (CCW) Piping and Letdown Heat Exchanger (P.O. 0714037/0, letter from Turner (DEI) to D.B. Meredith (WCNOC), L-4340-00-01, September 4, 2001.[7] This letter reviewed accomplishments of the Altran work, assessed rates of growth of existing SCC and recommended actions for minimizing future SCC.

5. "An Investigation of Microbiologically Influenced Corrosion at Wolf Creek Nuclear Generating Plant," Brenda J. Little, September 14, 2002.[17] This investigation reported on measurements of microbes and fungi taken from various locations in the CCW system.

6. "Wolf Creek Component Cooling Water System and Letdown Heat Exchanger Cracked Welds."[18]

7. "Examination of Cracking in Welds from the Wolf Creek Component Cooling Water System," CS-71300-ASD-001, Rev. 0, M.D. Wright, September 2002.[9] This reports on metallographic examinations and chemical analyses of cooling water and molybdate chemicals.

8. "Metallurgical Investigation into the Cause of Cracking in Piping for the Containment Cooling Water System at Wolf Creek," C. Wong and W.H. Cullen, December 5, 2002.[8] This reports on metallographic examinations.

3.0 Design of Wolf Creek CCW System

3.1 Locations and Chronology of SCC and Specimens

Figure 3.1 shows the CCW system piping as it exits from the letdown heat exchanger.[19] Many of the details in the original drawing are omitted to illustrate locations of SCC. The numbers locate specimens that were examined by Altran.[2,3,4,5,6] The numbers correspond with those on the chart of Table 5.1. Also noted on Figure 3.1 are the times when failures occurred. With respect to Figure 3.1 the following notes apply:

a. Welds 7 and 8 were not NDE (UT) inspected due to high radiation in the area.

b. Welds submitted to Altran were confirmed through destructive analysis to have circumferential cracks.

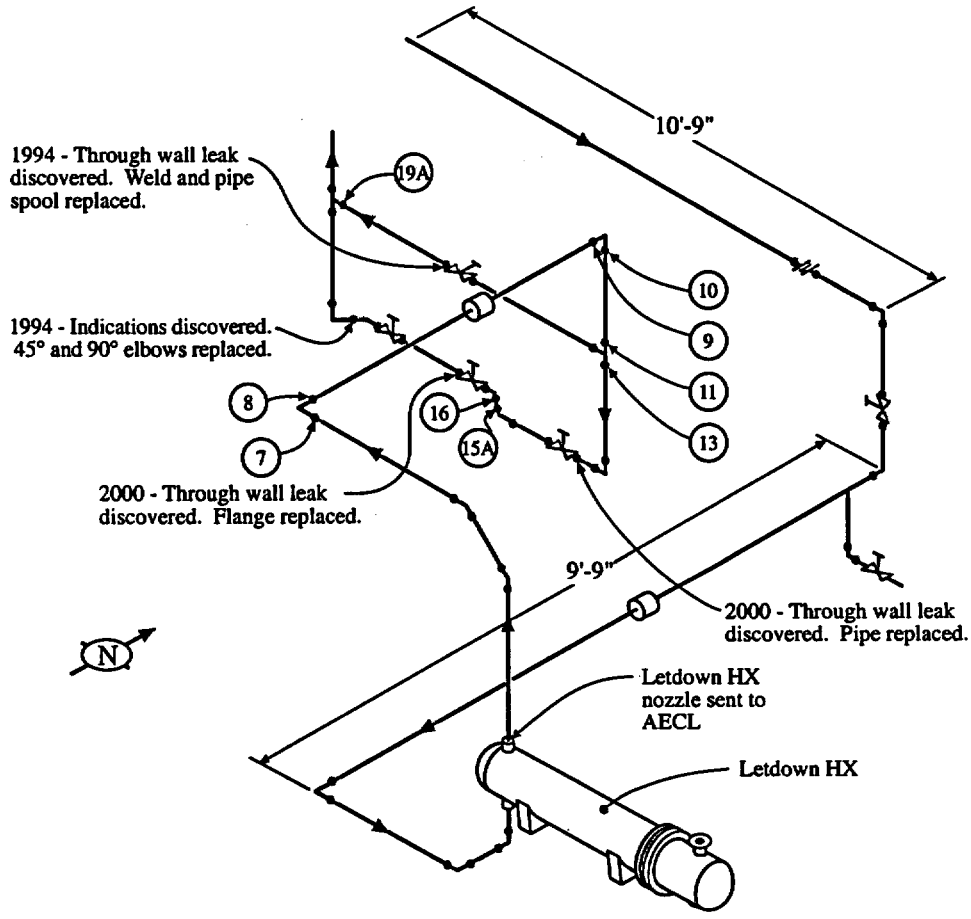

Figure 3.1 Schematic view of component cooling water system from drawing M-13EG06. Notation for specimens examined by Altran[2,3,4,5,6] shown in circles. Examples of metallographic examination by AECL shown in Figures 5.1-5.5 and 5.14 for the transition piece noted at the outlet of the letdown heat exchanger. Notes also shown for failures and their chronology. Data provided by Womelsdorf of W19CNOC.

c. Weld 57 was from the upper bearing cooler return line (4" Sch. 40, SA106Gr.B).

d. Welds 7-19A that were examined by Altran[2,3,4,5,6] were subjected to water in the range of 150-175°F.

e. Weld 57 was subjected to water of lower temperature in the range of 85-95°F.

Figure 3.2, 3.3 and 3.4 show locations of welds from which specimens were sent to the NRC and to AECL. These specimens are also identified in Table 5.1. Table 3.2 shows specimens sent to both NRC and AECL. The temperature of the water in these pipes is in the range of 85-95°F.

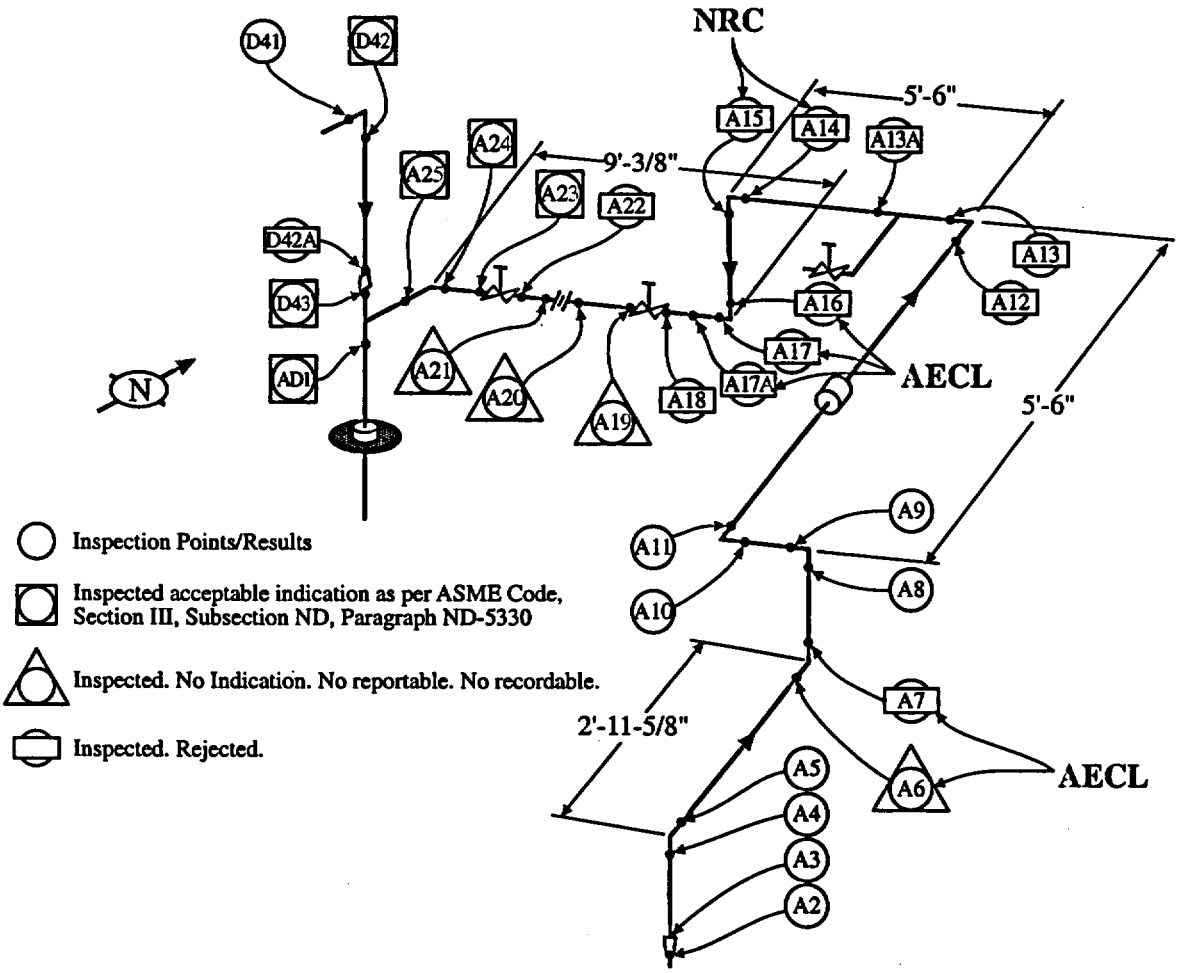

Figure 3.2 Schematic view of piping from which some specimens for NRC[8] and AECL[9] were taken. This schematic view is taken from the RCP "A" Thermal Barrier CCW System Return and is designated EID-0008. Notations refer to welds. Only specimen A-15 was examined by NRC[8] with the photo micrographs shown in their report.

Figure 3.3 shows specimens sent to NRC. The temperature of the water in these pipes is in the range of 85-95°F.

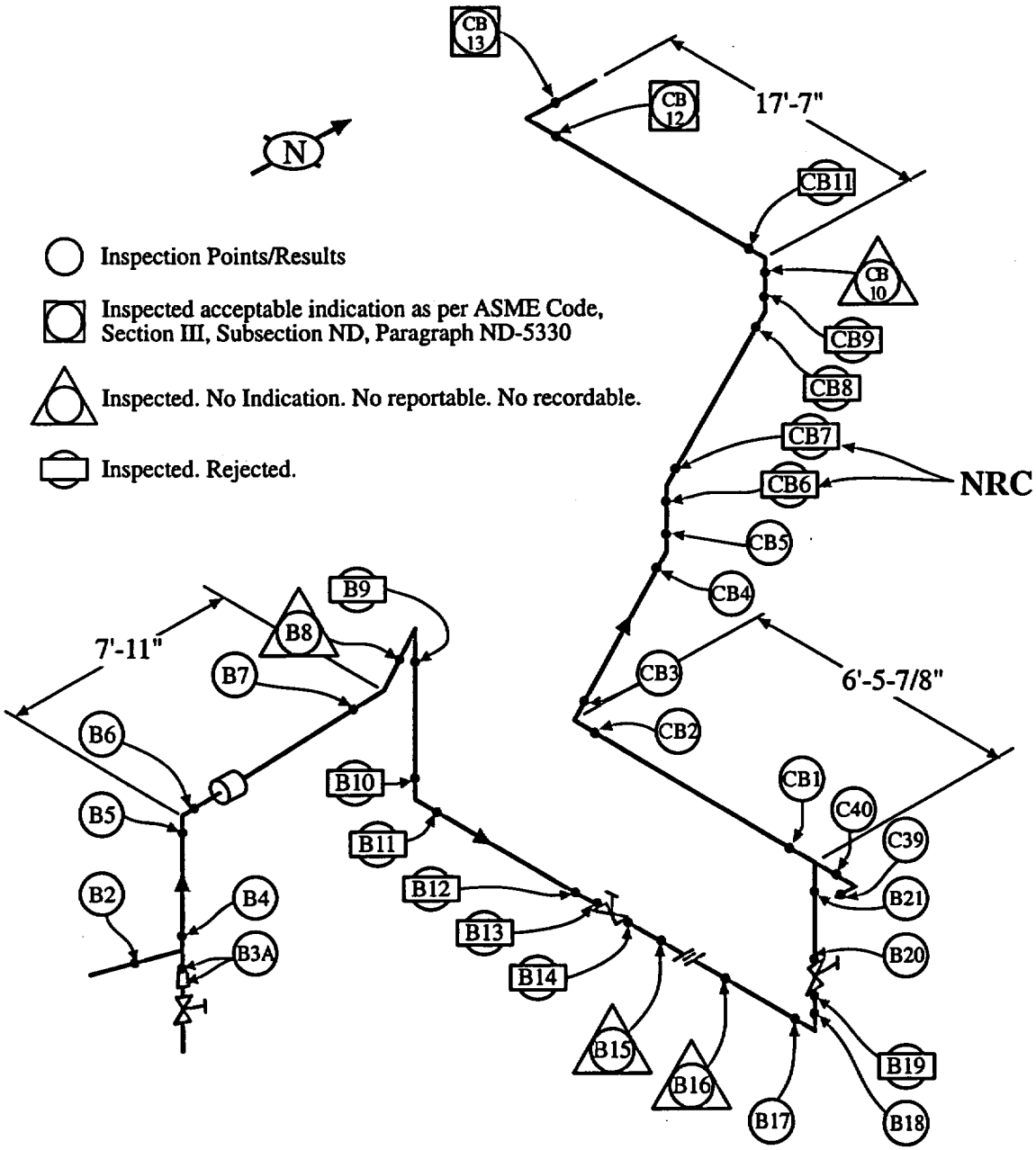

Figure 3.3 Schematic view of piping from which some specimens for the NRC were taken. This schematic view is taken from the RCP "B" Thermal Barrier CCW System Return and is designated EID-0007. Notations refer to welds. These specimens are identified in Table 5.1.

Figure 3.4 shows specimens sent to both NRC[8] and AECL.[9] The temperature of the water in these pipes is in the range of 85-95°F.

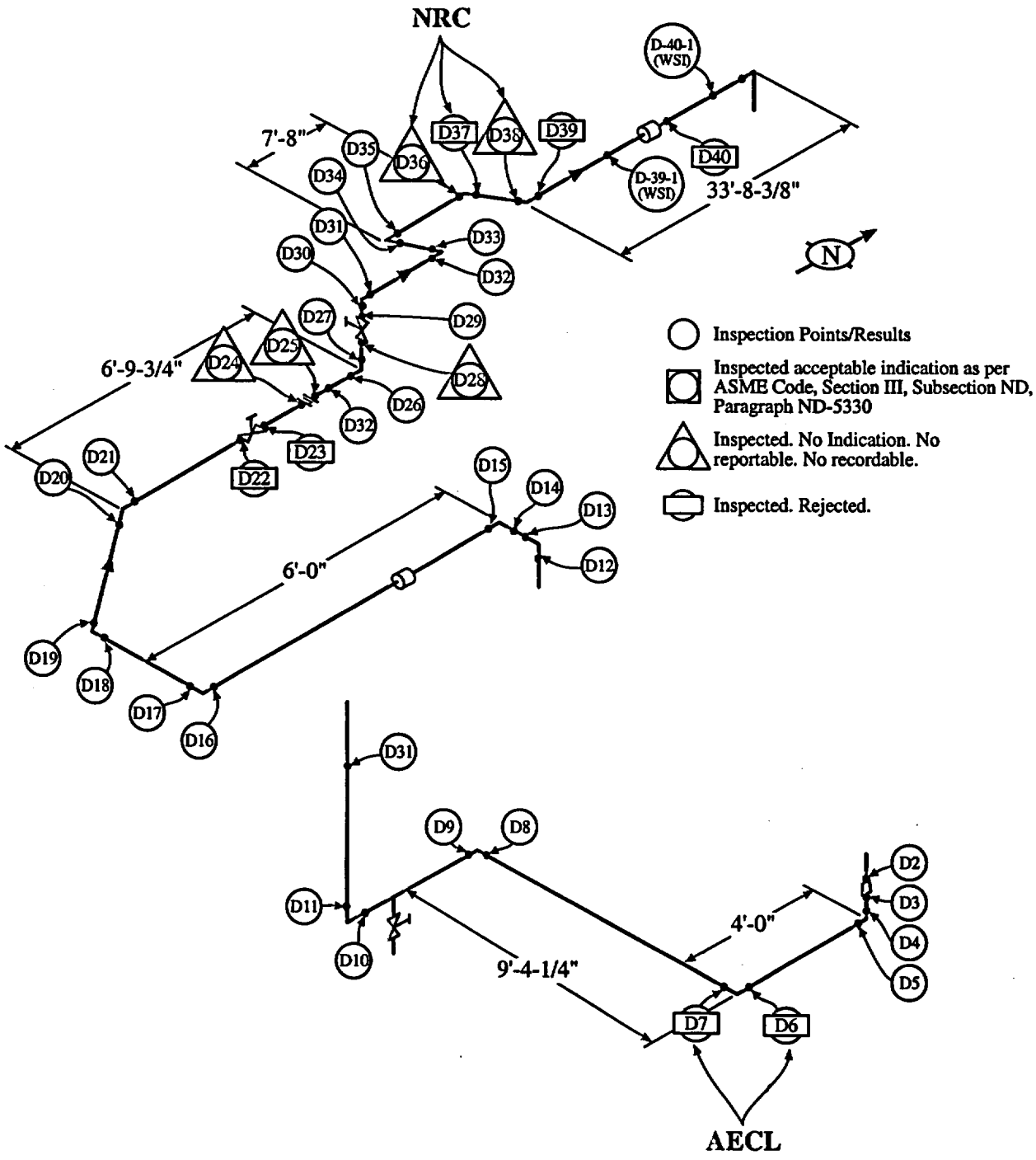

Figure 3.4 Schematic view of piping from which some specimens for NRC and AECL were taken. This schematic view is taken from the RCP "D." Examples of metallographic examination of welds D6 and D7 are shown in Figures 5.6-5.13. Thermal Barrier CCW System Return and is designated EID-0009. Notations refer to welds.

The chemistries of pipe samples and weld samples taken from the CCW system were analyzed by NRC[8] and by Altran[2,3,4,5,6] and results are given in Table 3.1. Relevant specifications are

given as supplied by Altran and the NRC. The chemistries of the piping appear to be in the right ranges. The weld chemistries are, in some cases, outside the specification noted for E7018 but this may not be the correct specification as noted by the NRC.

Table 3.1

Composition of Alloy SA 106Gr.B, w/o[6]

ASME SA 106Gr.B Spec.		Elbow[2]	Pipe[2]	E7018[4,5]	Weld [2]	Weld 22[3]	Weld 516[3]
C	0.30 max	0.246	0.267		0.125	0.098	0.10
Mn	0.29-1.06	0.95	0.75	1.25min	1.57	0.96	1.05
P	0.025 max					0.010	0.008
S	0.025 max	0.014	0.027		0.014	0.016	0.017
Si	0.10 min	0.15	0.16	0.90min	0.88	0.39	0.46
O		0.0034	0.0031		0.0045		
Cr[1]	0.40 max	0.015	0.019	0.20min	0.04	0.07	0.05
Cu[1]	0.40 max	0.038	0.018		0.26	0.10	0.16
Mo[1]	0.15 max	0.004	0.008	0.30min	0.005	0.02	0.03
Ni[1]	0.40 max	0.014	0.013	0.30min	0.028	0.08	0.03
V[1]	0.08 max			0.08min			
Al		0.026	0.014		0.26		

[1] These five elements shall not exceed 1% total
[2] NRC,[8] wet chemistry
[3] Altran[2]
[4] NRC,[8] identify as possible weld spec for SA106 material. This is not the actual specification.
[5] Sum of Mn, Ni, Cr, Mo+V<=1.5
[6] 4" schedule 120 has a 0.438" wall; 6" schedule 40 has a 0.280" wall

4.0 Environmental Chemistry

The purpose of this section is to provide bases for interpreting the effects of the chemical environments in the CCW system on the SCC. This section includes EPRI guidelines, internal WCNOC guidelines, chemical analyses from the present investigation and from those conducted by Altran[2,3,4,5,6] and the NRC.[8] Chemical analyses were obtained from the cooling water both in this investigation and by Altran, from the molybdate in this investigation, and from various deposits by Altran. Results from studies of microbial and fungal analyses are also included. Chronological data of the CCW system are included but they were not available in formats that permitted statistical analyses and are treated by estimation here; this approach, while not satisfying, is adequate for the present purposes.

4.1 EPRI Guidelines

The control of water chemistry in the WCNOC plant follows the "Closed Cooling Water Chemistry Guideline," TR 107396, prepared by the Electric Power Research Institute (EPRI) and dated October 1997.[10] Table 4-2 of their report, (Table 4.1 here) identifies the inhibitors that could be considered and are used for various CCW system applications:

The section on the use of molybdates from the EPRI guidelines[10] notes the following about the use of molybdates and is given directly or paraphrased. Wording used directly from the EPRI Guidelines is placed in "quotes" and [my comments are placed in brackets].

1. "*Mechanism*:" [Molybdate, is nonetheless a good inhibitor. The matter of need for oxygen recommended in the Guidelines is not supported by any experimental studies and has no fundamental basis.]

2. "*Applicable Metallurgy*: Ferrous alloys and aluminum." [Molybdates are applicable to more metals but this is not consequential here].

3. "*Control Range*: 200 to 1000 ppm as MO_4^{2-}. The minimum effective laboratory concentration for molybdate is on the order of 160 ppm as MO_4^{2-}. A typical dosage range for molybdate, when used alone, is 200 to 1000 ppm as MO_4^{2-} although in some cases lower dosages have been successful. In special applications, much higher dosages have been used. Initial (passivation) [should be inhibitive] dosages should be in the upper part of the typical operating ranges. There has not been an upper acceptable dosage established, based on pump seal degradation, as there has been for chromate and nitrite."

4. "*Associated Additives & Conditions*: Molybdate is often used with sodium hydroxide, sodium carbonate, sodium bicarbonate, an amine or borate to increase pH into the 8.5 to 10.5 range. This is based on the general impact of pH on corrosion rate for ferrous metallurgy. An azole is needed for copper corrosion inhibition."

5. "*Advantage*: Molybdate does not exhibit the toxicity of chromate, although it might have some environmental restrictions."

Table 4.1

Corrosion Inhibitors—Typical Control Ranges for Systems with Demineralized Water Makeup and Low Leakage.[10]

Inhibitor	Provides Protection Of	Typical Control range, ppm	pH Control Range	Comments
Chromate, CrO_4^{2-}	Fe, Cu, Zn, Al, Sol	150-300	8.5-10.5	
Nitrite, NO_2^-	Fe	500-1000	8.5-10.5	
Molybdate, MoO_4^{2-}	Fe, Al	200-1000	8.5-10.5	Dissolved oxygen conditions need to be considered
NO_2^-/MoO_4^{2-}	Fe, Al	Varies	8.5-10.5	
Hydrazine, N_2H_4	Fe, Cu	5-50	8.5-95 if Cu present; 8.5-10.5 if Cu absent	Ultra-low dissolved oxygen is critical for Cu control
Carbohydrazide	Fe, Cu	5-50	8.5-95 if Cu present; 8.5-10.5 if Cu absent	Ultra-low dissolved oxygen is critical for Cu control
Tolyltriazole/benzotriazole, TTA/BZT	Cu	5-30	8.5-10.5	
Mercaptobenzothiazole, MBT,	Cu, Sol	5-30	8.5-10.5	
Silicate	Fe, Cu, Al	20-50 above background	8.5-10.5	Not for use if pH<7; forms a fragile film—weak inhibitor
Pure Water*	Fe, Cu	N/A	Not established	Ultra-low dissolved oxygen is critical for Cu control

* It is not clear why pure water is recommended in this EPRI report as an inhibiting solution for Fe, especially. In neutral deoxygenated water, iron is unstable, as shown in Figure 7.1, and corrodes relatively rapidly. Pure deoxygenated water is acceptable only for Cu.

6. "*Disadvantage*: Molybdate does not inhibit microbiological growth, and it does not serve as a nutrient."

7. "*Radwaste considerations*: Molybdate-containing wastewater will compete with anionic radioisotopes for ion-exchange sites, resulting in reduced removal capacity for other ions such as iodine. The counter-ion (sodium or potassium) [they mean cation] will increase consumption of cation resin. Large volumes of resin are therefore required to process wastewater from molybdate-treated systems. If tetraborate is used as a pH buffer, the reactivity management concerns discussed above will also be of concern to BWR plants."

Chemicals used for inhibiting corrosion of copper alloys are discussed in the EPRI Guidelines, and the information affecting WCNOC is extracted here:

1. Use: "Chemicals used for copper corrosion control are nitrogen-containing organic compounds (azoles). Three chemicals of this type are used: mercaptobenzothiazole (MBT), tolyltriazole (TTA), and benzotriazole (BZT)."

2. "*Mechanism*: Azoles react with copper ions to form a thin film that reinforces the oxide film on the copper layer [This is a questionable interpretation of the mechanism]. MBT is the fastest film-former of its type.

   "Although TTA and BZT form a protective film more slowly than MBT, they are more stable under conditions of high temperature and chlorination. BZT and TTA are used in both open recirculating and CCW systems. Some suppliers blend TTA or BZT with MBT to incorporate both rapid film-forming properties and stability into a single formulation."

3. "*Applicable Metallurgy*: All three azoles are effective for copper alloys. MBT has been identified as the most effective for soft solder connections in emergency diesel generators."

4. "*Dosage Range*: In open recirculating systems (cooling tower systems), TTA and BZT minimum dosages of 1 to 2 ppm are used. In these applications, MBT is used at about three times the TTA or BZT dosage. There are no data available for minimum dosage in CCW systems. In CCW systems, however, typical TTA or BZT dosages are usually in the range of 5 to 30 ppm (or higher). Higher levels of TTA and BZT are required to protect the zinc in brasses although the information available is for open recirculating systems and might not apply to CCW systems. No maximum level for azoles has been established but this will be a function of TOC [total organic carbon] and pH limits."

5. "*Associated Additives & Conditions*: The azoles are typically used as additives to ferrous alloy inhibitors and are effective in the pH range of 8.5 to 10.5."

6. "*Advantages*:

   - The presence of an azole reduces deposition of copper ion on steel.

   - Azoles are low in toxicity compared to chromate.

7. "*Disadvantage*:

• Microorganisms degrade the MBT molecule rapidly and MBT is degraded by oxidants. TTA and BZT are not susceptible to significant microbiological degradation."

8. "*Radwaste Considerations*: At typical use concentrations (5-30ppm), radwaste processing of filming inhibitors such as TTA, BZT, or MBT is not of great concern. Since the inhibitors are sparingly soluble in water, high concentrations may lead to fouling of ion exchange resins. Since MBT degrades to sulfate, slightly higher sulfate concentrations could result in water treated with MBT. Continuous input of these chemicals to radwaste will increase the amount of organic loading on anion resins."

4.2 WCNOC Internal Guidelines

Table 4.2 describes the program of chemical analyses for the CCW system used by WCNOC. Table 4.3 describes specific values that apply.

Table 4.2

CCWA, CCWB, EB, and BTRS Chiller – All times.
(from WCNOC "Chemistry Surveillance Program" Rev. 15, page 36/40.)

Monthly	Quarterly	Semi-Annual
pH	Copper	Fluoride
Specific Conductivity	Iron	
Tolyltriazole	Heterotrophic Aerobic Bacteria (BART)	
Molybdate	Iron Related Activity (BART)	
Chloride	Sulfate Reducing Bacteria (BART)	
Sulfate		
Total ATP		
Gross Specific Activity		
Tritium		
Conductivity/Molybdate Ratio	Dissolved Oxygen	

4.3 Chemistry in the CCW System

I have reviewed data available from the period of 1984 through early 2001. However, I have not had sufficient resources to perform a detailed analysis. Thus, I have estimated ranges and averages from the plots. Since the plant did not start until September 1985, only subsequent values are relevant. Only the molybdate, tolyltriazole, chloride, and pH were available. No

microbial, oxygen, sulfate, nor iron analyses were available. These would all be helpful for developing a more thorough analysis.

Table 4.3

Chemistry Parameters for Component Cooling Water/BTRS Chiller. (Shell-side)
(From WCNOC Chemistry Specification Manual, Rev. 13, AP 02-003)

Parameter	Units	Norm Value	Supv Limit	Chem Limit
pH @ 25°C	pH	8.4	8.2-10.5	8.0-11.0
Chloride	ppb	<40	<50	<150
Fluoride	ppb	<40	<41	<150
Molybdates	ppm	300	200-400	150-450
Tolyltriazole	ppm	7	6-12	5-15
Makeup Water[1]	N/A	-	-	Primary Water Specs
Spec. Activity	mCi/ml	none	0	Monitor
Tritium	mCi/ml	1E-5	<5E-5	Monitor
ATP -Total	RLU	-	500	600
ATP - Free	RLU	-	450	550

[1] The specification for oxygen may be waived

Important trends should be considered together with the occurrence of SCC. The first SCC was observed in 1994. Since that time, more SCC was observed by 2001. These trends can be compared with the dominating trends of chemistry, which are apparent from Table 4.4:

1. The approximate average of the molybdate is in the range of about 220 to 510 ppm with lower values early, a peak in the middle at 1995, and lower values thereafter.

2. The tolyltriazole increases with time from about 5 ppm to range of 8 ppm starting in 1994.

3. The chloride impurity decreases from about 40-50 to 13-20 generally with time.

4. The pH decreases from a range of 9.1-9.3 to 8.4-8.6 by 2000 generally with time.

5. The SCC observed by 1994 seems associated with relative low molybdate, low tolyltriazole, higher chloride and higher pH.

6. The oxygen, while not given explicitly in the materials available to me, is understood to occur at about normal air saturation of 5-10 ppm since the system was open to air.

7. The occurrence of SCC in the range of 2000-2001 is not readily attributed to a period of chemistry since it is not clear when it initiated, although it can be assumed to have been developed over the life of the plant.

8. In one case a pipe that was inserted in 1994 exhibited SCC by 2000[5] although the SCC did not fully penetrate. Note that this indication had sustained six years of service; whereas, the SCC that was observed in 1994 had sustained nine years of service before going through wall. This suggests that the lowering of molybdate, increasing of tolyltriazole, decrease in chloride and lowering of pH contributed to the later SCC. However, the extent of the SCC relative to previous SCC was not given and no quantitative assessment is possible.

It seems that there is no clear relationship between the chemistry in the CCW system as shown in Table 4.4 and the occurrence of SCC. Also, there had been no significant change in chemistry through 2000 for six years.

Table 4.4

Chronology of WCNOC Chemistry for the CCW system Loops A and B.*

Year	Molybdate, ppm		Tolyltriazole, ppm		Chloride, ppb		pH	
	Avg.	Range	Avg.	Range	Avg.	Range	Avg.	Range
1984	50	2-83	0		800	50-1700	11	8-11.5
1985	80	5-150	0		60	7-120	9.5	9-10
1986	225	90-350	5	3-7	40	10-95	9.3	8.7-10.5
1987	250	180-400	5	2.5-6.5	45	3-105	9.4	9-10
1988	250	170-505	5	2-7.5	25	5-65	9.1	8.6-9.3
1989	300	250-345	5	4-6	27	13-40	9.1	8.8-9.9
1990	300	190-440	5	1.9-7	20	4-39	9	8.8-9.2
1991	280	210-450	5.3	3-7	30	6-45	8.8	8.5-9
1992	350	280-415	6	4-7	25	13-48	8.9	8.6-9
1993	340	270-450	6.5	4-9.9	15	6-38	8.6	7.9-9.1
1994	360	290-540	8	5-9.3	17	8-40	8.6	8-8.8
1995	510	440-550	7	5.8-8.2	20	9-33	8.6	8.4-9.5
1996	360	230-500	8.8	4.2-11	15	10-28	8.5	8.3-9.6
1997	340	200-380	8	5-10.6	18	10-34	8.5	8.3-8.6
1998	275	250-350	8	7.2-9.1	18	10-25	8.4	8-8.7
1999	240	210-260	8.5	6-10	14	10-27	8.4	8-8.7
2000	220	200-380	8	3.1-11	13	10-15	8.6	7.6-8.8

* All data are estimated from charts. Zero values were not included. Some points were omitted when it appeared that they were unreasonable.

4.4 Loop and Additive Chemistry

The chemistry of the A and B loops of the CCW system as well as the chemistry of the molybdate additive were measured at the AECL laboratories and reported in their final report. Their results are shown as Table 4.5 here.[9] There were no chemicals other than sodium molybdate that were significant in the analysis of the water. A small amount of copper was evident in the environment, which is probably related to the copper alloys in the heat exchangers. Similarly, there were no special species apparent in the molybdate additive

Table 4.5

Results of Molybdate and Water Sample Chemical Analysis.*

Customer ID	Units for water	CCW-A		CCW-B		Units for MoO_4	Molybdate-lot#43076F		Molybdate-lot#43120CA	
AECL QA #		30461		30462			30463		30464	
Rep #		1	2	1	2		1	2	1	2
pH		8.6		9.1						
Conductivity	mS	1.02		1.00						
Total Carbon	μg/L	28.7±1.4	27.0±1.4	26.3±1.3	26.0±1.3	μg/g				
Total Inorganic Carbon	μg/L	11.9±0.6	11.6±0.6	10.8±0.5	10.8±0.5	μg/g				
Total Organic Carbon	μg/L	16.8±1.6	15.5±1.5	15.5±1.4	15.1±1.4	μg/g				
Ion Chromatography Results										
sulphate	μg/mL	<0.2	<0.2	<0.2	<0.2	μg/g	<50	<50	<50	<50
chloride	μg/mL	<0.2	<0.2	<0.2	<0.2	μg/g	<50	<50	<50	<50
fluoride	μg/mL	<0.2	<0.2	<0.2	<0.2	μg/g	<50	<50	<50	<50
phosphate	μg/mL	<0.2	<0.2	<0.2	<0.2	μg/g	<50	<50	<50	<50
nitrate	μg/mL	<0.2	<0.2	<0.2	<0.2	μg/g	<50	<50	<50	<50
bromide	μg/mL	<0.2	<0.2	<0.2	<0.2	μg/g	<50	<50	<50	<50
Inductively Coupled Plasma Atomic Emission Spectroscopy Results										
Mo	μg/mL	430±40	440±50	420±50	440±60	wt %	41±4	41±4	40±4	40±4
Na	μg/mL	230±20	230±20	220±20	230±30	wt %	19.4±1.9	19.4±1.9	19.0±1.9	19.0±1.9

Table 4.5 (continued)

Customer ID	Units for water	CCW-A		CCW-B		Units for MoO_4	Molybdate-lot#43076F		Molybdate-lot#43120CA	
Ca	µg/mL	0.11±0.01	0.10±0.02	0.11±0.01	0.11±0.02	µg/g	100±17	86±12	84±11	89±15
Fe	µg/mL	<0.02	<0.02	<0.02	<0.02	µg/g	<24	<30	<28	<26
K	µg/mL	<0.2	<0.2	<0.2	<0.2	µg/g	<160	<220	<190	<170
Li	µg/mL	<0.01	<0.01	<0.01	<0.01	µg/g	<8	<11	<9	<9
Quantitative Inductively Coupled Plasma Mass Spectrometry Results										
Cr	ng/mL	<0.12	<0.12	<0.12	<0.12	µg/g	<0.1	0.2±0.1	<0.12	<0.11
Cu	ng/mL	2.3±0.2	2.6±0.3	3.4±0.4	3.4±0.4	µg/g	0.73±0.09	0.42±0.08	<0.05	<0.05
As	ng/mL	<0.7	<0.7	<0.7	<0.7	µg/g	<0.5	0.8±0.7	<0.6	<0.6
Se	ng/mL	<0.8	<0.8	<0.8	<0.8	µg/g	<0.5	<0.7	0.7±0.6	<0.6
In	ng/mL	0.47±0.07	0.51±0.08	0.54±0.08	0.60±0.08	µg/g	0.67±0.07	0.60±0.06	0.64±0.06	0.66±0.07
Semi-quantitative Inductively Coupled Plasma Mass Spectrometry Results										
Ag	ng/mL	0.05±0.02	<0.018	<0.018	<0.018	µg/g	0.02±0.01	<0.02	<0.017	0.02±0.02
Al	ng/mL	0.4±0.3	0.4±0.3	1±0.4	1±0.4	µg/g	6±2	5±2	1±0.5	1±0.6
Au	ng/mL	0.2±0.05	0.1±0.04	0.1±0.04	<0.04	µg/g	<0.03	0.1±0.04	0.04±0.03	<0.03
B	ng/mL	3±1	3±1	4±2	5±2	µg/g	2±0.9	2±1	2±1	2±0.9
Ba	ng/mL	<1	<1	<1	<1	µg/g	<1	<1	<1	<1
Be	ng/mL	<0.2	<0.2	<0.2	<0.2	µg/g	<0.17	<0.2	<0.2	<0.19
Ce	ng/mL	0.6±0.09	0.6±0.1	0.7±0.1	0.8±0.1	µg/g	0.8±0.1	0.7±0.1	0.7±0.1	0.7±0.1
Co	ng/mL	0.02±0.02	0.02±0.02	0.02±0.02	0.03±0.02	µg/g	0.01±0.02	0.03±0.02	0.04±0.02	0.02±0.02
Cs	ng/mL	0.08±0.02	0.07±0.02	0.1±0.02	0.11±0.02	µg/g	0.13±0.03	0.11±0.02	0.05±0.01	0.04±0.01
Dy	ng/mL	<0.03	<0.03	<0.03	<0.03	µg/g	<0.02	<0.03	<0.03	<0.02
Er	ng/mL	<0.02	<0.02	<0.02	<0.02	µg/g	<0.018	<0.02	<0.02	<0.019
Eu	ng/mL	<0.014	<0.014	<0.014	<0.014	µg/g	<0.011	<0.015	<0.013	<0.012
Ga	ng/mL	0.07±0.03	0.07±0.03	0.03±0.03	0.03±0.03	µg/g	0.04±0.02	0.03±0.03	0.03±0.03	0.03±0.03
Gd	ng/mL	<0.04	<0.04	<0.04	<0.04	µg/g	<0.03	<0.04	<0.04	<0.03
Ge	ng/mL	<0.08	<0.08	<0.08	<0.08	µg/g	<0.06	<0.08	0.1±0.07	<0.06

Table 4.5 (continued)

Customer ID	Units for water	CCW-A		CCW-B		Units for MoO_4	Molybdate-lot#43076F		Molybdate-lot#43120CA	
Hf	ng/mL	0.3±0.05	0.06±0.03	0.04±0.03	<0.03	μg/g	0.05±0.03	<0.03	<0.03	<0.03
Ir	ng/mL	<0.5	<0.5	<0.3	<0.3	μg/g	<0.014	<0.019	<0.016	<0.015
La	ng/mL	<0.008	<0.008	<0.008	<0.008	μg/g	<0.006	<0.008	<0.007	0.01±0.007
Lu	ng/mL	<0.008	<0.008	<0.008	<0.008	μg/g	<0.006	<0.009	<0.007	<0.007
Mg	ng/mL	0.6±0.3	0.5±0.2	0.6±0.3	0.6±0.2	μg/g	2±1	2±0.8	0.4±0.2	0.4±0.2
Mn	ng/mL	0.3±0.1	0.3±0.1	0.2±0.08	0.3±0.1	μg/g	0.1±0.06	0.1±0.06	0.1±0.07	0.1±0.05
Ni	ng/mL	<0.14	<0.14	<0.14	<0.14	μg/g	<0.11	<0.15	<0.13	<0.12
Pb	ng/mL	0.03±0.01	<0.012	<0.012	<0.012	μg/g	0.03±0.01	<0.013	0.02±0.01	<0.01
Pd	ng/mL	0.3±0.06	0.1±0.04	0.1±0.04	0.1±0.04	μg/g	0.05±0.03	0.1±0.04	0.06±0.04	<0.03
Pr	ng/mL	<1	<1	<1	<1	μg/g	<1	<1	<1	<1
Pt	ng/mL	<0.04	<0.04	<0.04	<0.04	μg/g	0.04±0.03	<0.04	<0.04	<0.04
Rb	ng/mL	1.1±0.2	1.1±0.2	1.1±0.2	1.1±0.3	μg/g	1.1±0.2	1.1±0.3	0.3±0.07	0.3±0.07
Re	ng/mL	9±1	9±2	9±2	8±1	μg/g	13±2	14±2	0.2±0.04	0.13±0.03
Rh	ng/mL	0.12±0.02	0.01±0.009	0.01±0.009	0.01±0.009	μg/g	<0.007	0.02±0.01	<0.008	<0.007
Ru	ng/mL	<0.03	<0.03	<0.03	<0.03	μg/g	<0.02	<0.03	<0.02	<0.02
Sb	ng/mL	0.2±0.04	0.09±0.03	0.1±0.04	0.2±0.04	mg/g	0.5±0.09	0.5±0.09	0.08±0.03	0.04±0.03
Sc	ng/mL	1±0.4	1±0.4	1±0.5	2±0.6	mg/g	1±0.5	1±0.6	1±0.4	1±0.4
Sn	ng/mL	0.3±0.07	0.4±0.07	0.4±0.07	0.3±0.07	mg/g	0.3±0.06	0.4±0.09	0.4±0.08	0.4±0.09
Sr	ng/mL	0.07±0.02	0.06±0.02	0.05±0.01	0.06±0.02	mg/g	0.13±0.03	0.06±0.02	0.02±0.01	0.02±0.009
Ta	ng/mL	0.09±0.02	0.04±0.01	0.02±0.01	<0.011	mg/g	<0.009	<0.012	<0.01	<0.009
Te	ng/mL	<4	<4	<4	<4	mg/g	<5	<5	<5	<5
Th	ng/mL	<0.014	<0.014	<0.014	<0.014	mg/g	<0.011	<0.016	<0.013	<0.012
Ti	ng/mL	4±1	4±1	7±2	7±2	mg/g	8±3	7±3	8±3	8±3
Tl	ng/mL	<0.016	<0.016	<0.016	<0.016	mg/g	0.15±0.03	0.12±0.03	0.11±0.02	0.12±0.02
Tm	ng/mL	<0.008	<0.008	<0.008	<0.008	mg/g	<0.006	<0.008	<0.007	<0.007
U	ng/mL	<0.016	<0.016	<0.016	<0.016	mg/g	0.2±0.04	0.3±0.05	0.05±0.02	0.08±0.02
V	ng/mL	0.5±0.2	0.6±0.2	0.6±0.2	0.7±0.2	mg/g	0.3±0.1	0.2±0.1	0.3±0.1	0.2±0.08
W	ng/mL	34±6	34±6	34±6	33±6	mg/g	70±10	75±10	79±10	77±10

Table 4.5 (continued)

Customer ID	Units for water	CCW-A		CCW-B		Units for MoO_4	Molybdate-lot#43076F		Molybdate-lot#43120CA	
Y	ng/mL	0.02±0.01	<0.01	0.01±0.01	0.02±0.01	mg/g	0.02±0.009	<0.011	<0.01	0.02±0.009
Yb	ng/mL	<0.03	<0.03	<0.03	<0.03	mg/g	<0.03	<0.03	<0.03	<0.03
Zn	ng/mL	<0.2	<0.2	<0.2	<0.2	mg/g	<0.17	<0.2	0.4±0.2	0.3±0.2
Zr	ng/mL	0.07±0.03	<0.02	<0.02	<0.02	mg/g	0.5±0.09	0.4±0.08	0.2±0.04	1±0.2

*Taken directly from AECL report.[9]

Data similar to that in Table 4.5 were taken in the Altran work[21] for the water in CCW System B and are shown in Tables 4.6 and 4.7. These data are not materially different from those in Table 4.4 and show generally good agreement considering that they were taken at different times, different places, and were analyzed in different laboratories. Only the iron concentration in Table 4.6 seems erroneous. Such a concentration of iron is not possible from a solubility point of view. The specimens must have contained some colloidal or particulate iron.

Table 4.6

Summary of Chemical Analyses of Metals in Water Sample CCW System "B" Level Transmitter Line 1700 4/4/97.[21]

Metal Analyzed	Concentration, mg/liter
Al	3.67
Sb	<0.76
As	0.03
Ba	<0.01
Be	<0.01
Cd	<0.01
Ca	1.90
Cr	0.07
Co	0.19
Cu	0.20
Fe	198
Pb	<0.38
Mg	0.17
Mn	3.02
Mo	231
Ni	1.23
K	0.28
Se	<0.76
Ag	<0.002
Na	55.2
Th	<0.02
Sn	0.058
V	<0.01
Zn	1.75

Table 4.7

Summary of Chemical Analyses from Water Sample from BTRS Chiller, Data Taken December 20, 2000.[20]

Species and Method	Filtered, ppm	Total, ppm
ICP-Inductively Coupled Plasma		
Aluminum (Al)	0.2	0.2
Barium (Ba)	<0.1	<0.1
Boron (B)	<0.1	<0.1
Cadmium (Cd)	<0.01	<0.01
Calcium ($CaCO_3$)	0.8	0.9
Calculated Hardness ($CaCO_3$)	0.80	0.90
Chromium (Cr)	<0.01	<0.01
Copper (Cu)	0.15	0.46
Iron (Fe)	0.48	7.0
Lead (Pb)	<0.1	<0.1
Lithium (Li)	<0.01	<0.01
Magnesium ($CaCO_3$)	<0.4	0.4
Manganese (Mn)	0.02	0.02
Molybdenum (Mo)	140	150
Nickel (Ni)	<0.1	<0.1
Phosphorus (P)	1.6	1.7
Potassium (K)	<0.2	0.7
Silica (SiO_2)	<0.2	0.7
Sodium ($CaCO_3$)	310	340
Strontium (Sr)	<0.01	<0.01
Vanadium (V)	0.13	0.15
Zinc (Zn)	<0.01	0.04
IC-Anions by IC		
Bromide (Br)		<0.3
Nitrite (NO_2)		<3.0
Chloride ($CaCO_3$)		<4.2
Nitrate ($CaCO_3$)		9.4
Sulfate ($CaCO_3$)		<7.8
ALK-Alkalinity		
Bicarbonate ($CaCO_3$)		210
Carbonate ($CaCO_3$)		29
Methyl Orange ($CaCO_3$)		240
Phenolphthalein ($CaCO_3$)		14
Others		
pH (pH units)		9.1
Conductivity, mmhos/cm		620

Chemical analyses were also performed by Altran on sludge from the "A" and "B" trains.[21] These specimens had been supplied by WCNOC to Altran and were taken on 4/1/97 and 4/4/97, respectively. Tables 4.8 and 4.9 summarize data obtained for constituents from sludge in the A and B train transmitter lines.[21] Table 4.8 describes the structures of the constituents and Table 4.9 describes the chemistry. Probably the most important observation is the high concentration of sulfur. Altran suggests that this may have resulted from sulfate reducing bacteria (SRB). However, Tables 4.5 and 4.7 show no such significant nutrient of dissolved sulfur. Thus, there is no explanation for the presence of the high sulfur. Also, neither the microbial analyses from Altran nor our present report show any indications of SRB as discussed in Section 4.5. It seems unlikely that this sulfur was significant in the SCC. Little[17] in her work did not find SRB.

Table 4.8

Constituents of Sludge Taken in the A and B Transmitter lines on 4/1/97 and 4/4/97.[21]

Constituent	Formula	Concentration, %	
		Train A, 4/1/97	Train B, 4/4/97
Quartz	SiO_2	10	Trace
Calcite	$CaCO_3$	6	
Siderite	$FeCO_3$	3	
Iron	Alpha-Fe	17	
Magnetite	Alpha-Fe_3O_4	12	10
Hematite	Alpha-Fe_2O_3	13	2
Goethite	Alpha-FeOOH	6	31
Akaganeite	Beta-FeOOH	14	
Lepidocrocite	Gamma FeOOH		12
Iron Oxide Hydroxide	FeOOH		25
Iron Sulfide	FeS	18	
Sphalerite	ZnS	1	
Isemanite	$Mo_3O_8 \cdot xH_2O$		20

4.5 Microbial and Fungal

A detailed study of the microbial and fungal species was conducted by Dr. Brenda Little. Her report is included as Appendix 1.0. D. Womelsdorf (WCNOC) and I accompanied her during her selection of samples on 02-07-02. These samples were selected from locations that would have the greatest likelihood of having high concentrations of microbes and fungi. Such locations were at the bottoms of storage vessels and in dead legs. These locations are identified in Appendix 1.0.

Table 4.9

Elemental Analysis by EDS of Chemical Species from Sludge from A and B Transmitter lines Taken on 4/1/97 and 4/4/97.[21]

Element	Concentration, %	
	Train A, 4/1/97	Train B, 4/4/97
Al	0.29	0.88
Si	10.98	
S	16.11	35.44
K	0.69	
Ca	5.8	
P		1.68
Ti	0.32	
Fe	64.91	62.00
Zn	0.92	

Immediately after taking the specimens, they were taken to Dr. Little's laboratory and cultured. The results of culturing are shown in Table 2.0 of Appendix 1.0.

Dr. Little concluded that there were no microbes nor fungi, as well as there being no SRB, present that would produce aggressive species from their metabolism that could accelerate corrosion. The main reason for this result is the absence of nutrients in the system.

The work of Altran,[3,5,6] as well, showed no evidence of microbial species that would contribute to accelerated corrosion. No SRB were noted.

5.0 Chronology and Characteristics of SCC at Wolf Creek

5.1 Locations Analyzed

Specimens exhibiting SCC have been taken from the CCW system piping as follows:

1. In 1994 specimens were taken from the CCW system, and results are summarized in the DEI report.[1] No photomicrographs nor descriptions are available.

2. In 2000 specimens were taken from the CCW system and analyzed by Altran. There is no information available on the circumferential extent nor is there information on most of the depths of penetrations at the welds. Also there is no survey of the IGC at locations other than at the sites of initiation of SCC.

3. In 2002 specimens were taken in connection with the present study and analyzed by AECL.[9] Significant features are shown in this section.

4. In 2002 specimens were taken in connection with the study by NRC[8] and metallographic findings are given in their report.

The disposition and character of the SCC of these specimens is given in Table 5.1. The locations of these species in the CCW system are shown in Figures 3.1 – 3.4.

5.2 Principal Features of SCC

The principal features of the IGC-SCC are described in the Altran,[2,3,4,5,6] AECL[9] and NRC[8] reports are as follows:

1. The SCC initiates at the inside surface of the pipe adjacent to the water.

2. The SCC is associated only with welds and the associated stress.

3. SCC proceeds either circumferentially or longitudinally but in close proximity to the weld in the heat affected zone.

4. The morphology is intergranular.

5. The advancing SCC branches.

6. The initiation stage is sometimes IGC but changes to IGSCC. Some of the IGC does not change if it is shallow, and the SCC may not develop significantly. In the IGC region, pearlite is observed to be preferentially dissolved by NRC[8] and Altran.[3]

Table 5.1

Summary of Specimens Taken From WCNOC CCW System from 1994 through 2002.
(These specimens are ones that were mainly examined metallographically.
Other specimens were taken and pieces were removed that are not described here.)

Reference	Approx Date of SCC Occur	Location	Description of Location	Approx Temp	Crack Character
	(Plant started Sept 1985)				
	1994		6" discharge between Letdown Heat Exch and 14" return header	150°F	Through wall, circum.
Altran Aug 2000	May 2000 Altran April 2001	W-22	6" piping BGV021, carbon steel Sch. 40 buttweld end, SA 106Gr.B, seamless, Class 150, ASME III, Class 3	150°F	IGC at initiation; multiple branching. SCC is entirely IG.
Altran Aug 2000	Same as W-22	W-1A	90° elbow in 6" piping, carbon steel Sch. 40, butt weld, SA 106Gr.B, seamless, Class 150, ASME III Class 3	150°F	No cracking; some pits/porosity
Altran Aug 2000	Same as W-22	FR-516	1" pipe, construction weld C-M03-EG-02, FW=516, carbon steel, Sch. 80, ASME SA 106Gr.B seamless, Class 150, ASME III, Class 3	150°F	SCC entirely in weld; interdendritic; IGC at initiation; grain deformation at tip indicating overload final failure and transgranular ductile perforation
Altran Feb 2001and subsequent reports	Same as W-22	Weld #7	Pipe to elbow, 6", carbon steel Sch. 40, SA 106Gr.B, Class 150, ASME III, Class 3	150°F	All welds sent to Altran had been inspected by WCNOC with NDE(UT) and locations of possible SCC identified. At Altran the presence of SCC was verified by destructive analysis when the pipe samples were broken open

Table 5.1 (continued)

Reference	Approx Date of SCC Occur	Location	Description of Location	Approx Temp	Crack Character
Same as Weld #7	Same as W-22	Weld #8 (F021)	Elbow to pipe, 6", carbon steel Sch. 40, SA 106Gr.B, Class 150, ASME III, Class 3.	150°F	See Weld #7
Same as Weld #7	Same as W-22	Weld #9	Pipe to elbow, 6", carbon steel Sch. 40, SA 106Gr.B, Class 150, ASME III, Class 3.	150°F	See Weld #7
Same as Weld #7	Same as W-22	Weld #10	Elbow to pipe, 6", carbon steel Sch. 40, SA 106Gr.B, Class 150, ASME III, Class 3.	150°F	See Weld #7
Same as Weld #7	Same as W-22	Weld #11	Pipe to tee--run;, 6", carbon steel Sch. 40, SA 106Gr.B, Class 150, ASME III, Class 3.	150°F	See Weld #7
Same as Weld #7	Same as W-22	Weld #13	Tee to pipe--run, 6", carbon steel Sch. 40, SA 106Gr.B, Class 150, ASME III, Class 3.	150°F	See Weld #7
Same as Weld #7	Same as W-22	Weld #15A	Elbow to pipe, 6", carbon steel Sch. 40, SA 106Gr.B, Class 150, ASME III, Class 3.	150°F	See Weld #7
Same as Weld #7	Same as W-22	Weld #16	Pipe to elbow, 6", carbon steel Sch 40, A 106B, Class 150, ASME III, Class 3.	150°F	See Weld #7
Same as Weld #7	Same as W-22	Weld #19A	Pipe to tee--branch, 6", carbon steel Sch 40, SA106Gr.B, Class 150, ASME III, Class 3. This pipe was inserted in 1994.	150°F	See Weld #7. No obvious defective welds; porosity within the weld metal but not the source of cracking or defective performance.
Same as Weld #7	Same as W-22	Weld #57 (F019)	Pipe to elbow, 4", carbon steel Sch. 40, SA106Gr.B, Class 150, ASME III, Class 3. This was installed in the CCW system return from an RCP upper bearing cooler, suggesting more portions than the return	150°F	See Weld #7

Table 5.1 (continued)

Reference	Approx Date of SCC Occur	Location	Description of Location	Approx Temp	Crack Character
			line but less SCC.		
NRC December 5, 2002			SA106Gr.B Class 3. 3" Sch. 160. Loop A, A-14 weld, Drawing EID-0006	90°F	No SCC but IGC at entry point between weld and pipe and some dissolution of pearlite.
NRC December 5, 2002			SA106Gr.B Class 3. 3" Sch. 160. Loop A, A-15 weld, Drawing EID-0006	90°F	No SCC but IGC at entry point between weld and pipe and some dissolution of pearlite.
NRC December 5, 2002			SA106Gr.B Class 3. 4" Sch. 160. Loop C, CB-6 weld, Drawing EID-0007	90°F	No SCC but IGC at entry point between weld and pipe and some dissolution of pearlite.
NRC December 5, 2002			SA106Gr.B Class 3. 4" Sch. 160. Loop C, CB 7 weld, Drawing EID-0007	90°F	No SCC but IGC at entry point between weld and pipe and some dissolution of pearlite.
NRC December 5, 2002			SA106Gr.B Class 3. 4" Sch. 160. Loop D, D-37 weld, Drawing EID-0009	90°F	No SCC but IGC at entry point between weld and pipe and some dissolution of pearlite.
NRC December 5, 2002			SA106Gr.B Class 3. 3" Sch. 160. Loop D, D-38 weld, Drawing EID-0009	90°F	No SCC but IGC at entry point between weld and pipe and some dissolution of pearlite.
NRC December 5, 2002			SA106Gr.B Class 3. 3" Sch. 160. Loop D, D-39 weld, Drawing EID-0009	90°F	No SCC but IGC at entry point between weld and pipe and some dissolution of pearlite.
AECL Report, Sept 2002			Welds A7, A6 from one pipe spool. SA106Gr.B Class 3. 3" Sch. 160. From RCP A thermal barrier return line	90°F	Limited evaluation; no SCC; some IGC
AECL Report, Sept 2002			Welds A16, A17, A17A from separate pipe spool from RCP A thermal barrier return line. SA106Gr.B Class 3. 3" Sch. 160.	90°F	Limited evaluation; no SCC; some IGC

Table 5.1 (continued)

Reference	Approx Date of SCC Occur	Location	Description of Location	Approx Temp	Crack Character
AECL Report, Sept 2002			Welds D6, D7 from single pipe length from RCP D thermal barrier return line. SA106Gr.B Class 3. 3" Sch. 160.	90°F	No significant circumferential SCC but IGC at initiation sites with some IGSCC as deep as 0.4 mm; significant longitudinal SCC up to 1.2 mm deep in weld, HAZ, matrix.
AECL Report, Sept 2002			Letdown heat exchanger from 8" nozzle to the letdown heat exchanger (8" to 6" reducer).	150°F	Longitudinal SCC. One fully penetrated. Three main cracks characterized and they are longitudinal. These all close. Crack #1 was through; #2 was not and used for EDS. Extensive Mo along the crack.

7. The SCC may be either circumferential or longitudinal. This seems to depend on the residual stresses. However, the mechanism of the SCC is the same and there is no evidence to the contrary.

8. The SCC may proceed through the weld, HAZ, and matrix indicating that it is independent of the metallurgy. This is observed especially if the cracks are longitudinal.

9. The rate of SCC depends on temperature.

10. The first SCC required about nine years to penetrate the 0.280" of a 6" pipe.

11. One pipe, weld 19A, that was replaced in 1994 sustained SCC by 2000.[3] The depth of this SCC was not determined but was not through wall.

12. The SCC has been observed with Mo at the crack tip and along the SCC; no other chemicals are significant along the SCC; for example, chloride is not observed and extensive Mo is also observed in the IGC region.

5.3 Metallography

In order to characterize the SCC as a part of the present work, specimens of piping were examined metallographically at AECL from two different locations in the CCW system.[9] One set of photomicrographs was taken from the saddle weld joint at a transition from 8" to 6" diameters from the exit of the letdown heat exchanger. Here, the longitudinal nature of the cracks could be observed from visual examination. A second set of photomicrographs was taken from welds D6 and D7. Here, the initial NDE (UT) had indicated that there was a large circumferential SCC about 360° and in some places about 90% through the wall. During a meeting among AECL, WCNOC, and me, it was determined that the circumferential SCC penetration was negligible and that the main SCC was longitudinal much like that in the saddle weld joint. It was determined that the large NDE (UT) indications arose from the inner weld joint and not from SCC.

Photomicrographs from the saddle weld joint are shown in Figures 5.1 through 5.5; photomicrographs from the welds in D6 and D7 are shown in Figures 5.6 through 5.13.

Figure 5.1 shows three cracks that are part through-wall and are numbered #1, #2, and #3 for convenience. The largest is #1. These cracks are growing from the inside surface and are away from the saddle weld. Figure 5.2 shows the #2 crack in detail, and Figure 5.3 shows the tip of crack #2 in more detail. Here, the details of branching and intergranular features are evident.

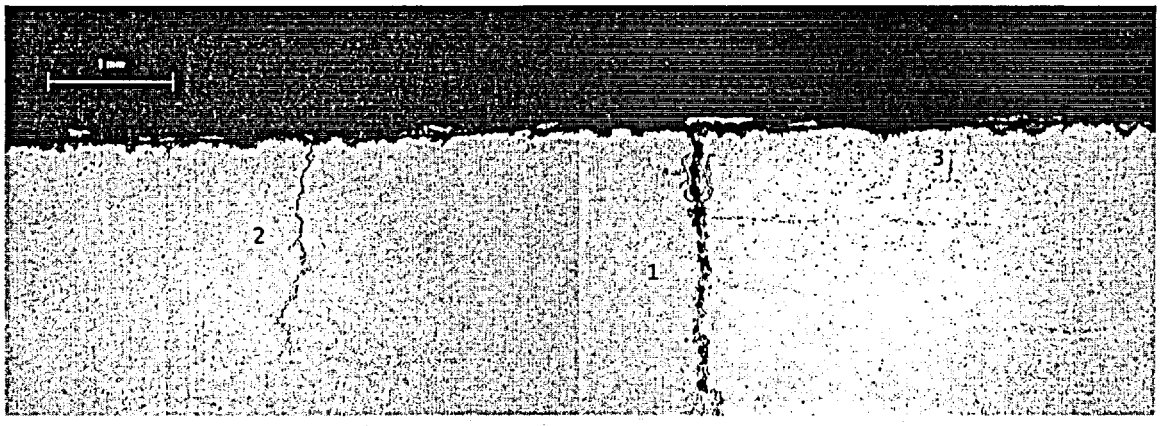

Figure 5.1 Photomicrograph of cross section of saddle weld showing three cracks labeled #1, #2, and #3 starting from the inside surface and moving away from the weld. From Figure 3 on page 4-7 of the AECL report.[9]

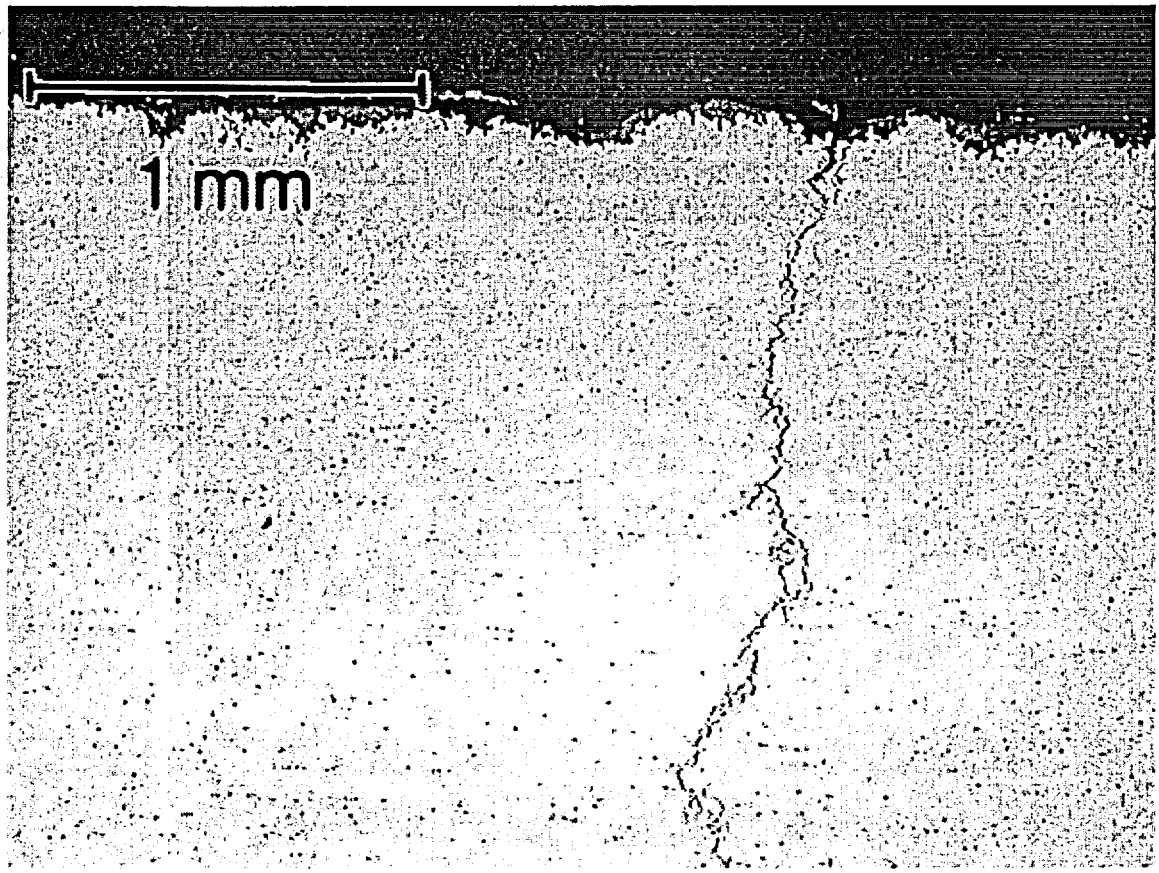

Figure 5.2 Photomicrograph of cross section of saddle weld showing cracking #2 starting from the inside surface. From Figure 4 on page 4-7 of the AECL report.[9]

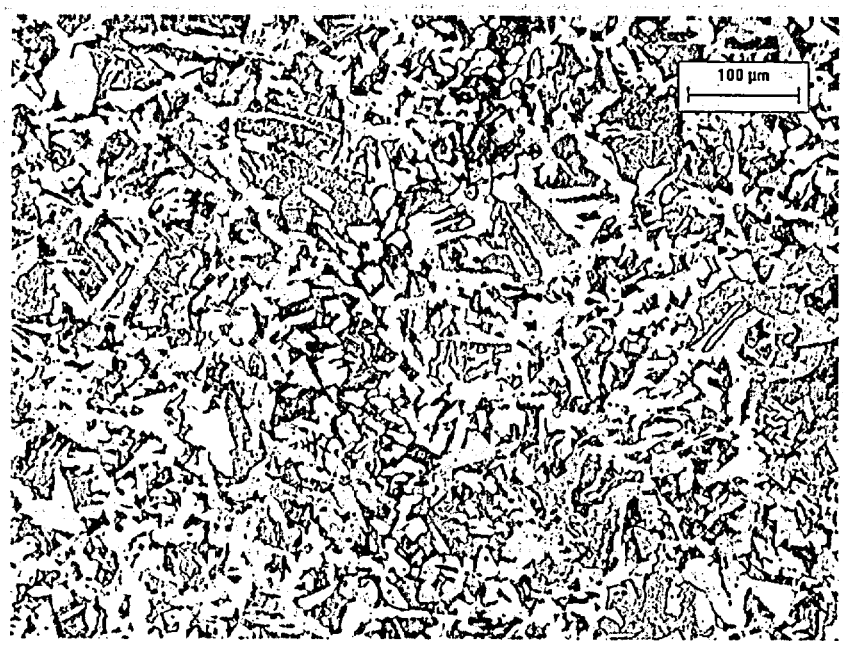

Figure 5.3 Photomicrograph of cross section of the tip of crack #2 from Figures 5.1 and 5.2. From Figure 7 on page 4-9 of the AECL report.[9]

The surface is extensively reacted as shown in Figure 5.4. This photomicrograph is near crack #3. Here, it is clear that the surface is reactive and that this reactivity has moved first along the boundaries of grains. A detailed view of Figure 5.2 is shown in Figure 5.3.

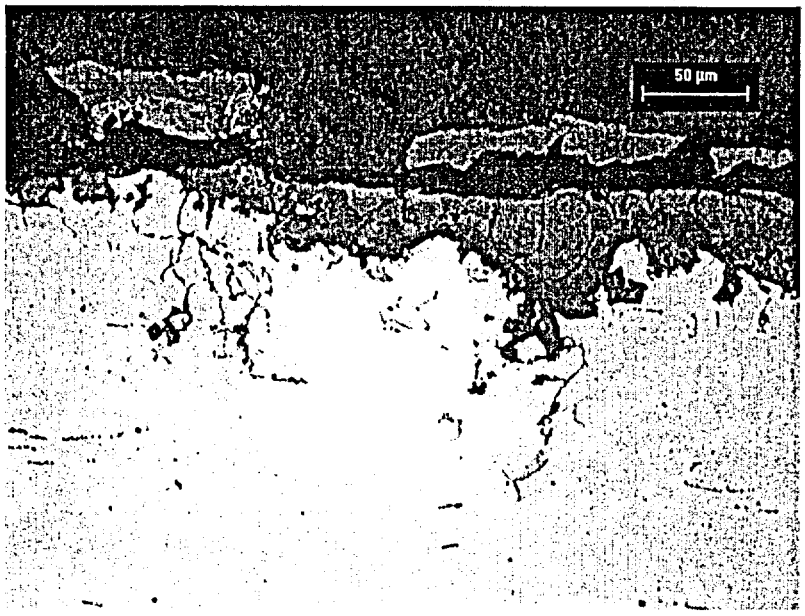

Figure 5.4 Photomicrograph of the surface edge on the inside surface near crack #3 showing extensive reactivity at the surface following the direction of the SCC. From Figure 8 on page 4-9 of the AECL report.[9]

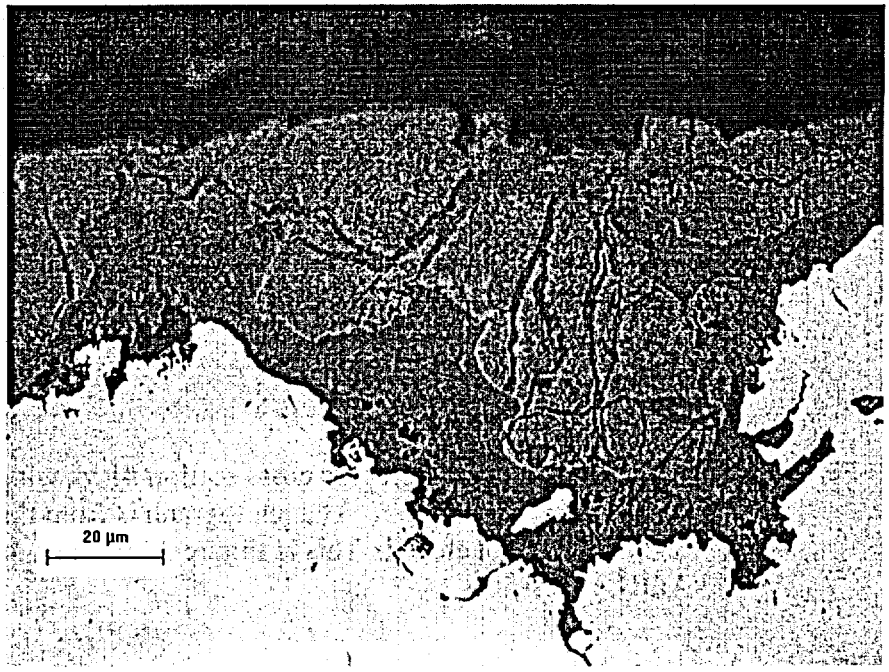

Figure 5.5 Photomicrograph of the surface edge showing a detail of Figure 5.4 where there is extensive reactivity at the surface following the direction of the SCC. From Figure 9 on page 4-10 of the AECL report.[9]

In examining D6 and D7 welds, it was first assumed, based on preliminary NDE (UT) work, that the SCC was intermittently 360° around and up to 90% intermittently through wall. This finding indicated that the SCC was extensively circumferential. Thus, the first metallographic work was organized to evaluate circumferential SCC. However, the first metallographic investigations found the maximum circumferential IGC-SCC was about 0.4 mm (0.016") although with extensive IGC; and it seemed that there must have been some error in either the NDE (UT) or the metallography. Ultimately, it was found that the NDE (UT) was erroneous and apparently had detected an ID surface geometry and not SCC. The metallography had found relatively shallow IGC and small amounts of SCC in the circumferential direction as shown in Figures 5.6 and 5.7.

Figures 5.6 and 5.7 are typical of all the SCC that proceeds circumferentially. These same features were observed in the Altran[2,3,4,5,6] and NRC[8] reports.

In addition to the SCC that is observed to proceed circumferentially as shown in Figures 5.6 and 5.7, IGSCC in the CCW system piping proceeds also longitudinally in the D6 and D7 specimens as shown also in the 6" piping in Figures 5.1 through 5.5. Figure 5.8 shows a cross section that was prepared to show longitudinal IGSCC. This was taken from weld D7. Figure 5.9 shows the detail of the surface of Figure 5.[8] Again, the preliminary IGC is evident regardless of whether the cross section is longitudinal or circumferential.

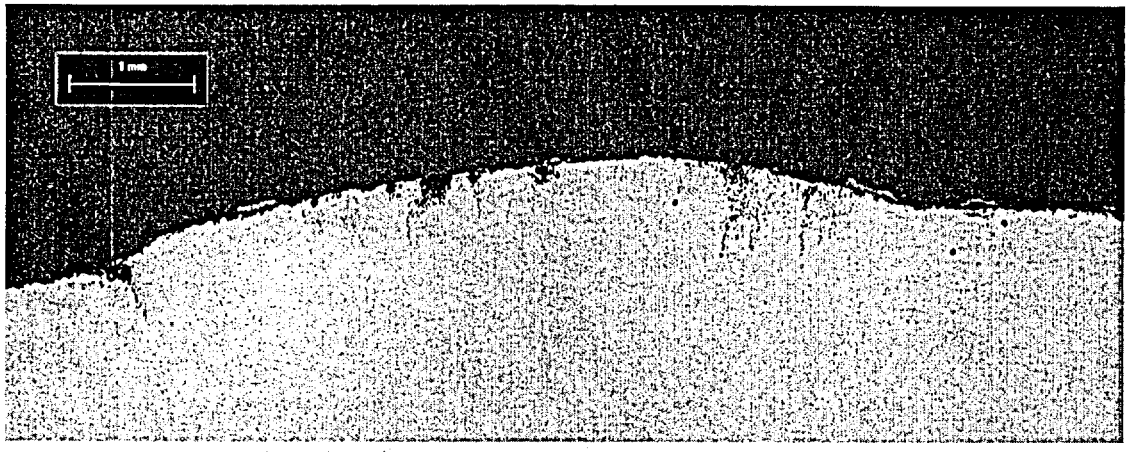

Figure 5.6 Weld D6 and metallographic cross section #1 viewing the circumferential direction. The photograph is from the weld root region and is not etched. This is Figure 38 from page 4-33 of the AECL report.[9]

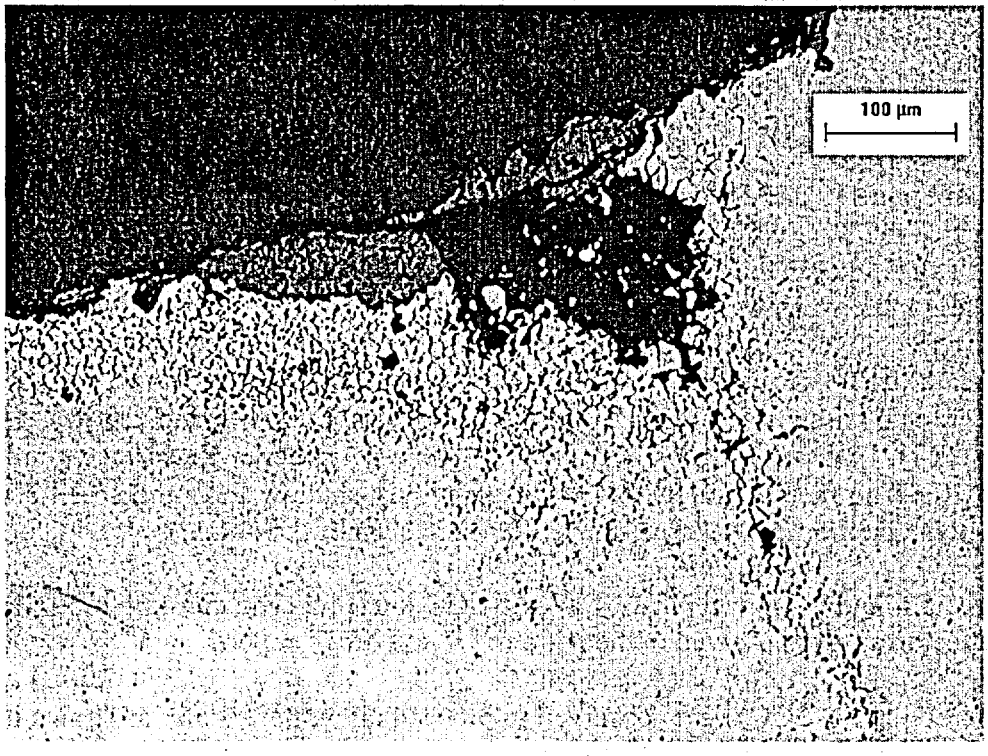

Figure 5.7 Weld D6 and metallographic cross section #1 viewing the circumferential direction. This view is a higher magnification of the penetration at the left of Figure 5.6. This photomicrograph is from the left side of Figure 5.6. This is Figure 39 from page 4-34 of the AECL report.[9]

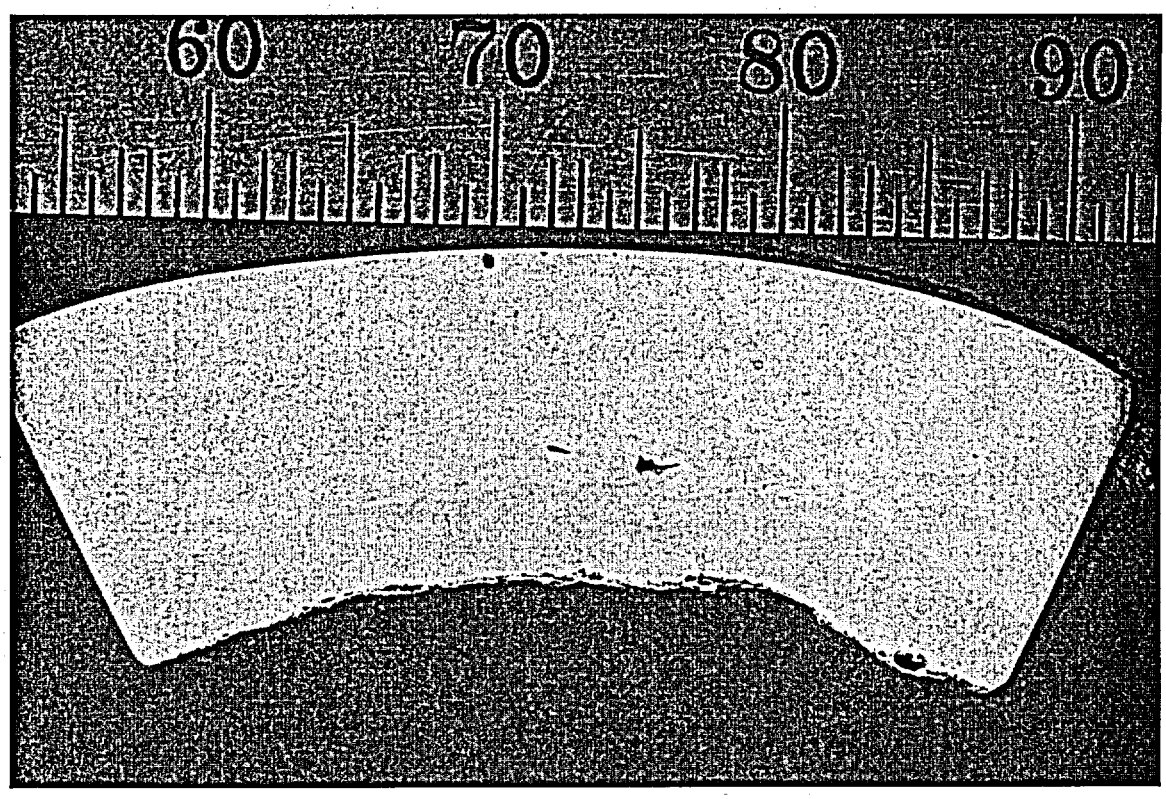

Figure 5.8 Weld D7 from the center of the weld taken in the circumferential section and includes about 60° of arc. This is intended to show features proceeding in the longitudinal direction that are perpendicular to the circumferential plane. This is Figure 78 from page 4-57 of the AECL report.[9]

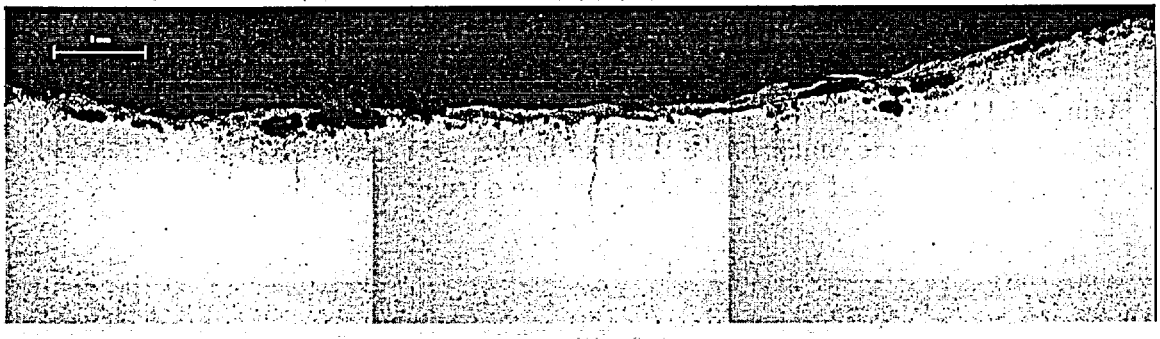

Figure 5.9 Weld D7 from the same mount as Figure 5.8 showing the inside surface of the circumferential plane. This is intended to show features proceeding in the longitudinal direction. This is Figure 79 from page 4-57 of the AECL report.[9]

The transition from IGC to IGSCC proceeding in the longitudinal direction is shown in Figure 5.10. This is taken from approximately the center of Figure 5.9 and extends approximately 1.2 mm into the metal. Once the IGSCC has developed, the IGC is no

longer present, and the IGSCC continues. This longitudinal SCC was much deeper than any penetration observed propagating circumferentially in the D7 weld, for example, as shown in Figures 5.6 and 5.7.

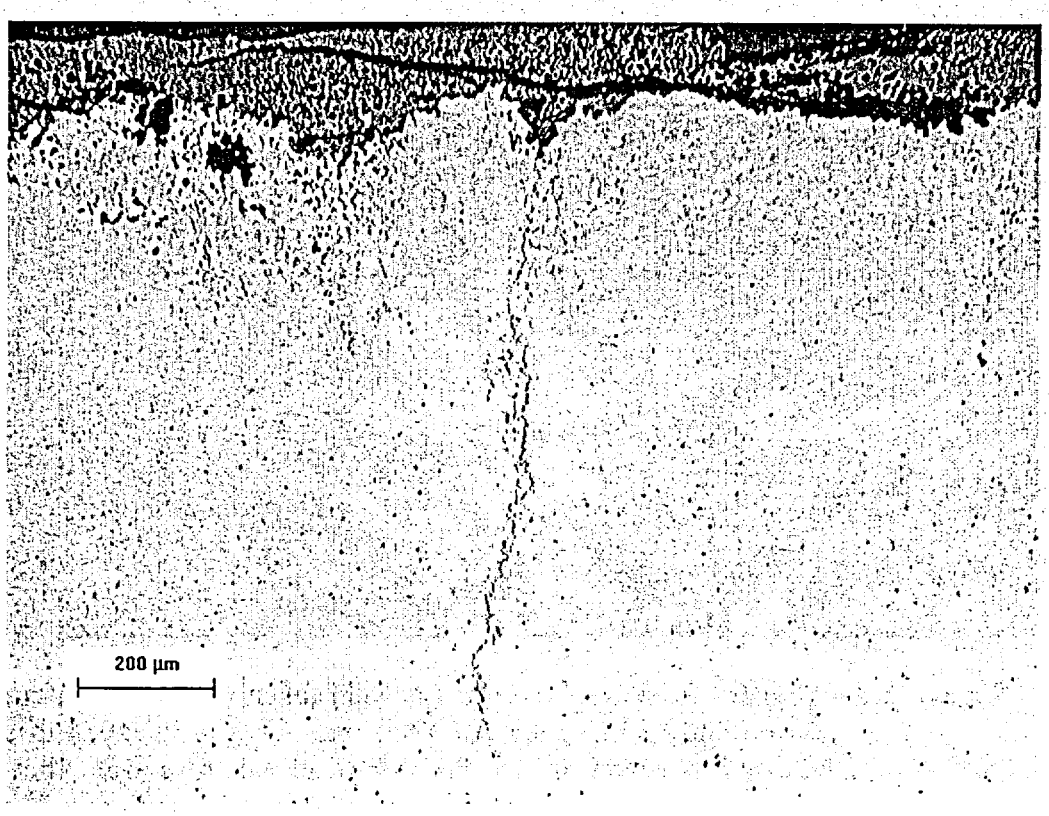

Figure 5.10 Weld D7 proceeding from the surface shown in Figure 5.9. This is taken from approximately the center of Figure 5.8 and shows the occurrence of an IGSCC proceeding longitudinally. This is Figure 80 from page 4-58 of the AECL report.[9]

Figures 5.11 and 5.12 show micrographs from successive grinding moving toward the fusion zone from the center of the weld as shown in Figures 5.8, 5.9, and 5.10. Figure 5.13 shows the detail of an SCC that proceeds in a longitudinal direction.

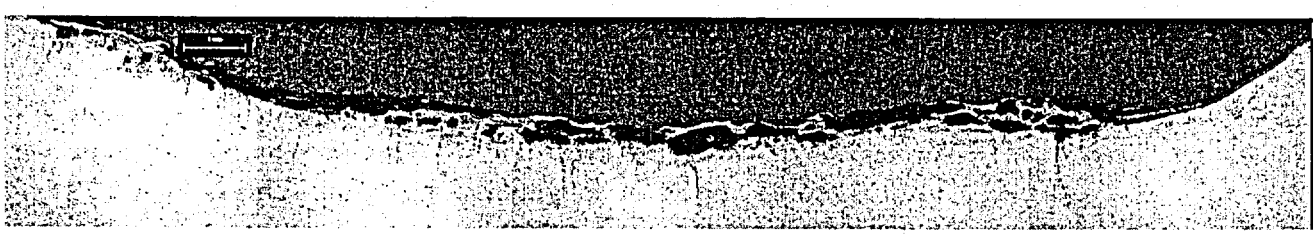

Figure 5.11 Weld D7 but 0.5 mm closer to the fusion boundary than in Figures 5.8-5.9. This is from Figure 82 on page 4-58 of the AECL report.[9]

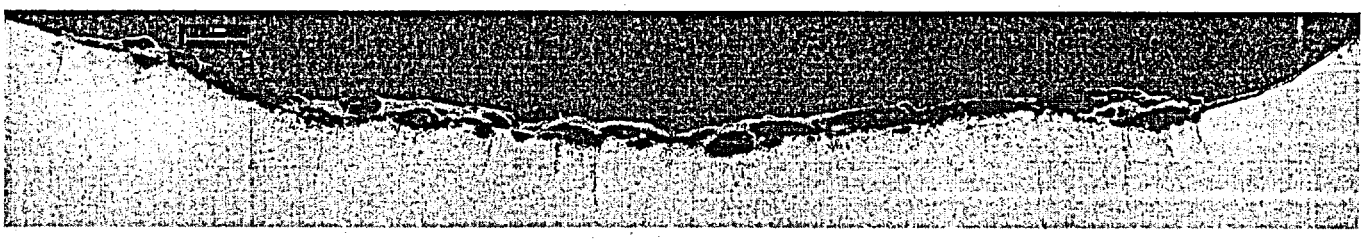

Figure 5.12 Weld D7 but 1.0 mm closer to the fusion boundary than in Figures 5.8-5.9. This is from Figure 83 on page 4-58 of the AECL report.[9]

There are two main features of the corrosion in the CCW system piping. One is the IGC that seems to be characteristic of the early stage of the penetration. The extent of this penetration is not great and seems to be no more than 100 to 200 μm. (0.006 to 0.008".) Figures 5.4, 5.5, 5.6 and 5.7 are typical of this early stage. The next stage is IGSCC and is shown clearly as different from IGC in Figures 5.1, 5.2, 5.3, 5.10, and 5.13. These patterns are shown also in the Altran reports.[3,5] This early IGC is also shown in the NRC report.[8]

5.4 Chemistry Inside SCC

Chemistry inside the advancing SCC as well as in the precursor near the surface region is described in Figure 5.14 from the AECL work. Here, the chemistry was investigated using EDS. Only molybdenum was observed in any significant amounts inside the SCC. Figure 5.14 summarizes only the readings for molybdenum as compared with iron. The main remaining species are oxygen. Therefore, the ratio of molybdenum to iron gives a good indication of the relative concentration of molybdenum.

The data in Figure 5.14 show that molybdenum is distributed more or less uniformly along the SCC. Being more quantitative is difficult since the EDS beam includes sides of the SCC and unknown depth data. Regardless, the semiquantitative data exhibit a clear indication of the distribution of molybdenum to the tip of the SCC.

Measurements of chemistry using EDS by Altran showed the following:

1. The fracture surface of W-22 was analyzed by EDS, and a significant amount of molybdenum was found. No other metallic nor contaminating elements were found.[2]

2. The fracture surfaces of welds 9 and 19A[3,5] were analysed and significant amounts of molybdenum were found. Small amounts of Al and Si were found. No other metallic nor contaminating elements were found. Altran does not give the semiquantitative data for species.

3. The inside surface of pipe #16 exhibited a significant amount of molybdenum and a slight amount of silicon compared with the expected high concentration of iron.

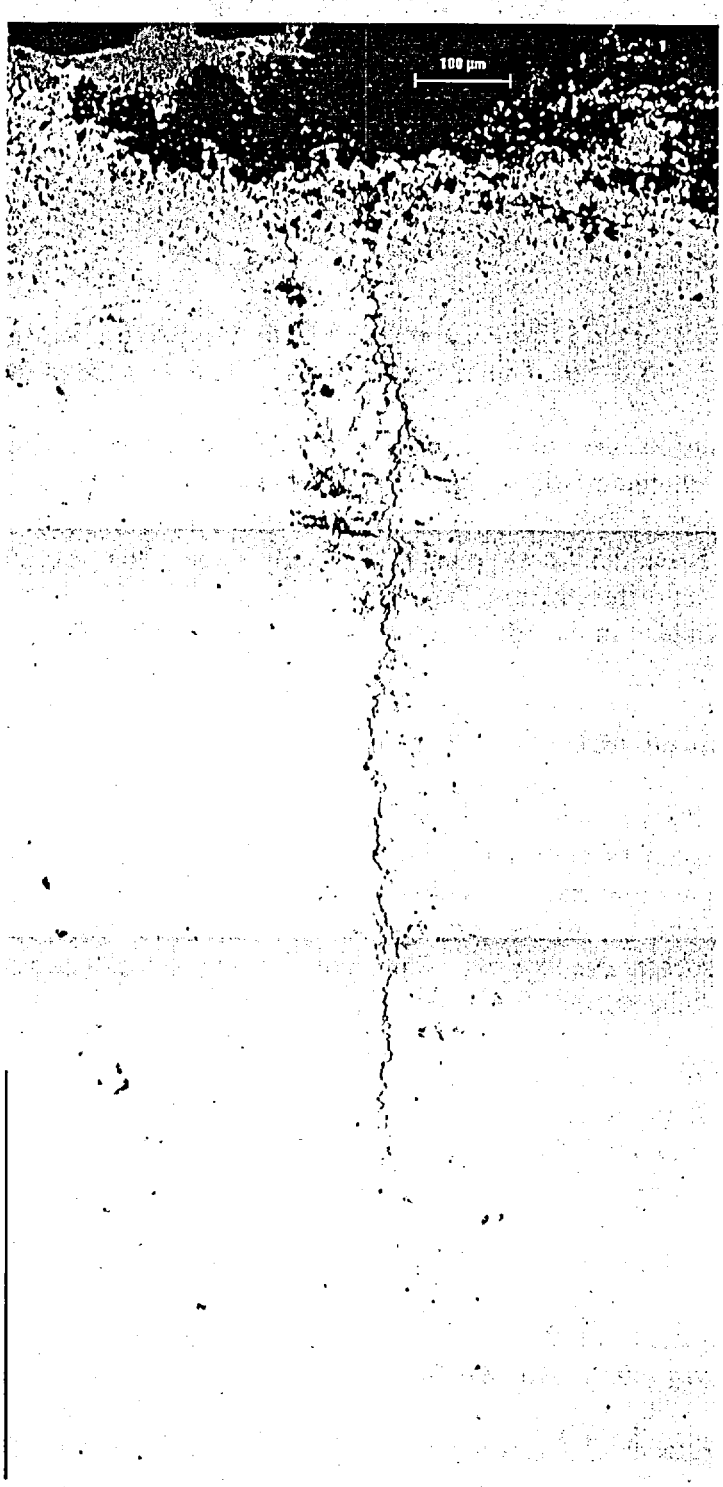

Figure 5.13 Weld D7 from about the middle of Figure 5.12. The depth of this SCC is about 1.2 mm. (0.047".) This is from Figure 84 on page 4-59 of the AECL report. [9]

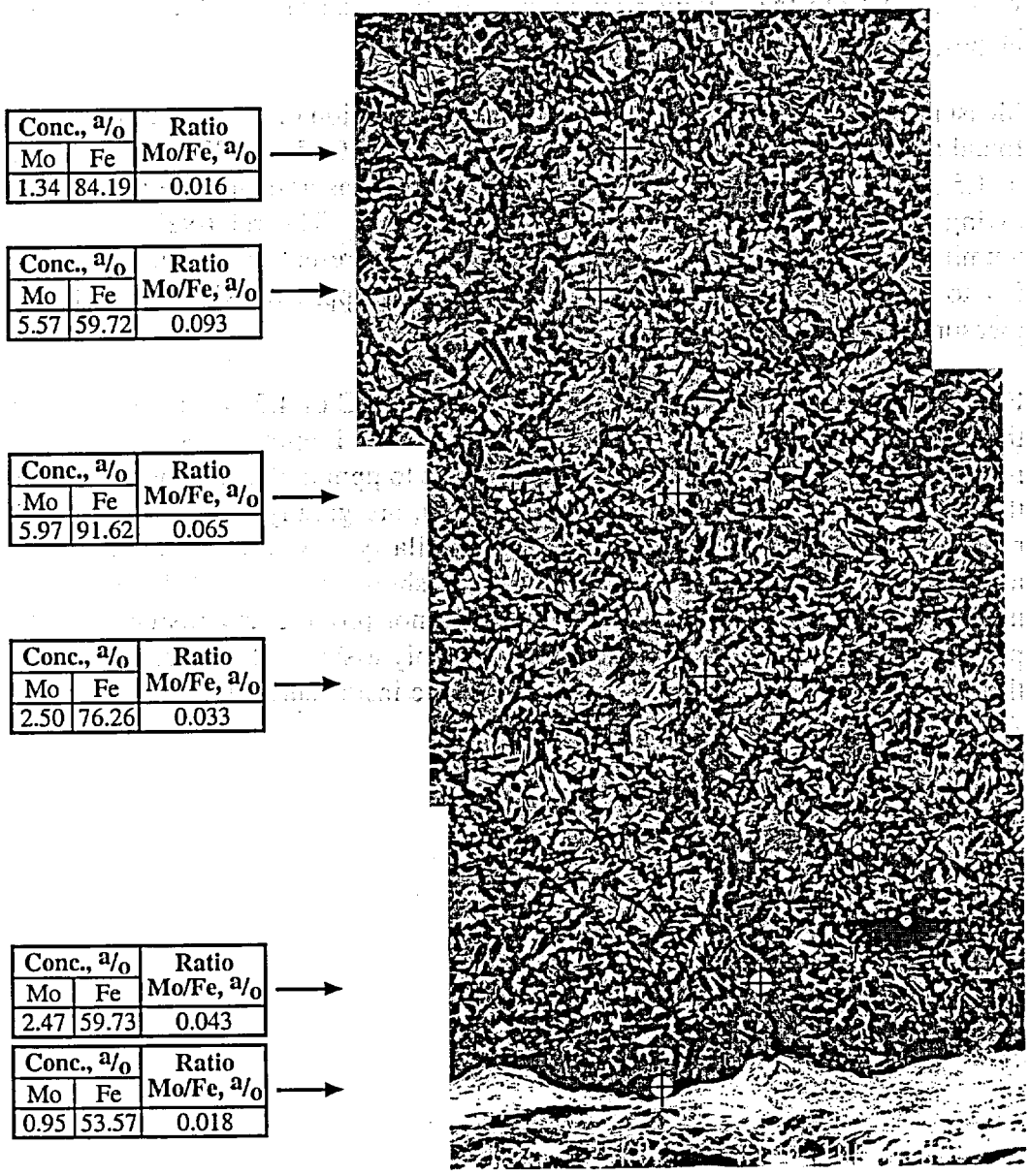

Figure 5.14 Crack #2, shown also in Figures 5.1, 5.2 and 5.3 (inserted here for convenience), with results for analyses by EDS of molybdenum and iron with ratio of molybdenum/iron based on atomic percentages. Based on a composite of 100x photomicrographs. From Figure 10 on page 4-11 of the AECL report for the morphology and Figures 11 to 18 for the EDS data.[9]

The Altran reports do not specify the locations of their measurements with respect to the crack tips, mid point and entrance. They also do not specify whether the measurements were taken from the metallographic edge or from the face of the SCC although their language suggests but does not confirm the latter.

Measurements from the NRC report[8] analyzed the region of the IGC at five locations and found ranges (weight percent, w/o) of: 3.6 to 4.7 Mo, 0.15 to 0.27 Al, 0.14 to 0.22 Si, 1.3 to 1.5 Mn, 52 to 60 Fe and 30 to 34 O. Carbon measurements are not usually reliable owing to usual contamination from SEM systems. The relatively large amounts of aluminum is surprising in view of the fact that it is present in the coolant in the range of 0.4 to 1 ppm as shown in Table 4.5 and as 8.67 ppm in Altran.[21] Silicon was not measured in the AECL work nor in the Altran work.

For an approximate comparison of the Mo in the IGC of 4.2 w/o relative to 300 ppm in the coolant with about 0.21 w/o of Al relative to 1 ppm in the coolant give ratios, respectively, 0.014 and 0.21 of w/o in the oxide to ppm in the environment. This implies that the aluminum, and presumably the silicon, are greatly enriched in the IGC region relative to the molybdenum. Note that similarly low values of silicon relative to aluminum were reported by Altran and are shown in Table 4.7. While there are numerous possible speculations here, it does not provide any insights for the present problem. The best interpretation here is probably associated with relative solubilities at the local pH. In the relevant range of pH on the inside surface, Mo is soluable and both Al and Si are much less soluble.

6.0 Experience of Other Plants

Experiences with CCW systems, their materials, chemistry, properties, inspection and failures in domestic plants are summarized in Table 6.1. This information was obtained from a telephone survey conducted by WCNOC. The frequency of types of inhibition is summarized in Table 6.2.

Experience with international plants is summarized in Table 6.3. This information was obtained by E mail requests. These data are also summarized in Figure 6.2 according to the number of plants in a particular system, e.g. it is assumed that all plants in the French Electricity (EDF) system use the same water chemistry. The data in Table 6.3 indicates that the predominantly used inhibitors are hydrazine and phosphate. Chromate, molybdate, and nitrite are used less and about equally. The use of hydrazine means that the environment is deoxygenated. The use of phosphate means that the chemistry on the surface is buffered.

Data from a previous investigation by Dominion Engineering (DEI) of SCC in CCW systems[1] are summarized in Table 6.4. Here are three plants aside from WCNOC that sustained SCC and all three used nitrite. The interpretation by DEI attributed these failures to effects of microbes oxidizing nitrites to nitrates with the speculative results that the SCC results from nitrates according to the patterns in Figure 7.15. However, there is little support for this interpretation of nitrate-SCC in terms of the relevance to available data for SCC that has been observed in nitrate solutions. The results in these cases are relevant to Wolf Creek in that the oxidizing potential achieved in the instances where failure occurred may be more important than the nitrate/nitrite chemistries. This is discussed in Section 7.3.1.

It should be noted that the Callaway plant is presently sustaining some SCC;[20] but the extent is not clear, and the rate seems less than that at WCNOC. In this context it should be noted that under the best circumstances the corrosion of tubing in steam generators is quite variable as discussed in connection with Figures 7.6, 7.7, and 7.8 in Section 7.2.4. Further, tubing in different steam generators in the same plant behaves often times quite differently. Nonetheless, it is possible that what appears to be less rapid SCC could be related to the fact that the cooling water in the CCW system in the Callaway plant runs at generally constant temperature from cooling towers; whereas, WCNOC uses lake water which is variable and may produce oscillations in stress that accelerate SCC as noted in Figures 7.49, 7.50 and 7.51 of Section 7.3.7.

The surveys in Tables 6.1 and 6.3, as summarized in Table 6.2, show that the use of molybdate by WCNOC is consistent with about 9% of other plants throughout the world.

Table 6.1
Use of Inhibitors in Domestic Applications of CCW Systems.

Survey of Materials, Inhibitors, Performance of Domestic CCW Systems.
(Survey conducted by WCNOC)

	Plant	Chemistry	Since Startup	Before/After?	Material	Evidence?	Miscellaneous
1	Arkansas Nuclear One	Nitrite Borax	Yes	N/A	Mixed	None	
2	Beaver Valley Power St.	Molybdate Nitrite	No	Chromate	Carbon Steel	None	Advice: Some biocides with chloride in them might be the cause of an attack to crack the steel?
3	Braidwood Station	Nitrite	No	Chromate	Carbon Steel	None	
4	Browns Ferry	Molybdate Nitrite	No	Nitrite	Carbon Steel	???	
5	Brunswick Steam	Nitrite	Yes	N/A	Carbon Steel	None	
6	Byron Station	Sodium Nitrite	Yes	N/A	Carbon Steel	None	
7	Callaway	Molybdate	?Yes	N/A	Carbon Steel	None	
8	Calvert Cliffs	Hydrazine	Yes	N/A	Carbon Steel	None	
9	Catawba Nuclear St.	Nitrite Borax	Yes	Going to Moly	Stainless	None	
10	Illinois Power Company	Molybdate	No	Nitrite	Carbon Steel	Yes	Many with complications not consistent with WCNOC conditions; including a two year shut

Table 6.1 (continued)

	Plant	Chemistry	Since Startup	Before/After?	Material	Evidence?	Miscellaneous
							down period
11	Columbia Energy NW	Dimin	Yes	N/A	Carbon Steel	None	
12	Donald C. Cook	Nitrite	Yes	Going to Moly	Carbon Steel	None	
13	Cooper Nuclear Station	Dimin	No	Nitrite	Stainless	None	Ion on the skid; some carbon steel also
14	Crystal River Unit 3	Hydrazine	No	Amonia	Carbon Steel	None	
15	Davis-Besse	Hydrazine	Yes	N/A	Carbon Steel	None	
16	Diablo Canyon	Molybdate Nitrite	No	Chromate	Carbon Steel	None	
17	Dresden Station						
18	Duane Arnold Energy	Molybdate Nitrite	No	???	Stainless	None	
19	Farley Nuclear Plant	Chromate	Yes	N/A	Mixed	None	
20	Fermi 2	Dimin	Yes	Maybe Inhibitor	Carbon Steel	None	
21	James A. Fitz Patrick	Dimin	Yes		Carbon Steel	None	
22	Fort Calhoun Station	Nitrite	No	Chromate	Carbon Steel	None	
23	R.E. Ginna Nuclear P	Chromate	Yes	N/A	Carbon Steel	None	
24	Grand Gulf	Nitrite	Yes	N/A	Carbon Steel	None	
25	Shearon Harris	Molybdate	No	Chromate	Carbon Steel	None	

Table 6.1 (continued)

	Plant	Chemistry	Since Startup	Before/After?	Material	Evidence?	Miscellaneous
26	E.I. Hatch	Molybdate Nitrite	No	Nitrite	Carbon Steel	None	
27	Hope Creek Gen St.	Same as Salem	Same as Salem	Same as Salem	Same as Salem	Same as Salem	
28	Indian Point 2	Molybdate Nitrite	No	Chromate	Stainless	None	
29	Indian Point 3	Molybdate	No	Chromate	Carbon Steel	None	
30	Kewaunee NPP	Molybdate Nitrite	No	Chromate	Carbon Steel	None	
31	LaSalle Station	Nitrite	No	???	Carbon Steel	None	
32	Limerick Generating	Nitrite	Yes	N/A	Mixed	None	Mixed Primarily with Carbon and Stainless
33	McGuire	Nitrite	Yes	N/A	Stainless	None	
34	Millstone Nuclear	Nitrite & Hydrazine	Yes	N/A	Carbon Steel	None	
35	Monticello	Chromate	Yes	N/A	Carbon Steel	None	
36	Ninemile Point 1	Dimin	Yes	N/A	Carbon Steel	None	
37	Ninemile Point 2	Dimin	Yes		Carbon Steel	None	
38	North Anna	Chromate	Yes	N/A	Carbon Steel	None	
39	Oconee	Chromate	Yes	N/A	Carbon Steel	None	
40	Oyster Creek Nuclear	Molybdate	No	Boron-nitrite	Carbon Steel	None	
41	Palisades Nuclear	Nitrite				None	

Table 6.1 (continued)

	Plant	Chemistry	Since Startup	Before/After?	Material	Evidence?	Miscellaneous
42	Palo Verde	Nitrite Borate	Yes	N/A	Carbon Steel	None	
43	Peach Bottom	Sodium Hydroxide?	Yes	N/A	Carbon Steel	None	
44	Perry Nuclear	Hydrazine	Yes	N/A	Carbon Steel	None	
45	Pilgrim Nuclear	Nitrite	No	Pure Water	Carbon Steel	None	
46	Point Beach	Chromate	Yes	N/A	Carbon Steel	None	
47	Praire Island Nuclear	Chromate	Yes	N/A	Carbon Steel	None	
48	Quad Cities Station	Nitrite	Yes	N/A	Carbon Steel	None	
49	River Bend Station	Dimin	Yes	N/A	Carbon Steel	None	
50	H. B. Robinson Steam	Chromate	Yes	N/A	Carbon Steel	None	
51	Salem Gen Station	Potassium Chromate	Yes	N/A	Carbon Steel	None	
52	San Onofore Nuclear	Nitrite	Yes	N/A	Carbon Steel	None	
53	Seabrook Station	Hydrazine	Yes	N/A	Carbon Steel	None	
54	Sequoyah Nuclear	Molybdate	Since 93	N/A	Stainless	None	
55	South Texas Plant	Nitrite	Yes	N/A	Mixed	None	
56	St. Lucie	Molybdate Nitrite	No	Chromate	Carbon Steel	None	
57	V.C. Summer Nuclear	Chromate	Yes	N/A	Carbon Steel	None	Some Cyclic Failure due to Vibration

Table 6.1 (continued)

	Plant	Chemistry	Since Startup	Before/After?	Material	Evidence?	Miscellaneous
58	Surry Power Station	Chromate	Yes	N/A	Carbon Steel	Some	General Corrosion rusting through. Did not considered cracks however.
59	Susquehanna	Nitrite	Yes	N/A	Carbon Steel	None	Did play with Molybdate for a short time about six years ago.
60	Three Mile Island	Molybdate	No	Nalco Oil then Moly/Nitrite	Carbon Steel	Some	Pitting and Through wall failures due to mechanical sources
61	Turkey Point	Molybdate Nitrite	No	Chromate	Mixed	None	Switched 15 yrs ago
62	Vermont Yankee	Molybdate Nitrite	Yes	N/A	Carbon Steel	None	
63	Vogtle Electric	Nitrite	Yes	N/A	Carbon Steel	None	
64	Waterford 3	Molybdate	No	Sodium Nitrite	Carbon Steel	None	
65	Watts Bar	Molybdate	Yes	N/A	Carbon Steel	None	
66	Laguna Verde						

Table 6.2
Summary of Present Usage of Inhibitors for CCW Systems.*

Inhibitor Type	Number Use from Table 6.1	International Use (number of plants, See Table 6.3)	Fraction of Total, %
Water without inhibitor	7	0	4.6
Hydrazine	4	22	17.2
NaOH	1	0	0.7
Chromate	12	5	11.2
Molybdate	9	4	8.6
Nitrite	16	0	10.6
Molybdate-Nitrite	10	0	6.6
Boron compound-Nitrite	3	0	1.9
Hydrazine-Nitrite	1	0	0.7
Phosphate	0	57	37.8
Total	63	88	

*Based on Tables 6.1 and 6.3

Table 6.3
Survey of International Use of Inhibitors in PWR CCW Systems

Country and Electric Utility	Piping Material for CCW System	Stress Relief	Heat Exchanger Material	Inhibitor and Chronology	Oxygen Concentration	pH	Conduc-tivity	Method of Deionization	Residual Impurity Chemistry	Microbes or Fungi	NDE (UT)	SCC Observed
France, EdF(about 56 plants)	Carbon Steel,	Not known; proprietary	Not know	Na_3PO_4 with 100-500ppm PO_4	Oxygenated	Limit: 10.8 to 11.5; expected 11.0-11.5, 10.0 to 10.8 acceptable 1 month, NaOH addition prohibited	2000-3000 mS/cm	Give same water as makeup for NPP which gives conduct of 0.06to 0.1microS/cm	Expected <20 ppb for Cl and F; limit <0.15 ppm	No analysis	No information	No information
Germany (about 14 plants)	Carbon steel St35, St37, stress relief not known	Stress relief not known	Old plants: Sondermessing 71 (German brass); in new plants either stainless steel or titanium, depending on cooling water quality.	N_2H_4 with 300-400 ppm or low N_2H_4 with 5-10 ppm or N_2H_2 free. No inhibitor	Oxygenated water is used for filling; for low N_2H_4 tight systems improved to avoid frequent make-ups. Oxygen expected to be <50 ppb. In N_2H_4 treated oxygen free water used.	High N_2H_4 9-10; low N_2H_4 about 9; oxygen free 6-7; pH not specified	High N_2H_4 <50mS/cm ; low N_2H_4 <10mS/cm ; oxygen free: <5 mS/cm	Use makeup water system	Low, not measured	No analysis	No information but not expected since no damage	None

Table 6.3 (continued)

Country and Electric Utility	Piping Material for CCW System	Stress Relief	Heat Exchanger Material	Inhibitor and Chronology	Oxygen Concentration	pH	Conduc-tivity	Method of Deionization	Residual Impurity Chemistry	Microbes or Fungi	NDE (UT)	SCC Observed
Japan, Kansai Electric Power (about 11 plants)	Carbon steel	None	Copper alloys	Four plants on chromate (>175 ppm), seven plants on N_2H_4 200<x<1000ppb	DO<100 ppb for N_2H_4	Chromate pH 8 to 9.7; for N_2H_4 pH 8-9.7	for N_2H_4 <10mS/cm	Use make up for secondary system	F<0.15ppm, Cl<0.05ppm	No analysis	None	None
Korea, Kori Unit 1, 2 (Two plants)	1/2 to 10" seamless or welded, ASTM A53 or ! 106 Grade A or B SC1140; 12 to 24" seamless or welded, ASTM A 53 or A 106 A or B Std, 3/8" wall	Not Stress relieved	Cu-Ni (90:10) for unit 1 and CuNi (70:30) for unit 2	Hydrazine 5-25 ppm since 1996; potassium chromate, 175-225 ppm as CrO_4 before 1996	None detected	8.0 to 9.5	not known	use demineralized water	<150 ppb for Cl and F each	None	No plan for inspection	No SCC observed
Korea, Kori Units 3 and 4(Two plants)	SA 106 GrB with rubber lining	Stress relieved following standard procedures	Cu-Ni (90:10); SB-111, No. 706	AVT since 1995; chromate before 1995; N_2H_4 5-25 ppm	None detected	8.5 to 9.5	No range	No purification demineralizer	Cl<0.15; F<0.15 ppm	Not analyzed	No inspection	No SCC observed

Country and Electric Utility	Piping Material for CCW System	Stress Relief	Heat Exchanger Material	Inhibitor and Chronology	Oxygen Concentration	pH	Conduc-tivity	Method of Deionization	Residual Impurity Chemistry	Microbes or Fungi	NDE (UT)	SCC Observed
Sweden, Ringhals (Three plants)	Type A106; Swedish rules do not accept carbon >0.25 and special precautions if welding when C>0.20%. Since welds below this value, no heat treatment	No heat treatment since carbon <0.20%	Original: Copper Alloy SB-111. R-2 replace with Ti. R-4 all four heat exchangers replaced with Ti (ASTM B338 Gr 2). Replacement starting at R-3	Before 2000 inhibitor was potassium chromate; R-2 still using chromate; R-3 and R-4 switch to 250-350 sodium molybdate with 20 ppm Tolyltriazol	Oxygen 7.0 to 10.0 ppm in Re and R4	8.5 to 10.5	700 - 900 mS/cm		Cl approx 300 ppb	Below detection	No regular NDE (UT); regularly inspect by Fe concentration	No SCC
Spain, Almaraz (Two plants)	SA 106B	No	Stainless steel 304 A 213	Potassium chromate 175 to 225 ppm until 1996, molybdate since the >120 ppm	Saturated	10-10.2 with NaOH	500mS/cm for 140-160 ppm molybdate	Water from Tajo river then inverse osmosis and then mixed bed resin	Less than detection limit	Organics are removed by osmosis	Visual	No SCC
Spain Vandellos (One plant)	ASTM A 105B	No	90/10 Cu-Ni	300-500 ppm Na_3PO_4	Saturated	11.5-12	1500-2000ms/cm	Mixed bed resins no inverse osmosis	Cl<150ppb	Analyzed for and none detected	Visual	No SCC

Table 6.4

Summary of Data from DEI 1995 Investigation and from Callaway Experience

Plant	Temperatures	Inhibitors and Additives	Other Chemistry	Microbes and Fungi	SCC	Locations	Source of Information
McGuire 1 and 2	Cracking in regions of 70°-80°F, 110°F and 150°F	Approximately 2000 ppm nominal inhibitor containing sodium nitrite, borax, sodium bicarbonate, benzotriazole, and Calgon H450 as biocide. About 2000 ppm inhibitor at 1984 but increased to about 2400 ppm inhibitor	Oxygen 200 to 1000 ppb		Observed after 13 years at McG 1 and 10 years at McG 2	Welds and deposits; SCC in weld, HAZ, matrix at welds	1995 DEI report to WCNOC
Cooper		Nitrite since startup until about 1980 when several IGSCC cracks occurred. Since then pure demineralized water has been used with no inhibitor. In 1994 two leaks occurred	Standard oxygenated since 1992; prior was low ppb oxygen	No good evidence except for appearance of nitrate	Early SCC considered due to nitrates; later IGSCC thought by GE due to left over nitrates; SwRI considers that pure water. SCC in 1979 five years service; 1994 20 years of service 24 with demin water	All at welds in weld, HAZ and adjacent to HAZ	1995 DEI report to WCNOC

Table 6.4 (continued)

Plant	Temperatures	Inhibitors and Additives	Other Chemistry	Microbes and Fungi	SCC	Locations	Source of Information
Cook 1 and 2		Sodium nitrite based inhibitor from 1974 and 1977 for Cook 1 and 2. SCC found in 1987. In 1991 more cracks observed. Nitrite maintained 500-1000 ppm and pH is 8.5 to 9.5 with NaOH if required.		After 1987 used Calgon LCS 60 and glutaraldehyde also. Current practice is to add biocides to 100 ppm if there is evidence of biological activity after draining if evidence from low nitrite or increase in pH	Westinghouse said that nitrite too low; cracks occur after 13 and 10 years of service for Unit 1 and Unit 2	All at welds	1995 DEI report to WCNOC
Callaway		Sister plant to Wolf Creek			SCC about half way through in time since about 1986.		Communication from DA Womelsdorf, WCNOC

7.0 SCC and Corrosion of Mild and Low Alloy Steel

7.1 Introduction

The purpose of this section is to provide background for understanding the reasons for the SCC occurring in the CCW system and for predicting future performance. Specific questions to be considered with respect to the piping materials and environments in the CCW system are:

1. What specific aspects of the chemical environment produce SCC in the piping material?

2. What are the effects of important variables such as stress, temperature, pH, potential, and species with respect to predicting and optimizing future performance?

3. What is the effect on SCC of heat treatment (e.g. PWHT) used to lower the residual stresses?

4. What is a reasonable approach to calculating the time for perforation of piping given various practical assumptions about pre-existing and non-pre-existing SCC?

5. What kinds of crack shapes might develop from the point of view of determining the likelihood of exceeding K_{Ic} and can these be reasonably attained?

The SCC of mild and low alloy steels occurs readily over the range of temperatures from room temperature (RT) to the range of at least 350°C. This work has been undertaken in connection with pipelines, steam turbines, refinery vessels, chemical processing equipment, and pressure vessels and pipes for nuclear and fossil power plants. Much of the work in the RT range has been conducted in connection with pipelines and the application of CERT testing methods. Relevant information from these investigations is considered in this section.

7.2 Background

There are five subjects that underlie the important dependencies of the SCC that occurred in the CCW system. First, SCC occurs in generally orderly patterns that can be best seen in mode diagrams such as the one shown in Section 7.2.1. Second, the occurrence of SCC depends on seven primary variables as described in Section 7.2.2; third, the SCC in the CCW system moved through initiation and propagation stages as described in Section 7.2.3; fourth, the SCC, like all SCC, is quite variable both within heats and from heat-to-heat as described in Section 7.2.4; fifth, the geometrical distribution of SCC over the component determines whether there are simply leaks or whether the entire component may fail as shown in Section 7.2.5.

7.2.1 Mode Diagram for the SCC of Steel

The occurrences of SCC in alloys in aqueous solutions tend to follow the thermodynamic boundaries as identified in the equilibrium diagrams of pH and potential. Figure 7.1 shows the E-pH diagram for iron in water at 25°C with some annotations that are relevant to this discussion.

Figure 7.1 indicates the following important patterns that are relevant to the operation of the CCW system:

1. Without oxygen in the water, the open circuit potential is constrained to be in the range shown by lines (1) and (2) over the full range of pH. Where Fe^{2+} is soluble, this range is shown by (1); where Fe is in equilibrium with Fe_3O_4 this range is shown by (2).

2. With oxygen in the water, the open circuit potential is constrained to be in a larger range as shown, where the range associated with Fe^{2+} is shown by the line (3); and the range associated with the formation of Fe_3O_4 is shown by the line (4). While the O_2/H_2O half cell is given by line (b), the practical upper limit for the open circuit potential is lower by about 200 mV owing to the sluggishness of the oxygen reduction reaction. This practical upper limit is given approximately by line (5) and takes its location from the data of Figure 7.10.

3. When the pH is less than about 7-8, iron in the deaerated range becomes more soluble; and iron corrodes progressively more rapidly with the decrease of pH as indicated by line (6).

4. When the potential is raised, the Fe_2O_3 is stabilized; and passivity improves as indicated by line (7).

5. When the pH is raised above about 8, especially in the deaerated condition, the solubility of magnetite and hematite are increasingly reduced with the minimum solubility at about pH 12.3 shown by line (8); and iron, so protected, becomes increasingly corrosion resistant. This pH of minimum solubility indicates where iron is maximally resistant to corrosion.

6. The range of potential and pH in which the CCW system operates or has operated is shown approximately in the cross-hatched region.

The occurrence of SCC tends to follow regular patterns that can be summarized within coordinates of pH and potential. Such a diagram for mild and low alloy steels in the range of room temperatures is shown in Figure 7.2. Here, data for the occurrence of SCC in several different environments are shown to plot regularly, especially in the acidic and alkaline ranges as shown in Figure 7.2a where the data are in the range of RT to 100°C. These data can be aggregated as shown in Figure 7.2b. This figure shows that there are four main regions where SCC occurs: alkaline SCC (AkSCC), low potential SCC (LPSCC), acidic SCC (AcSCC), and high potential SCC (HPSCC). Most of the work

underlying Figures 7.2a and 72b is from Parkins and Congleton and their co-workers, and is variously referenced in Section 7.0. Numerous workers have contributed to identifying the HPSCC region, and this region becomes more intense as the temperature increases. This region is discussed in detail in Section 7.3.1.

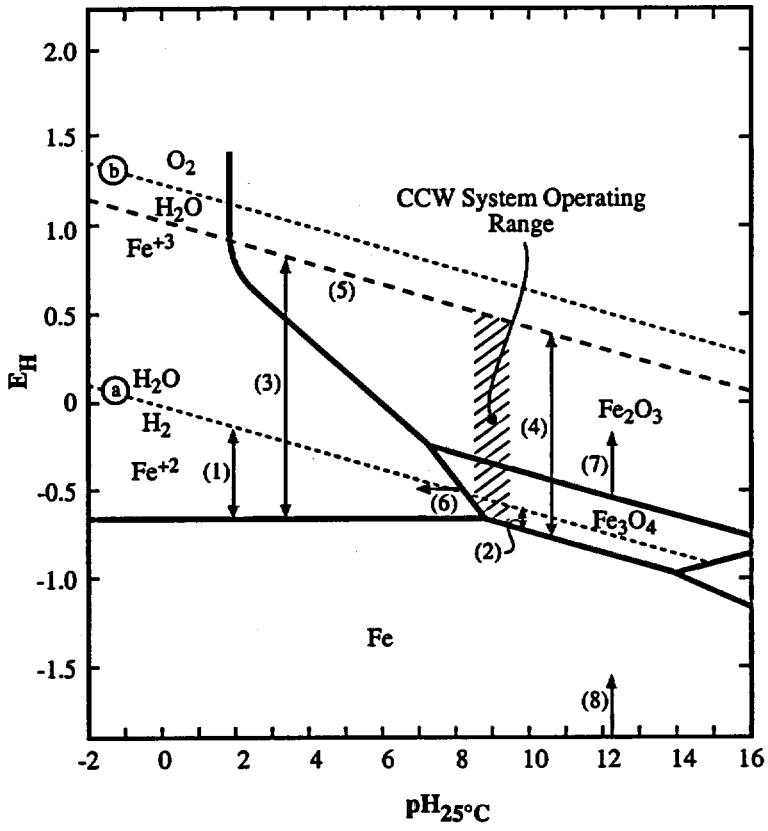

Figure 7.1 Potential vs. pH for the stability of iron at 25°C based on the diagram from Pourbaix.[22]

The patterns observed in Figure 7.2 indicate the following:

1. A range of SCC occurs below the H_2O/H_2 standard hydrogen half cell. This corresponds to low potential SCC (LPSCC) and is most likely related to some kind of hydrogen embrittlement.

2. There is a region of SCC above the H_2O/H_2 line that probably extends over a broad range of pH and corresponds to a high potential SCC (HPSCC). This region is most likely associated with the breakdown of the passive films at higher potentials. This is the region that is most likely associated with the CCW system problem, which is the subject of this report. The dependence of this region on pH is not well defined; but its dependence mainly on the breakdown potential of iron suggests that it may be independent of pH just as the LPSCC is independent on pH although for a different reason

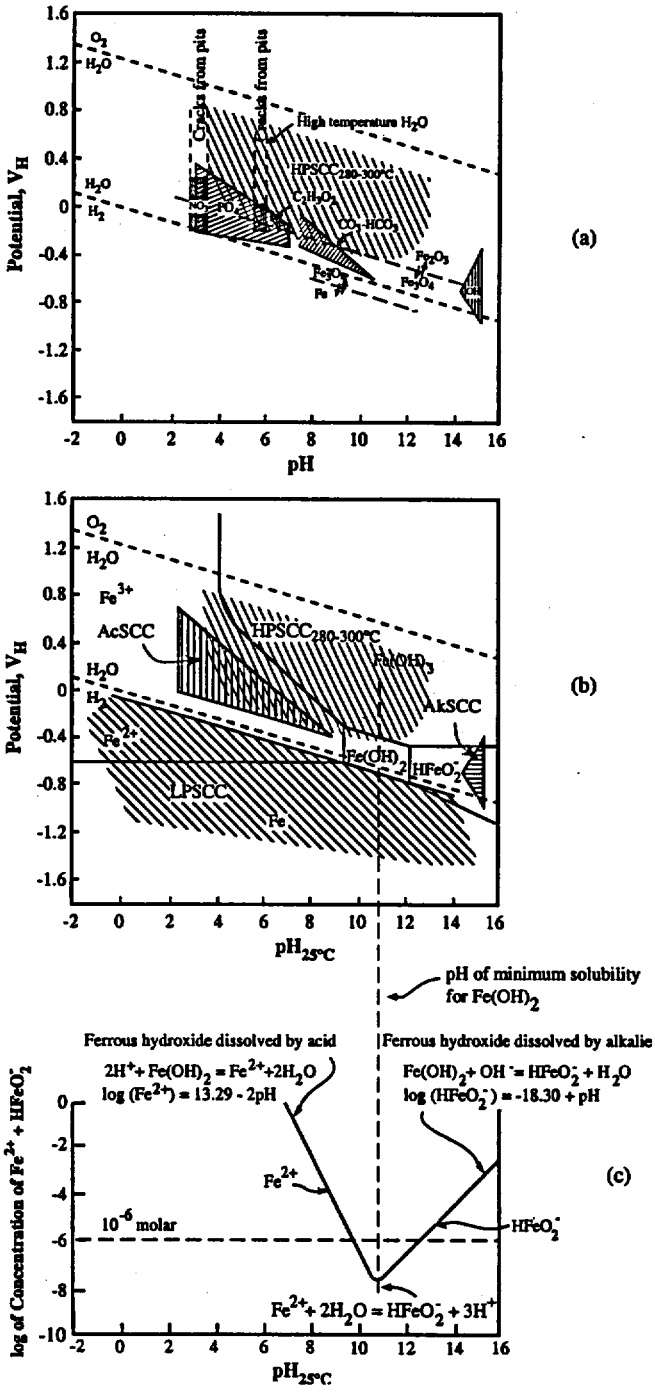

Figure 7.2 (a) Potential vs. pH for iron in water. Shaded areas show locations for occurrence of SCC of low alloy steels exposed to different environments at RT to about 150°C except for one in high temperature water which is generally in the range of 280 to 300°C. From Congleton et al.[45] (b) Aggregate of data to show patterns. From Parkins.[23] (c) Solubility of iron as a function of pH with the dotted line drawn from the minimum solubility to the region of no anodic SCC. From Pourbaix.[24]

3. In the acidic region above the H_2O/H_2 line there is a somewhat triangular region that corresponds to acidic SCC (AcSCC). This region seems approximately symmetric at about the Fe_2O_3/Fe_3O_4 half cell equilibrium. This is not surprising since such a susceptible region was predicted early by both Humphries and Parkins[25] and Staehle.[26]

4. In the alkaline region there is also a triangular region centered about on the same Fe_2O_3/Fe_3O_4 line but mainly adjacent to the region of solubility of the alkaline soluble iron corresponding to the alkaline SCC (AkSCC).

5. Between the regions of the AkSCC and AcSCC there seems to be a region where no SCC occurs along the symmetry of the Fe_2O_3/Fe_3O_4 line; this region of no or minimum SCC corresponds closely to the region of minimum solubility of Fe_2O_3 and Fe_3O_4. The fact that such a minimum should occur here is not surprising in view of the minimum in solubility as noted in Figure 7.2c. Such a minimum as a function of pH also suggests that moving the solution pH of the CCW system water toward this region could minimize or possibly eliminate SCC if it is of the AcSCC/AkSCC type.

Understanding the SCC in the CCW system involves appreciating the implications of Figure 7.2.

7.2.2 General Dependencies of SCC

Understanding the circumstances in which SCC is significant and the rate at which SCC penetrates involves understanding its dependencies upon seven "primary variables:" electrochemical potential, pH, species, alloy composition, alloy structure, temperature and stress. The general dependencies of the progress of SCC are illustrated in Figure 7.3 for the case of AkSCC. This figure also shows examples of some of these dependencies for the case of Alloy 600MA in secondary water of PWR steam generators. Defining the dependencies on these variables also is part of defining and differentiating the various submodes. Each of the submodes shown in Figure 7.2 depends differently on these seven variables as is evident from Figure 7.2 where each depends differently on the pH and potential.

Understanding the dependencies according to these primary variables shown in Figure 7.3 is necessary for predicting the occurrence of SCC in the CCW system. These dependencies that are relevant to the steel used in the CCW system piping, as well as relevant data from other steels, are described in Section 7.3.

7.2.3 Initiation and Propagation

The SCC that has occurred in the CCW system involves both initiation and propagation stages, and a perspective on these stages is useful. In general, initiation depends more on the chemistry on the surface while propagation depends less on surface chemistry and more on chemistry at the tip of the advancing SCC. However, this distinction does not necessarily mean that the overall dependencies are totally different; unfortunately, the

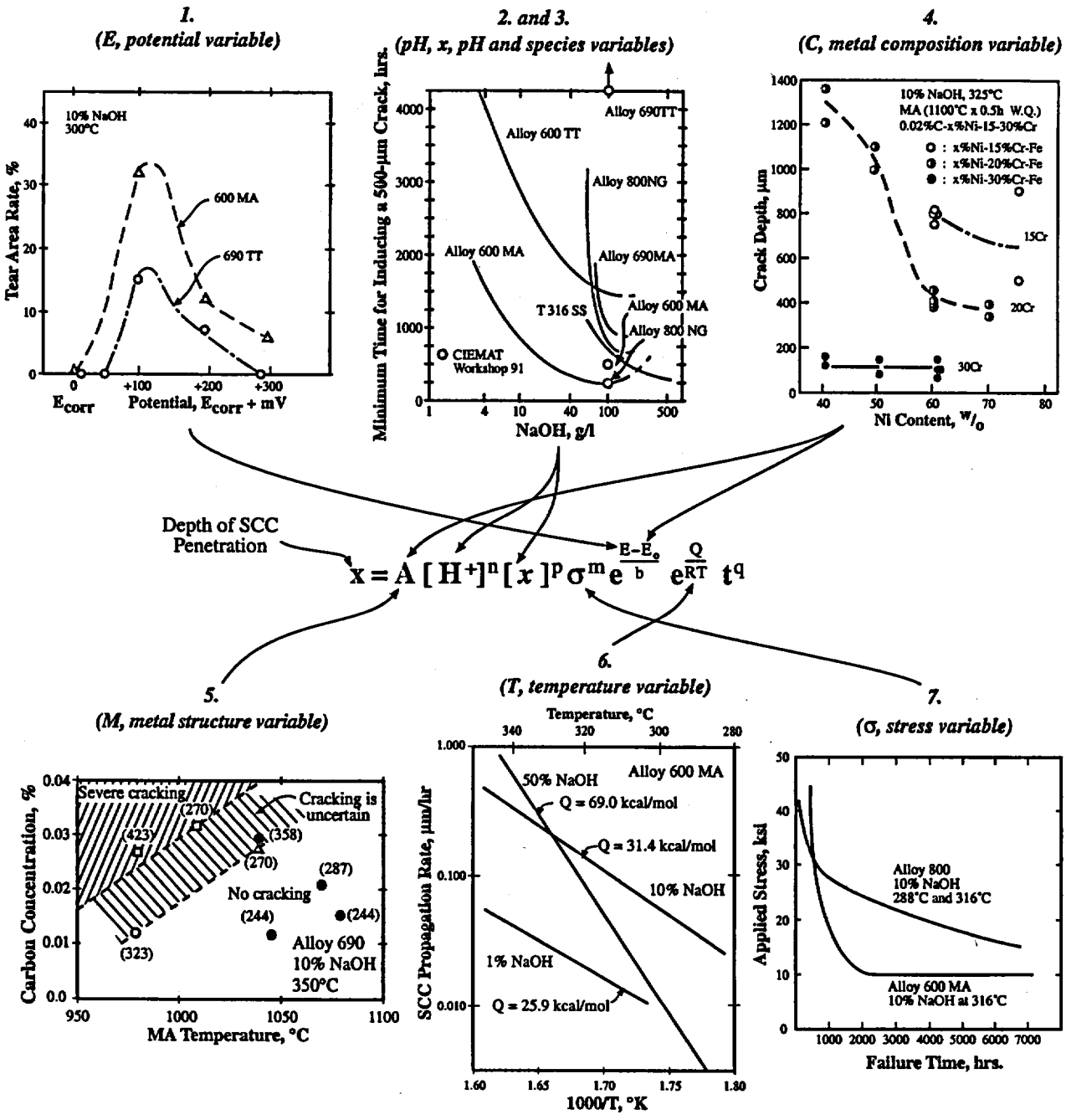

Figure 7.3 General relationship of penetration of SCC as a function of primary variables. Examples of patterns for the primary variables from AkSCC are shown adjacent to the equation. (1) From Suzuki.[27] (2 &3) The original curves of Berge and Donati[28] were redrawn, and data were added by McIlree.[29] (4) From Nagano et al.[30] (5) From Vaillant et al.[31] (6) From Jacko.[32] (7) From Wilson et al.[33]

relative dependencies of initiation and propagation have not been well studied. Figure 7.4 from the work of Parkins[35] shows that the dependence of SCC on potential is similar for both initiation and propagation. This is also true for the SCC of sensitized stainless steel in BWR water.[34] However, this may or may not follow with respect to species, pH, temperature, and mean stress. Also, the occurrence of SCC in the CCW system may be subject to variability that occurs within heats and from heat to heat as described in Section 7.2.4.

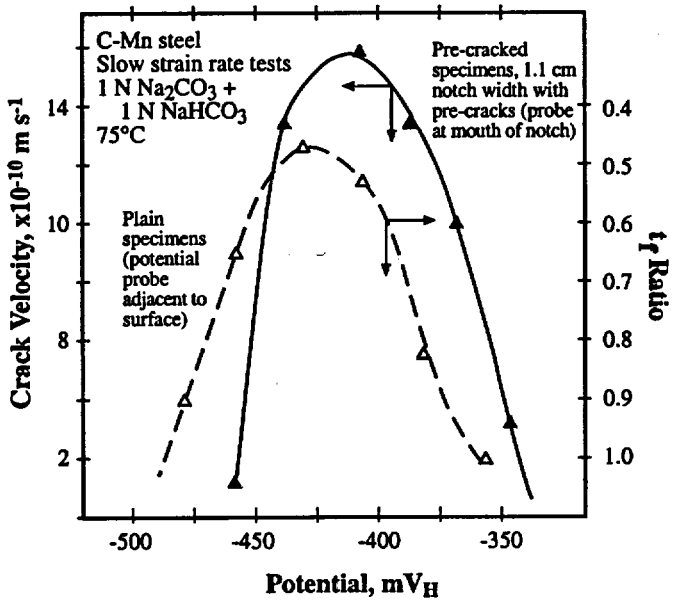

Figure 7.4 Crack velocity and time-to-failure ratio vs. potential for a C-Mn steel exposed to a 1N Na_2CO_3+1N $NaHCO_3$ solution at 75°C. Smooth specimen tested as CERT.[35]

Initiation often requires relatively high surface stresses if the chemical conditions are not in the region of highest propensity for SCC; also, the time of initiation of SCC may be quite variable since surface-related corrosion processes generally have large statistical dispersions. Initiation is greatly affected by conditions of the surface such as machining, grinding, polishing, and chemical cleaning. Propagation seems less sensitive to the chemical and mechanical conditions on the surface and may occur at lower mean stresses. Distinguishing between the conditions of initiation and propagation has always been controversial. Understanding the differences between initiation and propagation for the CCW system is especially important since it affects how the occurrences of future perforations should be predicted.

A straightforward means for distinguishing initiation and propagation is shown in Figure 7.5. Here, Figure 7.5a shows how conditions for initiation are determined. In general, the conditions for initiation are defined by testing specimens with smooth surfaces and determining the time at which failure occurs for a given stress. Such experiments yield a plot of stress vs. time-to-failure. These data usually give a threshold stress below which

SCC will not initiate. Sometimes there is a downward slope to this threshold with time, but the general idea of a threshold is a useful one.

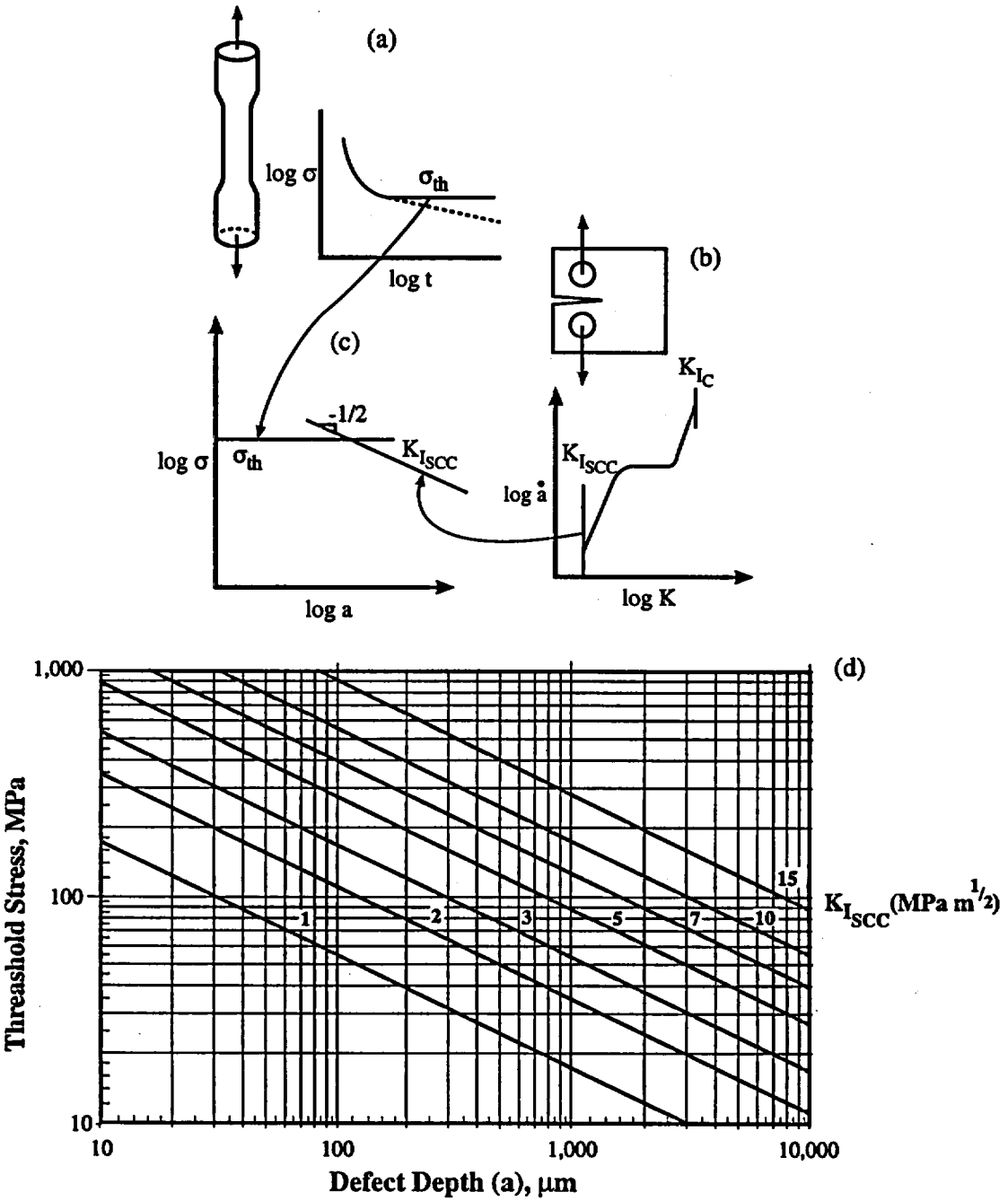

Figure 7.5 (a) Method for determining the dependence of initiation vs. stress. (b) Method for determining the value of K_{ISCC} involving crack velocity and stress intensity. (c) Schematic integration of (a) and (b). (d) Quantitative graphic for determining depth at which the transition from initiation to propagation occurs.

Diagrams resulting from measuring propagation are shown in Figure 7.5b. Here, propagation is measured generally using a specimen with a pre-crack with which the rate of growth or crack velocity is measured as a function of the stress intensity, K, as shown in Eqn. (7.1). The stress intensity depends generally on the mean stress and the depth of a crack. Of special interest to defining the transition from initiation to propagation is K_ISCC at which significant SCC begins. K_ISCC defines the set of values for the mean stress and crack depth for the propagation of SCC and produces a slope of –1/2 on a plot of stress vs. defect depth as shown schematically in Figure 7.5c and in detail in Figure 7.5d. Figure 7.5c shows schematically how the threshold stress that applies to initiation interacts with the locus of stress and crack depth as defined by K_ISCC. This intersection indicates that the transition from initiation to propagation control occurs where the threshold stress for initiation intersects the locus defined by K_ISCC.

$$K_I=\sigma_m(\Pi a)^{1/2} \qquad (7.1)$$

where:

K_I = stress intensity at the crack tip in the opening (I) mode
σ_m = mean stress
a = defect depth

Since it appears that the residual stress from welding for initiating SCC in the CCW system is relatively high, the transition from initiation to propagation may occur at relatively shallow depths of the initiated SCC.

7.2.4 Variability

When viewing the occurrence of SCC, especially these few occurrences from the CCW system, it is tempting to compare such observations directly and conclude something about relative rates as affected by stress and temperature. While such comparisons are useful qualitatively, they are sometimes misleading. Such comparative data needs to be tempered with the understanding that data for SCC are variable. The variabilities of SCC data are illustrated in Figures 7.6, 7.7 and 7.8. Such variability has been described in detail by Staehle,[36,37] Stavropoulos et al.,[38] and Staehle et al.[39]

Figure 7.6 shows how SCC in thin wall heat transfer tubing occurs with time for various locations and according to various modes in PWR steam generators. While this application is different from the CCW system piping, this kind of occurrence over time could be similar to the CCW system piping application. Further, this variability would probably be greater at the lower temperatures of the CCW system application compared with the approximately 300°C for Figure 7.6 since the dispersion of data tends generally to increase as the stressors (e.g. temperature) decrease.

Figure 7.7 shows data for the failure of stainless steel pipes exposed to oxygenated water in the range of 288°C in BWR applications. These data, like those of Figure 7.6, are plotted in the coordinates of Weibull statistics and show the percent failed (the

probability) versus time of exposure. The dimensions of these pipes are in the same range as those of the CCW system. Figure 7.7 shows that the dispersion of these data is large even at 288°C. Such a dispersion of data could also be relevant to the CCW system. Not everything sustains SCC at once, and SCC initiates and grows at different rates.

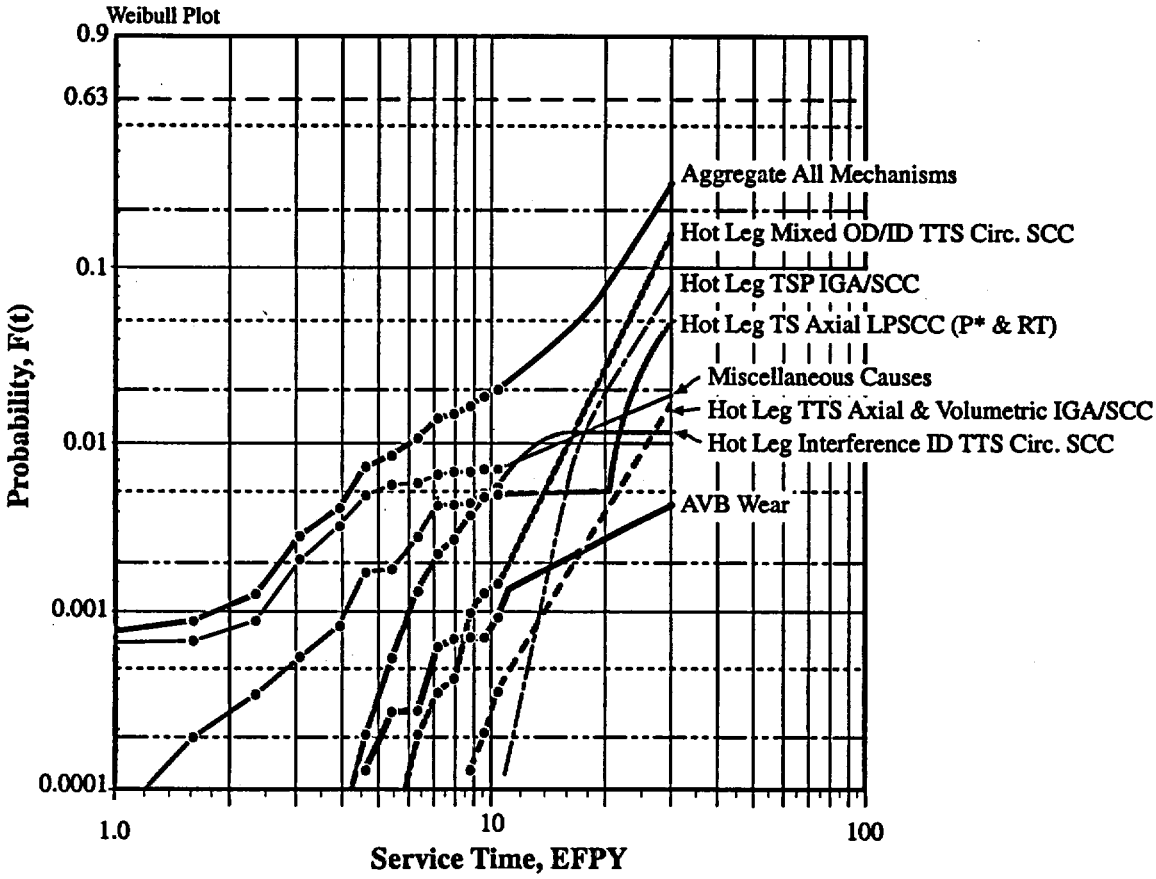

Figure 7.6 Probability of failure vs. equivalent full power years for Ringhals 4 PWR for various mode-location cases and for the aggregate probability. Alloy 600MA tubing. From Björnkvist and Gorman.[40]

A somewhat different illustration of variability is shown in Figure 7.8 from the work of Scott.[43] Here, data are shown from corrosion, mostly SCC, taken from the primary and secondary sides of PWR steam generators. The abscissa indicates chronologically successive heats of material all prepared in the same facility. The ordinate indicates the percent of each heat with indications of failure. At the top of each bar is the number of tubes of that heat used in the respective heat exchanger. These data show a broad range of occurrence of SCC from none to as high as about 40% of tubes. The trends do not correlate with the succession of heats. Similar data for the occurrence of SCC in stainless steels has been published by Clarke and Gordon.[41]

The data of Figure 7.8 indicate the reasonable possibility that the various locations of CCW system pipes may sustain SCC at various times regardless of their nominal similarity. Further, each weld may correspond itself to a different heat of material. Such

heat-to-heat patterns as illustrated in Figure 7.8 suggest that detailed comparisons among plants, e.g. Callaway, and from location to location within the CCW system of WCNOC may not provide reliable comparisons in detail.

7.2.5 Distribution of SCC, Longitudinal and Circumferential

Serious failures due to SCC depend on how the SCC is distributed. There are two general geometric patterns for the distribution of SCC that occur in pipes: longitudinal and circumferential. These are illustrated in Figure 7.9.

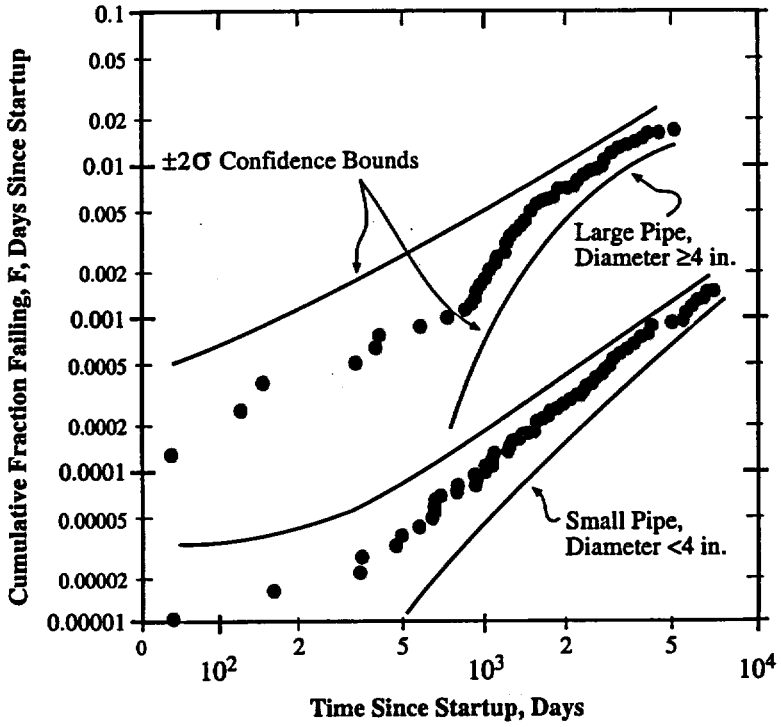

Figure 7.7 Cumulative fraction of welds failed in terms of repair rates in stainless steel pipes designated as "large diameter, ≥4 inches" or "small pipe diameter, < 4 inches" from BWR type nuclear plants. The larger diameter pipes include only IGSCC, and the smaller pipes include all failure modes. The Weibull characteristic, θ, and the Weibull slope, β, for the larger diameter data are about 500 years and 0.57 and for the smaller diameter are about 4200 years and 0.59, respectively.[42]

SCC in the longitudinal direction is shown schematically in Figure 7.9a. Here, while perforation is not desirable, mainly, the result is leaking. The longitudinal SCC has no clear path for linking of cracks. Such perforations occurred in the transition piece as shown in Figures 5.1 to 5.5 and in welds D6 and D7 in Figures 5.10 to 5.12 of Section 5.0. However, in the latter, the temperature was lower, and the SCC has progressed only about 1.2 mm. No significant perforation in the CCW system piping is likely soon as described in Section 8.2.2.

SCC in the circumferential direction is shown schematically in Figure 7.9c, 7.9d and 7.9e and is more serious from a failure point of view. First, if the SCC proceeds fully around the periphery, the pipe sustains a double-ended pipe rupture, and the entire contents of the system can be quickly emptied. The question to be answered, then, is how immanent is such an event for the CCW system?

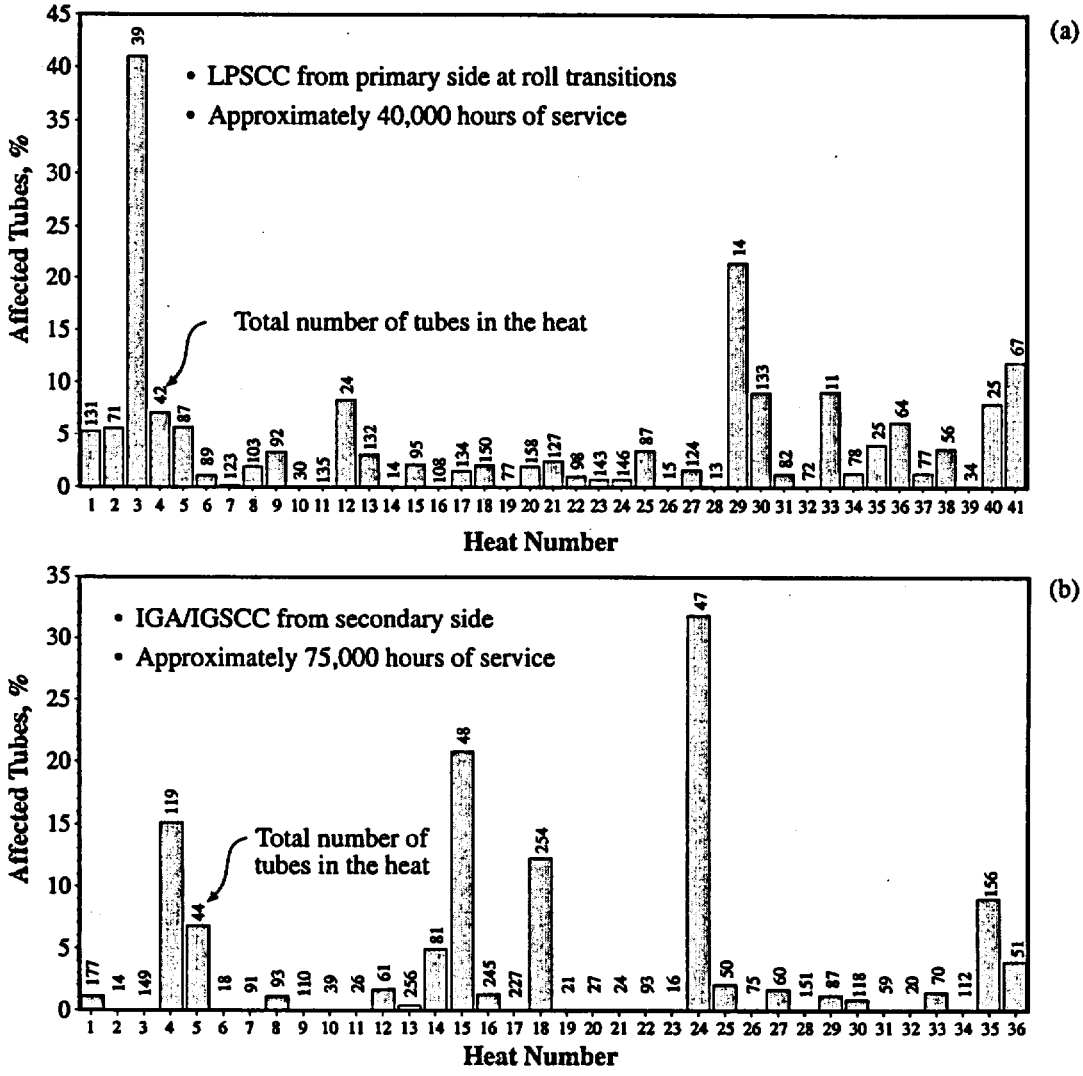

Figure 7.8 (a) Percent of tubes affected by LPSCC from the primary side of a PWR steam generator vs. heat number determined at roll transitions after approximately 40,000 hours of service. Primary surface temperature at this location is about 310°C. All heats are from the same manufacturer and were produced in the sequence shown. Environment is primary water. (b) Percent of tubes affected by IGA and IGSCC vs. heat number from the secondary side of a PWR steam generator in heat transfer crevices after approximately 75,000 hours of service. From Scott.[43]

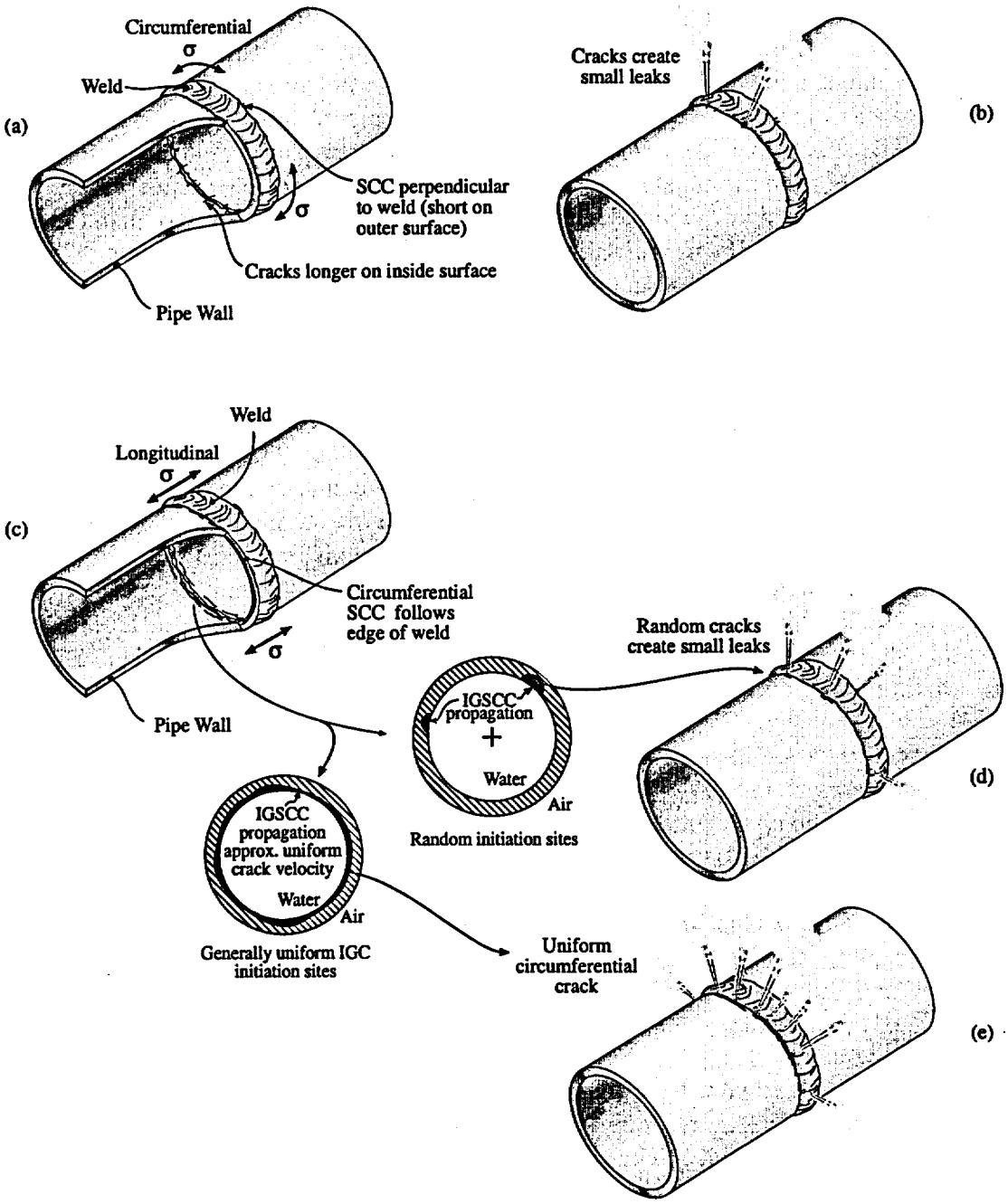

Figure 7.9 Schematic views of effects of direction of stress on the type of SCC. (a) and (b) Stress is circumferential and produces longitudinal SCC the length of which is limited by the stress field produced by the weld. Small leaks are the maximum damage that can be produced. (c), (d), and (e) Stress is longitudinal and produces circumferential SCC. If the initiation of SCC is random, as in (d), the resulting propagation will produce minor leaks. If the initiation is generally uniform around the periphery of the inside surface, the propagation can propagate around the circumference.

The Altran reports,[2,3,4,5,6] indicate that some of the specimens, which they examined as noted in Table 5.1, sustained circumferential SCC. They did not measure nor report the peripheral extent nor the depths of these SCC. The extent to which such SCC reach a critical extent in the combined peripheral and depth directions depends on the general uniformity of stress, the material conditions around the periphery, and the time required for initiation. For the piping studied here, it seems then that alloy structure in the region of the welds is not a significant factor in propagation. There are then two main questions affecting whether a uniformly circumferential SCC will develop. One is whether the stress is uniform around the circumference. Second, is whether the initiating conditions are generally uniform. These issues are illustrated in Figure 7.9 and are discussed in Section 7.3.7 in connection with Figure 7.47.

With respect to the uniformity of the initiating condition around the inner periphery, it appears that this is somehow related to the occurrence of the IGC shown in Figures 5.1, 5.2, 5.4, and 5.5. This IGC seems to be focused on one side or the other or both of the weld root. There were no specific studies of the uniformity of this IGC around the periphery. It is reasonable to assume that there is some uniformity since it was observed in the circumferential photomicrographs prepared by Altran[2,3,4,5,6] as well as the NRC and AECL work. In view of the consistent occurrence of IGC among the three laboratories it should be assumed that this IGC is uniform around the periphery and that there is a basis for initiating SCC around the periphery on more or less a uniform basis.

With respect to the uniformity of stress around the periphery, SCC was observed in most of the specimens examined by Altran and noted in Table 5.1. Since these specimens were from the same type of material and since their metallography was taken more or less randomly, it should be assumed that propagation around the periphery could be more or less uniform. Further, the rate of propagation in the plateau region is generally independent of the stress intensity. Such a condition would support also a generally uniform crack front. Thus, with the relatively uniform initiation conditions around the periphery and the relative uniform rate of propagation, assessing a break before leak (BBL) should be considered.

Altran did not investigate the circumferential extent of the SCC: i.e., using multiple metallographic cross sections around the periphery. Thus, there is no basis for assessing the possible circumferential SCC as illustrated in Figure 7.9.

The fact that the CCW system does not operate at high pressures mitigates against ready separation of the circumferential type. However, the possibility of such a mode of failure should be considered. The necessary stress for separation could come from fit-up stresses or other configuration stresses.

7.3 Dependencies of SCC on Primary Variables

In this section each of the primary variables as illustrated in Figure 7.3 is discussed as they relate to the CCW system and to the quantitative requirements both for prediction and recommending changes.

7.3.1 Electrochemical Potential

The variable of electrochemical potential is important to the CCW system since the environment contains dissolved oxygen with the result that a broad range of potentials can be realized as noted in Figure 7.1 and Figure 7.2. This broad range of potentials enables the occurrence of HPSCC in the range of relatively high potentials. This possibility of a broad range of potentials is the basis for some utilities using hydrazine in their CCW systems as described in Section 6.0 and Tables 6.1, 6.2 and 6.3. Hydrazine lowers the electrochemical potential, since it is a reducing species, and causes the potential to be relatively low and generally constant.

The primary variable of electrochemical potential relates directly to the concentration of oxygen in the environment as is shown in Figure 7.10. Considering the primary variable of electrochemical potential needs to (1) identify the minimum potential above which SCC occurs and (2) determine the rate at which SCC can proceed for the relevant potentials in the range of temperatures in the CCW system. These two topics are discussed in this section. Before a credible prediction can be discussed, the effects of temperature, as in Section 7.3.6, also need to be discussed. The combined contribution of these variables for predicting performance is discussed in Section 8.2.

The effect of dissolved oxygen on the open circuit electrochemical potential of steel is shown in Figure 7.10. The pattern shown in Figure 7.10 has been confirmed by many investigators. These results indicate that there is an approximately 600 mV increase in the open circuit potential as oxygen is added to deaerated water. Figure 7.10 also shows that above about 0.1 ppm of dissolved oxygen the potential does not change significantly. This effect of oxygen on the potential is important relative to the framework of potential and pH that can occur in the WCNOC CCW system as shown in Figures 7.1 and 7.2. These results mean that the line (5) in Figure 7.1 is defined by the upper plateau in Figure 7.10.

The potential, above which HPSCC can occur, is shown by Figure 7.11 although higher temperatures are emphasized. Figure 7.11a shows that SCC occurs readily above about –0.2 volts. This is well within the upper boundary of potential that is produced by dissolved oxygen as shown in Figure 7.10. A similar boundary of potential is shown in Figure 7.11b for work at 288°C. These figures, despite the data being at temperatures higher than the CCW system, show that the range of potentials sustained in the CCW system are within the range for HPSCC.

The crack velocity for A 508Cl2 steel in pure water as a function of oxygen concentration for various temperatures is shown in Figure 7.11b. Figure 12a shows the effect of oxygen on the average velocity of SCC for A 508Cl2 steel; and Figure 12b shows the effect of temperature for three concentrations of oxygen for a 533GrB steel. While these data are not at the temperature range of the CCW system, they come close; and extrapolations to temperatures of the CCW system are discussed in Section 8.2.

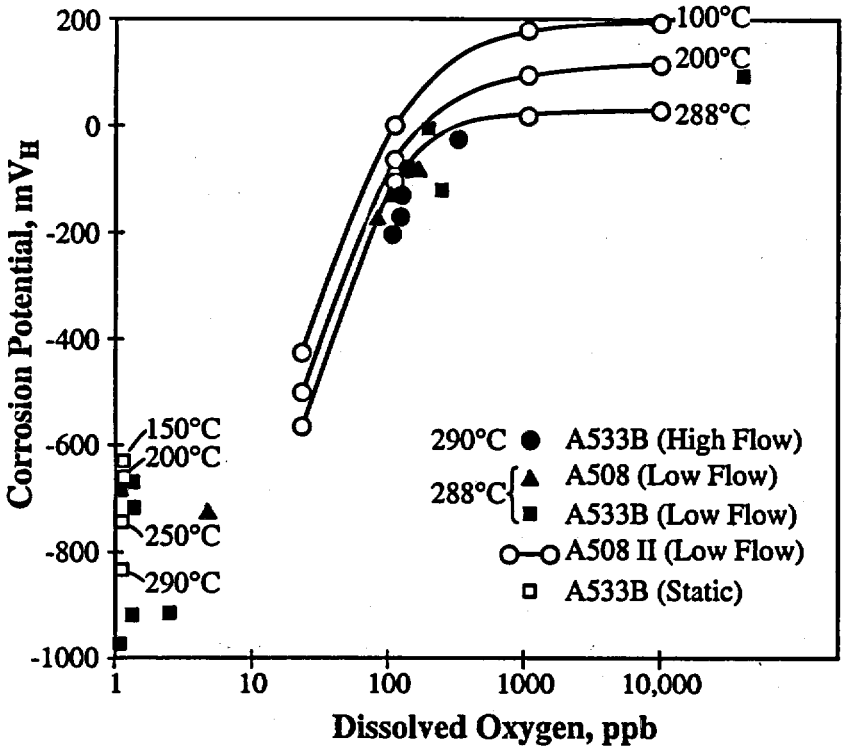

Figure 7.10 Corrosion potential vs. dissolved oxygen in pure water for pressure vessel steels at various temperatures. From Scott and Tice.[44]

Figure 7.13 shows the crack growth rate vs. dissolved oxygen for pressure vessel steels. Figure 7.13a shows the crack growth rate vs. oxygen for pressure vessel steel in 288°C water. It appears that the cyclic growth in fatigue is independent of the oxygen; whereas, the SCC data depend strongly on dissolved oxygen. In Figure 7.13b, a similar plot shows more data and comparisons with the literature. This figure provides an indication of the scatter of data in the literature.

Figure 7.14 integrates a large amount of data from various authors and shows the effect of potential on the crack growth rate as normalized by the temperature on the ordinate scale. These data show, again, that the potential of steel in the CCW system significantly exceeds the values above which HPSCC is significant. Figure 7.14 integrates effects of temperature by using an exponential expression on the ordinate to normalize the data.

While the CCW system is essentially one of oxygenated pure water, with the dilute additives of molybdate and tolyltriazole, and while this system does not sustain SCC so rapidly at the relatively low temperatures of the CCW system, SCC of mild steels occurs readily at these low temperatures but in more concentrated solutions; Figure 7.15 shows examples of the dependence of SCC on potential in these more concentrated solutions in the general range of temperatures sustained by the CCW system. These data are part of the data set that has been used by Parkins, Congleton and their colleagues[23,24,45] to prepare the mode diagram of Figure 7.2. Figure 7.15 is shown to indicate that SCC can occur readily at relatively low temperatures but in more concentrated solutions.

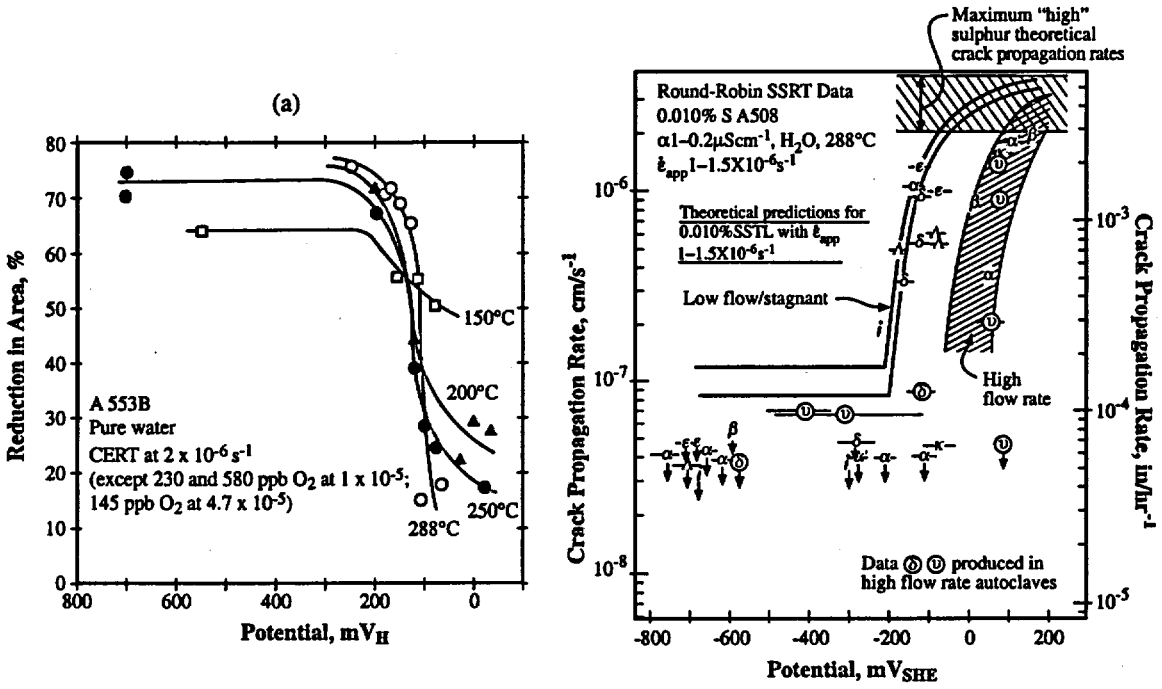

Figure 7.11 (a) Reduction in area vs. the open circuit potential inferred from the oxygen concentration as a function of temperature for steel. From Congleton et al.[45] (b) Crack propagation rate as a function of corrosion potential for an A508 steel at 288°C. From Ford et al.[46]

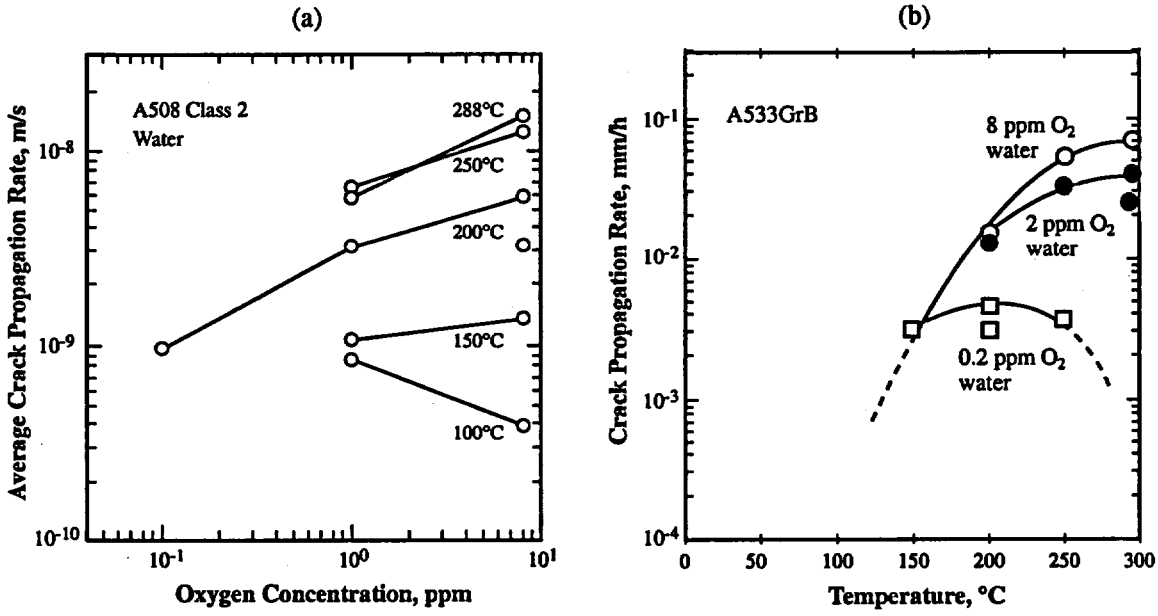

Figure 7.12 (a) Average rate of crack propagation as a function of concentration of oxygen for A508Cl2 steel in pure water for a range of temperature. From Waid and Ault.[47] (b) Crack propagation rate vs. temperature for three oxygen concentrations in pure water for A 533GrB. From Kuniya et al.[48]

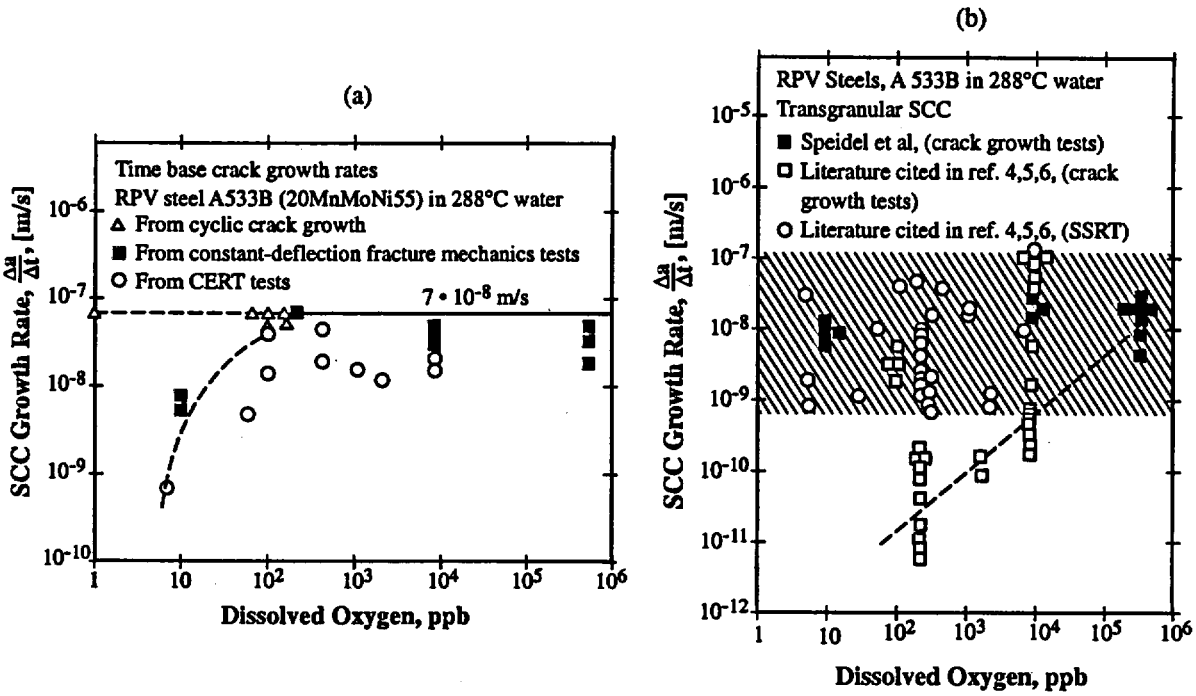

Figure 7.13 (a) SCC and CF crack growth rate vs. dissolved oxygen for a reactor pressure vessel steel, A 533B, in pure water at 288°C. From Speidel.[49] (b) SCC crack growth rate vs. dissolved oxygen for reactor pressure vessel steels exposed at 288°C in pure water. From Speidel and Magdowski.[50]

Figures 7.15a and 7.15b show the effects of potential on the SCC of mild steel in NaOH solutions. In one case, Figure 15a, three strain rates are tested; in the other three temperatures are tested. The potential at which SCC occurs is the same, except that different reference electrodes are used. Figure 7.15c shows the effect of potential on the details of corrosion morphology also for phosphate solutions; and Figure 7.15d shows the dependence of average velocity of SCC on the potential as a function of pH for two forms of phosphates, Na_3PO_4 and Na_2HPO_4 tested at room temperature. Thus, phosphate produces SCC over a broad range of pH and potential at room temperature in mild steels.

Figure 7.15e shows the effect of strain rate on the SCC in phosphate solutions tested at –1 V_{SCE}. Here SCC is in a 1M H_3PO_4 solution. These results show the clear dependence of SCC on strain rate.

Figure 7.15f shows the dependence of SCC measured as reduction in area vs. potential for temperatures to 90°C in a carbonate-bicarbonate solution. This environment is widely used for studying the SCC of pipeline steels.

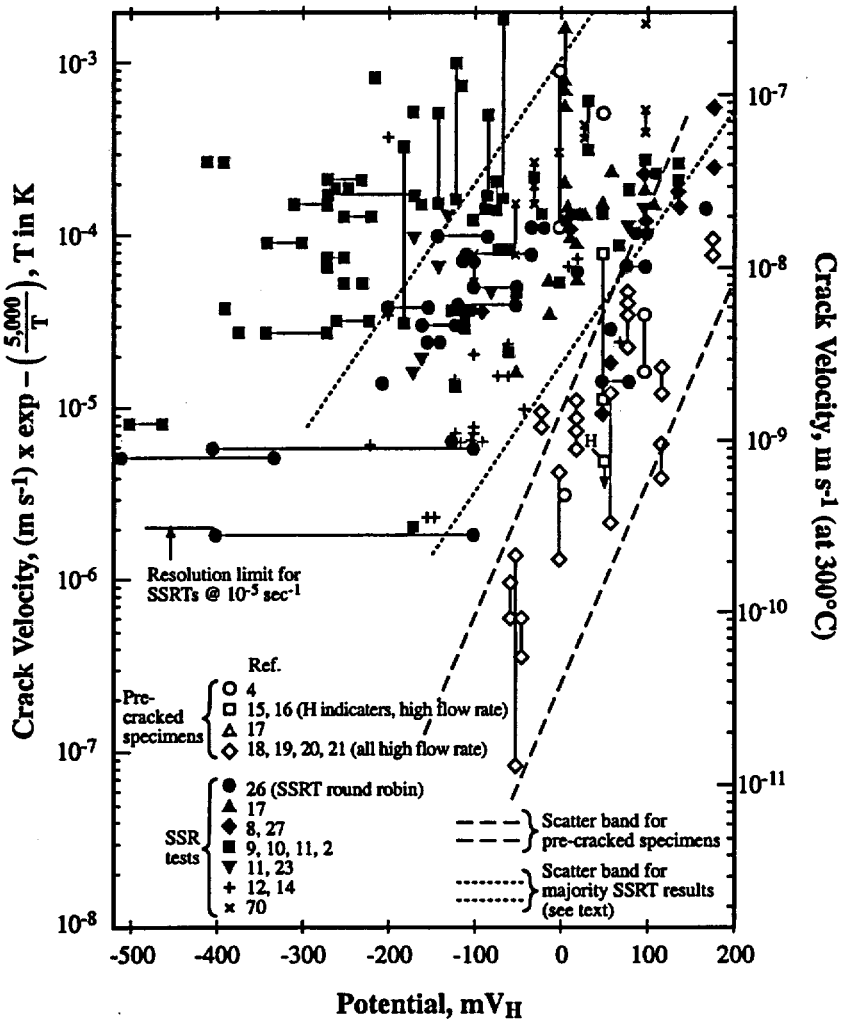

Figure 7.14 Crack velocity as normalized by temperature vs. potential for SCC of pressure vessel steels exposed to pure water where testing has been conducted both by statically loaded pre-cracked specimens and by CERT. From Scott and Tice.[44]

Figure 7.15g shows the effect of potential on the SCC of Alloy En25 in 1M ammonium acetate at pH 7 at 90°C. As with all of SCC, there are transitions from hydrogen embrittlement, to ductile, to general corrosion, to SCC and to ductile morphologies.

Figures 7.15h, 7.15i, and 7.15j show various views of SCC in nitrate solutions. Nitrates are significant here because there has been some speculation, as in Table 6.4 based on the 1995 report of DEI,[1] that the SCC in several plants has resulted from the microbial oxidation of nitrite inhibitors to nitrate and subsequent SCC according to well known effects of nitrate environments producing SCC of steel. Figure 7.15h shows the effect of potential and temperature on the SCC of mild steel in a nitrate solution where lowering the temperature lowers the onset of SCC. Figures 7.15i and 7.15j show the combined effects of nitrate and nitrite. Figure 7.15i shows that adding nitrite to nitrate inhibits the SCC for a potassium nitrate solution by raising the minimum potential for the onset of

SCC. Figure 7.15j shows an integrated interaction of potential and nitrite on the SCC of a C-Mn steel in boiling 8M KNO_3 tested with CERT. Clearly, the nitrite inhibits SCC even in the concentrated solution in which tests were carried out. Figures 7.15i and 7.15j indicate that the microbially induced oxidation of nitrite to nitrate would be unlikely to produce a sufficiently large relative amount of nitrate that would produce SCC in the presence of the original nitrite. Further, it is likely that the non-oxidized nitrite would inhibit SCC in nitrate.

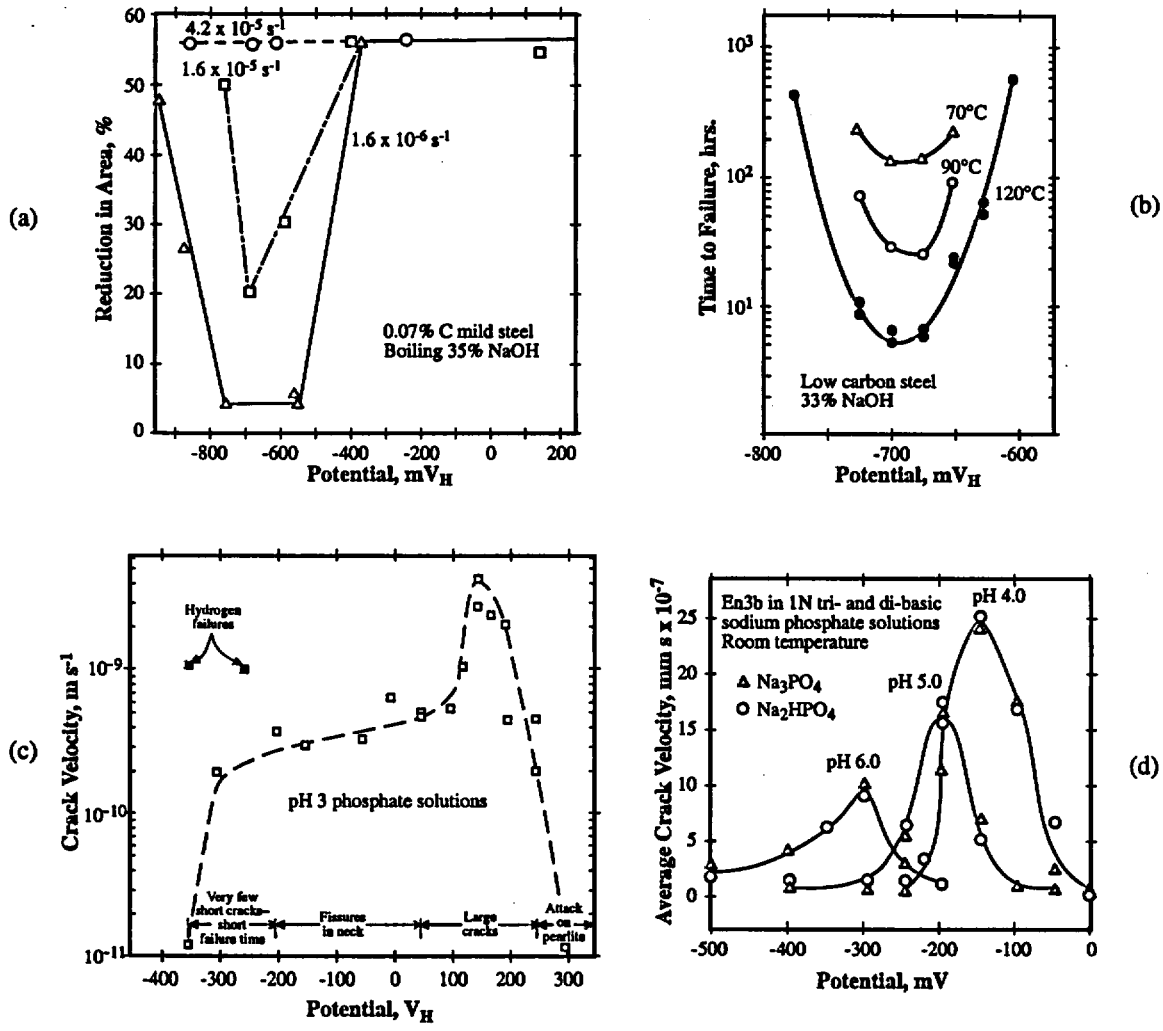

Figure 7.15 (a) Reduction in area vs. potential for mild steel exposed in boiling 35% NaOH tested at three strain rates. From Parkins et al.[51] (b) Time-to-failure vs. potential for three temperatures for a low carbon steel in 33% NaOH. From Singh[52] reporting on Bohnenkamp.[90] (c) Crack velocity vs. potential for a mild steel (two steels used: 0.23 w/o C and 0.88 Mn and 0.14 C at 0.91 Mn) tested in Na_2HPO_4+ H_3PO_4 at pH 3 showing morphologies of corrosion. From Parkins et al.[53] (d) Average crack velocities vs. potential for En3b (w/o C 0.12, Si 0.05, Mn 0.81, S0.029, P 0.008) steel in Na_3PO_4 and Na_2HPO_4 tested at RT function of pH. From Holroyd.[13]

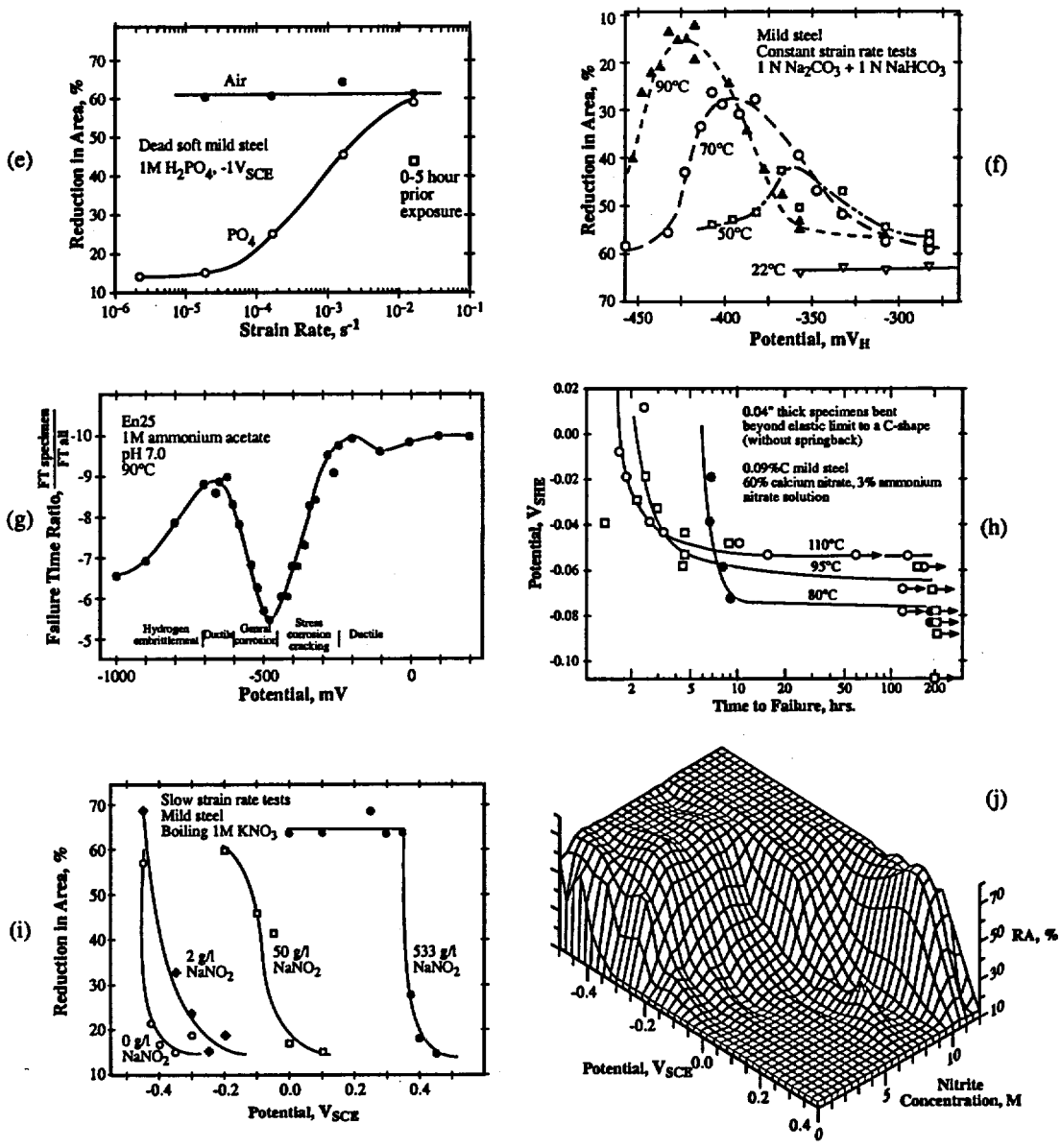

Figure 7.15 (e) Reduction in area vs. strain rate for a dead soft mild steel in air and 1M H_2PO_4 at $^-1.0$ V_{SCIE}. From Parkins.[54] (f) Reduction in area vs. potential for mild steel exposed to carbonate-bicarbonate solutions at various temperatures and tested in CERT. From Ogundele.[55] (g) Failure time ratio (failure time in solution vs. failure time in oil) of En25 steel (w/o C 0.35, Si 0.28, Mn 0.66, S 0.005, P 0.001, Ni 2.54, Cr 0.67, Mo 0.58) vs. potential for 1 M ammonium acetate at 90°C and pH 7.0 tested in CERT at $2x10^{-6}$ sec^{-1}. From Holroyd.[13] (h) Potential vs. time-to-fail for three temperatures for mild steel (0.09%C) exposed in a 60% $CaNO_3$+3% NH_4NO_3 solution. From Mazille and Uhlig.[56] (i) Reduction in area vs. potential for mild steel exposed in boiling 1M KNO_3 in CERT as a function of concentration of NaOH. From Parkins.[57] (j) Reduction in area vs. potential and concentration of nitrite for a C-Mn steel in boiling 8M KNO_3 tested in CERT. From Parkins.[58]

7.3.2 pH

The variable of pH is important because small changes produce large changes in the solubility of iron as shown in Figure 7.2. Increasing the solubility increases the corrosion rate and permits more rapid SCC. Thus, changes in the pH at Wolf Creek, as identified in Table 4.4 could influence both general corrosion and SCC.

Figures 7.1 and 7.2 show that iron oxide is most insoluble in the range of 12.3. This means that iron-base alloys will be the most optimally corrosion resistant at this pH. These diagrams also indicate that oxygen will raise the potential (see line (5) of Figure 7.1) into the range where Fe_2O_3 is stable. Fe_2O_3 is more insoluble and therefore more resistant to corrosion than Fe_3O_4.

Figure 7.2 provides the main insight into the effect of pH on SCC and shows that a minimum in the combination of AkSCC and AcSCC occurs at the solubility minimum for the oxides. However, it is not clear that either of these submodes is relevant to the CCW system. Rather, it appears that the HPSCC submode is relevant as shown clearly in connection with the development of Figure 8.1, but there is little information on the pH dependence of this submode. In principle, this submode is probably independent of pH since it is more defined by the breakdown of the protective films at higher potentials; on the other hand, it could be dominated by the solubility of Fe_2O_3 or (Fe, Mo)O_x which would suggest a strong dependence on pH. Regardless, the correct expectation for the dependence of HPSCC on pH is not known.

It is probably reasonable to keep the pH relatively high in order to minimize the solubility of iron and to minimize SCC if it were to depend on pH.

7.3.3 Species

The category of "species," as one of the seven primary variables as identified in Figure 7.3, is concerned with those species mainly that are not so critical to potential or pH. The nominal chemistry of the CCW system is discussed in Section 4.0 with Tables 4.2, 4.3, and 4.4. The species of specific interest to the CCW system are the following:

1. Oxygen: Oxygen is important mainly as it affects the potential as described in Section 7.3.1. Its main effect on affecting the electrochemical potential is shown in Figure 7.10. Oxygen is not included in this section but in 7.3.1.

2. Molybdate: Molybdate is included in this section since it is an important addition in the CCW system as a corrosion inhibitor. The addition of molybdate as an inhibitor to the CCW system and its concentration over time are described in Section 4.0.

3. Tolyltriazole: Tolyltriazole is included in this section since it is added specifically as an inhibitor to minimize the corrosion of the copper alloy tubes of the heat exchangers in the CCW system. The addition of tolyltriazole as an inhibitor is described in Section 4.0.

4. Chloride: Chloride is present in small amounts, as shown in Tables 4.4 and 4.5, but is the only significant impurity present in the CCW system. Its concentration is in the range of several tens of ppb and is therefore not important, especially since there is no means for concentrating it as there is in heat transfer crevices in steam generators.

5. Microbes and fungi: Microbes and fungi are often important in water systems as they produce metabolic products that are corrosive or lead to corrosion. However, there are negligible nutrients in the CCW system and microbes and fungi cannot grow. The work of B. Little[17] shown in Appendix 1.0 for this project as well as the summary in Section 4.5 indicate the microbes and fungi have not caused nor can the present species produce aggressive corrosion. The reports of Altran[2,3,4,5,6] conclude the same.

6. Nitrites: While nitrites as inhibitors are used in CCW systems in the nuclear industry, as shown in Tables 6.1, 6.2, and 6.3, they are not used at the WCNOC. However, the 1995 report of DEI, as shown in Table 6.4, identified three cases of SCC in CCW systems that they attributed to the oxidation of nitrites to nitrates, which, in turn, were hypothesized to produce SCC. A discussion of nitrites and nitrates is important in this section; and the SCC observed in these other cases, as suggested in the DEI report, is probably more related to the type of HPSCC observed at Wolf Creek with the matter of nitrites and nitrates being unimportant.

7. Sulfur: Sulfur species were observed in the Altran studies[2,3,4,5,6] in significant amounts as shown in Tables 4.8 and 4.9. The presence of such relatively large amounts of sulfur indicates possibly the presence of SRB at WCNOC as well as at the utilities identified in Table 6.4. However, there is not sufficient sulfate in the water, as shown in Section 4.0, to provide the necessary nutrient for the action of SRB. Possible action of SRB are not considered here based especially on the findings of Little in Appendix 1.0.

The specific species of interest are discussed as follows:

1. Pure water including oxygen

The role of oxygen is discussed in detail in Section 7.3.1. Mild and low alloy steels sustain SCC in high purity water containing oxygen. Generally, the intensity of such SCC increases as the potential (or oxygen) increases. SCC of mild and low alloy steels in pure water has been studied for both PWR and BWR applications in pressure vessels and piping as well as for turbines. This work has included a range of oxygen concentrations for both PWR and BWR applications.

There is a definable submode of SCC, high potential SCC (HPSCC) that is distinguished from AkSCC and AcSCC, and this is shown on Figure 7.2. The latter two require that certain acidities or alkalinities are present; these submodes also depend on potential as shown in Figure 7.15. The minimum potential above which HPSCC of steels occurs is described in Section 7.3.1 and shown in Figures 7.11 and 7.12. As shown in Figure 7.1, the range of potentials that can exist in the CCW system can readily support the occurrence of HPSCC.

2. Molybdate

Molybdate is widely used as an inhibitor for steels exposed to aqueous solutions at temperatures up to at least 100°C. Molybdenum is used both as a dissolved species, i.e. the molybdate, and as an alloy species. In general, it appears that molybdenum functions in the same way in both applications. One of the attractions of molybdate is its lack of toxicity, while at the same time providing good inhibition.

When the potential-pH diagram for Mo in water is assessed, it appears that molybdenum is almost totally soluble. It would seem from such properties, that Mo would provide no inhibition in terms of insoluble compounds by comparison with chromium and iron where the inhibitive predictions are solidly based on thermodynamic predictions. On the other hand, there seem to be two regimes for the inhibitive action of the molybdates.

1. The first basis was recognized by Pourbaix and is shown in Figure 7.16 in the E-pH diagram for Mo in water. This basis for inhibition occurs both in the formation of MoO_3 and MoO_2. The MoO_3 is effective in minimizing pitting, i.e. as the pH in the pit

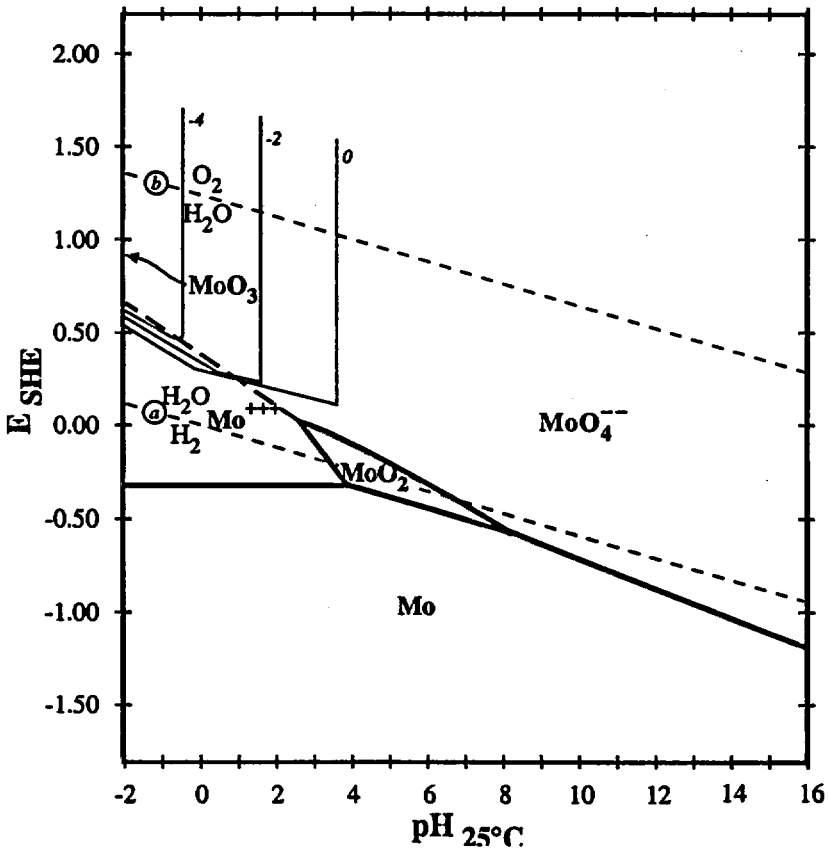

Figure 7.16 Potential vs. pH for molybdenum in water at 25°C. States of molybdenum noted. From Pourbaix.[22]

decreases, the molybdenum becomes less soluble, especially in the range of potentials where the passivity of iron-base alloys breaks down. The MoO_2 is effective over only a modest range of potentials and at generally mildly acidic pH. This compound does not appear to provide significant protection based on Figures 7.19 and 7.21a. The role of molybdates in forming the insoluble MoO_3 is most likely the basis for the success of Mo as an alloying addition in Type 316 stainless steel.[59]

2. The second basis for the beneficial effect of Mo has been more empirical. It has been established experimentally that molybdenum is an effective inhibitor in the range of neutral and alkaline pH despite the solubility shown in Figure 7.16. On the other hand, Figure 7.16 shows that the MoO_2 is not stable above about pH 7 nor is there a broad range of stability in the direction of potential even to pH 2. This suggests that Mo at higher values of pH does not act by forming insoluble MoO_2; but rather acts by forming a mixed oxide of greater stability than Fe_3O_4, over a broader range of pH, when compared with Figure 7.1. The additional stability of such mixed oxides is a well established pattern as with the mixed oxides of: $(Fe,Cr)O_x$ which accounts for the stability of stainless steels and high nickel alloys; the $(Ni,Cr)O_x$ which accounts for the stability of the family of Alloy 600, 690; and the $(Fe,Ni,Cr,Zn)O_x$ which accounts for the beneficial effects of zinc additions in water cooled nuclear plants. Possible inhibition due to the formation of a mixed $(Fe,Mo)O_x$ has been suggested by Robertson and others as shown in Figure 7.29. This seems to be the most plausible interpretation for inhibition at mid-to alkaline pH as well as over a range of potentials. However, such a mixed oxide for $(Fe,Mo)O_x$ does not seem to be characterized by good thermodynamic constants as do the mixed oxides of Fe, Cr, and Ni.

Empirically, it appears that both effects produce improved alloys as well as good inhibitors via the addition of molybdenum.

A good overview of the effects of molybdate additions is shown in Figure 7.17 where the effects of concentration, pH, and temperature in low hardness water are shown using dynamic polarization scans. Here, increasing the concentration of molybdate through 2000 ppm lowers the passive current density. This benefit improves as the pH is increased from pH 3.0 to 9.0. The effect decreases as the temperature is increased from 21 to 60°C. Note that these data have been determined by dynamic polarizations so that the curves tend to occur at higher currents than for steady state, potentiostatic, or open circuit control.

Figure 7.18 shows some finer gradations for the polarization results. Figure 7.18 shows results from aerated DI water with concentrations from 50 to 500 ppm MoO_4^{2-}. Figure 7.18a is best compared with Figure 7.17c. These figures differ in several ways. First, owing to the aeration of the environment in Figure 7.18a, the corrosion potential is about 600 mV higher and in accord with the data of Figure 7.10. Second, the passive current densities in the DI water are much lower than those in the low hardness water. Third, in both cases the passive current densities decrease with increasing concentrations of MoO_4^{2-}. Fourth, the anodic peaks in Figure 7.17c compared with Figure 7.18a are lower and would decrease in potentiostatic or steady state experiments.

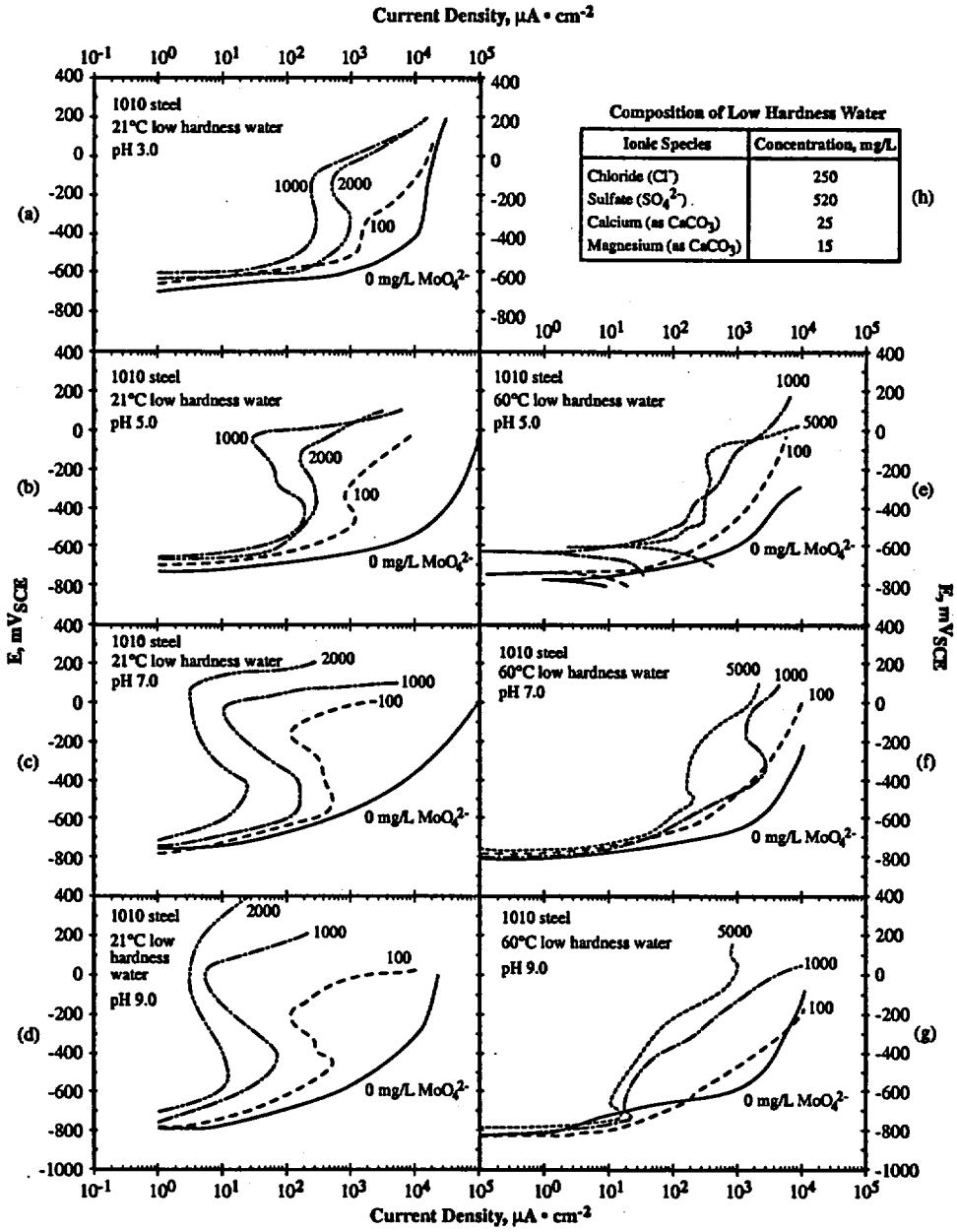

Figure 7.17 Potential vs. current density as a function of concentration of molybdate from 0 to 2000 ppm, pH from 3.0 to 9.0, and temperature at 21 and 60°C for an SAE 1010 steel exposed to an deaerated synthetic low hardness water containing Cl 250 mg/L, SO_4^{-2} 520, Ca^{2+} 25 and Mg^{2+} 15. The pH of each solution adjusted with NaOH or H_2SO_4 as required. Potentiodynamic data taken at 0.2 mVs^{-1}. (a) 21°C, pH 3; (b) 21°C, pH 5; (c) 21°C pH 7; (d) 21°C pH 9; (e) 60°C, pH 5; (f) 60°C, pH 7; (g) 60°C, pH 9; (h) Table with composition of synthetic low hardness water. From Stranick.[60]

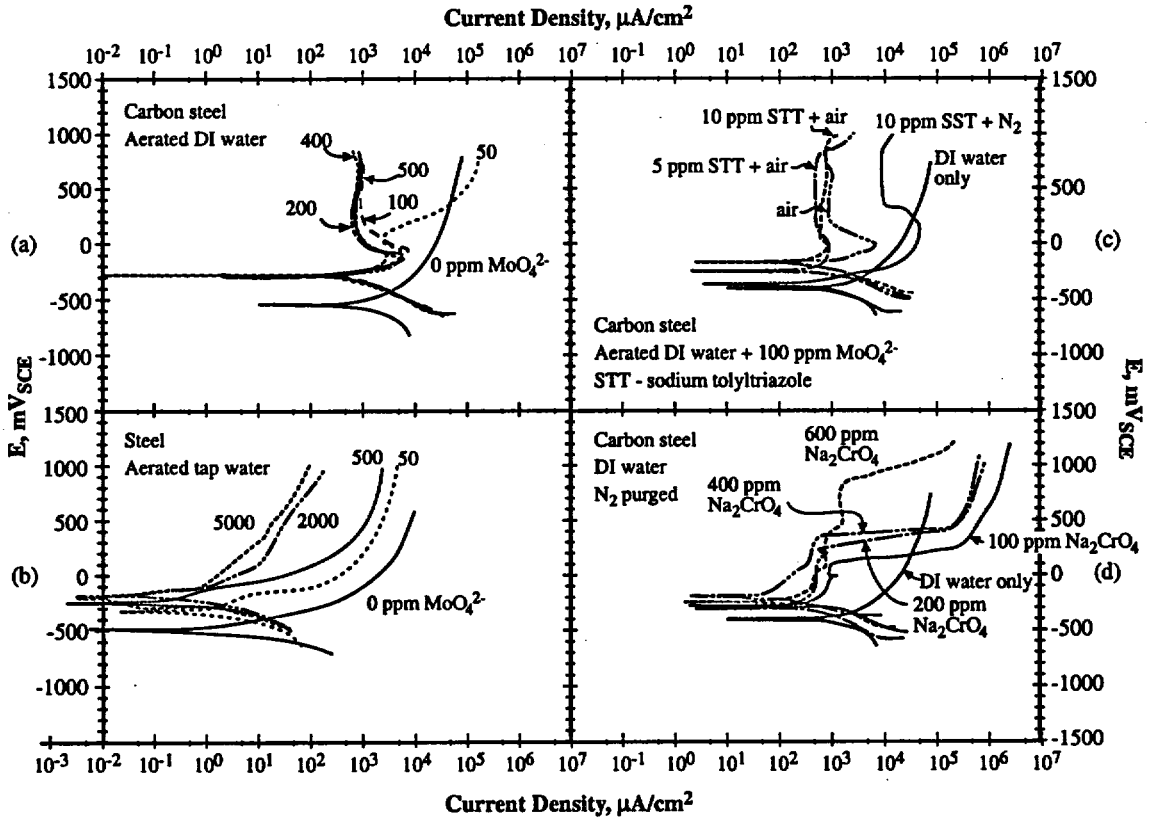

Figure 7.18 (a) Potential vs. log current density for carbon steel exposed to aerated DI water with varying amounts of Na_2 and MoO_4^{2-} at RT using potentiodynamic polarization with a scan rate of 0.1 mVs^{-1}. From Alexander and Moccari.[71] (b) Potential vs. log current density for steel in aerated and simulated tap at RT with varying amounts of MoO_4^{2-}. Tap water low hardness with 250 mg/L Cl, 520 of sulfate, 25 of calcium, and 15 of magnesium at RT. From Oung and Wang.[61] (c) Potential vs. log of current density for DI water with MoO_4^{2-}, STT, and aeration and deaerated environments at RT. From Alexander and Moccari.[71] (d) Potential vs. log current density for aerated DI water with additions of Na_2CrO_4 at RT. From Alexander and Moccari.[71]

A broader set of data showing the effect of MoO_4^{2-} but in the aerated condition is given in Figure 7.18b where concentrations from 0 to 5000 ppm are used in aerated and simulated tap water. These data should be compared with Figure 7.17c, and the results seem similar.

Figure 7.18c shows the effect of sodium tolyltriazole STT in addition to the MoO_4^{2-} in cases of being aerated and nitrogenated (deaerated). Here, the STT lowers the anodic peak significantly, and the passive current densities are not changed significantly. A

surprising observation in Figure 7.18c is the high value for the curve for the MoO_4^{2-} with STT and N_2 bubbling. These data are not consistent with those in Figure 7.17.

Finally, for background, Figure 7.18d shows the effects of chromates that can be compared with data for molybdates over the range to 600 ppm. In the passive range the current densities are not significantly different. However, the protection conferred by chromate breaks down at relatively low potentials. This results from the transition of the Cr_2O_3 to the CrO_4^{2-}.

A general view of the effect of the concentration of molybdates is shown in Figure 7.19 where the open circuit potential is plotted vs. the concentration of molybdates for 21°C and various values of pH. Here, it is clear that a substantial improvement in corrosion resistance occurs at pH 5.0 and above. This is evident from the increase in potential that is due to the formation of a stable passive film. It is also clear that a large fraction of the beneficial effect of molybdate in the low hardness water occurs by 100 ppm, but the benefit of molybdate increases at higher concentrations. Figure 7.19 also shows that the MoO_2 is not significantly protective by comparison with Figure 7.16 since the protective quality of the molybdate is much less in the range of stability of MoO_2, i.e., below pH 6.

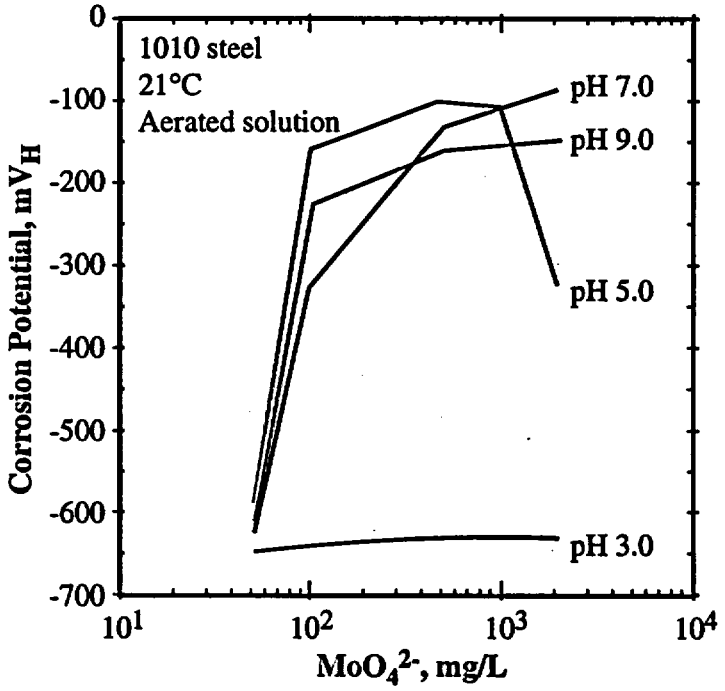

Figure 7.19 (a) Open circuit potential vs. concentration of molybdate for four values of pH at 21°C exposed to aerated synthetic low hardness water. From Stranick.[60]

Studying the corrosion of steel and projecting data forward sometimes requires acceleration. One means for accelerating corrosion is to conduct tests with a galvanic couple, and for steel a practical couple is comprised by copper and steel. A couple

between copper and steel is also a model for such couples in hot water systems. A series of experiments has been conducted to evaluate effects of molybdate inhibitors by Mustafa and Shahinoor Islam Dulai[62] using steel-copper couples exposed to a simulated cooling water. Effects of area ratio and pH on these couples are shown in Figure 7.20. Figure 7.20a shows the expected result of the steel corroding more rapidly when coupled and Figure 7.20b shows the expected result of the corrosion rate of steel increasing with the copper/steel area ratio.

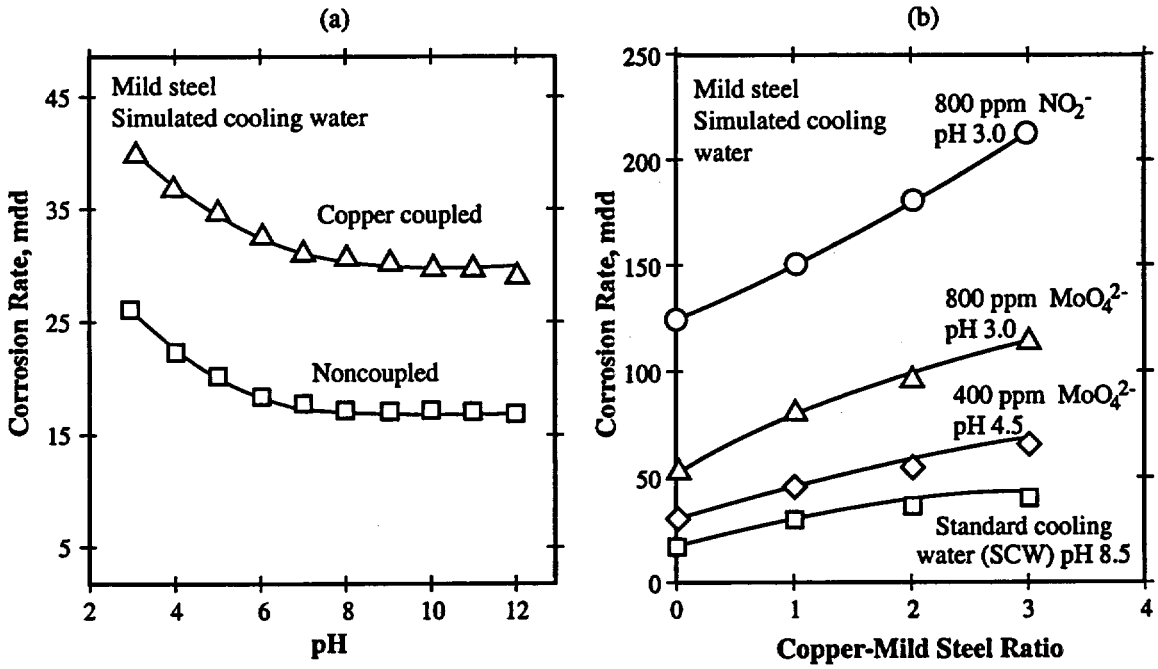

Figure 7.20 (a) Corrosion rate vs. pH for the coupled and non-coupled condition for mild steel/copper couples. (b) Corrosion rate vs. copper/steel area ratio. From Mustafa and Shahinoor Islam Dulai.[62]

The effect of concentration of MoO_4^{2-} is shown in Figure 7.21. Figures 7.21a and 7.21b from Mustafa and Shahinoor Islam Dulai[62] show the effect of MoO_4^{2-} on the corrosion rate from pH 3.0 to pH 9.0. Here, the corrosion rate begins to decrease with increasing pH; and at pH 5 the corrosion rate begins to decrease significantly. The corrosion rate decreases at pH 6 and by pH 9 it is significantly decreased. Also, these data show that the optimal amount of molybdate is in the range of 500 ppm similar to the result of Figure 7.19. Figure 7.21c shows a similar result in low hardness water for a mild steel.[61] As with Figure 7.21b, the optimum concentration of MoO_4^{2-} is about 500 ppm. Figure 7.21d shows that increasing the MoO_4^{2-} decreases the corrosion rate even at 200 ppm, which is the highest concentration used.

The interactions of MoO_4^{2-} with chloride and sulfate are shown in Figure 7.22. Figure 7.22a shows that at 250 mg/L of MoO_4^{2-} up to 100 mg/L chloride does not increase the rate of corrosion significantly, and a similar result applies to the effect of sulfate as

shown in Figure 7.22b. Increasing these impurities increases the rate of corrosion, but the concentration of 250 mg/L of MoO_4^{2-} tends to be optimum although higher concentrations were not investigated.

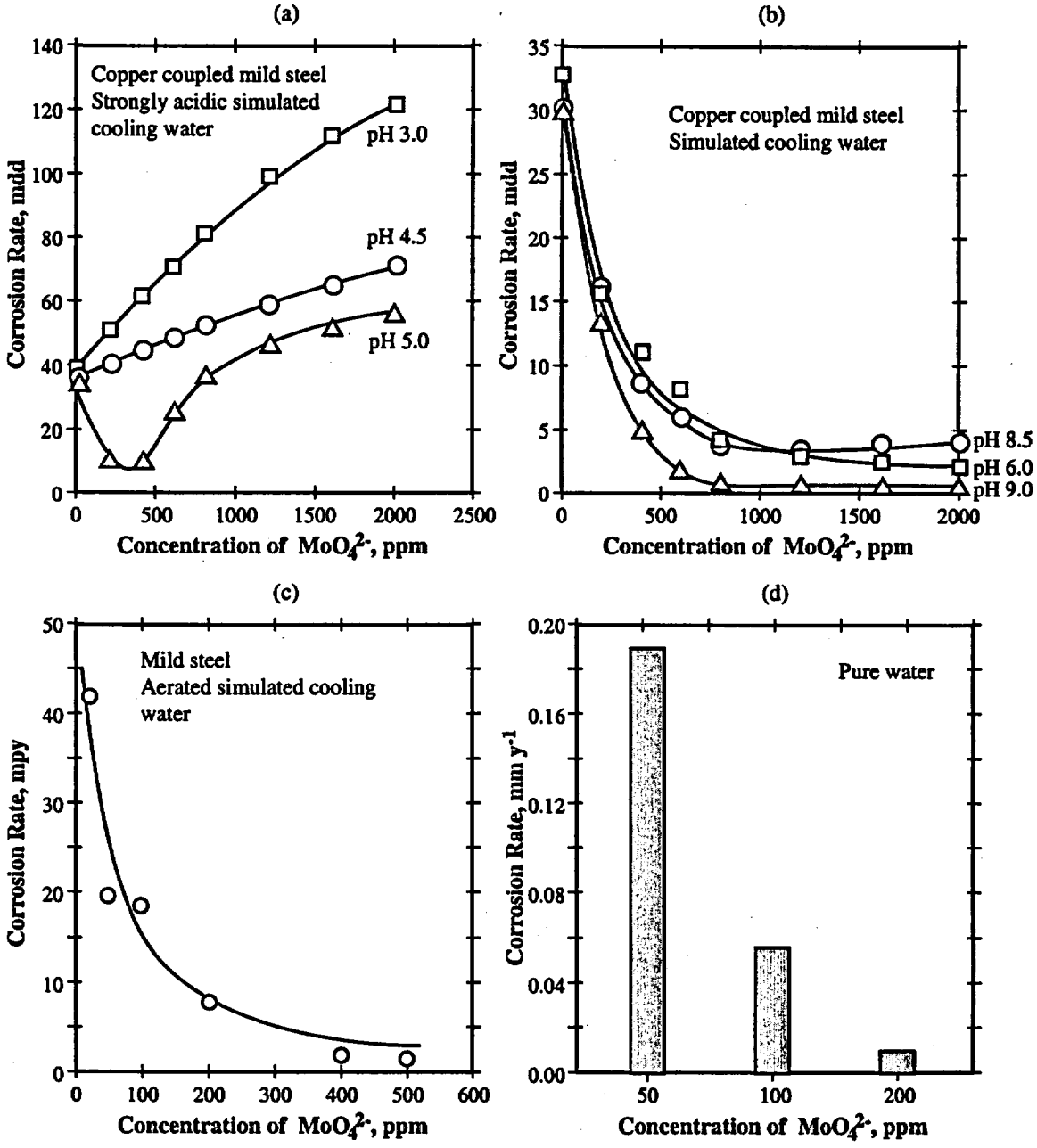

Figure 7.21 (a) (b) Corrosion rate vs. concentration of MoO_4^{2-} in simulated cooling water for a mild steel from pH 3.0 to pH 9. From Mustafa and Shahinoor Islam Dulai.[62] (c) Corrosion rate of mild steel in low hardness (Cl 250 mg/L, sulfate 520, Ca 25, Mg 15) vs. MoO_4^{2-}. From Oung and Wang.[61] (d) Corrosion rate vs. concentration of MoO_4^{2-} in solutions containing only MoO_4^{2-} for AISI 1020 steel at 27°C. From Torres et al.[63]

Table 7.1 shows results from studying the combined effects of MoO_4^{2-}, Cl^-, and temperature in an aerated solution on the corrosion of cold rolled 1010 steel. Here, it seems that the optimum concentration of MoO_4^{2-} is about 500 ppm.[64]

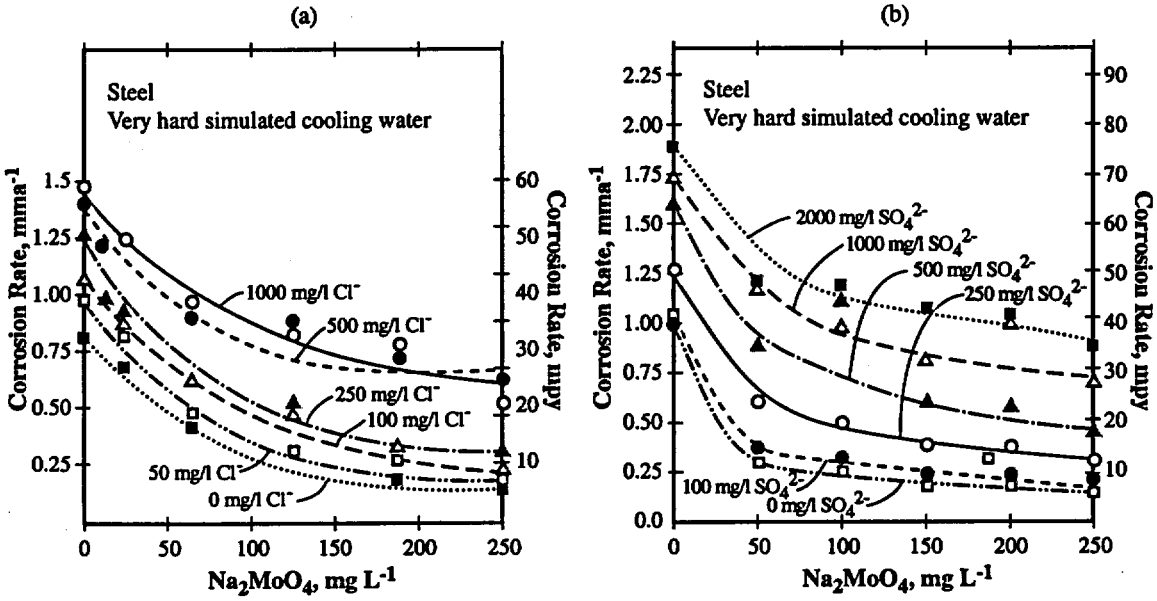

Figure 7.22 (a) Corrosion rate vs. concentration of Na_2MoO_4 for concentrations of chloride from 0 to 1000 mg/L. Experiments using very hard water with mild steel at 25°C. (b) Corrosion rate vs. concentration of Na_2MoO_4 for concentrations of chloride from 0 to 2000 mg/L. Experiments using very hard water with mild steel at 25°C. From Robitaille.[65]

Table 7.1

Corrosion Rates for Cold-Rolled Steel, 1010 as Affected by Concentration of Molybdate, in Aerated Solutions Containing 352 ppm SO_4^{2-}, 123 HCO_3^- and 14 ppm CO_3^{2-} at Two Temperatures and Two Concentrations of Cl^-. From Lizlovs.[64]

Conc of $Na_2MoO_4 \cdot 2H_2O$, ppm	Corrosion Rate, mg-dm^{-2}day^{-1}			
	152 ppm Cl^-		304 ppm Cl^-	
	RT	70°C	RT	70°C
0	105	157.0	129	85.0
5			85	
10			104	
50			69.8	
100	48.7	222.0	65.5	124.0
250	nil	44.2	7.8	71.6
500	nil	15.2	0.1	10.0
750	nil	4.2	nil	5.1
1000	nil	5.5	nil	1.1

The effects of pH and hardness as affected by the concentration of MoO_4^{2-} are shown in Figure 7.23. Figure 7.23a[62] shows that, with increasing pH, a pH of 6 seems to be the value above which the corrosion rate does not change significantly for both 200 and 800 ppm in the coupled and non-coupled cases. This is the same result as shown in Figure 7.21. A similar result is shown in Figure 7.23b where the lowest pH is 5.5. While there is a clear benefit of pH 9.5 compared with pH 5.5, the difference is not so large as shown also in Figure 7.23a. In Figure 7.23b, again, the optimum concentration of Na_2MoO_4 seems to be in the range of 500 mg/L. Figure 7.23c, which compares hardness, shows also that 500 ppm MoO_4^{2-} is optimum for three different harnesses.

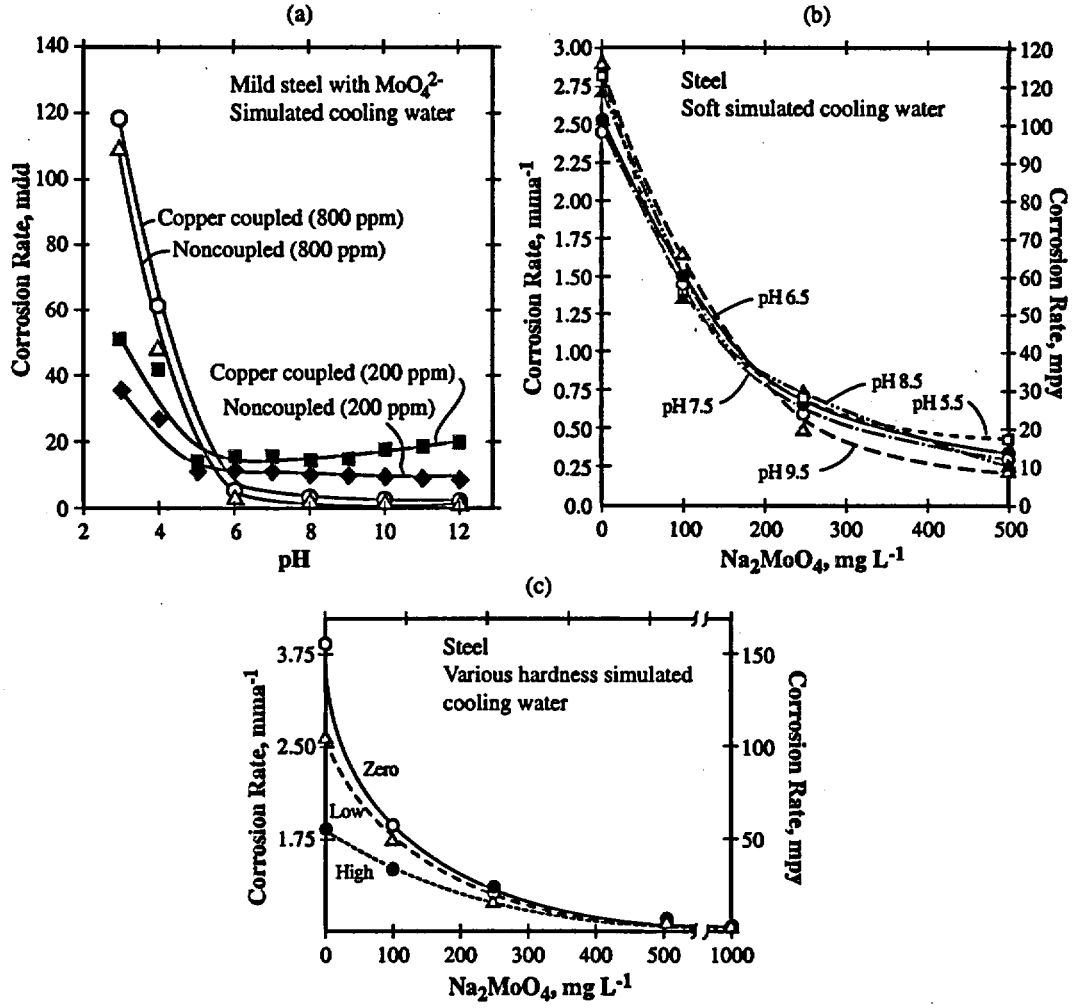

Figure 7.23 (a) Corrosion rate vs. pH for 200 ppm concentrations of Na_2MoO_4 in the coupled and non-coupled cases for simulated cooling water for mild steel. From Mustafa and Shahinoor Islam Dulai.[62] (b) Corrosion rate vs. concentration of Na_2MoO_4 for pH of 5.5 to 9.5 at 49°C for mild steel in soft simulated cooling water (Ca^{2+} 25 mg/L, Mg^{2+} 15, Cl^- 250, SO_4^{2-}520, $NaHCO_3$ 170, Na_2CO_3 25). From Robitaille.[65] (c) Corrosion rate vs. Na_2MoO_4 for mild steel for three hardnesses of water at 49°C and pH of 8.5. From Robitaille.[65]

The effect of molybdate on the initiation of fatigue damage to 1020 mild steel has been studied by Husain et al.[66] in three different environments including air, tap water and brine. This work was carried out at RT with a cyclic frequency of 1.65 Hz. Figure 7.24 compares results for the initiation of SCC as a function of concentration of MoO_4^{2-}. Here, initiation was defined as the number of cycles required to penetrate 0.25mm. This work shows that molybdate substantially increases the time to initiate, i.e., inhibits initiation.

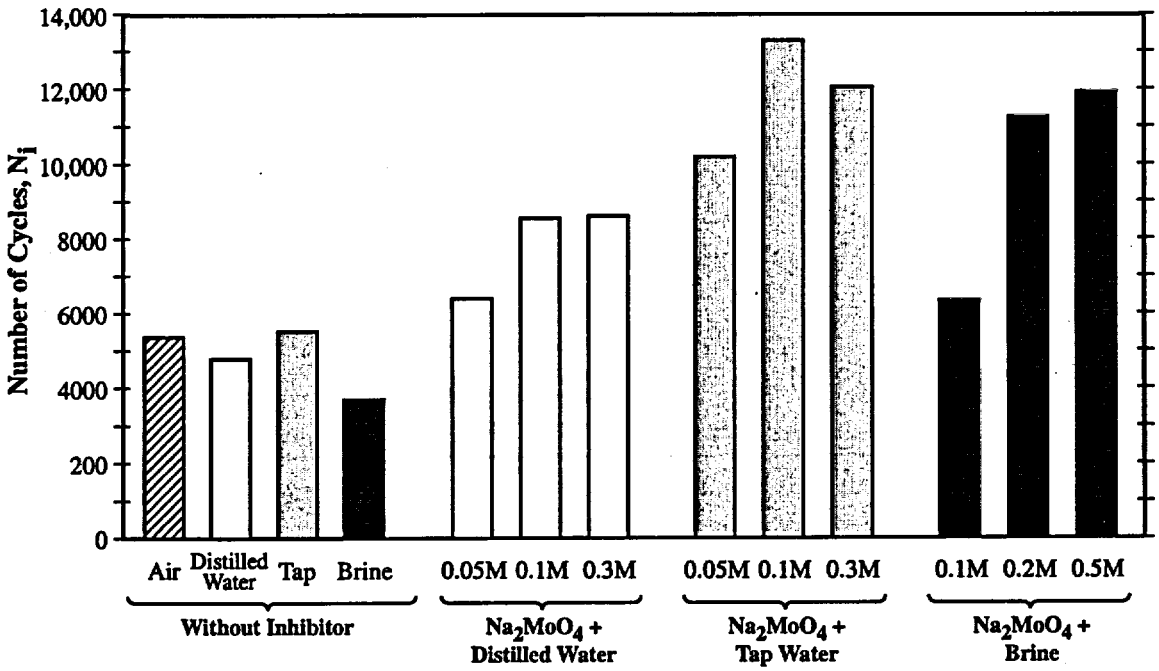

Figure 7.24 Number of cycles required for crack initiation to 0.25mm depth at 1.65 Hz for a mild steel using a notched bar exposed to full bending for three concentrations of Na_2MoO_4 at RT. From Husain et al.[66]

Figure 7.25 shows fatigue crack growth rates that correspond to the initiation in Figure 7.24. In Figure 7.25, the fatigue crack growth rates are measured as a function of stress intensity in the same environments as in Figure 7.24. These data show, not surprisingly, that the crack growth rate in dry air is the slowest although the increment relative to the aqueous environment is probably not significant. Further, the inhibitor is effective in reducing the crack propagation rate in the 0.05M and 0.1M concentrations. Similar inhibition was observed in the case of samples tested in inhibited distilled water except that the inhibition is more effective in 0.1M and 0.3M concentrations. On the other hand the crack growth rate tested in brine was independent of the concentration of inhibitor. The morphology for all cracking was transgranular.

The effectiveness of various inhibitors on the fatigue crack growth rate of Type 4340 steel is shown in Figure 7.26. A notched bar was used for testing and the cyclic frequency was 0.167Hz. The inhibitors were dissolved in an organic solution of a phase

transfer catalyst of Adogen 464 which is a methyl trialkyl (C_8-C_{10}) ammonium chloride. A 0.1M stock solution of Adogen 464 was prepared in either mineral spirits or xylene and 10 mil of this solution was mixed with a approximately 1 gram of solid inhibitor compound. While this environment is not an aqueous solution, the results provide some basis for comparing the effectiveness of inhibitors. The molybdate was similarly effective as the chromate.

SCC of En25 steel has been studied in a 0.2% $(NH_4)_2MoO_4$ solution having a pH 4.63 as a function of potential at 90°C. Results from this work are shown in Figure 7.27. Figure 7.27a shows the effect of potential on the morphology of corrosion, the final pH, the average velocity of SCC and the current density at constant potential. Figure 7.27b shows the potential-pH (after the experiment) superimposed on a partial E-pH diagram for both Fe and Mo. Locations of various morphologies are also shown. The SCC in Figure 7.27 is not relevant to the situation in the CCW system since the regime of SCC is within the range of relatively rapid corrosion as shown in Figures 7.19 and 7.23. Further, the regime of SCC is below that of the regime of potentials for the CCW system as compared with the relationship of potential vs. oxygen concentration shown in Figure 7.2.

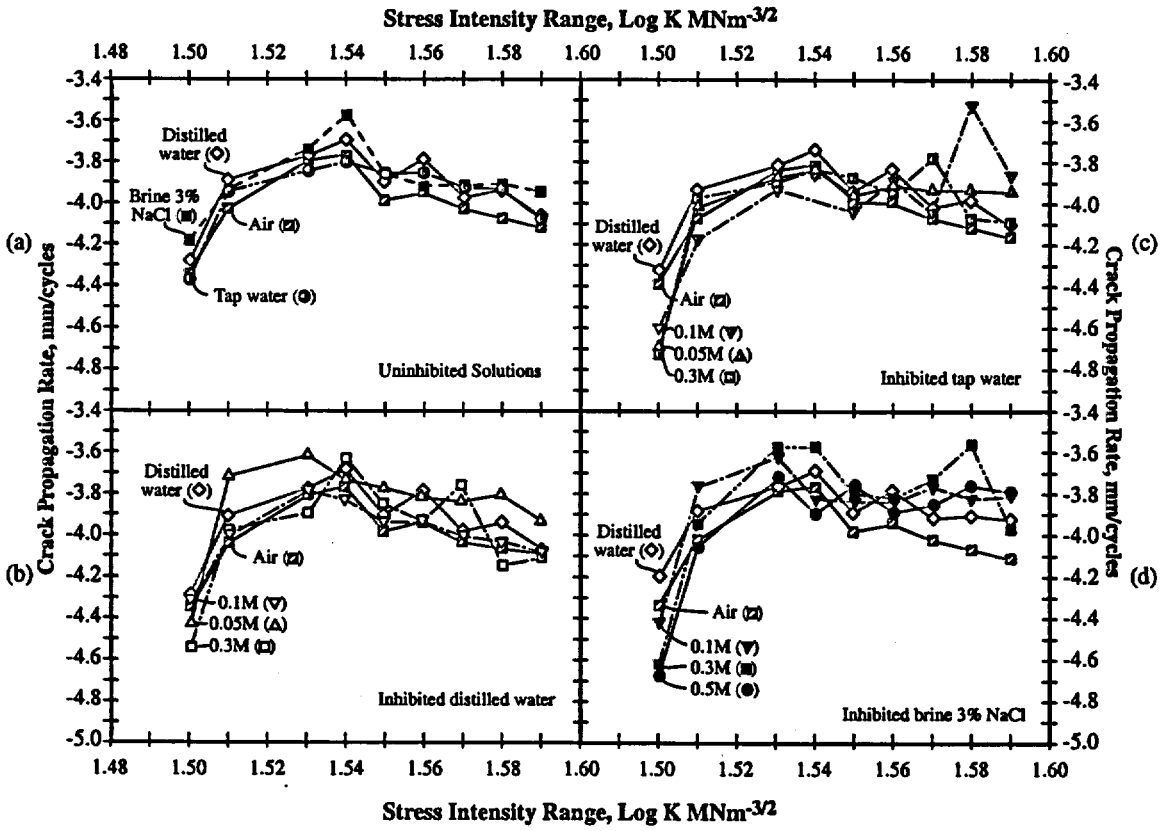

Figure 7.25 Crack propagation rate vs. range of stress intensity for mild steel tested at 1.67Hz at RT. (a) Non-inhibited solutions. (b) Distilled water. (c) Tap water. (d) Brine. From Husain et al.[66]

Indications of the effectiveness of molybdates on the dissolution transients associated with the advance of SCC are shown in Figure 7.28. Figure 7.28a shows the oxidation current density relevant to molybdate and borates as affected by sulfur species. These currents have been measured after 10^{-2} seconds. The data show that the presence of molybdate substantially inhibits the transient current relative to borate. Figure 7.28b shows the current density vs. time from pulsing with potential comparing a 0.01M Na_2SO_4 with a 0.01M Na_2MoO_4 environment. These data are similar to those in Figure 7.28a in that the presence of the molybdate accelerates the decay of current. This result, as with that in Figure 7.28a, implies that the rate of crack growth in a molybdate solution is retarded relative to either borate or sulfate solutions.

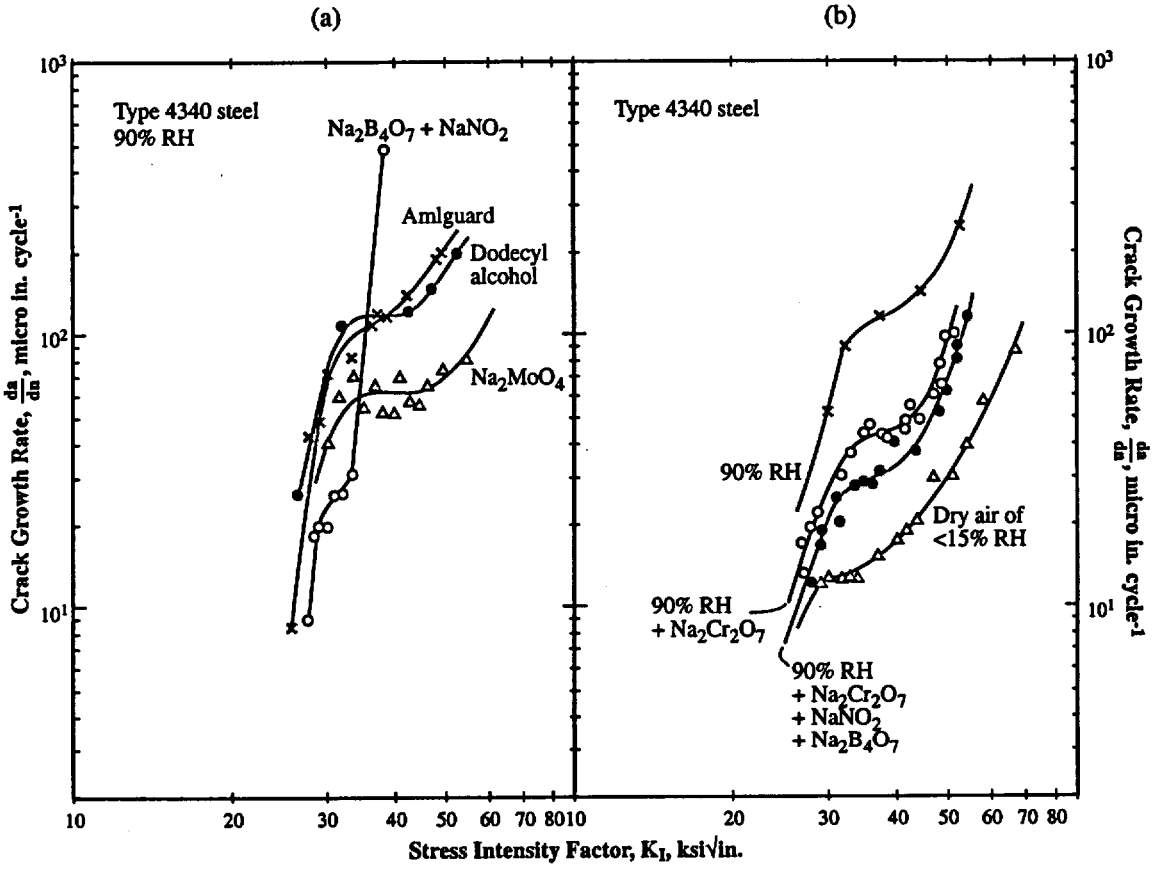

Figure 7.26 Crack growth rates vs. stress intensity range for Type 4340 steel exposed at RT and 0.167 Hz for various inhibitors dissolved in an Andogen 464 plus mineral spirits or xylene solution. (a) One set of environments. (b) Other set of environments. From Agarwala and DeLuccia.[67]

Details of the inhibition by molybdate as well as other inhibitors have been studied by Robertson[11] and by Pryor and Cohen.[12] Results from their work are shown in Figure 7.29. The most important result of their work is the low concentration at which molybdate, as well as nitrite, inhibits corrosion. In the experiments shown in both Figures 7.29a and 7.29b, both nitrate and molybdate were equally effective in terms of the minimum

amount of species required to produce significant inhibition. Both were more effective than chromate. These data show that both species produced effective inhibition at concentrations approximately as low as 10^{-5} N in aerated solutions.

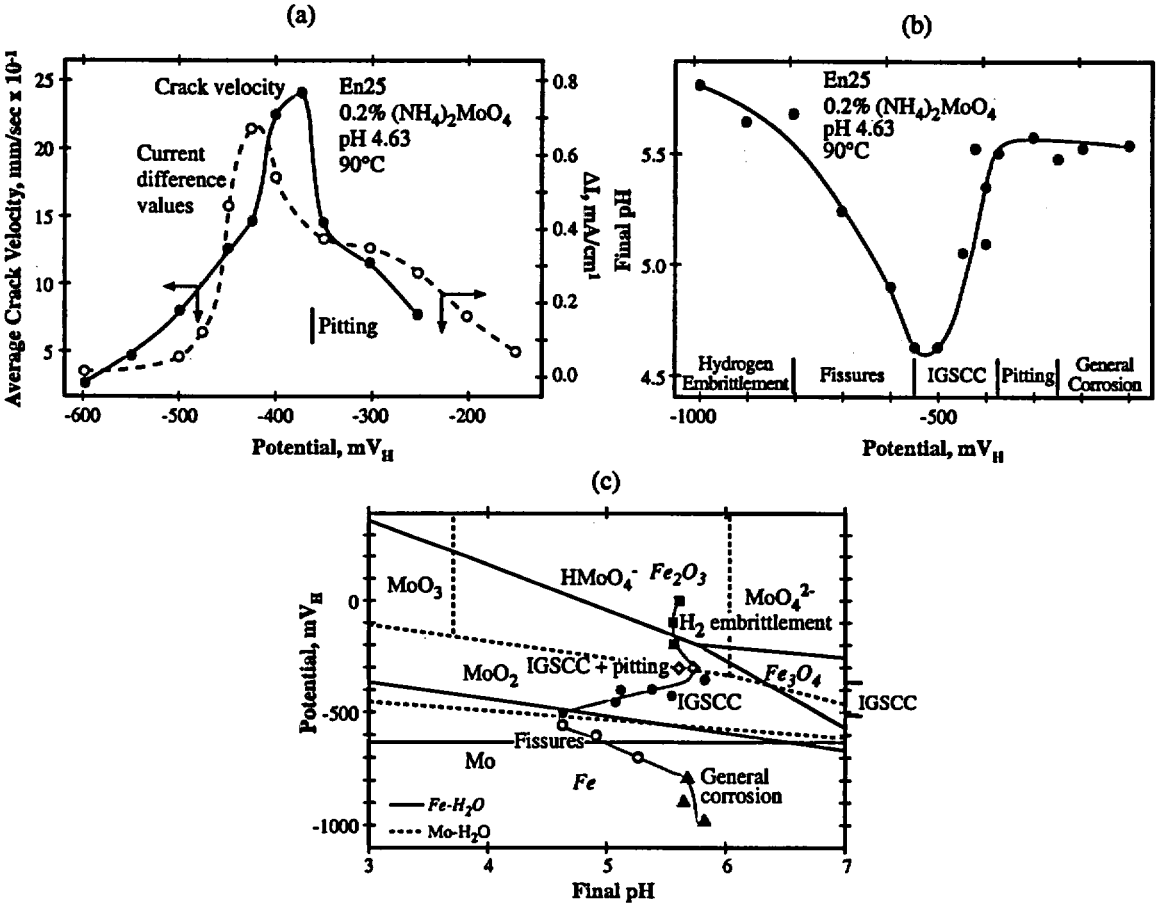

Figure 7.27 (a) Final pH, corrosion morphology, average crack velocity, and current density vs. potential for En25 at 90°C exposed in $(NH_4)_2MoO_4$ at 90°C with SCC measured by CERT. (b) Potential vs. pH for both Fe-H_2O and Mo-H_2O with the pH at the end of test vs. potential and the corrosion morphology noted. (c) Potential vs. final pH showing morphologies of corrosion. From Holroyd.[13]

As suggested in Figure 7.30, more MoO_4^{2-} is required for effective inhibition as Cl^- increases. Further, it appears that molybdenum acts the same whether it is an alloying element or dissolved in the aqueous solutions. Figure 7.30 shows results from a study by Sugimoto and Sawada [68] where a 20Cr+25Ni alloy was investigated in chloride solutions in the range of temperatures less than about 50°C. This alloy is different from the mild steel of interest in this report; however, the data from the Sugimoto and Sawada study are relevant in view of the general patterns of interactions between the molybdate and chloride.

The significant fundamental knowledge concerning the role of the molybdate additive to the CCW system is the following:

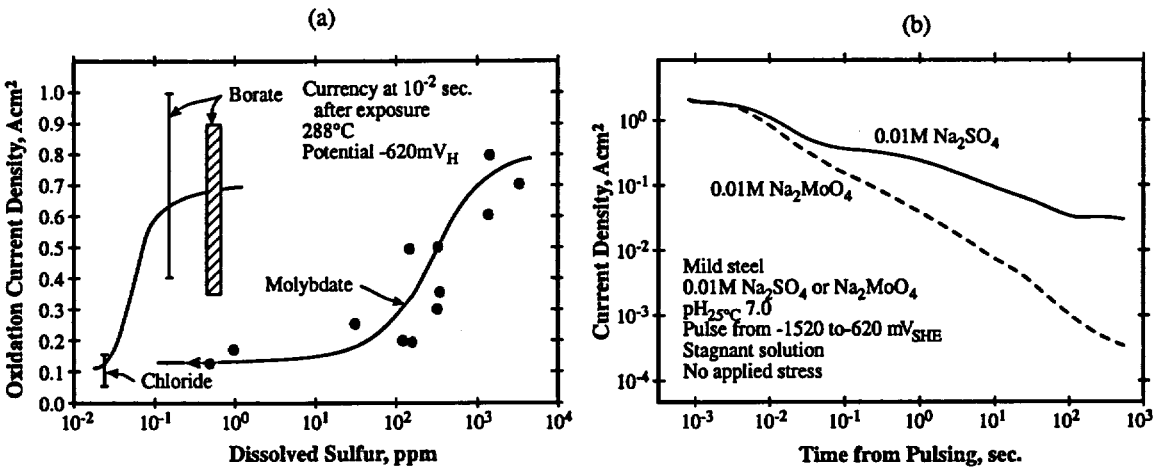

Figure 7.28 (a) Oxidation current density on the surface of Fe exposed to borate, chloride or molybdate-based electrolytes at 288°C. These oxidation rates are measured at 10^{-2} seconds after exposure of the surface and while exposed to 620 mV_H. From Ford and Combrade.[69] (b) Current density vs. time from pulse for mild steel exposed to Na_2SO_4 and Na_2MoO_4 environments at 288°C for a RT pH of 7.0. The pulse involved a change from 1520 mV to –620 mV_H.[70]

1. The E-pH diagram in Figure 7.16 provides the fundamental thermodynamic basis for the solubilities. Inhibition of pitting usually results from the formation of MoO_3 at the base of advancing pits as they progressively acidify. The stability of MoO_3 increases as solutions become more acidic as shown in the diagram. Except for a narrow range of stability of MoO_2, Mo is completely soluble in aqueous solutions. This pattern suggests that Mo would not be protective.

2. The MoO_4^{2-} seems to provide effective inhibition despite its broad range of solubility.

3. Inhibition by molybdate, in general, is not effective until the pH is above about pH 6 as shown in Figures 7.19 and 7.23. The occurrence of inhibition in this range seems to result from a mixed oxide, such as $(Fe,Mo)O_x$ that forms and is stabilized with increasing pH above about pH 6. However, there is little support for such a compound. Regardless, the various speculations in the literature about how MoO_4^{2-} works are probably baseless except for the reasonable possibility for the formation of a mixed oxide.

4. As the pH decreases below about pH 5-6, the molybdenum no longer provides significant protection as shown in Figures 7.19 and 7.23. Such a tendency is quite likely related to the SCC described in Figure 7.27 from the work of Holroyd.[13] Thus, the SCC observed by Holroyd and shown in Figure 7.27 is very likely related to a less

protective film in the region of pH 4-5 where the SCC was observed; it is unlikely that this same SCC would occur at pH greater than about pH 6.

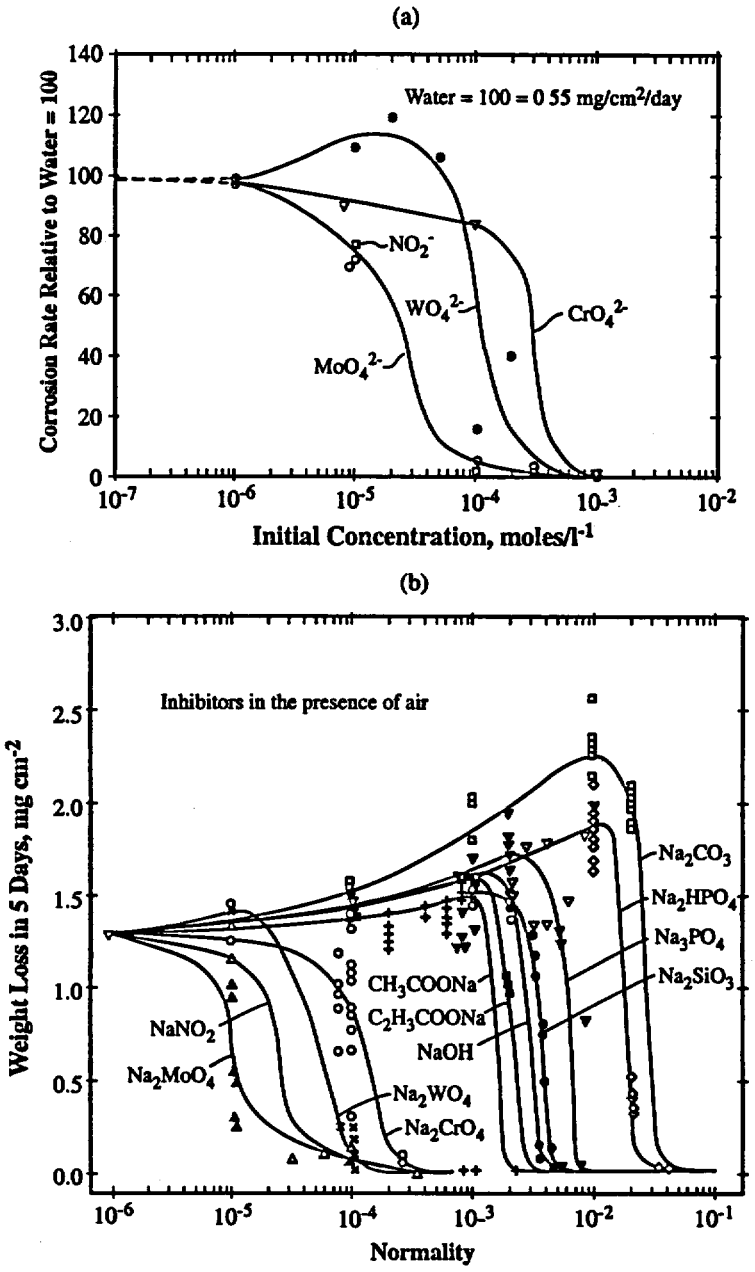

Figure 7.29 (a) Corrosion rate vs. concentration for four inhibitors in aerated water at RT. Tests conducted for seven days. Experiments conducted in distilled water in the pH range of 6.5 to 7.5. Specimens cut from cold worked mild steel strip with 0.033 w/o carbon. From Robertson.[11] (b) Weight loss vs. concentration of inhibitors for a nominal (laboratory-fabricated) autobody steel with 0.052 w/o carbon for tests at 25°C for 5 days in aerated distilled water. From Pryor and Cohen.[12]

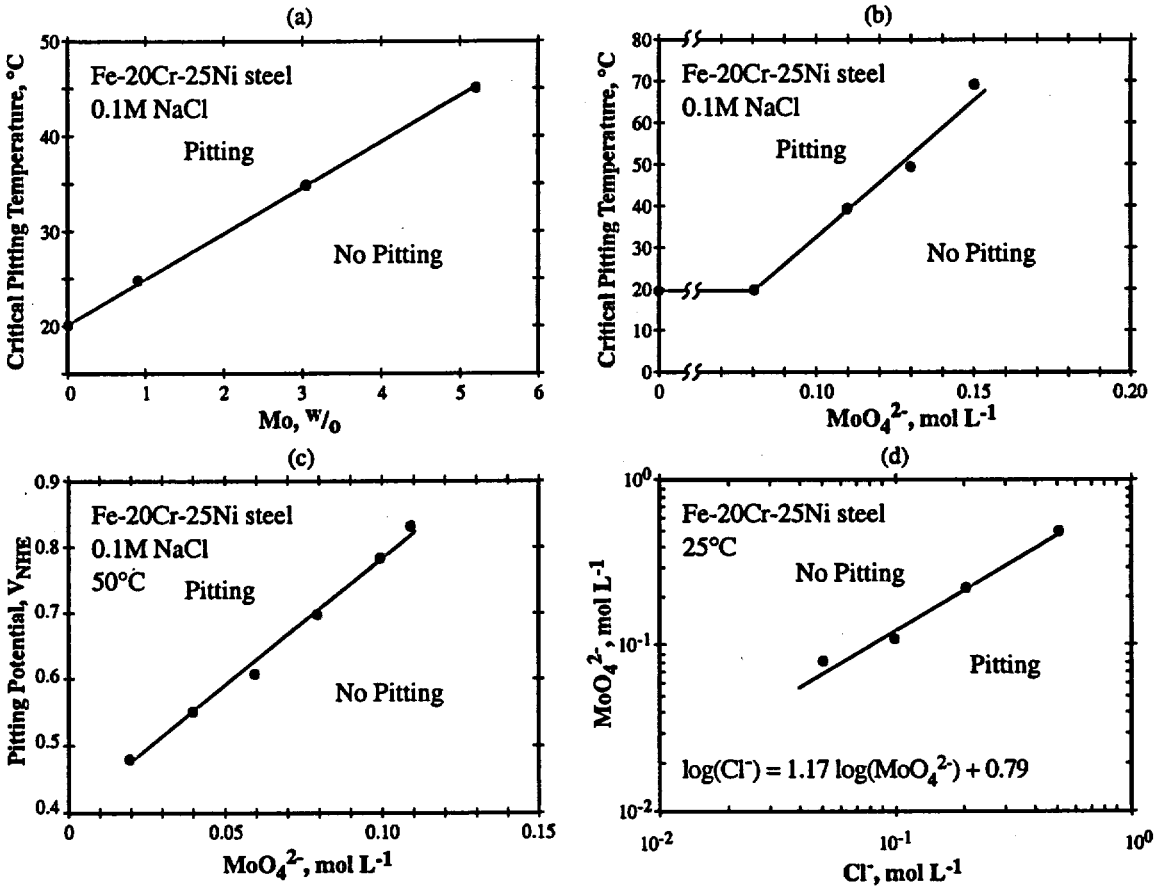

Figure 7.30 Pitting as affected by Mo dissolved in the alloy and in the aqueous environment when a Fe-20Cr-25Ni alloy is exposed to NaCl solutions at less than 50°C. (a) Critical pitting temperature vs. concentration of Mo in alloy for a 0.1M NaCl solution. (b) Critical pitting temperature vs. concentration of MoO_4^{2-}concentration in a 0.1M NaCl solution. (c) Pitting potential vs. MoO_4^{2-}concentration in a 0.1M NaCl solution at 50°C. (d) MoO_4^{2-}vs. Cl- for conditions of pitting and no pitting at 25°C. From Sugimoto and Sawada.[68]

5. Molybdate retards the transient processes that comprise the advance of SCC as demonstrated in Figure 7.28.

6. In some ranges of pH, molybdate seems equivalently effective as chromate as shown in Figure 7.29.

This set of fundamental observations, which are supported by references in this section, show that it is not likely that molybdates are critically related to the SCC at WCNOC in the CCW system. As indicated in Section 8.0, the SCC in the CCW system is more related to HPSCC and depends critically on the oxygen concentration.

3. Tolyltriazole in combination with molybdate and oxygen

Tolyltriazole is widely accepted as a standard inhibitor for copper base alloys. Tolyltriazole is used in the CCW system of the WCNOC in the range of 4-8 ppm as shown in Tables 4.3 and 4.4. However, little work showing effects of tolyltrizole alone and with molybdate has been conducted except for one study by Alexander and Moccari.[71] Their results are shown in Figure 7.18c; for comparison, Figure 7.18a shows the effects of molybdate on the potentiodynamic polarization curves for SA106Gr.B exposed to DI water at RT. These data are similar to those in Figure 7.18b.

The data in Figure 7.18c show that tolyltriazole produces two important effects in combination with molybdates. First, it significantly lowers the active peak suggesting that its main contribution occurs at lower potentials. Second, without dissolved air the passive current density is significantly increased. Tolyltriazole seems to produce little effect on the passive current density of molybdate-containing solutions when air is present. These effects produced by tolyltriazole suggest important interactions that have no explanation. The effects produced by tolyltriazole as shown in Figure 7.18c are unusual and suggest that additional work should be undertaken, especially with respect to understanding its effect on SCC.

4. Chloride

While chloride is present in the CCW system, the concentrations are low as shown in Tables 4.3, 4.4 and 4.5; and there is no means for significantly concentrating such species. Chloride should not be regarded as an important species in the corrosion or SCC of the CCW system.

5. Microbes and Fungi, Sulfur

The presence and importance of microbes and fungi in the CCW system has been reviewed in detail by Dr. Little;17 her report is attached in Appendix 1.0. She concluded that there was no evidence of species that would lead to aggressive corrosion; further, she noted that there was not sufficient concentration of nutrients to support the growth and proliferation of such species.

The matter of microbes was also investigated by Altran.[2,3,4,5,6] They also found no evidence of aggressive species.

However, Altran also observed a concentration of sulfur as noted in Section 4.0, Tables 4.8 and 4.9. They suggested that such sulfur could be produced by SRB which is a reasonable observation. However, there is not sufficient sulfur in the CCW system to provide the nutrient. Also, no SRB were detected either by Little[17] or by Altran.[2,3,4,5,6]

For the present, it must be concluded that there are no aggressive microbes or fungi of significance in the CCW system; and, further, they have not affected SCC in the past.

6. Nitrites

Nitrites are not used by WCNOC for treating the CCW system although this is used by about 11% of the domestic and international utilities that were contacted as noted in Tables 6.1, 6.2 and 6.3. However, in the 1995 report by DEI, they noted that three failures occurred, as noted in Table 6.4, that were attributed variously to the oxidation of nitrites by microbes to nitrates. They speculated that the SCC was due to the presence of these nitrates that would have produced SCC according to the effects of nitrates shown in Figure 7.15.

In preparing this report, I asked Dr. Little whether she was familiar with any case where the oxidation of nitrites to nitrates has lead directly to a verifiable occurrence of nitrate-related SCC. She indicated that she was aware of no such instance.

Furthermore, the work on SCC due to nitrates as affected by nitrites is described here in Figures 7.15f, 7.15g and 7.15h. In all cases, the magnitudes of concentrations in which experiments with nitrate have produced SCC exceed what is reasonably available from the oxidation of nitrites. Further, the presence of nitrites inhibits SCC in the nitrate as noted in Figure 7.18. In fact, it is more likely that the SCC sustained by the utilities described in the DEI 1995 report is due to the high oxygen concentrations or to the increased potential produced by the nitrites similar to the effect of oxygen, as is considered to be critical in this report.

7.3.4 Alloy Composition

The composition of Alloy ASME SA106Gr.B used in the CCW system is shown in Table 3.1. Changing this alloy is not an option nor is it necessary. Table 3.1 also shows the composition of weld metal. These compositions are in normal ranges.

It is nominally surprising that this mild steel sustains SCC as a normal matter since the generally expected degradation of these alloys is more associated with general corrosion. Nonetheless, as shown in Section 7.3.1, Figure 7.15, mild steel sustains SCC in concentrated solutions in the range of boiling to lower temperatures.

7.3.5 Alloy Structure

The alloy structures of interest in the CCW system application at WCNOC is simply that from nominal fabrication of the pipes and from welding as it involves weld metal and the HAZ. There is nothing special about these structures.

The SCC has proceeded intergranularly but there is nothing about the heat treatment nor fabrication that suggests a special reason for such an intergranular path. Many alloys sustain such intergranular SCC without special considerations of heat treatment or composition. These same alloys sustain TGSCC in different environments.

The only aspect of structural preference in the CCW system piping aside from the IGSCC and IGC seems to be the preference of early corrosion to react with the pearlite. Both the NRC8 and Altran[2,3,4,5,6] investigations observed this pattern. However, once the SCC begins to propagate as a fully IGSCC, such special localized corrosion stops. This localized corrosion of the pearlite seems confined to the early IGC region.

7.3.6 Temperature

In this section, I identify and discuss available data showing the effects of the primary variable of temperature on HPSCC. These data, with others concerning potential, are integrated with Section 7.3.1, concerning effects of potential, to rationalize the occurrence of the HPSCC in the CCW system in Section 8.2.

There seem to be two dominating patterns of SCC in steels with respect to the primary variable of temperature. First, there are the data that have been obtained in nominally pure water, mainly in connection with pressure vessel steels and turbines for PWR and BWR applications, some of which have been described in Section 7.3.1 in connection with the discussion of the dependence of SCC on potential. Second, there are the data that have been obtained in concentrated solutions such as those in Figure 7.15 of Section 7.3.1 in connection with the concentrated solutions of nitrates, carbonates, phosphates, acetates, molybdates, and alkalies. The discussion in this section is mainly concerned with the first group since the water in the CCW system is closer in composition, not withstanding the several hundred ppm of molybdate, to the pure water in primary and secondary systems of PWRs and BWRs. In fact, in primary systems, the additions of lithium and boron species produce the same kind of conductivity and pH that occurs in the CCW system.

In applying the data from the temperature dependence of SCC in pure water to interpreting the HPSCC in the CCW system, there are three considerations that need to be accounted for. First, there is a tendency for the dependence of the crack growth rate data to be bi-modal with respect to temperature as illustrated in Figure 7.31. In the lower temperature range, the crack growth rate depends positively on temperature; in the higher temperature range above 200-250°C the crack growth rate sometimes depends negatively on temperature. Other data for the dependency of temperature do not exhibit such behavior although this bi-modal behavior is sufficiently common to exercise care in extrapolating from higher temperatures to lower ones of interest to the present analysis. Regardless, the extrapolation to the CCW system range of temperatures should use the lower temperature dependence depending on an appropriate intercept.

Second, the crack growth rate depends on the alloy composition although some of the data used in this analysis are from pressure vessel steel. Figure 7.32 shows that increasing the sulfur concentration increases the crack growth rates. Here, the heat A contains about the same concentration of sulfur as the piping in the CCW system as noted in Section 3.0 and Table 3.1.

Third, the crack growth rate also depends on the concentration of impurities or conductivity of the solution. Figure 7.33 shows this dependence although the contribution of impurities

seems to decrease with decreasing temperature and with the sulfur concentration similar to that in the CCW system pipes. How this contribution of conductivity should be treated in extrapolating data from higher temperatures is not clear.

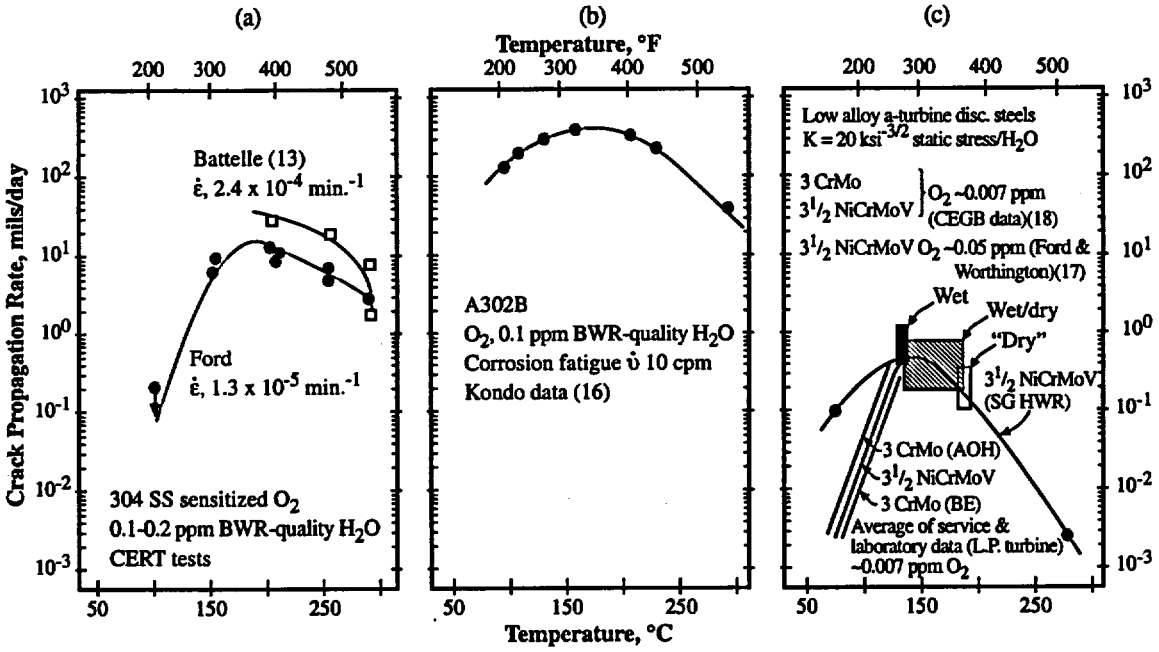

Figure 7.31 Crack propagation rate vs. temperature. (a) Type 304 sensitized stainless steel in 0.1-0.2 ppm BWR water. From Ford and Povich.[72] (b) A 302B in 0.1 ppm BWR water at 0.167 Hz. From Kondo et al.[73] (c) Low alloy turbine disc steels with K=20 $ksi^{-3/2}$, low oxygen. From Weinstein.[74]

Data from which rates at higher temperatures can be extrapolated to the CCW system temperatures are shown in Figures 7.12a, 7.12b, 7.14, 7.31, 7.32, and 7.33. In addition, rates can be extrapolated according to Figures 7.34 through 7.41.

Figure 7.34 shows two sets of data from Speidel and Magdowski[75] for various pressure vessel steels as well as work from Rahman and Ruscak.[76] The first two plots in this figure have been taken from numerous references[77,78,79,80,81,82] and include various concentrations of oxygen and stress intensities. Regardless, they provide a general pattern of the dependence of SCC on temperature. Figure 7.34b indicates that the low alloy steels in general exhibit lower crack growth rates than the higher alloy pressure vessel materials. Further, these data show that high oxygen environments exhibit consistently more rapid crack velocities although it should be noted that the stress intensities are generally higher for their data. Figure 7.34c shows similar results but are taken from a single heat of material and at a single concentration of oxygen.

Figure 7.35 compares crack velocities for aerated and deaerated environments for two heats of material, one an A 333-6 carbon steel and the other an A 508-2 low alloy steel at approximately the same stress intensities. Clearly, the crack velocities in the aerated

environments are more rapid. This seems contrary to the pattern in Figure 7.34b. Both figures exhibit the bi-modal pattern shown in Figure 7.31.

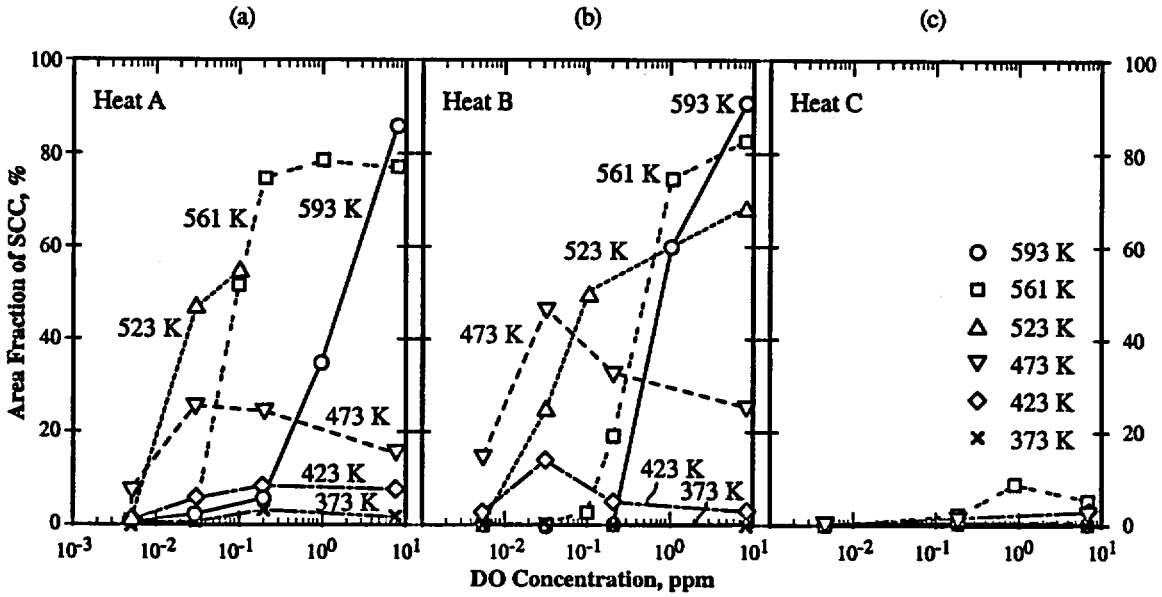

Figure 7.32 Area fraction of SCC vs. concentration of dissolved oxygen at temperatures from 373K to 593K. Data obtained with CERT at $4.2 \times 10^{-7} s^{-1}$, conductivity <0.06 μScm^{-1}. Concentrations of alloying species in w/o: (a) C-0.22, P-0.018, S-0.021 (b) C-0.22, P-0.01, S-0.015 (C-0.18, P-0.003, S-0.001). From Arai et al.[83]

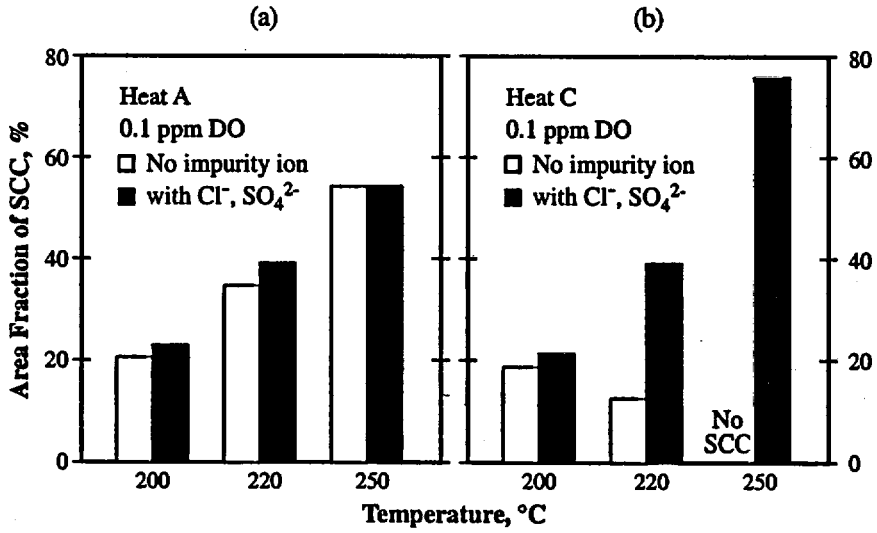

Figure 7.33 Area fraction of SCC vs. temperature for two heats of material (the low and high sulfur heats of Figure 7.32) for specimens exposed to pure water environments with and without impurities and both heats exposed to 0.1 ppm of oxygen and tested at $4.2 \times 10^{-8} s^{-1}$. From Arai et al.[83]

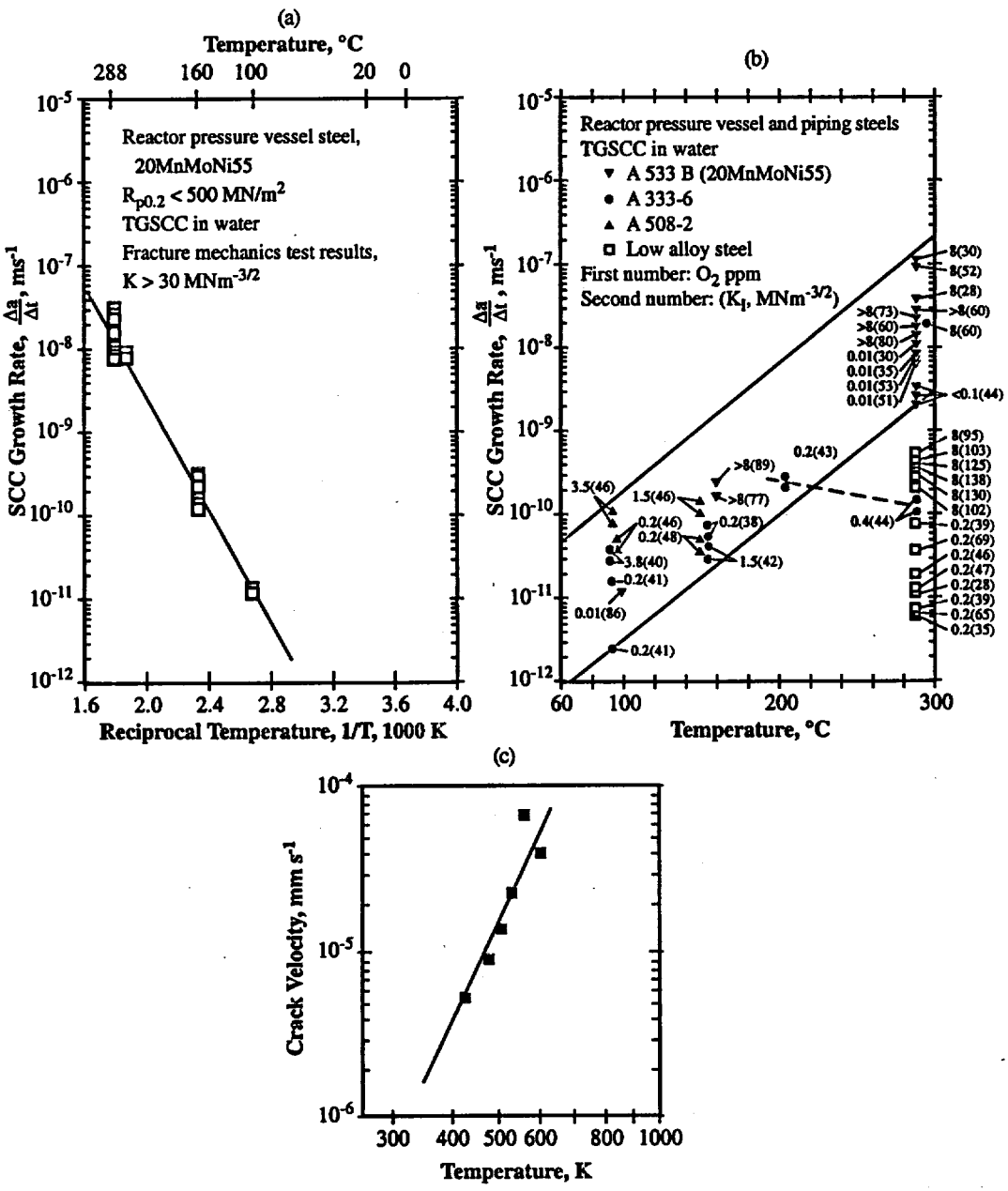

Figure 7.34 (a) Crack growth rate vs. reciprocal temperature for a pressure vessel steel 20MnMoNi55. The oxygen concentrations and stress intensities have been taken from various authors and are various. From Speidel and Magdowski.[75] (b) Crack growth rate vs. temperature for pressure vessel steels at various concentrations of oxygen and various stress intensities. From Speidel and Magdowski.[75] (c) Crack growth rate for a 15Kh2NMFAA alloy at 8 ppm oxygen vs. temperature for low alloy steel (C 0.16, P 0.009, S 0.01Cr 2.2, Ni 1.29). Testing in 0.6% boric acid and 6 ppm potassium hydroxide pH_{RT} 6.7, CERT at $1x10^{-6}$ and $2x10^{-7}s^{-1}$. From Rahman and Ruscak.[76]

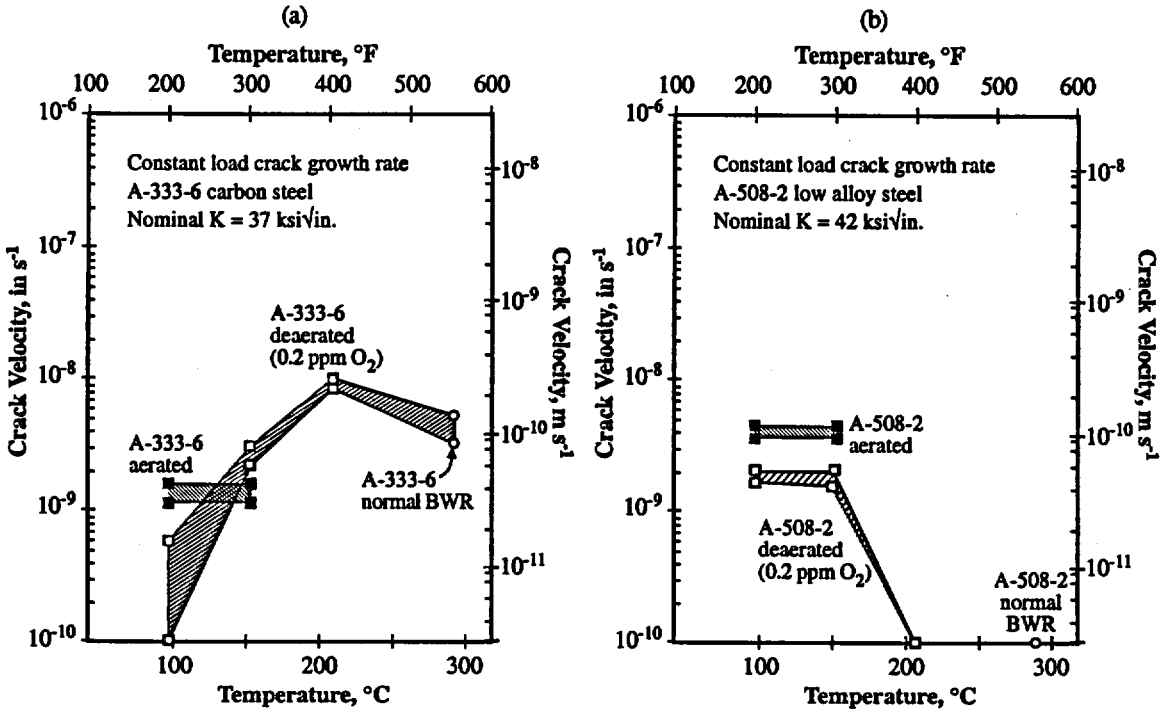

Figure 7.35 (a) Crack growth rate vs. temperature for a A333 carbon steel at a nominal K=37ksi $in^{1/2}$ for aerated and deaerated pure water environments. (b) Crack growth rate vs. temperature for an aerated and deaerated pure water environment with an A 508-2 low alloy steel having a nominal K=42 ksi $in^{1/2}$. From Hale.[78]

Figure 7.36a includes the same range of temperature as Figures 7.34 and 7.35 but considers two different compositions of mild steel; the designations being the same as Figure 7.32. The "BWR" specimens were exposed to environments of 0.1 to 0.2 ppm oxygen while the "PWR" specimens were exposed to 0.005 ppm oxygen. Clearly, higher oxygen and higher sulfur accelerate the SCC. Figure 7.36b shows a similar pattern.

Data from the work of Ritter and Seifert[84] are shown in Figure 7.37 where they investigated pressure vessel type steels from the point of view of what is called by some "strain induced corrosion cracking" (SICC). This nomenclature is both erroneous and misleading. The phenomena being investigated is simply the same SCC as discussed in this section. Figure 7.37a shows the crack velocity for several alloys vs. temperature for high dissolved oxygen and a dynamically opening crack. Figure 7.37b, shows equivalent experiments with the cyclic frequency applied to a weld material; here, the effect of cyclic frequency is inverse to usual effect of cyclic frequency. Figure 7.37c shows data from experiments equivalent to those in Figure 7.37b but the specimens are wrought rather than welded. The welded specimens exhibit a somewhat more rapid crack velocity. Figure 7.37d shows what is effectively a $K_{I_{SCC}}$ vs. temperature for wrought pressure vessel materials and one welded material. The figures in Figure 7.37 all, more or less, exhibit the bi-modal dependence of SCC on temperatures in the sense of Figure 7.31.

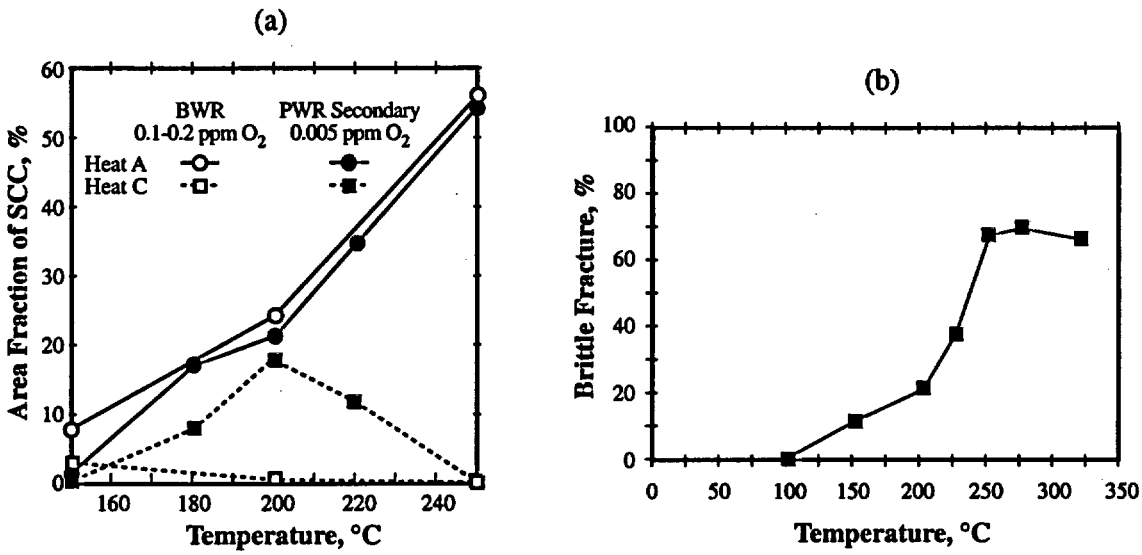

Figure 7.36 (a) Area fraction of SCC vs. temperature for two heats of material with dissolved oxygen 0.1 to 0.2 ppm and CERT strain rate 4.2×10^{-7} s^{-1}. Compositions of alloys are the same as the high and low sulfur of Figure 7.32. From Arai and Mayuzumi.[85] (b) Brittle fracture (SCC) % vs. temperature for specimens tested at 8 ppm dissolved oxygen for 15Kh2NMFAA (same composition as Figure 7.34) in CERT testing of $1 \times 10^{-6} s^{-1}$ and $2 \times 10^{-7} s^{-1}$. From Rahman and Ruscak.[76]

Figure 7.38 gives data for stresses to initiate SCC as a function of temperature. These data for dependence of stress on temperature were obtained using tapered specimens. The value for initiation stress at 150°C approaches the yield stress at RT. This is not surprising. However, no SCC was observed to initiate at 100°C.

Figure 7.39 shows the effect of temperature and oxygen on the S-N fatigue life of a carbon steel tested in high purity water.[86,87] In general, higher oxygen lowers the fatigue life by increasing amounts at higher temperatures.

Figure 7.40 shows the combined effect of potential and temperature on crack growth from CERT testing of a A508 alloy by Congleton and Shoji.[88] Here, the crack growth rate increases with increasing potential. However, the dependence upon temperature follows the bi-modal pattern of Figure 7.31.

It is clear from Figure 7.41 that the effect of oxygen on the occurrence of SCC remains generally constant above about 0.5 ppm. Thus, in extrapolating effects of temperature, using data in the range of 0.5 to 10 ppm oxygen should provide credible bases.

One of the features of the SCC at the CCW system at WCNOC has been the early IGC. Figure 7.42 shows that both pitting and miscellaneous cracking on the crack face can occur in the range of temperatures of the CCW system. Further, Figure 7.42c shows that there is a good correlation between the number of pits and the number of these cracks

suggesting high chemical reactivity at the surface. These phenomena may or may not be directly relevant to the initiation sites; but the chemical reactivity, especially, of the pits suggest such reactivity.

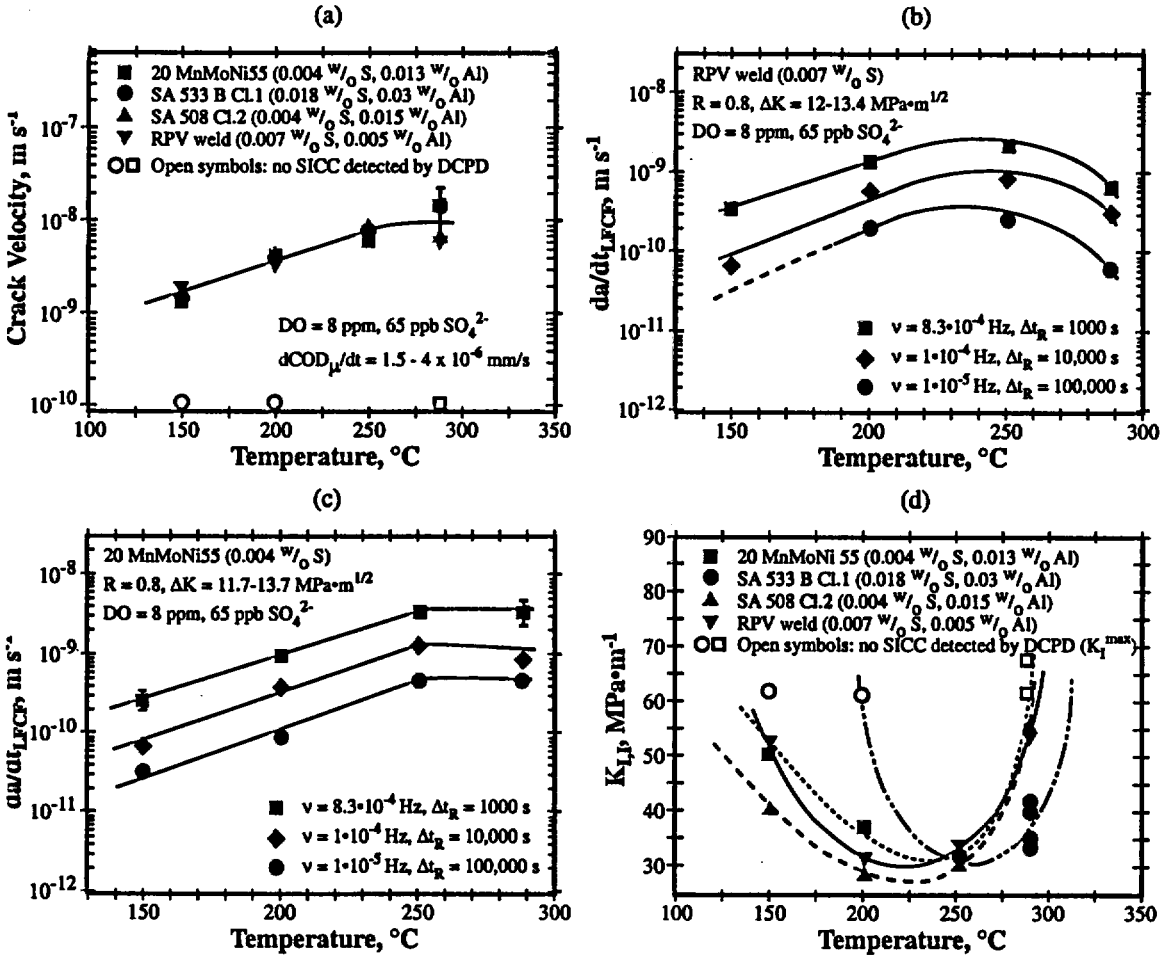

Figure 7.37 (a) Crack growth rate vs. temperature for pressure vessel steels and a weld for 8 ppm oxygen and a dynamically opening crack. (b) Crack growth rate in low cycle corrosion fatigue for a weld material in 8 ppm oxygen for three cyclic frequencies. (c) Crack growth rate vs. temperature in low cycle corrosion fatigue for a wrought pressure vessel steel at three frequencies exposed in 8 ppm oxygen. (d) Stress intensity for initiation of SCC vs. temperature for wrought and weld materials, exposed in 8 ppm oxygen. From Ritter and Seifert.[84]

7.3.7 Stress

Stress is the seventh primary variable as shown in Figure 7.3. Stress is particularly important here because it is clear from the patterns of circumferential and longitudinal SCC, which are shown in Section 5.0, that stresses due to welding, together with the dependence on oxygen described in Section 7.3.1, control both the occurrence and

direction of the SCC. No SCC was observed to initiate in the CCW system piping in the absence of welds being present; while, at the same time, SCC was observed to be present in the regions of welds where the SCC penetrated the weld, heat affected zone and matrix. Further, Table 5.1 shows that a weld inserted in 1994 sustained SCC by 2000, although it was not through wall, as identified by NDE (UT) at WCNOC and by Altran.

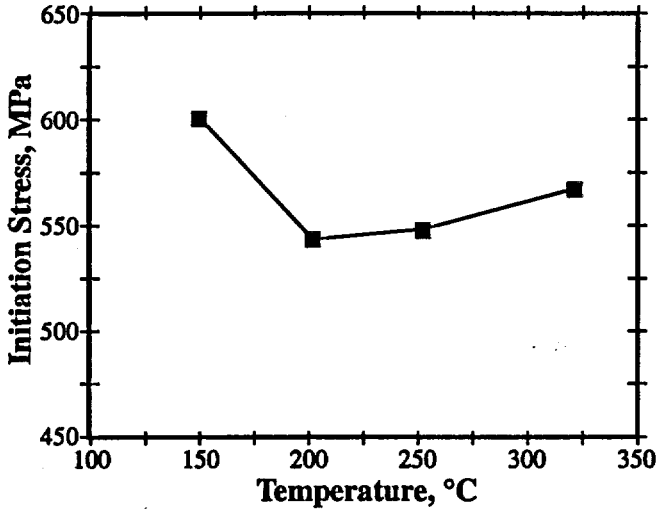

Figure 7.38 Initiation stress vs. temperature for the 15Kh2NMFAA alloy exposed to solutions with 8 ppm oxygen for low alloy steel (C 0.16, P 0.009, S 0.01Cr 2.2, Ni 1.29). Testing in 0.6% boric acid and 6 ppm potassium hydroxide pH_{RT} 6.7. Statically loaded smooth surface tapered specimens used. From Rahman and Ruscak.[76]

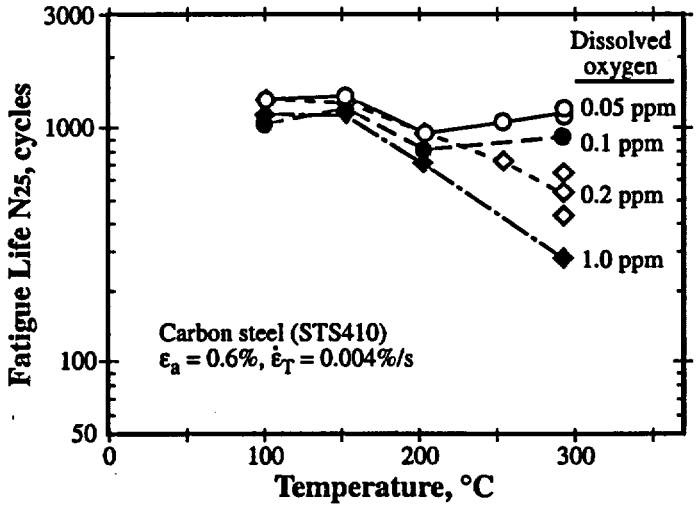

Figure 7.39 Fatigue life vs. temperature for carbon steel at four concentrations of oxygen in pure water. Fatigue stressing fully reversed. Original data from Nakao et al.[87] From James and Van Der Sluys.[86]

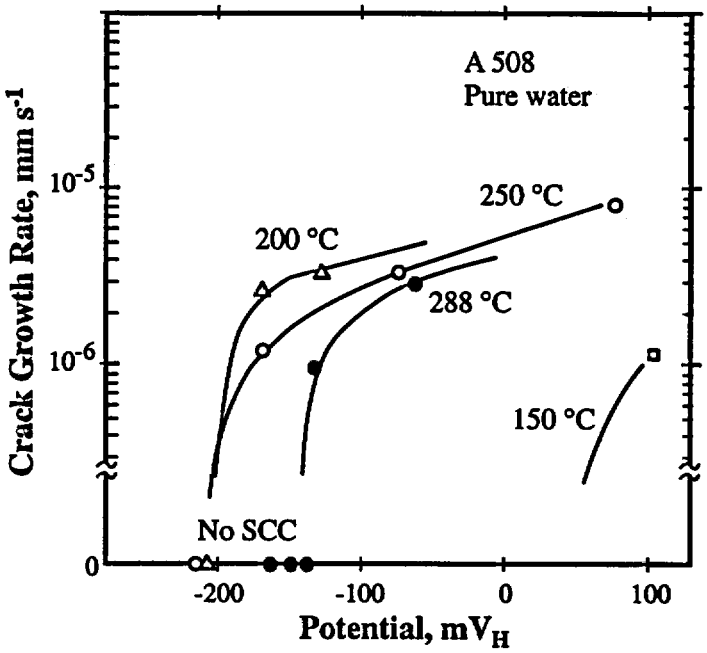

Figure 7.40 Crack growth vs. potential for Alloy A508 in oxygenated pure water at four temperatures. From Congleton and Shoji.[88]

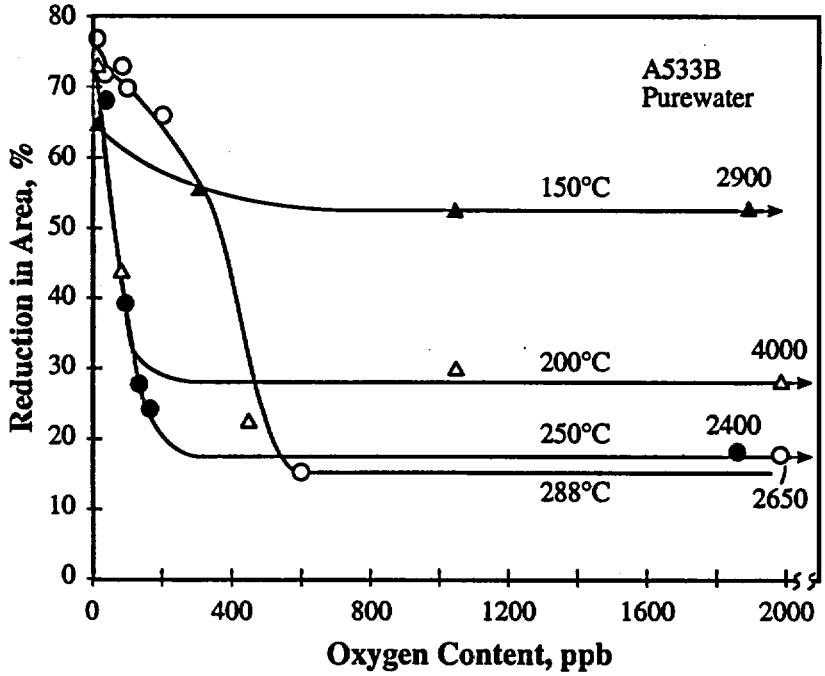

Figure 7.41 Reduction in area vs. oxygen concentration for A533B steel for four temperatures tested in CERT at $2x10^{-6}$ s^{-1}. From Congleton et al.[45]

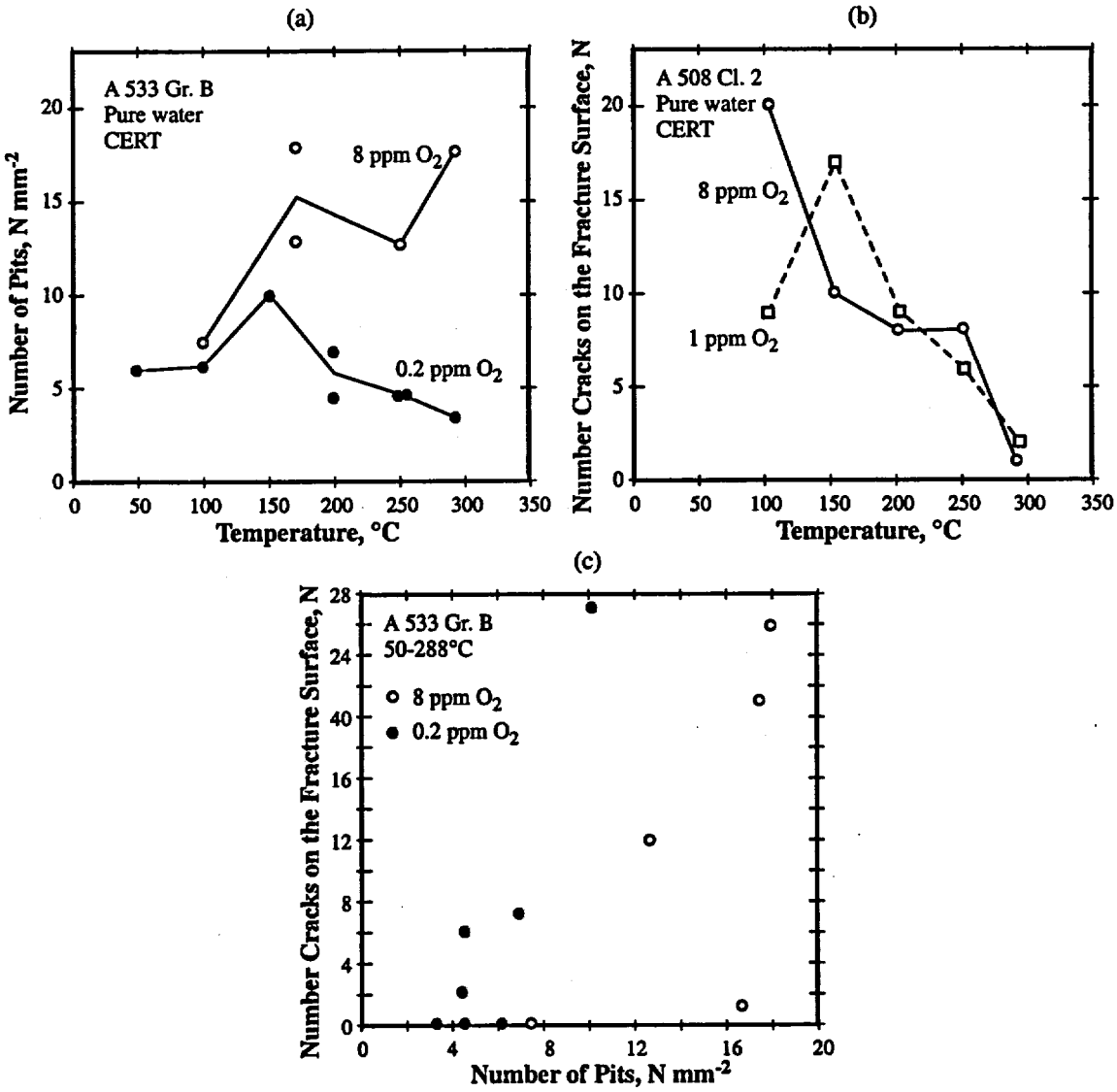

Figure 7.42 (a) Number of pits vs. temperature for A533GrB for two concentrations of oxygen. From Kuniya et al.[89] (b) Number of cracks on the fracture surface vs. temperature for A508Cl2 steel for two concentrations of oxygen. From Waid and Ault.[47] (c) Number of cracks on the fracture surface vs. number of pits for A533GrB CERT specimens over a temperature range 50-288°C for two concentrations of oxygen. From Kuniya et al.[48]

The purpose of this section is to describe how stress is incorporated into predicting the course of SCC. In the present case of the CCW system most, if not all, of the stress that affects SCC is due to residual sources, mainly weld stresses. Quantifying the magnitude of residual stresses is difficult, and reasonable assumptions are required. Residual stresses are often assumed to be at the yield stress.

The main elements in considering stress and the main quantitative data are included here:

1. Initiation and propagation

Predicting the perforation of pipes at the present time requires that both initiation and propagation stages be considered as illustrated in Figure 7.5. The stage of initiation is controlled by stresses and chemistry on the surface. Important aspects of chemistry at the surface are discussed in Sections 7.3.1 (potential), 7.3.2 (pH) and 7.3.3 (species). This section is concerned primarily with stress as it affects both initiation and propagation.

The stage of initiation concerns a relatively thin layer of metal at the inside surface of the pipe. The thickness of such an initiation layer can be assessed according to Figure 7.5d. For example, with a threshold surface stress of 200 MPa and a K_ISCC of 10 MPa $m^{1/2}$, the depth of the initiation layer is about 700 μm. Once the penetration exceeds this depth, the SCC is in the stage of propagation.

The length of time that SCC is in the initiation and propagation stages varies greatly. Figure 7.43 illustrates the main cases for combinations of initiation and propagation. There are essentially four cases as shown in Figure 7.43. First, (I) SCC may be dominated by propagation and proceed more or less linearly from initiation to propagation. This is not usual but represents an assumption that gives a lower bound of the rate of propagation. Fourth, (IV) SCC may be dominated by the initiation stage, and the propagation is rapid and contributes little to the overall time of perforation. In this case the rate of propagation is the highest. The Cases (II) and (III) are intermediate and comport more with actual behavior. Which of these Cases dominates depends on whether conditions for propagation are favored as for Case (II) or conditions for initiation are favored as for Case (III); Case (III) is most as most likely in the CCW system case.

Figure 7.43 also shows the bounding conditions for rates of propagation. Since the general time to perforation for the CCW system is known as a function of temperature from the evaluation of the specimens in Table 5.1, t_f is fixed and is approximately 9 years at 150°F. Also, from the work at AECL[9] and as shown in Section 5.0, Figures 5.10 through 5.12, the depth of SCC at 90°F is also known to be about 1.2 mm after 15 years.

It is most likely that the stage of initiation, t_i, is mainly associated with the development of the IGC as shown in Figures 5.1-5.3. In the three investigations, e.g., NRC, Altran, and AECL reports, the metallography shows that the stage of initiation is IGC; further, the extent of the IGC penetrations observed in the three investigations is about the same. Since the environment in the CCW system is quite dilute and further is effectively inhibited by the molybdate, this initiation stage is probably slow. This IGC seems to have a strong chemical dependence in view of the several observations of dissolved pearlite and extensive IGC. Also, these initiation sites seem to be associated with extensive general corrosion as shown in Figure 5.4 and 5.5. This extensive chemical corrosion may be the reason for the relatively low activation energy for the SCC in the CCW system SCC as shown in Figure 8.1. This low activation energy may provide a clue that initiation, as in Case (III) of Figure 7.43, is the best characterization.

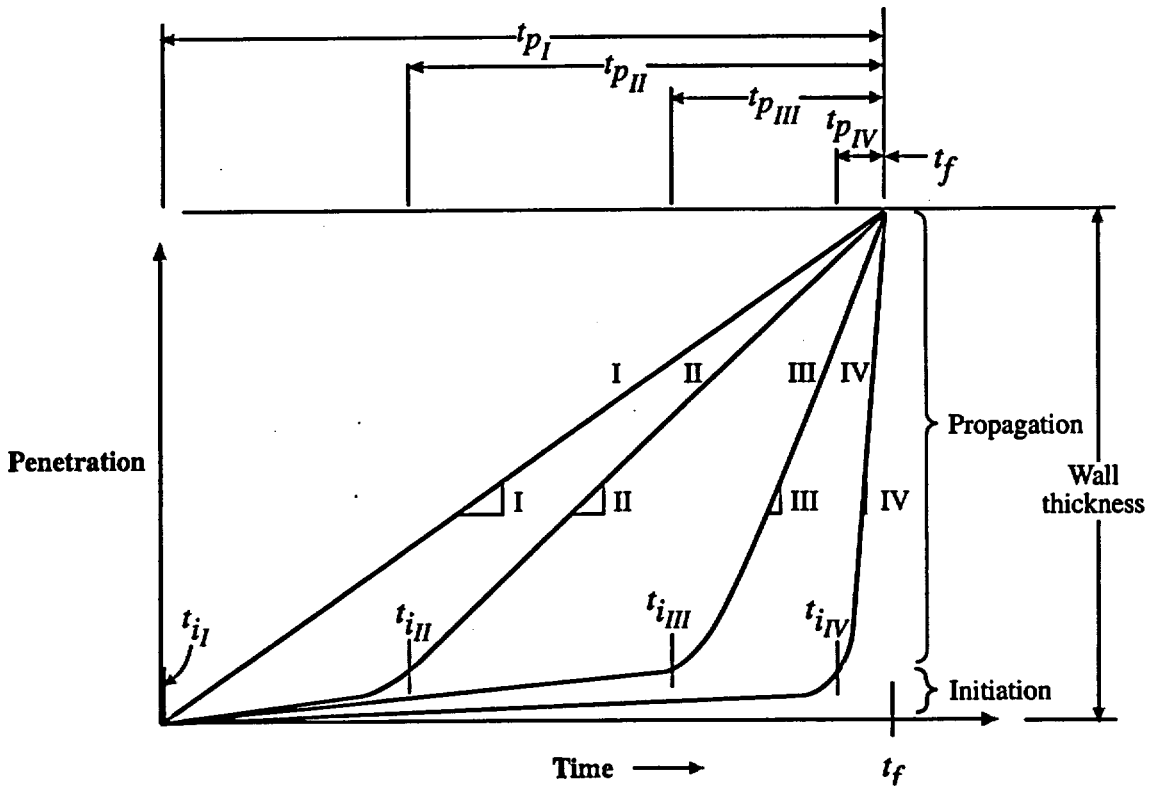

Figure 7.43 Schematic illustrations of contribution of initiation and propagation to total failure time for four typical cases. $t_f=t_i+t_p$ is shown for each of four cases.

Deciding on which of the four cases represents the situation at the CCW system is a matter of judgment since there is not much intermediate information nor is there definitive information on the rate of penetration during the initiation step. The simplest assumption about the progress of SCC is to assume Case (I), i.e. the progress of SCC is linear and that initiation is not evident. The case I assumption is the most optimistic bounding case, i.e. here the rate of propagation is the slowest. The more likely assumption is Case (III) where the rate of the propagation is probably about three times that for Case (I).

Identifying these cases as shown in Figure 7.43 is important since it affects how data from the literature are applied to prediction and assessment. For example, much of the data for SCC is obtained in the laboratory by directly measuring the rate of propagation of SCC either with a pre-cracked specimen or with a CERT specimen. Such data apply only to the propagation stage. Therefore, the assumption that propagation is a Case (I) type in Figure 7.43 is not consistent with the relevant data in the literature. The data from the literature would be more likely consistent with the t_{pIII} in Figure 7.43. This problem is considered in Section 8.2.

2. Dependence of initiation and propagation on stress

Figure 7.44 shows data from the dependence of SCC in the initiation stages. These data are similar to the schematic views in Figure 7.5. This view of SCC is relatively simple. SCC does not initiate until some threshold is exceeded. This threshold depends on the concentration of species, the potential, pH, the alloy and other factors. The threshold for initiating SCC depends also on the state of the surface and whether it is polished, abraded, lightly machined, heavily machined or ground. The details are not important here, but the effects of surface conditions on initiation are quite variable. There is also a view that there is no such concept as a stress threshold; however, practically, as shown in Figure 7.44 a stress threshold for SCC initiating from a smooth surface is a generally useful concept.

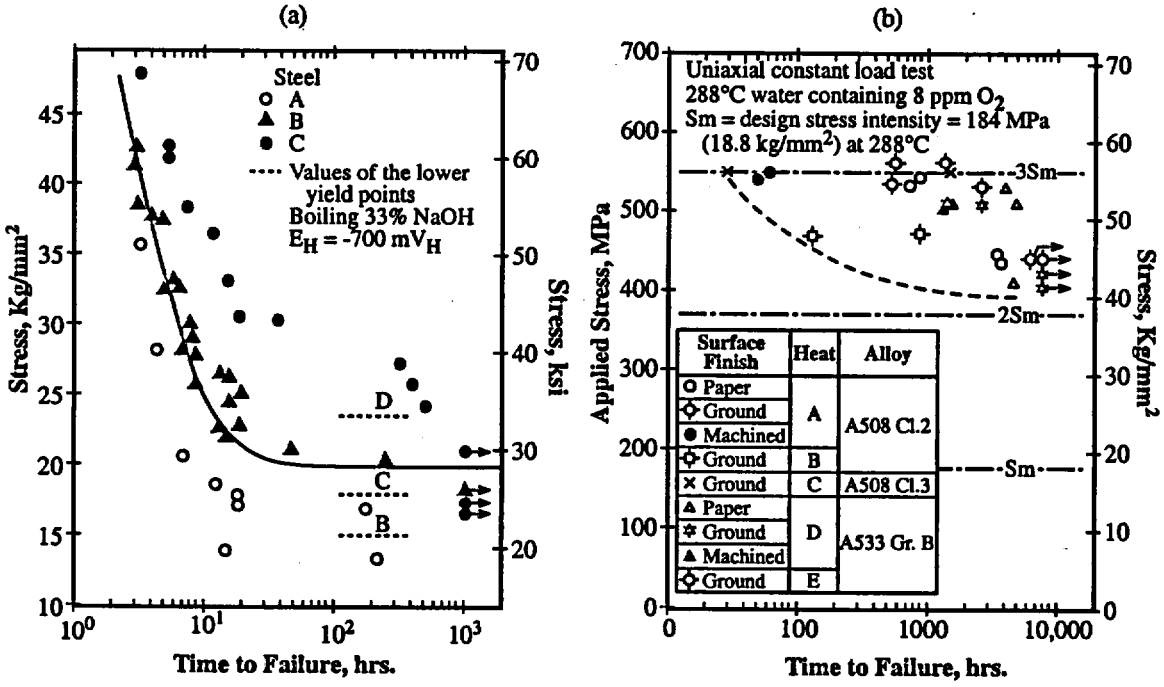

Figure 7.44 (a) Stress for failure by SCC for three steels exposed to 33% boiling NaOH at –700 mV_H. From Bohnenkamp.[90] (b) Applied stress vs. time-to-failure for uniaxial constant load at 288°C in water containing 8 ppm O_2. Design stress, Sm=184 MPa at 288°C. From Kuniya et al.[48]

The general dependence of initiation of SCC on stress is illustrated in Figure 7.3 where the rate of SCC (or time to some depth) depends on stress to some power. This formulation applies strictly to the initiation of SCC. The exponent on the stress varies but is usually taken as about 4.0 for purposes of estimating effects of stress. The possibly broad range of stress exponents has been discussed in detail by Jiang and Staehle,[91] and Figure 7.45 gives results of their work showing that the stress exponent for an initiation dominated condition may vary from about 0.5 to 9.0. Thus, using a possibly typical but

not necessarily correct stress exponent of 4, which is commonly used, the time for initiating SCC for the CCW system is increased by a factor of 16 when the stress is reduced by a factor of two. This is the reason for the interest in PWHT. It should be noted that this factor of change applies only to initiation.

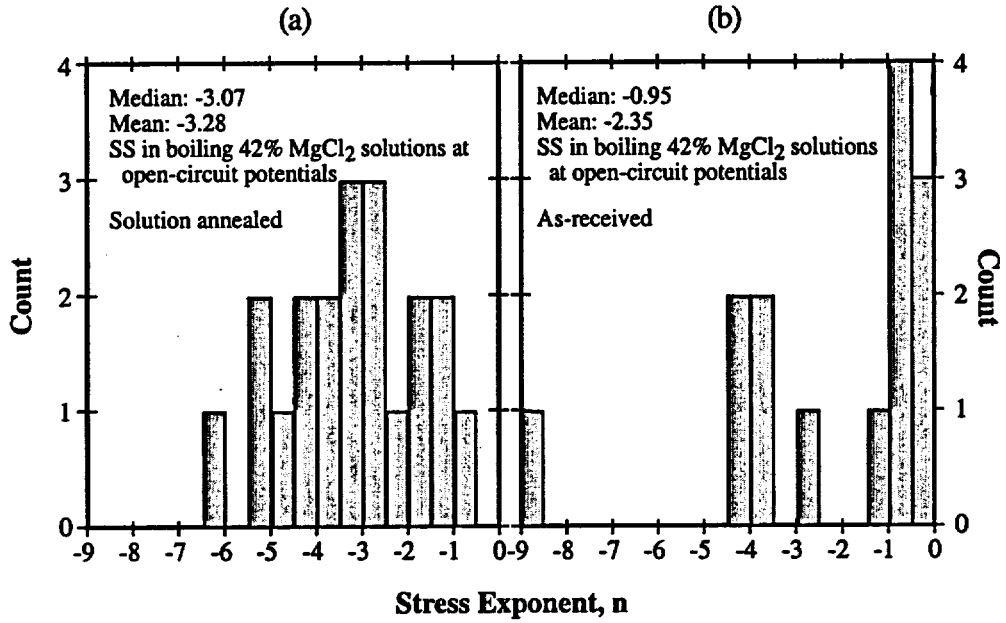

Figure 7.45 Number of observed stress exponents (n) for stainless steel specimens in boiling 42% $MgCl_2$ solutions at open circuit potential. (a) Solution annealed. (b) As-received. From Jiang and Staehle.[91]

Unfortunately, there are few data for estimating the stress exponent relevant to initiation in the present subject. More data, as described in Sections 7.3.1 and 7.3.6 are available for estimating the SCC velocity, and these data are used in Section 8.2 to rationalize the rate of HPSCC at temperatures in the range of the CCW system.

The interaction of propagation with stress follows, generally, a pattern shown in Figure 7.46. This is the prototypic response for the propagation of SCC. The value of $K_{I_{SCC}}$ is somewhat arbitrarily defined, but is the point where the crack velocity becomes practically negligible. Since the dependence of Stage I is so steep only the plateau region is relevant for prediction. The plateau region, practically, is not always completely independent of K, and its width varies. There is little information about V-K curves for mild steel in the range of temperatures of the CCW system. However, there is no reason to expect that they would differ in shape from the behavior of other steels in other aqueous environments.

The effect of stress during the propagation stage is different. According to the illustration in Figure 7.5b, once stress exceeds the K_ISCC, the SCC proceeds rapidly until the plateau range is reached where the SCC proceeds at a rate generally independent of stress intensity. The dependence of crack velocity in this range is more complex in that the

stress intensity depends on the product of mean stress and the square root of the crack depth as noted in Eqn. 7.1. If the mean stress is more or less constant, then the stress intensity increases as the crack depth increases.

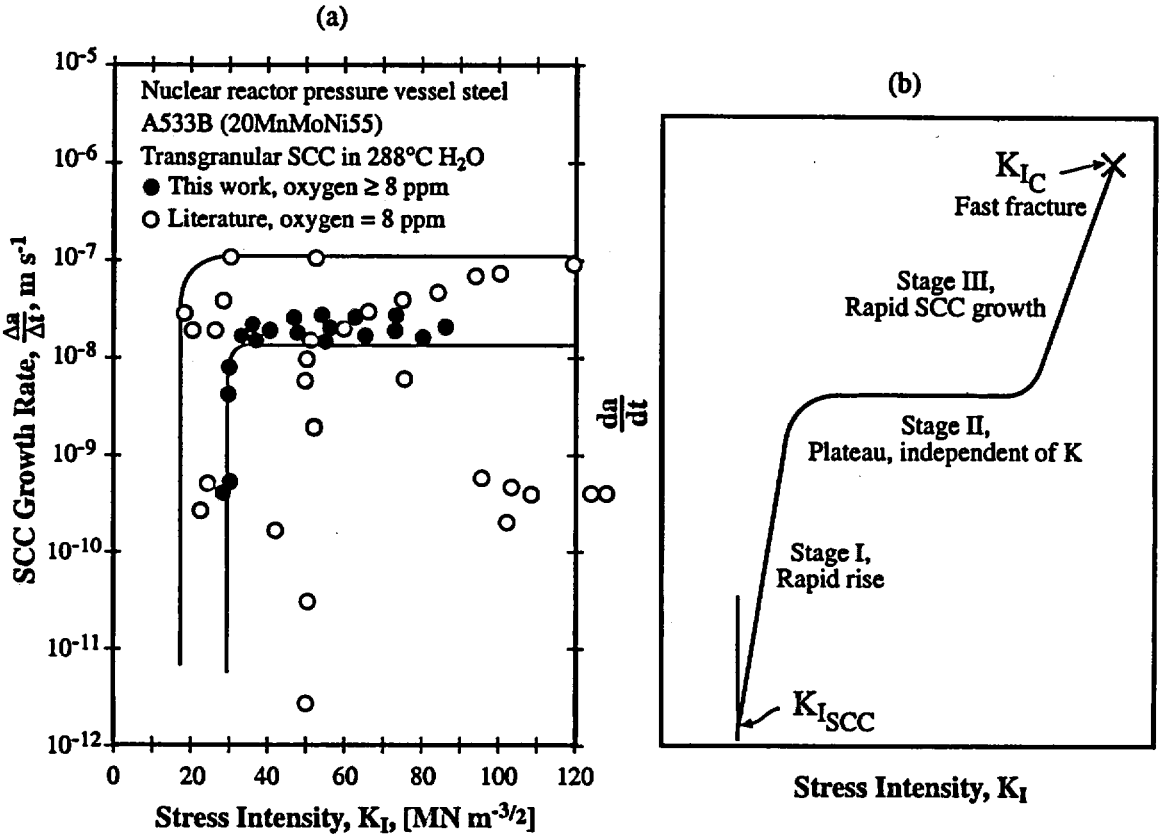

Figure 7.46 (a) SCC crack growth rate vs. stress intensity (V-K curve) for an A533B pressure vessel steel at 288°C and 8 ppm oxygen. From Speidel and Magdowski.[92] (b) Schematic view of V-K curve showing three stages of SCC.

3. Consequence of stress-dependent initiation and propagation for CCW system piping: longitudinal and circumferential SCC

Stress and the direction of SCC are important to the outcome of predictions for the magnitude of SCC in the CCW system. If the stress is predominantly peripheral, the SCC will proceed longitudinally as shown in Figures 5.1 to 5.5 and 5.10 to 5.12. Further, it is not likely that longitudinal SCC will extend much beyond the weld region since the high stresses diminish away from the weld. This case is illustrated in Figures 7.47a and 7.47b. This geometry, as constrained by stresses in the weld, limits the crack length and therefore the stress intensity and its approach to K_{IC}.

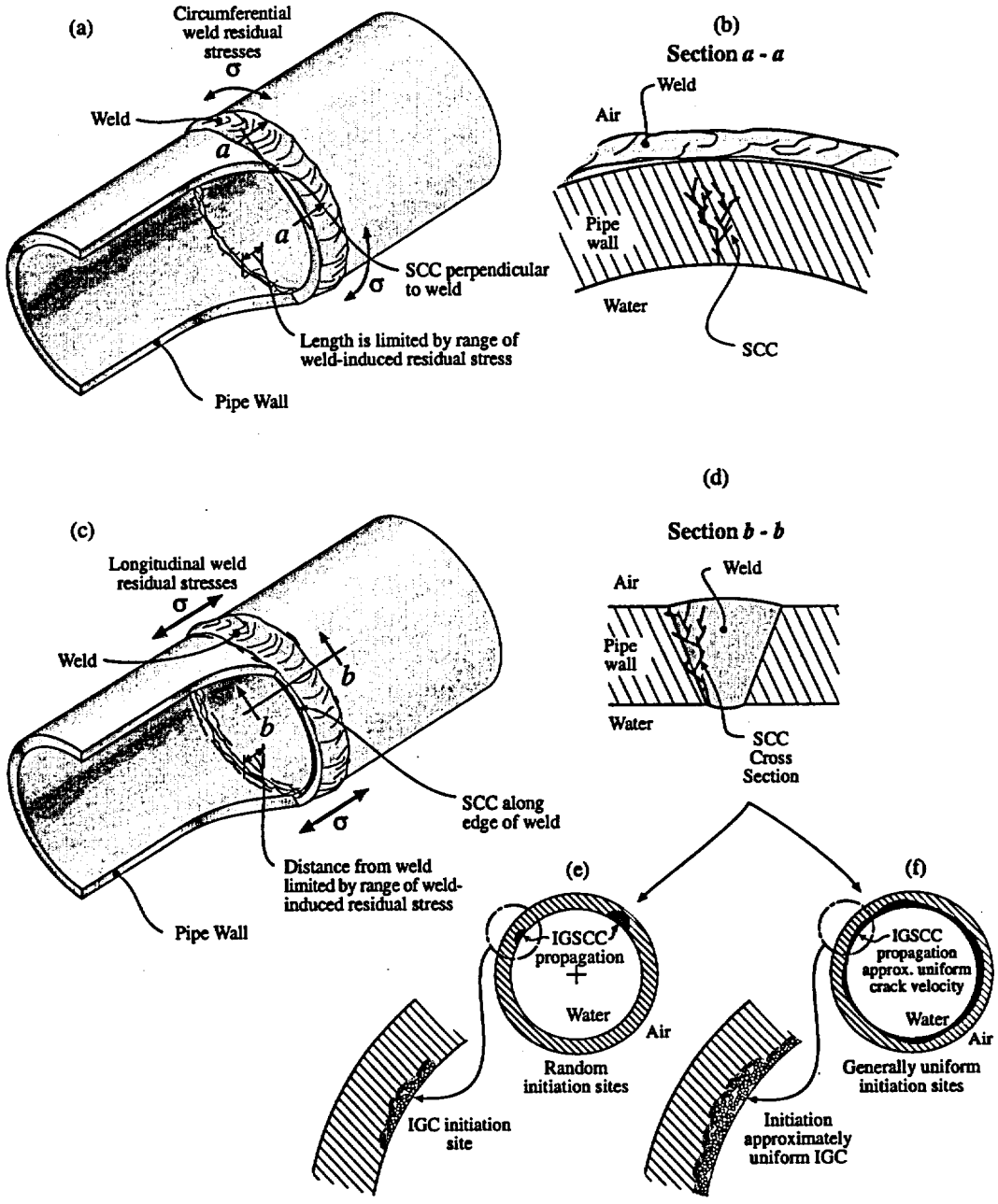

Figure 7.47 Schematic view of the details of SCC that results from circumferential and longitudinal stresses associated with welds. (a) and (b). Circumferential stresses produce longitudinal SCC that extend for relative short distances near the welds. The longitudinal morphology at section a-a is shown in (b). (c) and (d) Longitudinal stresses at the weld produce circumferential SCC. (e) Random initiations produce random SCC. (f) Uniform initiations produce uniform SCC.

If the weld stress is predominantly longitudinal in the weld region, the SCC will be confined to the weld and will be circumferential as was observed in the Altran studies.[2,3,4,5,6] Here, the SCC proceeded along the edge of the weld and heat affected zone. In the case of circumferential SCC, a completely different problem of predication applies relative to longitudinal SCC; there are two essential issues here as illustrated in Figure 7.47b:

a. If the initiation is more or less continuous, the time for starting the propagation phase will be more or less the same. If the initiation is not so continuous, the propagation can only start at fewer sites as shown in Figure 7.47b-5.

b. The velocity of propagation after initiation occurs may be independent of the stress, as indicated I Figure 7.46, over the width of the plateau. Thus, the velocity of the SCC will be more or less constant around the periphery and would produce a generally uniform front depending on the extent and contiguity of the sites of initiation.

The pattern shown in Figures 7.47c, 7.47d, and 7.47f suggests that the penetration of the weld region could be more or less uniform and lead to conditions for an extensive circumferential SCC. In support of this possibility, all of the photomicrographs from Altran, AECL and NRC showed this region of IGC of about the same intensity. Predictions based on this model are discussed in Section 8.2.

4. Consequences of existing SCC and PWHT

The application of PWHT could be expected to reduce residual stresses about a factor of two. If PWHT is applied from the point of view of affecting initiation, the SCC would be eliminated. Lowering the surface stress a factor of two would most likely lower the stress below any threshold or at least increase the time for initiation by the power law relationship as shown in Figure 7.3. This consequence is illustrated in Figure 7.48a.

The case of pre-existing SCC, when SCC is in the propagation stage, as is possibly the case for the CCW system at this time, there is some question as to whether PWHT would produce a benefit. Figures 7.48b and 7.48c show two cases: in Figure 7.48b the initial stress intensity is at the early stages of the plateau. The PWHT is applied, the initial stress intensity is lowered below K_{ISCC} and the relative SCC growth is negligible. In Figure 7.48c the stress intensity is higher and a PWHT only lowers K to an earlier location on the plateau. In this case the crack velocity is not changed and PWHT, then, is not effective. The cases for 7.48b and 7.48c depend on the initial size of the SCC, the prevailing stresses, and the effectiveness of the PWHT.

5. Cyclic stressing

The illustration of initiation and propagation as shown in Figure 7.43 are idealized patterns. These apply to experiments where the stress is constant. In practical applications, the stress is cyclic, even if low amplitude and infrequent. There are two

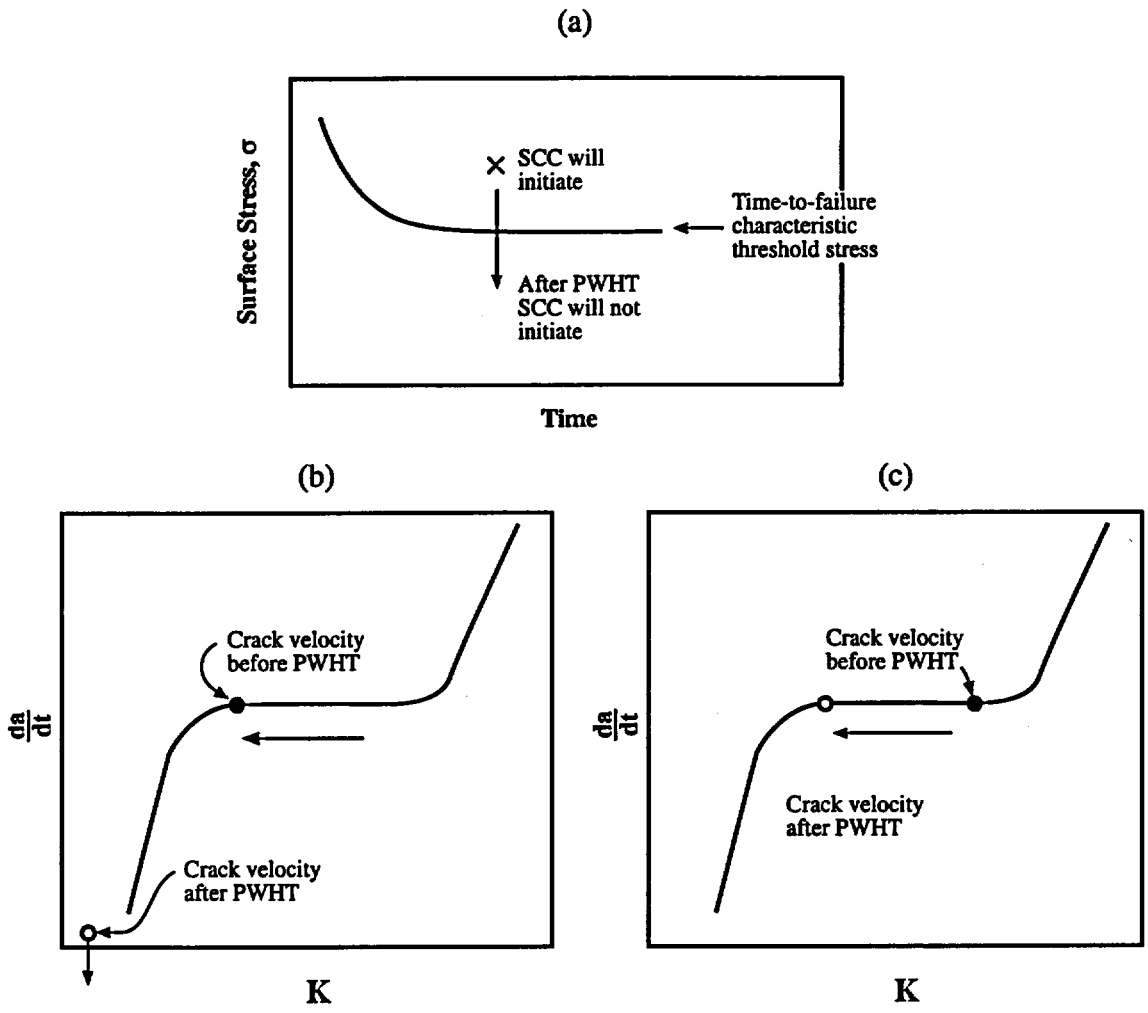

Figure 7.48 (a) Effect of lowering surface residual stress by PWHT on initiation. (b) Results from PWHT produce a negligible da/dt for a K less than $K_{I_{SCC}}$. (c) Lowering stress intensity by PWHT if both initial and final conditions remain in the plateau region.

aspects of this cyclic stress that are relevant to the CCW system. One is the acceleration of SCC that occurs with low amplitude stress ripples imposed on mean stresses. The other is the accentuation of this effect that occurs as the cyclic frequency is lowered. Both of these probably occur in the CCW system and may contribute to the occurrence of SCC in the temperature range of the CCW system.

Figure 7.49 shows the effect of a superimposed ripple stress of small magnitude together with the effects of cyclic frequency for C-Mn exposed to a carbonate-bicarbonate solution at 82°C. These small stress ripples significantly lower the threshold stress for SCC, and the decreasing frequency decreases the threshold still further.

Figure 7.50 shows that changing from a relatively high frequency of 11Hz to a lower one, 0.19Hz, produces a major change in minimum K for initiation and in the range of intergranular morphology. Figure 7.50b shows the same pattern as for Figure 7.49: lowering the cyclic frequency accelerates the initiation and propagation of SCC. The effect of temperature in addition to that of cyclic frequency is shown in Figure 7.51 over a range of temperatures for oxygenated water with 65 ppb of SO_4^{2-} that is somewhat typical of the CCW system case. These results show clearly a pattern that can be extrapolated to the temperature range of the CCW system.

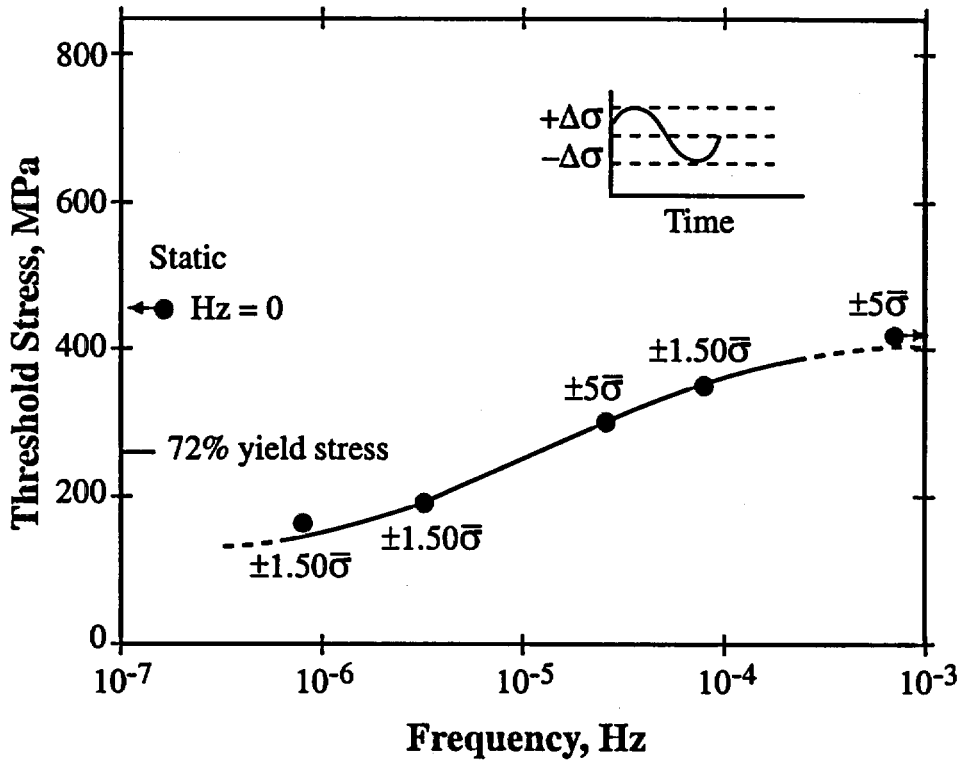

Figure 7.49 Threshold stress vs. frequency for low fluctuations of stress for a C-Mn steel in a carbonate-bicarbonate solution at -650 mV_{SCE} and 82°C. From Parkins.[93]

6. Residual stresses and weld cold work

Residual stresses are the most common contributor to SCC. Design engineers are generally unaware of this contribution and assume that calculated stresses define the influence on SCC. This, of course is wrong, and many serious failures have resulted from this mistake. Figure 7.52 illustrates the occurrence of LPSCC in a pressurizer due to welding stresses. Clearly, the welding stresses are effective in producing LPSCC. Figure 7.46 illustrates how readily residual stresses due to welding can produce SCC; this is similar to what has occurred in the CCW system.

7. Surface cold work

SCC can be initiated, that otherwise would not, when high local residual stresses occur on the surface. Figure 7.53 shows that scratches on the free span of a tube in a steam generator of a PWR on the cold leg cause SCC to initiate. Once initiated, this SCC continues rather than being stifled owing to the lower temperature and no high local chemical concentrations as occurs in crevices. This propagating SCC is most likely LPSCC on the secondary side. Figure 7.53, like Figure 7.52, illustrates the importance of residual stresses, except in the case of Figure 7.53 the residual stresses are produced by surface abrasion.

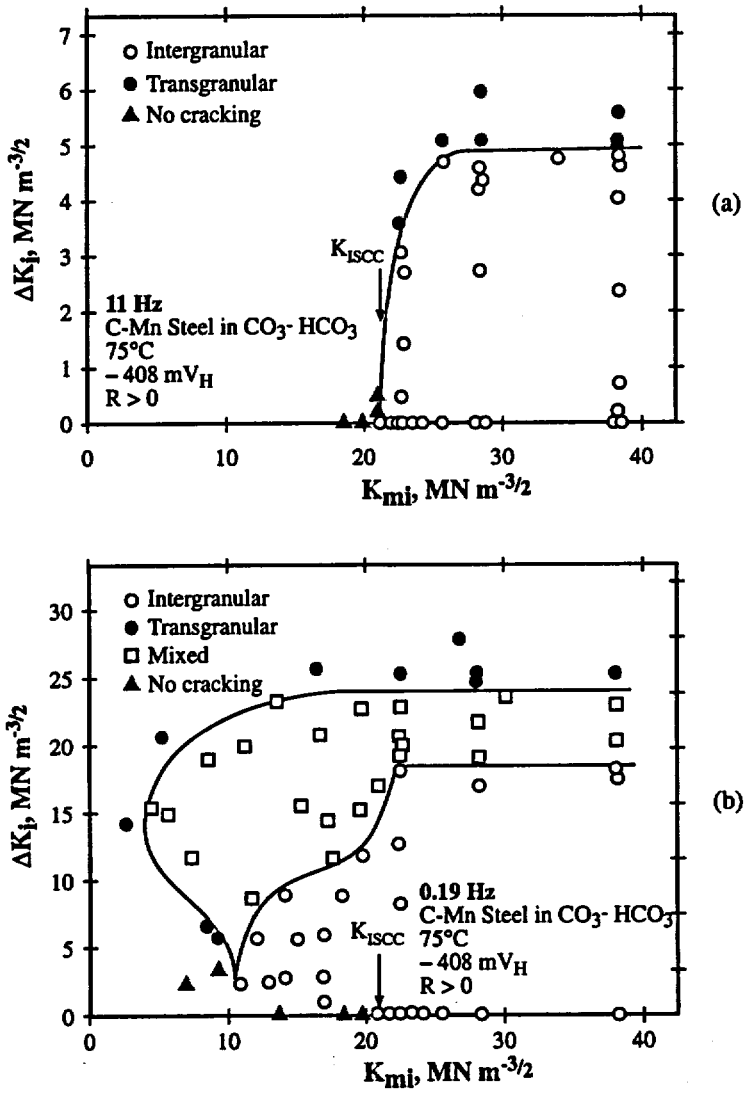

Figure 7.50 ΔK_i vs. K_{mi} for a C-Mn steel immersed in a carbonate-bicarbonate solution at 75°C and -650 mV_{SCE} for R>0. (a) 11Hz. (b) 0.19Hz. From Parkins and Greenwell.[94]

8. Relief of stresses – The PWHT Process

Table 6.3 in Section 6.0 shows that PWHT is not common for the CCW system piping. It should be noted that PWHT is not required by ASME code for CCW system piping of this diameter and thickness. However, PWHT has been used in Kori 3 and 4 and is presumed there to be conducted by a standard ASTM procedure. A detailed study of PWHT has been conducted by Goodwin et al.[95] and their results for the effect of temperature and time on PWHT relaxation of stresses for a SA533Gr.B steel are shown in Figure 7.5.4.

The data in Figure 7.54 show that the residual stresses can be substantially reduced by PWHT. Since a 50% reduction in the residual stress can increase the initiation time of SCC by a factor of about 16, using PWHT is nominally beneficial at least for initiation as described in Section 7.3.7-4.

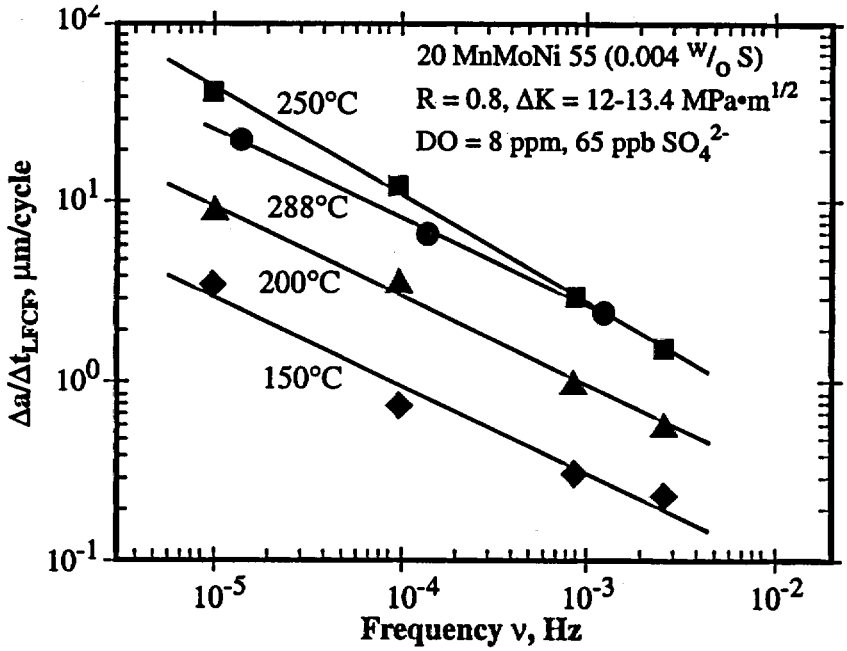

Figure 7.51 Δa/ΔN vs. frequency for low cycle corrosion fatigue for a 20 MnMoNi55 steel exposed to 8 ppm oxygen and 65 ppb SO_4^{2-} tested at four temperatures. From Ritter and Seifert.[96]

An important concern about using PWHT is whether the resulting microstructure could be more prone to SCC. This should be investigated. Also, the benefit of using PWHT, once cracks have initiated and propagated some distance, may be marginal as shown in Figure 7.48 and discussed in Section 7.3.7-4.

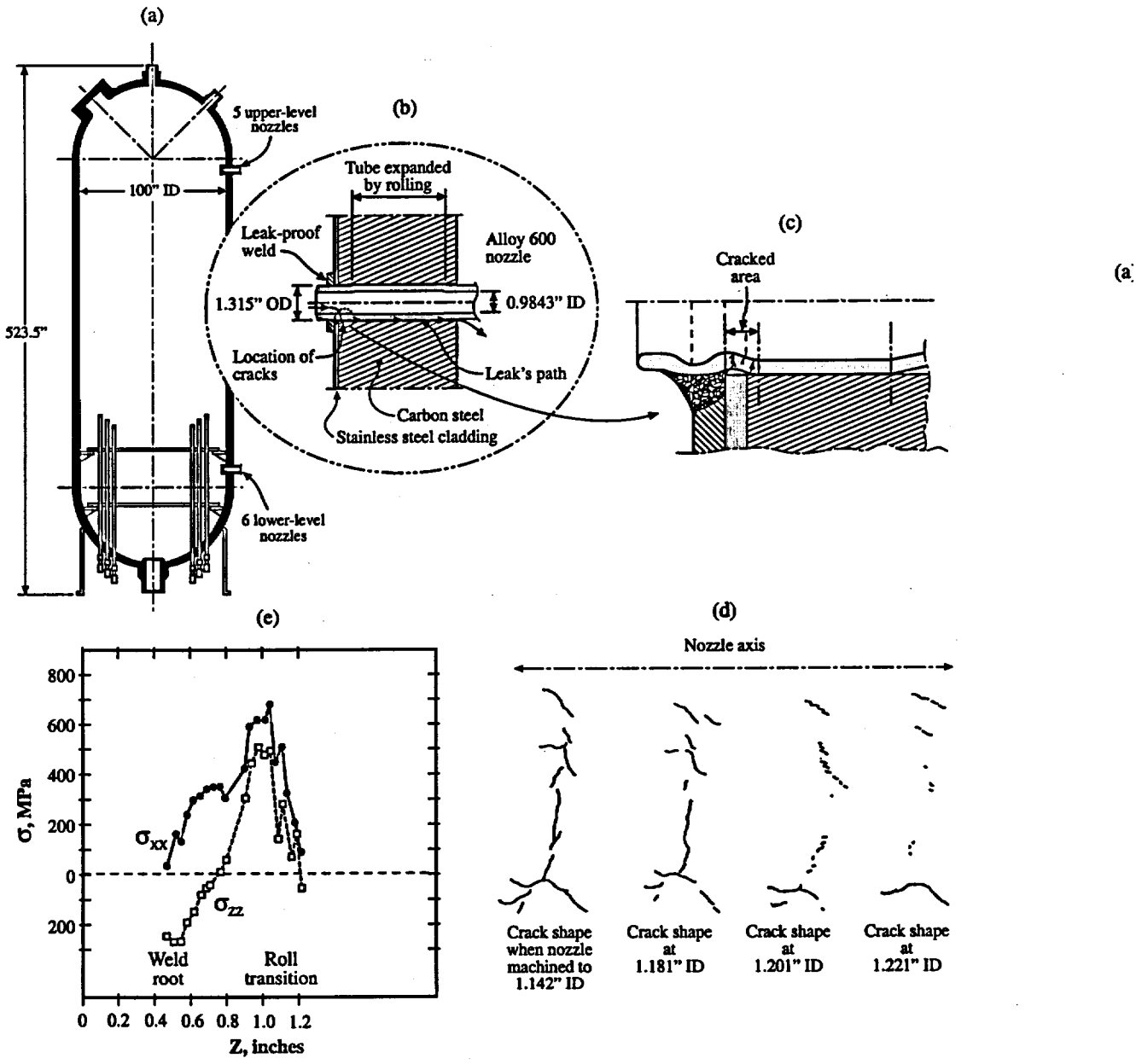

Figure 7.52 (a) Overall view of pressurizer from 1300 MW PWR plant showing locations of instrument nozzles. (b) Overview of nozzle showing locations of weld and leaks. (c) Detailed view of nozzle showing effect of welding on the roll transition zone and location of cracks. (d) Detailed view of SCC with dimensions given in terms of ID and successive machining to reveal shape of SCC. Destructive examination of one nozzle from Flamanville-2. (e) X ray diffraction measurements of the inner surface residual stresses. From Alter et al.[97]

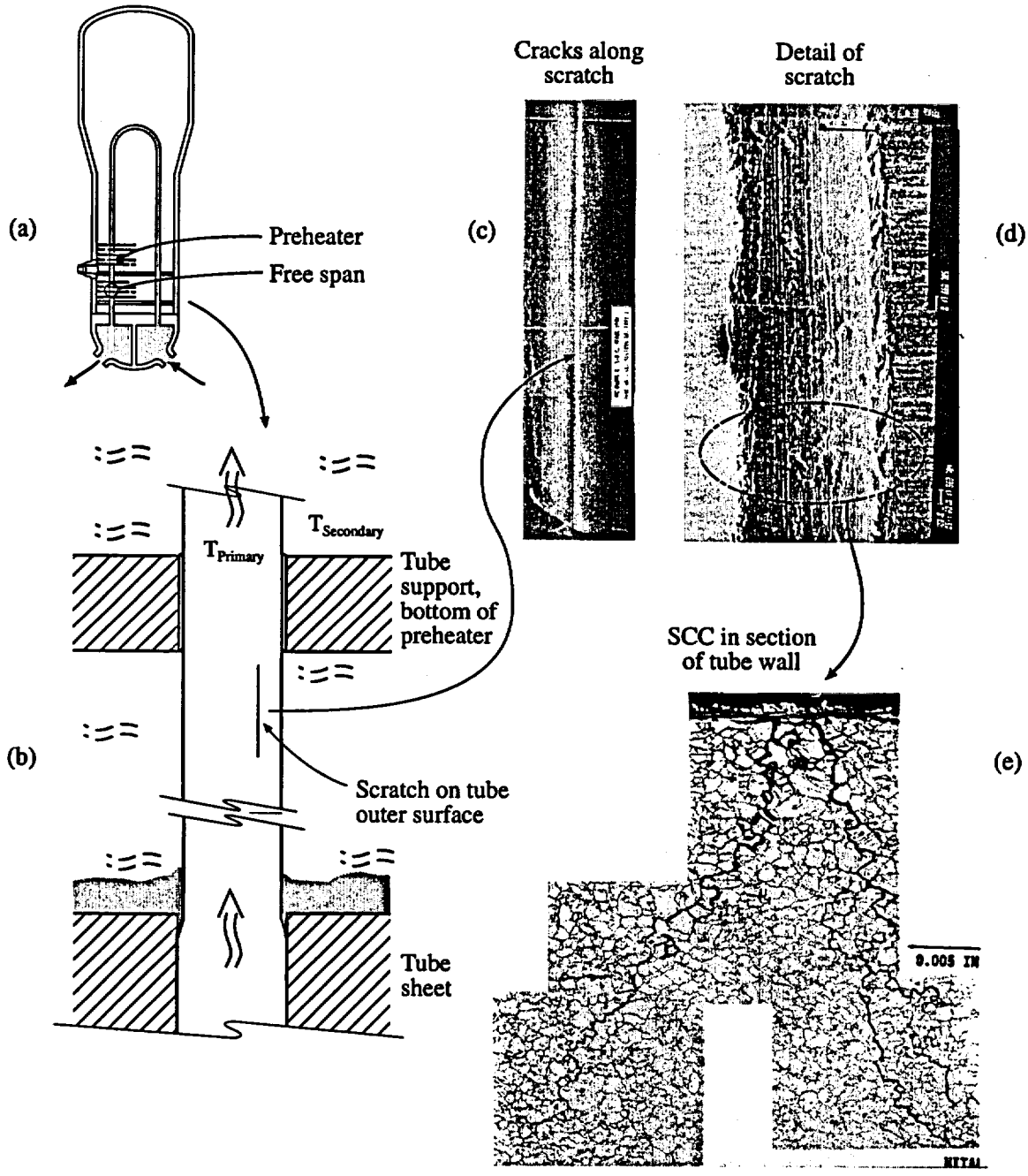

Figure 7.53 SCC at free span cold leg at McGuire Unit-2 in an Alloy 600MA tube. (a) General location of scratch and SCC. (b) Schematic view of location of SCC. (c) OD of tube showing scratch. (d) Detail of scratch with SEM. (e) Cross section of SCC. From Eaker.[98]

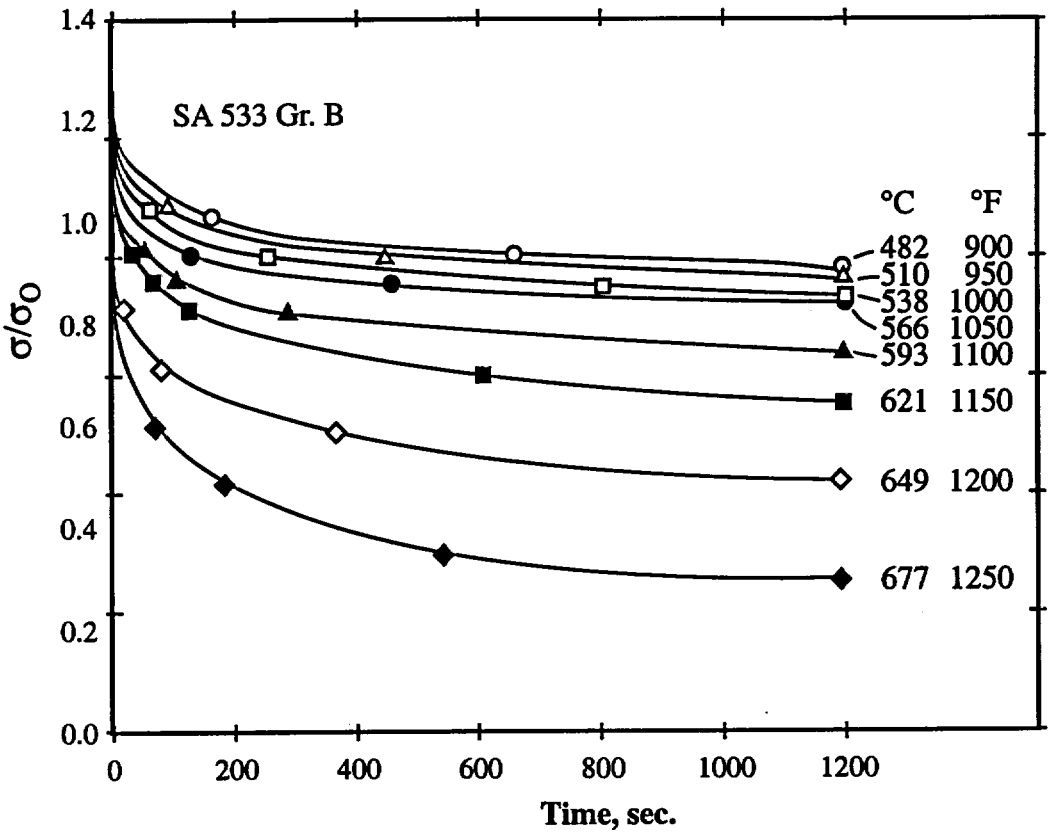

Figure 7.54 Stress ratio at time and temperature vs. initial stress vs. time for temperatures from 482 to 677°C for SA533Gr.B steel. Reduction of residual stresses with heat treatment. From Goodwin et al.[95]

8.0 Predicting SCC in the CCW System

8.1 Available Information and Meaning

While direct information from operating equipment is not available that permits precise interpretations of the SCC, useful information is, nonetheless, available and can be applied reasonably to deciding on a course of action for the CCW system at WCNOC. In this section this information and its significance are summarized. The core of the available information is given first, as underlined and the significance follows:

8.1.1 Integrity

1. Over the years of operation since 1986 there have been no significant chemical upsets, as shown in the water chemistry in Table 4.4 as well as the background from which it is taken, that indicate that the SCC is due to some special chemical aberration. Since the first SCC had taken at least eight years to perforate, whatever chemistry is relevant to producing the SCC would have to persist, more or less, steadily. Further, the chemistry in the 1986 to 1994 period, after which the first SCC was observed, would have to be similar to that in the 1994 to 2000 period after which additional SCC was observed. Note that a pipe inserted in 1994 (Weld 19A), as identified in Table 5.1 had sustained part-through SCC by 2000.[2,3,4,5,6] The pattern for SCC in the CCW system here is systemic and not accidental. Further, there is no evidence of adventitious chemical species inside the advancing SCC except for the molybdate, which is discussed in Sections 4.0 and 5.0. Also, the only contaminant, chloride, is present at such low concentrations that it cannot be taken as significant; further, there is no credible mechanism for the chloride concentrating as it does at heat transfer crevices in SGs.

2. The chemical analyses of piping, as shown in Table 3.1, indicates that the composition of the SA106Gr.B alloy is within established specifications. These results indicate that there was nothing defective in the chemistry of the alloy used in the piping.

3. In none of the piping and welds examined metallographically by Altran, AECL or the NRC were any defects observed in either the welds or piping that suggests that the material of construction was defective. It can be concluded that the SCC in the CCW system is not related to defective material.

4. NDE (UT) identified the fact that SCC in the 4" piping was about 360° intermittently around and up to 90% intermittently deep. This observation was later shown to be erroneous by direct metallographic comparison between these results and the NDE (UT) during a meeting at AECL. The NDE (UT) readings apparently had resulted from reading the weld discontinuity. The methods of NDE (UT) are being improved with the assistance of EPRI.

5. The SA106Gr.B and similar alloys are widely used for CCW systems. Tables 6.1 and 6.3 show that most of the CCW systems are fabricated from a mild steel. The chemistry

and properties of these steels are about the same. Thus, the use of the CCW system material at WCNOC is within industry patterns.

8.1.2 Use of Molybdate

1. Molybdate is a widely used inhibitor for water in steel piping. The broad use of molybdate as an inhibitor for steel exposed to aqueous coolants in industrial applications is discussed in Section 7.3.3. Molybdate is often used together with other inhibitors to achieve synergistic benefits. For example, a combination of molybdate and nitrites is sometimes used. Further, molybdate is regarded as effective as chromates in some investigations.[11,12] While molybdate is not the most widely used inhibitor in other CCW systems in the nuclear industry, Table 6.2 shows that molybdate is used by approximately 9% of present plants.

2. Most other CCW system applications use various water chemistries, including molybdates, hydrazine, pure water, phosphates, chromates, and nitrites. The plants using these various inhibitors are summarized in Table 6.2. According to Table 6.4, three plants with nitrite inhibition and one other plant using molybdate have sustained SCC. The uses of all of these inhibitors are within EPRI guidelines and/or standard industrial practice. Further, each of these has disadvantages. Hydrazine is toxic and must be used with increased pH or steel will corrode rapidly; deaeration and distilled water, unless with increased pH, accelerates the corrosion of steel; tri-sodium phosphates can produce concentrated alkalinity, and lower pH phosphates produce SCC of mild steel as in Section 7.3.1; chromates are toxic; and nitrites can be converted to nitrates by some microbial actions thereby raising the potential and possibly moving into potential ranges where SCC is accelerated. Further, the fact that no other SCC has been detected may relate more to the lack of inspection of CCW systems.

3. Molybdate is the only environmental species in the WCNOC CCW system that is observed by AECL, Altran, and NRC investigations to occur more or less uniformly along the SCC. While it is tempting to ascribe the SCC to molybdate for this reason, it is inevitable that molybdate should be inside the SCC regardless: it is present in relatively large quantities in the bulk environment; it is negatively charged; and the high oxygen provides a significant gradient in potential along the SCC to accelerate the movement of negative charges to the crack tip.

4. It is unlikely that molybdate is critically related to the occurrence of the SCC in the CCW system. There is strong evidence that molybdate is an effective inhibitor and is judged by investigators to be as effective as chromate.[59,60,62,63,64,65,66,67,69] Molybdenum alloying increases the resistance to pitting at the tips of advancing pits. Molybdate retards the advance of SCC in high temperature water despite its contribution of conductivity as shown in Figure 7.28. The observation that molybdate can produce SCC from the work 13of Holroyd does not apply to the CCW system. Holroyd's work was in a range of pH where molybdate is not an effective inhibitor as shown in Figures 7.19, 7.21a and 7.23a. Further, the concentration used was high relative to the concentrations in the CCW system. Thus, molybdate cannot be regarded as an accelerator of the SCC.

5. The present range of concentration of molybdate added as an inhibitor may be too low in view of the patterns in Figures 7.21 through 7.24. The data from these figures show that an optimum concentration should be in the range of 300 to 700 ppm with an average of 500 ppm. There does not appear to be significant improvement above this concentration.

6. There are suggestions, which are erroneous, in the literature that oxygen should be present for molybdate to exert its inhibitive action. However, there is no direct nor fundamental evidence that this co-dependence is valid. It appears that the necessity for oxygen is more related to the fact that most experiments have been conducted in the presence of oxygen since this is perceived as a worst case, and that many systems treated with inhibitors are aerated. However, there is no definitive set of experiments that demonstrate that oxygen is required for molybdate to be effective. Furthermore, there is no fundamental basis for assuming that molybdate will not be effective in deaerated water.

8.1.3 Mechanism and Principal Dependencies of IGSCC in the CCW System

Submode of SCC

1. The most likely submode of SCC that occurs in the CCW system is HPSCC as shown in Figure 7.2. This is based on the oxygen present, the similarity of crack velocities to extrapolations, as discussed in Section 8.2, and the absence of any support for a critical role of molybdate in accelerating SCC.

2. At the beginning of every SCC in the CCW system piping there is some amount of IGC regardless of whether the SCC is longitudinal or transverse. Such a pattern is observed in the work by AECL, NRC, and Altran; and it is common in many cases for IGC to occur when the conditions for SCC are close to a boundary between SCC and none such as those identified in the mode diagram of Figure 7.2. If the conditions, e.g. the oxygen or potential, are well within the region of SCC, the IGC tends not to occur. The occurrence of the IGC suggests that the SCC in the CCW system is occurring close to the boundary of the HPSCC region. For this reason, the rate of SCC is also slow.

3. There is no evidence to support that microbial or fungal action is critical to the occurrence of the SCC in WCNOC. Critical locations in the CCW system have been analyzed and no evidence of significant microbes or fungi has been found based on the report in Appendix 1.0. Further, there is no evidence that molybdates support the growth of microbes and fungi. Altran reached the same conclusions. It should be noted that there is evidence for high concentrations of sulfur as shown in Tables 4.8 and 4.9 from the work of Altran.[2,3,4,5,6] However, the source of this sulfur is not obvious since, as for all microbes and fungi, growth depends on a source of nutrients. The concentration of sulfate in the CCW system is negligible. Also, there is no evidence of sulfur on the faces of the SCC. This result showing high sulfur must be considered spurious and irrelevant to the occurrence of SCC.

Relevance of nitrate and microbial data

4. The occurrences of SCC in CCW systems of other (than WCNOC) plants, as possibly related to nitrates interacting with nitrite-oxidizing microbes, should be considered as follows, as indicated in the DEI Report,[1] and as shown in Table 6.4.

a. McGuire 1 and 2, Cooper, and Cook 1 and 2, all of which sustained SCC in their respective CCW systems1 were on nitrite water chemistry. There is some evidence for the presence of nitrite-oxidizing microbes producing nitrates which have been shown to produce SCC. This evidence is not strong in any of these cases.

b. The evidence that the SCC in these three plants is causally related to the presence of nitrates is not strong and is generally speculative. In fact, in some of the cases no microbes were found and neither were nitrates. In view of the high concentrations of nitrates required as shown in Figure 7.15, a substantive role for nitrates is not credible. Further, nitrites inhibit SCC of steel in nitrates.

c. There is no evidence that the concentrations necessary to produce a nitrate-related SCC could be or were achieved. Note that data in Section 7.3.1 Figure 7.15 require much higher concentrations of nitrates to produce SCC than are conceivably produced by the superficial reactions of nitrites on surfaces in the CCW system piping. Also the presence of nitrites inhibits SCC associated with nitrates as shown in Figure 7.15i and 7.15j.

d. There is no information on the concentration and pH dependence of nitrate-produced SCC in the range of pH and local conditions expected in these three plants.

e. It is more likely that the SCC observed in these three plants is related to high potentials that are also achieved where oxygen is the main oxidizing species. The nitrate equilibrium that is associated with the presence of the microbially-induced nitrate will stabilize this higher half cell potential that is equivalent to the presence of dissolved oxygen.

pH

5. There is some question as to whether raising pH from the past values to higher values will mitigate SCC. The desirability of raising the pH is based on two sets of evidence. One is the fact that pH 12.3 is the point where the solubilities of the iron oxides are minimum. The second is the fact that the AcSCC and AkSCC are also minimum at the same location as the solubility minimum, as shown in Figure 7.2. However, there are two countervailing arguments here: First, the protective oxide in the molybdate solution, which is most likely a $(Fe,Mo)O_x$, is probably stable over a range from at least pH 5-6 to pH 13. In the direction of potential the $(Fe,Mo)O_x$ is stable from about the average of the

Fe_3O_4/Fe half cell and the MoO_4^{2-}/Mo half cell to about the potential of hematite breakdown demonstrated in polarization tests. Whether this responds in the same way to pH as the hematite is not clear. Further, the lower boundary of the HPSCC has never been investigated as a function of pH, but its onset is probably related to the potential of breakdown of Fe_2O_3. Thus, while increasing the pH in the CCW system is probably a good idea, the bases for the effectiveness of this change are not obvious. Probably, the benefit obtained from raising the pH by addition of phosphates at the other plants noted in Table 6.3 is more related to their buffering action inside tight geometries.

Tolyltriazole

6. There is no evidence that tolyltriazole can be excluded from being considered as a possible contributor to the occurrence of SCC. Figure 7.18e shows that tolyltriazole in the range used at WCNOC does not affect significantly the passivity produced by molybdate. On the other hand, tolyltriazole is a film former and, in principal, could supply the necessary conditions for abetting SCC. Further, as shown in Figure 7.18e its effect on the polarization behavior raises several questions about its behavior as discussed in Section 7.3.3-3

Stress

7. No SCC has been observed exclusively in the piping although the metallographic observations of longitudinal SCC in Section 5.0 show that SCC can extend from the welds into the matrix. This indicates that the occurrence of the SCC depends critically upon stress, the highest stresses being associated with the welds. Further, the fact that both circumferential and longitudinal SCC occur indicates that the stresses favoring both directions depend on the geometry of the joint and the nature of the weld. These data support lowering the stresses at welds by a process like "post weld heat treatment" (PWHT). It is important, however, to assure that the PWHT does not increase the tendency for IGC, pitting, or general corrosion as well as SCC. These possibilities should be verified by direct experiments.

8. The fact that Callaway has observed SCC that is about half the depth of that in WCNOC and that they use a similar water chemistry and have a similar life suggests that the cyclic nature of the cooling water temperature may accelerate SCC at WCNOC according to the results in Figures 7.49, 7.50 and 7.51. Cyclic stressing, even with small amplitudes, and with low cyclic frequency greatly accelerates SCC. This could explain the difference between the two plants. Of course, such differences can be explained by statistical variations, different stresses, and slightly different chemistries as discussed in connection with Figures 7.6, 7.7 and 7.8.

9. The longitudinal and circumferential SCC are part of the same mechanism. Both orientations sustain the same characteristic of SCC. There is IGC at the beginning of the SCC, the SCC is intergranular, molybdenum is found along the SCC, and it occurs at locations of high stresses.

Metallurgy

10. The occurrence of SCC is independent of the metallurgy. The SCC observed at WCNOC occurs in the welds, HAZ and matrix. This is especially obvious in the longitudinal SCC shown in Section 5.0. Such independence of metallurgy emphasizes the importance of residual stresses from the welds and chemistry of the environment.

11. The preferential dissolution of pearlite has been observed in the NRC and Altran reports in the early IGC. However, this preferential dissolution does not occur along the SCC. This preferential dissolution is most likely due to the solubility of carbon in the iron carbide as studied by Staehle et al.[99,100]

12. As noted in Figures 7.6, 7.7 and 7.8 the occurrence of SCC, in general, is variable due to not well defined metallurgical factors. There is no reason to assume that the CCW system steel is any different. This implies, for example, that the occurrence of SCC among plants and within the CCW system at WCNOC would be variable. Thus, reaching conclusions about rates must recognize that there are limited data here and they are part of a larger distribution of data.

8.1.4 Comments on Other Mechanistic Proposals

Recommendations and interpretations have been supplied by DEI 1995, Altran, Turner, and NRC.[2,3,4,5,6,7,8] Their main ideas are summarized followed by my comments where the present report suggests differences:

1. DEI 1995[1]

   a. No plausible chemical interpretation is supportable. There are positive and negative aspects to the possible SCC due to high potential, mainly due to oxygen.

   b. Much of the observed SCC due to high potentials seems intergranular but this is not always so.

   c. Nitrates seem to be causally related to the SCC as they result from the microbial oxidation of nitrite.

   d. Some aspect of the weld crevice may be important.

   e. High weld stresses are a significant part of the reason for SCC.

   f. There is some evidence of reduced sulfur that may be important and may indicate the presence of sulfate reducing microbes.

Of the ideas in this report, the one about nitrite is not supportable. The nitrate SCC as described by Parkins and colleagues[53,54,57,58] is based on relatively high concentrations of nitrates. Further, there are no examples in the literature nor in practical experience[101] of SCC resulting from the oxidation of nitrites also.

While there is little question about the presence of sulfur as noted in Tables 4.8 and 4.9, this seems spurious since there is no sulfur in the SCC nor is there sufficient sulfate in the water to serve as a nutrient for the SRB.

2. Altran, June 2001, Root Cause Report.[6]

    a. Low pH reduces effectiveness of molybdate.

    b. Molybdenum concentration is too low.

    c. High temperatures reduce the effectiveness of the molybdate in providing protection.

    d. Chloride spikes may be important.

    e. Residual stresses, especially at the toe of the weld, accelerate SCC.

    f. The special corrosion at the initiation site suggests an active local electrolyte.

    g. Thermal cycling seems not to be important.

    h. The observed corrosion is "stress assisted intergranular corrosion."

The comments on molybdate, pH, concentration and temperature are dealt with elsewhere in this report, mainly in Section 7.3.3.

There is not sufficient chloride on an integrated basis to affect SCC.

Thermal cycling is important, even in the event of relatively small amplitudes and low frequencies as shown in Figures 7.49, 7.50 and 7.51.

The propagation of the SCC is not "stress assisted IGC." It is clearly SCC. However, the initiation sites are clearly IGC, and it appears that some stress is involved.

3. Turner, September 4, 2001.[7]

    a. No clear mechanistic explanation is obvious.

    b. Without a good experimental program, working out a substantive predictive interpretation is not possible.

c. Note the oxygen present, and oxygen is required to produce molybdate passivation through forming a soluble molybdate.

d. With respect to forming a stable molybdate the concentration of molybdate is too low, the pH is too low, the temperature in the high temperature region is too high, and the local turbulence at the weld geometry may de-stabilize the passivity.

e. The low rate of general corrosion indicates that the molybdate has been effective on normal surfaces.

f. The occurrence of microbes over time and the evidence of sulfides indicate that the CCW system is not sterile.

g. The stresses are high and the cyclic stresses are not significant.

h. Rates of SCC can be rationalized by taking the depth of observed cracking and comparing it to length of time over which such SCC may have occurred. This gives a rate. Such estimates suggest that SCC below 105°F is not a problem.

The cyclic stresses may be quite significant as indicated in Section 7.3.7.

While the SCC is now known to be less at the 105°F range, it is not negligible as described in Sections 5.0 and 8.2. Unfortunately, there are not sufficient data to assess the variability of SCC in this region of temperature.

There is no evidence that oxygen dissolved in the water is required for molybdate to be an effective inhibitor. While the CCW system is not sterile, the report by Little notes that there are no species that are aggressive in a corrosion sense.

The questions about the adequacy of molybdates are considered in Section 7.3.3.

4. NRC.[8]

a. No deep cracks observed despite the initial concerns and the problem is inadequate NDE (UT) technique. Also, the welding may have extensive undercuts.

b. Some localized corrosion at pearlite.

c. High concentration of carbon in the IGC.

The NRC report did not study longitudinal SCC as noted in Section 5.0 so their assumption about lack of SCC is incomplete.

The carbon observed is virtually always observed in the EDS of SEM and results from contamination. There is no evidence that this source has been separated from whatever may occur as a part of corrosion. Also, the carbon, if it is not due to system contamination, could result from the preferential corrosion of the pearlite.

The conclusions and comments presented in these reports reflected what was known at the time and were based on speculations from relatively limited data.

8.2 Prediction and Rationalization

8.2.1 Extrapolation and Comparison

The purpose of this section is to develop a quantitative basis for predicting the future occurrence of SCC and to determine whether the SCC observed in the CCW system in the range of 90 (32.2°C) to 150°F (65.56°C) is consistent with other data from the literature mainly taken at higher temperatures. A problem in developing this basis relates to the fact that there are few data at such lower temperatures, with most of the data having been obtained above 100°C. In order to relate the SCC in the CCW system to work reported in the literature, it is necessary to extrapolate from the higher temperatures to the lower temperatures of the CCW system.

The extrapolation of SCC from higher temperatures to temperatures of the CCW system was obtained by the following steps:

1. The failures that have occurred in the CCW system were taken as the following:

    a. In 1994 a through wall SCC penetration in the circumferential direction of 0.280" was observed after eight years. This corresponds to an average crack velocity of 2.82×10^{-11} m/s.

    b. In 2001 a maximum penetration of 1.2 mm in the longitudinal direction was observed after 15 years of service. This corresponds to an average crack velocity of 2.54×10^{-12} m/s.

    These data points are plotted on Figure 8.1 as line (1). These and other data are plotted in terms of an abscissa taken as 1/T since this is the conventional, as well as useful, way of analyzing rate processes in the temperature coordinate.

2. Data from the published literature for comparison with the CCW system were taken from figures in this report as follows:

    a. Line (2) is taken from Speidel and Magdowski[75] and is from Figure 7.34a. These data are based on using pre-cracked specimens of 20MnMoNi55 pressure vessel steel with $K>30$ $MNm^{-3/2}$ over a temperature range from 100 to 288°C.

b. Line (3) is taken from Speidel and Magdowski[75] and is from Figure 7.34b. In this case four lines are used. These data include a broad range of stress intensities and oxygen concentrations. 3-1 and 3-2 are the upper and lower boundaries of data from reactor pressure vessel steels tested at various oxygen concentrations and stress intensities. Points 3-3 and 3-4 are based on "low alloy steels" with 8 ppm oxygen and 0.2 ppm oxygen respectively. It is probably reasonable to take the same slopes as for lines 3-1 and 3-2 but this is not necessary since the implication is obvious.

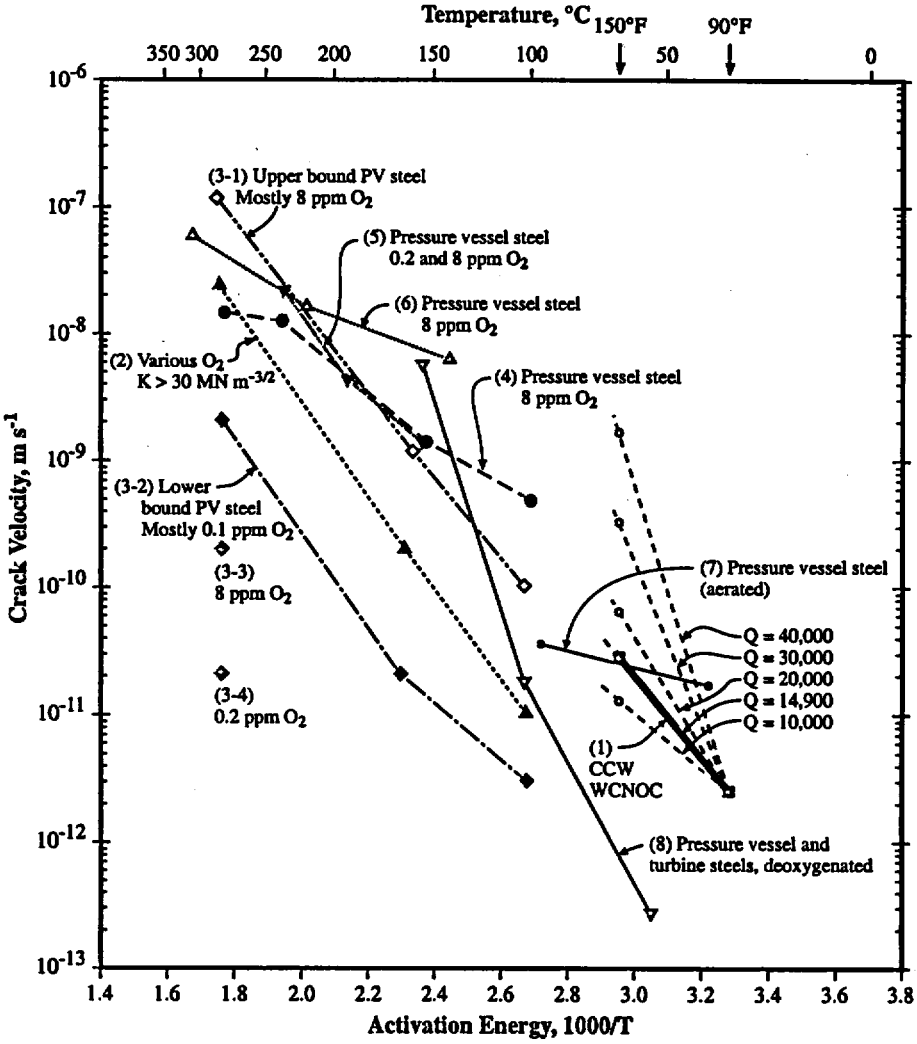

Figure 8.1 Rate of SCC vs. 1/T for steels exposed to water in the oxygenated and non oxygenated cases.

c. Line (4) is taken from Waid and Ault[47] and is from Figure 7.12a. These data were obtained by CERT testing of A508Cl2 steel in pure water with oxygen additions. The data for line (4) used only data from 8 ppm oxygen. These data are coincident practically with that of line (1). Such a similarity is reasonable

since both had the same oxygen concentration although the types of steel are different.

d. Line (5) is taken from Kuniya et al[48] and is from Figure 7.12b. These data were obtained by CERT of A533GrB from testing in pure water with additions of oxygen. The data in the temperature range of 200-250°C seemed to follow the same kind of maximum behavior as shown in Figure 7.31. Therefore, the lower temperature part of this dependence was used with a line containing points from 200°C and 150°C for three different oxygen concentrations.

e. Line (6) is taken from Rahman and Ruscak[76] and from Figure 7.34c. These data are from oxygenated environments in the temperature range of 400-600K and are pressure vessel steels.

f. Line (7) is taken from Hale[78] and from Figure 7.35a. These data were taken from aerated points and were taken from the lowest temperature points of 200°F with a slope parallel to the deaerated points for which there are more temperature-dependent data points.

g. Line (8) is taken from Ford and Andresen[102] and from Figure 7.31c where the data points are from studies of pressure vessel and turbine steels in pure water and deaerated environments. These data are taken from only lower temperature region below the peak in the temperature dependent data.

The plots of data in Figure 8.1 permit the following observations and are based on the following assumptions:

1. Most important, it appears that the CCW system SCC data are in the mainstream of data from higher temperatures, especially for the data with oxygen concentrations similar to the CCW system. These data supply the conclusion that the submode of HPSCC is the one that occurs in the CCW system.

2. The apparent activation energy of the CCW system SCC is 14.9 Kcal/mol and assumes that the SCC starts at the beginning of operation and proceeds linearly. Activation energies of 10, 20, 30 and 40 are illustrated with their apex at the 90°F data point for the CCW system data. This activation energy for the CCW system data is low relative to those for Alloy 600 in steam generators.

3. The data plotted in Figure 8.1 implicitly assume that stress is not a factor and that all data can be compared according mainly to their environments and materials. Such an assumption is certainly questionable, but there are not sufficient data for stress dependencies to be evaluated. This approach to correlation is reasonably justifiable by the generally applicable plateau behavior of the V-K curve as shown in Figure 7.46.

4. The data assume that it is legitimate to compare crack velocities from both pre-cracked specimens and CERT specimens. This is also a questionable assumption; but, again, there are not sufficient data to do otherwise.

5. The assumption that the SCC starts when the plant starts does not consider the time involved in the initiation phase. It is not uncommon for the initiation phase to consume half to two thirds of the total time to perforation as illustrated in Figure 7.43. The evidence of the IGC shown in Figures 5.1-5.3 suggests that some time was consumed in an initiation processes different from the SCC. There is no credible means for evaluating the division of the time that should be allocated to propagation and initiation according to Figure 7.43. If some time is allocated to initiation, then the actual rate would be greater and possibly as high as three times greater. Such values would suggest that the steel used in the CCW system is especially prone to HPSCC relative to the other data in Figure 8.1.

6. The data in Figure 8.1 also do not account for any accelerations produced by cyclic stressing possibly due to variations in temperature. According to Figures 7.49-7.51 such additional and possibly small cyclic stresses would increase the rate and suggest that the inherent rate without the cycling could be a factor of ten less than that which was observed and shown in Figure 8.1. There is no credible way to evaluate such a correction.

7. The data on the SCC from other plants given in Table 1 of the DEI[1] report should be included in Figure 8.1, but the data on temperatures at which SCC occurred are not available although it is likely that the SCC that was observed occurred in the range of 150°F.

8.2.2 Prediction of SCC at WCNOC

While there are uncertainties in understanding the bases for the data that apply to WCNOC as discussed in Section 8.2.1, the plot of line (1) in Figure 8.1 is probably the best basis for predicting the occurrence of SCC for the following reasons:

1. Line (1) includes whatever cyclic patterns of stress are inherent.

2. Line (1) includes whatever patterns of residual stress exist.

3. Line (1) includes whatever contribution of initiation that exists.

4. Line (1) includes both the circumferential SCC that was examined in the Altran reports[2,3,4,5,6] and the longitudinal SCC that was examined in the AECL report.[9] This line should apply to the rate of both orientations of SCC.

The disadvantage of using Line (1) is that whatever step of initiation is required has already occurred so that the rate of the propagation of the remaining SCC will be more rapid than the average used for Line (1).

Predicting future perforation by SCC at WCNOC for piping now in place and not having PWHT should proceed as follows:

1. Choose a mean temperature for the location of interest.

2. Use this mean temperature to determine the rate of SCC from Figure 8.1.

3. Assume that the rate of SCC applies from the start of the plant.

4. Assume that the present depth of SCC is that determined from Line (1).

5. Assume that the time to perforate is determined by the rate from Line (1) calculated with respect to the wall thickness of the pipe. i.e. time to perforate is determined by Eqn. (8.1):

Time to perforate=(thickness of the wall)/(rate at temperature from Line (1)) (8.1)

Modifications in the application on this time to perforate that should be considered are:

1. If a conservative penetration is appropriate, and some such conservatism should be considered, then the time to perforate should include a conservative thickness such as one half of the nominal wall thickness.

2. If a conservative form of Line (1) is appropriate, a factor of two increase in the rate is probably adequate. This would account for the time involved with initiation as shown in Figure 7.43. Further this would account for the fact that SCC would have already initiated. This would be consistent with extrapolations from higher temperature data.

3. If the expected direction of the SCC is longitudinal, such as that shown in the AECL report, then it is not necessary to apply either the thickness or rate conservatisms. Here, a "leak before break" (LBB) is assured. Further, the length of the SCC will be short and not reach a K_IC condition based on the limitation of length over which the residual stresses from the weld can apply.

4. If the expected direction of the SCC is circumferential, such as those shown in the Altran report, then the conservatisms of #1 and #2 should be applied since the possibility of LBB is not assured. The extent of prior penetration before reaching K_IC should be determined. However, past testing at WCNOC has shown that SCC that has occurred has produced LBB.

9.0 Recommendations

9.1 Specific Recommendations for the CCW System

I recommend that the following specific actions be taken to mitigate or prevent SCC in the CCW system at WCNOC. While these actions do not affect the immediate operation of the plant, they are important for assuring future reliable operation of the CCW system.

1. The present possibilities of "leak before break" (LBB) or "break before leak" (BBL) according to Section 8.2.2 and Figure 7.47 should be analyzed for present piping.

2. Applying PWHT to the welds in the CCW system should be considered especially for the higher temperature locations. This would reduce further significant growth of SCC with the caveat concerning how the V-K curve interacts with existing SCC as illustrated in Figure 7.48. This action should be preceded by determining whether this PWHT treatment increases the susceptibility of the alloy to SCC to an extent that exceed the benefit of lowering the stress. Lowering the residual stress by a factor two reduces the time to initiate SCC by a factor of about 16 assuming a stress exponent of 4.0. However, lowering the residual stress for a propagating SCC may produce much less to negligible benefit if there are already existing SCC and the resulting stress intensity remains in the plateau range as illustrated in Figures 7.46 and 7.48. It is possible that a lowering of the mean stress by a factor of two would produce no decrease in the rate of propagation.

3. Leaving the present molybdate water chemistry is acceptable so long as the PWHT is instituted. It should be recognized that this treatment will not prevent SCC so long as the system is oxygenated regardless, to a first order, of the concentration of molybdate or the pH. Also, there is no evidence that the molybdate water treatment accelerates SCC. While there is evidence in Figures 7.24, 7.25d and 7.28 that MoO_4^{2-} decreases the intensity of SCC, it appears that the present water chemistry does not prevent SCC.

4. The molybdate water treatment is applicable primarily to lowering the general corrosion rate. In this circumstance, the data in Section 7.3.3 indicate that the optimum concentration of molybdate is about 500 ppm at a pH of about 9. These values should be the mean of the continuing program in water chemistry.

5. A water treatment that would greatly minimize, if not prevent, the SCC which is now occurring, is the AVT//hydrazine described in Section 6.0. This treatment should be considered.

6. Institute a regular program of qualified NDE (UT) inspections with intervals that respond to the rate of crack growth.

7. Periodically assess the microbial/fungal environment.

8. Maintain graphical water chemistry records that can be inspected periodically including measurements of molybdate, chloride, sulfate, tolyltriazole, pH, conductivity, and oxygen.

9. The water temperatures at several critical locations in the CCW system should be monitored and recorded, partly to assess the cyclic nature of thermal stress.

10. Maintain a current knowledge of the performance of CCW systems in other plants.

9.2 Recommended Supporting Work

There are several open questions in the above options, and some experimental work should be undertaken as follows although completing this work does not affect the near term reliable operation of the plant:

1. The PWHT should be evaluated to assure that the residual stresses are adequately relieved. This should include measuring existing residual stresses and residual stresses after the heat treatment using conventional X ray methods.

2. After the PWHT the material should be subjected to a SCC test, such as CERT, to determine how the heat treatment has changed the proneness of the alloy to SCC.

3. There is a possibility that lowering the residual stresses will not reduce the rate of propagation of existing SCC as described in Figure 7.48. This situation should be analyzed.

4. The role of tolyltriazole with respect to accelerating SCC should be evaluated; a CERT test would be adequate.

5. Future metallography of any perforation or significant signal from the NDE (UT) should include:

    a. The depth of the SCC should be determined over its length in the longitudinal or circumferential directions.

    b. Especially for circumferential SCC, the depth should be recorded at least in four locations 90° apart.

    c. For longitudinal SCC, it should be evaluated if circumferential SCC is not observed; and the length of the SCC should be determined.

    d. The extent and uniformity of the IGC should be evaluated.

6. Data for K_IC for the SA106Gr.B, in the wrought, HAZ and welded conditions, should be reviewed and assessed for application to the SCC in the CCW system.

7. Some critical location in the CCW system piping should be monitored with a strain gage to assess cyclic stressing.

10.0 Acknowledgements

In preparing this report I appreciate the many important contributions from WCNOC and especially from Dave Meredith, Art Turner and Dan Womelsdorf. At AECL I appreciated the important contributions of Mike Wright, who managed the project, Marina Totland, who coordinated the chemical analyses from AECL in Section 4.0, and Allan Lockley, who handled the metallography. I appreciate Brenda Little for her always professional and expert collaboration on the microbial/fungal work in Appendix 1.0.

In my office, I continue to appreciate the energetic and professional contributions of Mary Ilg, Barb Lea, Erin Kate Parrish-Siggelkow, Julie Daugherty, and John Ilg.

11.0 Appendix

1.0 Brenda J. Little, "An Investigation of Microbiologically Influenced Corrosion at Wolf Creek Nuclear Generating Plant," 14 September 2002

2.0 Roger W. Staehle Curriculum Vitae

3.0 Michael D. Wright Curriculum Vitae

4.0 Brenda J. Little Curriculum Vitae

An Investigation of Microbiologically Influenced Corrosion at Wolf Creek Nuclear Generating Plant

Prepared by Brenda J. Little

14 September 2002

Abstract: There is no evidence that microorganisms are influencing corrosion in the CCW carbon steel piping systems at Wolf Creek Nuclear Generating Plant. The numbers and types of organisms isolated from waters and carbon steel surfaces within the system are typical of low nutrient waters. There were no consistent enrichments of organisms on surfaces.

Introduction: The CCW system is cooled by lake water in carbon steel heat exchangers. Under the current operating conditions molybdate (700 ppm) is added and pH is controlled at 9.5 with sodium hydroxide. The system is operated as a closed system and chemicals are added in demineralized water. Non-destructive testing had indicated some surface corrosion on the nozzle and a single line of the letdown heat exchanger. Water and surface deposits were removed from the system to determine whether microorganisms influenced the potential corrosion.

Methods and Materials: Water from ten locations within the CCW carbon steel piping system of Wolf Creek Nuclear Generating Plant was collected in individual sterile 50 ml plastic containers on 7/2/02. Valve locations are listed in Table 1.

Table 1. Valve descriptions

BGV0558	Letdown heat exchanger CCW return header drain.
EGV0155	CCW chemical addition tank (TEG02) drain.
EGV0168	CCW surge tank A (TEG01A) drain.
EGV0179	CCW surge tank B (TEG01B) drain.
EGV0307	CCW heat exchanger EEG01A outlet header drain.
EGV0308	CCW heat exchanger EEG01B outlet header drain.
EGV0382	Demineralized water to CCW surge tank TEG01A.
EGV0384	Demineralized water to CCW surge tank TEG01B.

At the same time, surface films were collected from nine locations using sterile Dacron® swabs. Each swab was transferred to a vial containing 5 ml sterile buffer solution. Samples were packed with a frozen gel refrigerant and shipped overnight to the laboratory. On 7/3/02, water samples and suspensions of surface samples in buffer were used to inoculate liquid media specific for anaerobic bacteria (ANA), aerobic bacteria (AERO), sulfate-reducing bacteria (SRB) and acid-producing bacteria (APB). Composition of media and buffer are included in Appendix A. Each sample was diluted to 10^{10}. Water and swab samples were streaked directly on plates of potato dextrose agar for determination of the presence of fungi. Water samples collected 6/5/02 by plant personnel were treated similarly. Media were examined over a one-month period for growth.

1.RESULTS

Results are summarized in Table 2. The highest number of bacterial cells were cultured from surge tank (A and B) waters that had been collected 6/5/02 and stored in plastic bottles at room temperature until 7/3/02. The microbial content of water in the CCW system collected 7/2/02 varied with location. Lake water contained higher numbers of aerobic bacteria than water from locations within the CCW system. The demineralized water contained roughly the same numbers of aerobes and anaerobes, approximately 10^{3-4}, each. Half the water samples collected on 7/2/02 were negative for SRB. The highest concentration of SRB was found in a surface swab sample from EG-V155. All other swab samples were negative for SRB. The numbers and types of organisms isolated from the surfaces were not markedly different from those in water samples on from the same locations.

Discussion:

Microbiologically influenced corrosion (MIC) is localized corrosion resulting from the presence and activities of microorganisms, including bacteria and fungi. Pope (1986) made the following generalizations about microorganisms:

- Individual microorganisms are small (from less than two-tenths to several hundred micrometers (μm) in length by up to two or three μm in width. Bacterial and fungal colonies can grow to macroscopic proportions.

- Bacteria may be motile, capable of migrating to more favorable conditions or away from less favorable conditions, e.g., toward food sources or away from toxic materials.

- Bacteria have specific receptors for certain chemicals and can move to higher concentrations of those substances. Surfaces, including metals, adsorb nutrients.

- Microorganisms can withstand a wide range of temperatures (at least -10 to 99 °C), pH (about 0 - 10.5) and oxygen concentrations (0 to almost 100% atmospheres).

- Microorganisms grow in colonies making survival more likely under adverse conditions.

- Microorganisms reproduce very quickly (generation times of 18 minutes have been reported).

- Individual cells can be widely and quickly dispersed.

- Many can quickly adapt to a variety of different nutrient sources, including sugars, lipids, alcohols, phenols, organic acids, etc.

- Many microorganisms form extracellular polysaccharide substances (EPS). EPS trap organisms and debris (food) and resist penetration of some toxicants (e.g., biocides and corrosion inhibitors).

- Many bacteria and fungi produce spores which are very resistant to temperature (some even resist boiling for over 1 hour), acids, alcohols, disinfectants, drying, freezing, and many other adverse conditions. Spores may remain viable for hundreds of years and germinate on finding favorable conditions.

- Microorganisms are resistant to many chemicals (antibiotics, disinfectants, etc.) by virtue of their ability to degrade them or by being impenetrable to them (due to slime, cell wall or cell membrane characteristics).

The most aggressive MIC takes place in the presence of microbial consortia in which many physiological types of bacteria interact in complex ways within the structure of biofilms. MIC does not produce a unique form of localized corrosion. Instead, MIC can result in pitting, crevice corrosion and underdeposit corrosion, in addition to enhanced galvanic and erosion corrosion.

The microorganisms that are most frequently cited as causing microbiologically influenced corrosion in carbon steel piping exposed to natural waters are SRB, APB and fungi. SRB concentrations are always positively correlated with sulfate concentration. SRB grow in soil, fresh water, or salt water under anaerobic conditions. Many species of SRB have been identified, differing in morphology and in organic substances that they can metabolize. They have in common the ability to oxidize certain organic substances to organic acids or carbon dioxide by reduction of inorganic sulfate to sulfide. In the absence of oxygen, the metabolic activity of SRB causes accumulation of hydrogen sulfide near metal surfaces. This is particularly evident when metal surfaces are covered with biofilms. The concentration of sulfide is highest near the metal surface. Iron sulfide forms quickly on carbon steels and covers the surface if both ferrous and sulfide ions are available. Formation of iron sulfide minerals stimulates the cathodic reaction. Once electrical contact is established a galvanic couple develops with the mild steel surface as an anode, and electron transfer occurs through the iron sulfide. At low ferrous ion concentrations, adherent and temporarily protective films of iron sulfides are formed on the steel surface, with a consequent reduction in corrosion rate. Aggressive SRB corrosion requires exposure to oxygen. Accordingly, structures that are exposed under fully deaerated conditions generally experience low corrosion rates despite the presence of high concentrations of SRB.

Both bacteria and fungi can produce organic acids. Most of the final products of APB are short-chained fatty acids, i.e., acetic, formic and lactic acids. The role of APB in MIC is controversial. Some propose that APB produce biogenic organic acids that are directly responsible for corrosion in the absence of SRB. Others report that the main role of APB is to provide the environment and nutrients for SRB growth. The corrosion rate of carbon steel in fresh waters is independent of pH between 4.5 and 9.5 (Metals Handbook, 1985).

This has been confirmed in tap water and distilled water. Over this range of pH values corrosion is controlled by oxygen diffusion. At pH 4.0 or below hydrogen evolution takes place and corrosion increases rapidly.

Microorganisms can also affect corrosion of carbon steel by creating differential aeration cells on the surface of the metal and fixing the location of anodic sites beneath colonies of microorganisms. The organisms most often cited as causing differential aeration cells are those organisms capable of depositing iron and manganese oxides. Manganese oxidation and deposition is coupled to cell growth and metabolism of organic carbon. The reduced form of manganese (Mn^{+2}) is soluble and the oxidized forms (Mn_2O_3, MnOOH, Mn_3O_4, MnO_2) are insoluble. As a result of microbial action, manganese oxide deposits are formed on buried or submerged materials including metal, stone, glass, and plastic, and can occur in natural waters that have manganese concentrations as low as 10 to 20 ppb. For mild steel corrosion under anodic control, manganese oxides can elevate corrosion current. The current may be significant for biomineralized oxides that provide large mineral surface areas. Given sufficient conductivity, manganese oxide may serve as a cathode to support corrosion at an oxygen-depleted anode within the deposit.

Iron-oxidizing bacteria produce orange-red tubercles of iron oxides and hydroxides by oxidizing ferrous ions from the bulk medium or the substratum. Iron-depositing bacteria are microaerophilic and may require synergistic associations with other bacteria to maintain low oxygen conditions in their immediate environment. Deposits of cells and metal ions create oxygen concentration cells that effectively exclude oxygen from the area immediately under the deposit and initiate a series of events that individually or collectively are very corrosive. In an oxygenated environment, the area immediately under individual deposits becomes deprived of oxygen. That area becomes a relatively small anode compared to the large, surrounding oxygenated cathode. Cathodic reduction of oxygen may result in an increase in pH of the solution in the vicinity of the metal. The metal will form metal cations at anodic sites. If the metal hydroxide is the thermodynamically stable phase in the solution, the metal ions will be hydrolyzed by water, forming H^+ ions. If cathodic and anodic sites are separated from one another, the pH at the anode will decrease and that at the cathode will increase. The pH at the anode depends on specific hydrolysis reactions. In addition, Cl^- ions from the electrolyte will migrate to the anode to neutralize any buildup of charge, forming heavy metal chlorides that are extremely corrosive. Under these circumstances, pitting involves the conventional features of differential aeration, a large cathode-to-anode surface area, and the development of acidity and metallic chlorides.

All water samples collected from the CCW system were taken as the first draw sample, i.e., the system was not flushed prior to sample collection. The first draw sample may contain higher numbers of microorganisms than water samples taken after flushing. The liquid and solid media used in this study provide optimum growth conditions for a small percentage of the natural population. Only 1-10% of the bacteria in any natural population can actually be cultured. Therefore, the numbers for bacteria in Table 1 may be gross underestimations. Alternatively, bacteria and fungi that were cultured may not be active in the system and may grow only when provided with nutrients. Despite the

uncertainties and limitations of microbial culture techniques several observations can be made. Bacteria and fungal cells from all samples taken from the CCW system grew slowly, with the first evidence of growth after one week to 10 days. Both APB and fungi were isolated from the raw lake water and from waters within the plant. The distribution of these organisms does not appear to be related to chemical additions or specific locations. Furthermore the organisms that cause corrosion are usually in biofilms on corroding surfaces. There were no indications that microorganisms of any particular type were associated with surface films. Only limited numbers of SRB could be isolated from any location in the system. There were no indications of iron or manganese deposits.

Three operating conditions limit the distribution and growth of microorganisms in the CCW system: addition of molybdate and elevated temperature and pH. The molybdate ion, a structural analogue of sulfate, inhibits sulfate reduction. The effect is extremely specific and effective in natural waters. Each organism has a pH and temperature range within which growth is possible and each usually has a well-defined optimum pH. Most natural environments have pH values between 5 and 9, and organisms with optima in this range are common. Only a few species can grow at pH values of less than 2 or greater than 10. Most fungi grow best in slightly acidic media. Bacteria and fungi can grow over the complete range of temperatures in which life is possible, but no one organism can grow over this entire range. Microorganisms can be grouped in three categories based on the temperature required for growth: psychrophiles (cold-loving), mesophiles (growing at moderate temperature) and thermophiles (heat loving). Each organism is restricted of +/- 30°C and can grow well that narrower range. The upper limit for fungal growth is 62-65°C. Most fungi are mesophilic, growing at temperatures between 10-35°C. A temperature of 90°C (194° F) is required to kill spores.

Bacteria in stored samples (collected 6/5/02) were orders of magnitude higher than in water samples collected 7/3/02 from the same locations, reflecting growth of organisms during the storage period or contamination. In either case, water from the surge tanks can support a higher microbiological population than was measured on 7/2/02. Subtle changes in operating conditions will influence the numbers and types of organisms in the CCW system.

References

Metals Handbook Desk Edition (1988) Carbon and alloy steels. ed. C. Mitchell Chapter 4 91-92.

D. Pope, "A Study of Microbiologically Influenced Corrosion in Nuclear Power Plants and a Practical Guide for Countermeasures," Electric Power Research Institute Report NP-4582, May 1986.

Appendix 2.0

ROGER WASHBURNE STAEHLE

Vital

Born: February 4, 1934, Detroit, Michigan, U.S.A.

Residence

North Oaks, Minnesota, USA

Education

- B. Met. Engr., The Ohio State University, 1957
- M.S. Met. Engr., The Ohio State University, 1957
- Westinghouse Reactor Engineering School, (6 months), 1959
- Ph.D., The Ohio State University, 1965

Employment

- Naval Officer and Nuclear Engineer with United States Navy and Atomic Energy Commission (with Vice Admiral H. G. Rickover). Naval Nuclear Reactor Development, 1957-1961
- Graduate Student, Research Associate, and International Nickel Fellow, The Ohio State University, 1961-1963
- Graduate Student, Research Associate, and Battelle Fellow, The Ohio State University, 1963-1964
- Assistant Professor, The Ohio State University, 1965-1967
- Associate Professor, The Ohio State University, 1967-1970
- Professor, The Ohio State University, 1970-1979
- Director, Fontana Corrosion Center, 1975-1979
- Dean, Institute of Technology, University of Minnesota, 1979-1983
- Professor, Chemical Engineering and Materials Science, Institute of Technology, University of Minnesota, 1983-1988.
- President & Chairman, Automated Transportation Systems, Inc. (now Taxi-2000) Minneapolis, 1984-1986. (On leave from University of Minnesota)
- Industrial Consultant, North Oaks, MN, 1986-Present
- Adjunct Professor, University of Minnesota, 1988-Present

Honors

- Electrochemical Society (ECS) Fellow Award, 2000
- TMS Meeting, "Chemistry and Electrochemistry of Corrosion and Stress Corrosion," in honor of R.W. Staehle, New Orleans, February 2001
- NACE Fellow Award, 1993
- NACE T.J. Hull Award, Corrosion'92, Nashville, TN
- Distinguished Alumnus, The Ohio State University, College of Engineering, April, 1989
- Willis Rodney Whitney Award from NACE for Outstanding Contributions to Corrosion Research, 1980
- Research in Progress meeting of NACE; special award (1979) for organizing the first conference
- National Academy of Engineering, 1978
- International Nickel Professor of Corrosion Science and Engineering, 1971-1976
- ASM Fellow, 1975
- College of Engineering awards for achievement (three awards) 1966, 1969, and 1970
- Ohio ASEE Award for Innovative Teaching, 1975

Publications

- 22 Edited volumes
- 37 Major Review Articles
- 126 Research Articles
- 82 Technical Reports for various national and international government organizations including DOE, EPRI

Boards of Directors

- Data Card Corporation, 1979-1983
- Donaldson Company, Inc., 1979-1983
- Teltech, Inc., 1984-1987
- Great Northern Iron Ore Properties- 1982-present

Appendix 3.0

MICHAEL D. WRIGHT

Technical Specialty:	Metallurgical Engineering
Current Position:	Corrosion Specialist, Heat Exchanger Technology Branch
Education:	Ph.D. (Metallurgical Engineering) Birmingham (1989) B.Sc. (Hons. Metallurgy & materials Science) Birmingham (1985)
Experience:	Employed at AECL since 1993. Total of 13 years work experience in stress corrosion, fatigue and welding. Corrosion engineer specializing in: • stress corrosion cracking of steam generator tubing, stainless steels and carbon steels • fatigue/corrosion fatigue of CANDU materials in high temperature water • materials/corrosion consulting for AECL • fitness for service/root cause assessments, including failure analyses
Experience Prior to AECL:	The Welding Institute (UK): Welding of medium and high-strength steels; stress corrosion/corrosion fatigue of carbon and stainless steels. Contract R&D, failure investigations and consulting.
Publications:	15 papers and publications

Appendix 4.0

Brenda J. Little January 2003

Home Address: 6528 Alakoko Drive, Diamondhead, MS 39525
Tel. (228) 255-9353
blittle@worldnet.att.net

Work Address: Naval Research Laboratory (NRL), Code 7303, Stennis Space Center, MS 39529 Position (8/96 - present) Senior Scientist

Education: B.S.(Biology/Chemistry), Baylor University, Waco, TX,1967
Ph.D. (Chemistry), Tulane University, New Orleans, LA, 1983

Adjunct Faculty Positions:

University of Southern Mississippi, Dept. of Marine Sciences, Hattiesburg, MS
Montana State University, Chemical Engineering Dept., Bozeman, MT

Memberships

American Chemical Society, National Association of Corrosion Engineers, Sigma Xi, Mississippi Academy of Sciences.

Publications

Peer-reviewed journal articles 77
Book Chapters 21
Books 1
Technical papers in symposium proceedings 96
Technical reports 10

Awards

3/02	NRL Alan Berman Research Publication Award
3/00	NRL Alan Berman Research Publication Award
3/99	National Association of Corrosion Engineers - International Technical Achievement Award
6/98	Outstanding Performance Award
3/98	National Association of Corrosion Engineers - International Fellow Award
3/95	1995 Women in Science and Engineering Award for Scientific Achievement

Selected Recent Publications

Little B (with) T Daulton, K Lowe, and J Jones-Meehan (2002) A Technique for Examination of Microbial Chromium (VI) Reduction. Journal of Microbiological Methods Vol 50. pp 39-54.

Little, B, and R Ray, (2002) A Perspective on Corrosion Inhibition by Biiofilms. Corrosion Vol 58, No. 5, pp 424-428.

Little B (with) J Banfield, J Moreau, C Chan, and S Welch (2001) Mineralogical Biosignatures and the Search for Life on Mars. Astrobiology 1(4) pp 447-467.

Little B and R Ray (2001) A Review of Fungal Influenced Corrosion. Corrosion Reviews Vol. XIX Nos. 5-6. pp 401-417.

Little B (with) T Daulton, K Lowe, and J Jones-Meehan, J (2001) In Situ Environmental Cell - Transmission Electron Microscopy Study of Microbial Influenced Reduction of Chromium (VI). Microscopy and Microanalysis Vol 7 pp 470-485.

Appendix 4.0 (continued)

Little B and R Staehle (2001) Fungal Influenced Corrosion in Post-tensioned Structures. Interface Winter 2001 pp 44-48.

Little B, R Staehle, R Davis (2001) Fungal Influenced Corrosion of Post-tensioned Cables. Biodeterioration and Biodegradation 47:71-77.

Little B (with) R Pope and R Ray and (2000) Microscopies Spectroscopies and Spectrometries Applied to Marine Corrosion. Biofouling Vol. 16(2-4) pp 83-92.

Little B (with) R Ray and R Pope (2000) Analysis of Hydrated Biological Specimens in the TEM: *Pseudomonas* Attachment to Corroding Iron. Microscopy and Analysis July pp 27-29.

Little B (with) M Franklin, D White, R Ray and R Pope (2000) The Role of Bacteria in Pit Propagation of Carbon Steel. Biofouling 15(1-3):13-23.

Little B, R Ray and R Pope. 2000 The Relationship Between Corrosion and the Biological Sulfur Cycle: A Review. Corrosion 56(4): 433-443.

Little, B, R Ray, P Wagner, J Jones-Meehan, C Lee and F Mansfeld. 1999 Spatial Relationships Between Marine Bacteria and Localized Corrosion. Biofouling 13(4): 301-321.

Little, B and M McNeil. 1999 The Use of Mineralogical Data in Interpretation of Long-Term Microbiological Corrosion Processes: Sulfiding Reactions Journal of the American Institute for Conservation 38:186-199.

Little, B, P Wagner, K Hart, R Ray, K Nealson and C Aguilar, 1998. The Role of Biomineralization in Microbiologically Influenced Corrosion. Biodegradation 9:1-10.

Little, B, R Ray and P Wagner (1998) Engineering Parameters that Affect Microbiologically Influenced Corrosion. Chemical Engineering Progress. September 1998; pp. 51-60.

Little, B (with), J Puh, P Wagner and W Bradley, 1998. The Effects of Biofouling on Graphite/Epoxy Composites. Journal of Composites Technology and Research,Vol. 20(1):pp. 59-67.

Little, B and P Wagner, 1997. Myths of Microbiologically Influenced Corrosion. Materials Performance 36(6):40-45.

12.0 References

1. Review of McGuire and Wolf Creek Component Cooling Water System Cracking, Dominion Engineering Report R-4323-00-2, Revision 0, May 1995.
2. Failure Analysis of Cracked Welds in Component Cooling Water Piping, Altran Technical Report No. 00617-TR-001, Rev. 0, Vol. 1/1, August 2000.
3. Failure Analysis of Cracked Component Cooling Water System Welds, Altran Technical Report No. 00628-TR-001, Rev. 0, Vol. 1/1, February 2001.
44. Root Cause Investigation of CCWS System Weld Cracking, Altran Technical Report No. 00628-TR-002, Rev. 0, Vol. 1/1, April 2001.
5. Failure Analysis of Cracked Component Cooling Water System Welds, Altran Technical Report No. 00628-TR-001, Rev. 1, Vol. 1/1, May 2001.
6. Root Cause Investigation of CCWS System Weld Cracking, Altran Technical Report No. 0068-TR-002, Rev. 1, Vol. 1/2, June 2001.
7. A.P.L. Turner, "Stress Corrosion Cracking of Component Cooling Water (CCW) Piping and Letdown Heat Exchanger (P.O. 0714037/0)," letter to D.B. Meredith (WCNOC), L-4340-00-01, September 4, 2001.
8. C. Wong and W.H. Cullen, Metallurgical Investigation into the Cause of Cracking in Piping for the Containment Cooling Water System at Wolf Creek, NRC Report, December 5, 2002.
9. M.D. Wright, Examination of Cracking in Welds from the Wolf Creek Component Cooling Water System; AECL CS-71300-ASD-001, Revision 0, Atomic Energy Canada Limited, September 2002.
10. K.A. Selby, G.A. Loretitsch, and D.J. Robinette "Closed Cooling Water Chemistry Guideline; TR-107396, EPRI, Palo Alto, October 1997.
11. W.D. Robertson "Molybdate and Tungstate as Corrosion Inhibitors and the Mechanism of Inhibition," Journal of the Electrochemical Society Vol. 98, 1951, p. 95.
12. M.J. Pryor and M. Cohen, "The Inhibition of the Corrosion of Iron by some Anodic Inhibitors," Journal of the Electrochemical Society Vol. 100, 1953, p. 203.
13. N.J.H. Holroyd, Environmental Aspects of Stress Corrosion Cracking of Ferritic Steels, Ph.D. Thesis, University of Newcastle-upon-Tyne, 1977.
14. B. Reischmann, M. Mukherjee, and J. Holland "Component Cooling Water Piping Stress Corrosion Cracking of Let Down HX Piping," draft dated 3/13/95.
15. B.J. Agle, "Failure Analysis of Cracked 6 Pipe and Elbows," Sherry Laboratories.
16. J. Gorman (DEI) and B. Reishmann, (WCNOC), Telecon., March 21, 1995.
17. B.J. Little, An Investigation of Microbiologically Influenced Corrosion at Wolf Creek Nuclear Generating Plant, 14 September 2002.
18. Wolf Creek Component Cooling Water System and Letdown Heat Exchanger Cracked Welds, Wolf Creek presentation to Electric Power Research Institute.
19. Private communication with D. Womelsdorf, WCNOC.
20. D. Meredith, NALCO Analytical Resources Chemistry Analysis Report NW0028064 for BTRS Chiller Water Sample, Fax, December 20, 2000.

21. Sherry Laboratories Chemical Analysis Rep, MLTS: 97-2549-1, April 22, 1977, Data Provided by WCNOC During Altran's Site Visit October 2000.
22. M. Pourbaix, Atlas of Electrochemical Equilibria in Aqueous Solutions, NACE, Houston, 1974.
23. R.N. Parkins, "Synthetic Solutions and Environment Sensitive Fracture," The Use of Synthetic Environments for Corrosion Testing: STP-971, P.E. Francis and T. S. Lee, eds., ASTM, Philadelphia, 1988, p. 132.
24. M.J. Pourbaix, Thermodynamics of Dilute Aqueous Solutions, Edward Arnold, London, 1949.
25. M.J. Humphries and R.N. Parkins, "The Influence of Oxide Films on Stress Corrosion Cracking of Carbon Steels," Fundamental Aspects of Stress Corrosion Cracking: NACE-1, R.W. Staehle, A.J. Forty and D. van Rooyen, eds., NACE, Houston, 1969, p. 384.
26. R.W. Staehle, "Stress Corrosion Cracking of Fe-Cr-Ni Alloy Systems," Theory of Stress Corrosion Cracking, J.C. Scully, ed., NATO Scientific Affairs Division, Brussels, 1971, p. 222.
27. S. Suzuki, "IGA Resistance of TT Alloy 690 and Concentration Behavior of Broached Egg Crate Tube Support Configuration," Proceedings of the Fifth International Symposium on Environmental Degradation of Materials in Nuclear Power Systems -Water Reactors, D. Cubicciotti, chair., American Nuclear Society, Chicago, 1992, p. 752.
28. Ph. Berge and J.R. Donati, "Materials Requirements for Pressurized Water Reactor Steam Generator Tubing," Nuclear Technology Vol. 55, 1981, p. 88.
29. Private communication with A.R. McIlree, EPRI, Palo Alto, November 1999.
30. H. Nagano, K. Yamanaka, T. Minami, M. Inoue, T. Yonezawa, K. Onimura, N. Sasaguri, and T. Kusakabe, "Effect of Alloying Elements and Heat Treatment on the Corrosion Resistance of Alloy 690," Proceedings: Workshop on Thermally Treated Alloy 690 Tubes for Nuclear Steam Generators: NP-4665S SR, C.E. Shoemaker, ed., EPRI, Palo Alto, 1986, p. 10/1.
31. F. Vaillant, D.Buisine, B. Prieux, J.C. Fournel, and A. Gelpi, "Effects of Microstructure and Mechanical Properties of Alloys 600 and 690 on Secondary Side SCC," Control of Corrosion on the Secondary Side of Steam Generators, R.W. Staehle, J.A. Gorman, and A.R. McIlree, eds., NACE, Houston, 1996, p. 321.
32. R.J. Jacko, Corrosion Evaluation of Thermally Treated Alloy 600 Tubing in Primary and Faulted Secondary Water Environments: NP-6721, EPRI, Palo Alto, 1990.
33. I.L.W. Wilson, F.W. Pement, R.G. Aspden, and R.T. Begley, "Caustic Stress Corrosion Behavior of Fe-Ni-Cr Nuclear Steam Generator Tubing Alloys," Nuclear Technology Vol. 31, 1975, p. 70.
34. P.L. Andresen, "Conceptual Similarities and Common Predictive Approaches for SCC in High Temperature Water Systems," Paper No. 96258, Corrosion '96, NACE, Houston, 1996, p. 96258/1.
35. R.N. Parkins, "Predictive Approaches to Stress Corrosion Cracking Failure," Corrosion Science Vol. 20, 1980, p. 147.

36. R.W. Staehle, Bases for Predicting the Earliest Penetrations Due to SCC for Alloy 600 on the Secondary Side of PWR Steam Generators; NUREG-CR-6737,U.S. Nuclear Regulatory Commission, Washington, 2001.
37. R.W. Staehle, "Predicting the First Failure," presented at NACE Corrosion 2003, San Diego, March 16-20, 2003, to be published by NACE, Houston, 2003.
38. K.D. Stavropoulos, J.A. Gorman, R.W. Staehle, and C.S. Welty, Jr., "Selection of Statistical Distributions for Prediction of Steam Generator Tube Degradation" Fifth International Symposium on Environmental Degradation of Materials in Nuclear Power Systems -- Water Reactors, E. Simonen and D. Cubicciotti, eds., American Nuclear Society, La Grange Park, Illinois, 1991, p. 731.
39. R.W. Staehle, J.A. Gorman, K.D. Stavropoulos, and C.S. Welty, Jr., "Application of Statistical Distributions to Characterizing and Predicting Corrosion of Tubing in Steam Generators of Pressurized Water Reactors," Life Prediction of Corrodible Structures, R.N. Parkins, chair., NACE, Houston, 1994, p. 1374.
40. Private communication with L. Björnkvist of Vattenfall and J. Gorman of Dominion Engineering, April, 1999.
41. W.L. Clarke and G.M. Gordon, "Investigation of Stress Corrosion Cracking Susceptibility of Fe-Ni-Cr Alloys in Nuclear Reactor Water Environments," Corrosion Vol. 29, 1973, p. 1.
42. E.D. Eason and L.M. Shusto, Analysis of Cracking in Small-Diameter BWR Piping, NP-4394, Electric Power Research Institute, Palo Alto, 1986.
43. P.M. Scott, "2000 F.N. Speller Award Lecture: Stress Corrosion Cracking in Pressurized Water Reactors – Interpretation, Modeling, and Remedies," Corrosion Vol. 56, 2000, p. 771.
44. P.M. Scott and D.R. Tice, "Stress Corrosion in Low Alloy Steels," Nuclear Engineering and Design Vol. 119, 1990, p. 399.
45. C.J. Congleton, T. Shoji, and R.N. Parkins, "The Stress Corrosion Cracking of Reactor Pressure Vessel Steel in High Temperature Water," Corrosion Science Vol. 25, 1985, p. 633.
46. F.P. Ford, H.D. Solomon, and P.L. Andresen, "Life Prediction for Low Alloy Steels Subject to Stress Corrosion and Corrosion Fatigue in High Temperature Water," VGB Tech. Ver. Grosskraftwerksbetr, VGB-TB 513, 1995, p. 21/1.
47. G.M. Waid and R.T. Ault, "Effects of Composition on Stress-Corrosion Cracking Resistance of Ultrahigh-Strength Steels," Stress Corrosion – New Approaches; ASTM STP 610, 1976, p. 199.
48. J. Kuniya, I. Masaoka, R. Sasaki, H. Itoh, and T. Okazaki, "Stress Corrosion Cracking Susceptibility of Low Alloy Steels Used for Reactor Pressure Vessel in High Temperature Oxygenated Water," Transactions of the ASME, Vol. 107, 1985, p. 430.
49. M.O. Speidel, "Stress Corrosion Cracking and Corrosion Fatigue of Nuclear Reactor Pressure Vessel Steels in Hot Water," J. Materials Engineering Vol. 9, 1987, p. 157.

50. M.O. Speidel and R.M. Magdowski, "Stress Corrosion Cracking of Nuclear Reactor Pressure Vessel and Piping Steels," International Journal of Pressure Vessels and Piping, Vol. 34, 1988, p. 119.
51. R.N. Parkins, F. Mazza, J.J. Royuela, and J.C. Scully, "Stress Corrosion Test Methods," British Corrosion Journal Vol. 7, 1972, p. 154.
52. V.K. Singh, "Stress Corrosion Cracking of Low-Carbon and Low-Alloy Steels," Steel India Vol. 11, 1988, p. 53.
53. R.N. Parkins, N.J.H. Holroyd, and R. R. Fessler, "Stress Corrosion Cracking of C-Mn Steel in Phosphate Solutions," Corrosion Vol. 34, 1978, p. 253.
54. R.N. Parkins, "A Critical Evaluation of Current Environment-Sensitive Fracture Test Methods," Environment-Sensitive Fracture: Evaluation and Comparison of Test Methods, STP 821, S.W. Dean, E.N. Pugh and G.M Ugiansky, eds., ASTM, Philadelphia, 1984, p. 5.
55. G.I. Ogundele, Feeder Cracking Evaluation: I – Review of Threshold Conditions to Cause Stress Corrosion Cracking of Feeder Pipe (Carbon Steel) Material; COG-JP-97-007-V6, Ontario Hydro Technologies, July 1998, Appendix F to G.J. Field, Feeder Cracking Joint Project Final Report; COG-JP-97-007, CANDU Owners Group, Toronto, 2000.
56. H. Mazille and H.H. Uhlig, "Effect of Temperature and Some Inhibitors on Stress Corrosion Cracking of Carbon Steels in Nitrate and Alkaline Solutions," Corrosion Vol. 28, 1972, p. 427.
57. R.N. Parkins, "Prevention of Environment Sensitive Fracture by Inhibition or Electrochemical Manipulation," Embrittlement by the Localized Crack Environment, R.P. Gangloff, ed., AIME, Philadelphia, 1983, p. 385.
58. R.N. Parkins, "Mechanistic Aspects of Intergranular Stress Corrosion Cracking of Ferritic Steels," Corrosion Vol. 52, 1996, p. 363.
59. J.R. Galvele, J.B. Lumsden, and R.W. Staehle, "Effect of Molybdenum on the Pitting Potential of High Purity 18% Cr Ferritic Stainless Steels, J. Electrochem. Soc. Vol. 125, No. 8, 1978, p. 1204.
60. M. Stranick, "The Corrosion Inhibition of Metals by Molybdate. Part I. Mild Steel," Paper No. 311, Corrosion '83, 1983, p. 311/1.
61. J.C. Oung and T.Y. Wang, "Study of Molybdate-Based Inhibitor in a Synthetic Cooling Water System," Corrosion Australasia Vol. 13, 1988, p. 19.
62. C.M. Mustafa and S.M. Shahinoor Islam Dulai, "Molybdate and Nitrite as Corrosion Inhibitors for Copper-Coupled Steel in Simulated Cooling Water," Corrosion Vol. 52, 1996, p. 16.
63. F. Torres, L. Sathler, and J.A.C.P. Gomes, "Evaluation of Molybdate at Low Concentrations as Steel Corrosion Inhibitor in Cooling Water Systems," Proceedings of the 9th European Symposium on Corrosion Inhibitors, Ann. Univ. Ferrara, N.S., Sez V, Suppl. 11, 2000, p. 873.
64. E.A. Lizlovs, "Molybdates as Corrosion Inhibitors in the Presence of Chlorides," Corrosion Vol. 32, 1976, p. 263.
65. D. R. Robitaille, "Sodium Molybdate as a Corrosion Inhibitor in Aqueous Environments," Water Corrosion Seminar, NACE, Houston, 1977, p. 1.

66. A. Husain, K. Habib, and R. Jarman, "The Inhibition Effect of Sodium Molybdate on the Corrosion Fatigue of 1020 Mild Steel," Microstructural Science Vol. 21, 1994, p. 181.
67. V.S. Agarwala and J.J. De Luccia, "New Inhibitors for Crack Arrestment in Corrosion Fatigue of High Strength Steels," Corrosion, Vol. 36, 1980, p. 208.
68. K. Sugimoto and Y. Sawada, "The Role of Alloyed Molybdenum in Austenitic Stainless Steels in the Inhibition of Pitting in Neutral Halide Solutions," Corrosion Vol. 32, 1976, p. 347.
69. F.P. Ford and P. Combrade, "Electrochemical Reactions on Bare Surfaces and Their Use in a Crack Prediction Model for the Low-Alloy Steel/Water System," Proceedings of the Second International Atomic Energy Agency Specialists Meeting on Subcritical Crack Growth; NUREG/CP-0067, W.H. Cullen, ed., 1985, p. 231.
70. F.P. Ford and P.W. Emigh, "Mechanistic Interpretation of Corrosion Fatigue of Low Alloy Steels in Deoxygenated Water," Paper No. 173, Corrosion '84, NACE, Houston, 1984, p. 173/1.
71. D.B. Alexander and A.A. Moccari, "Evaluation of Corrosion Inhibitors for Component Cooling Water Systems," Corrosion Vol. 49, 1993, p. 921.
72. F.P. Ford and M.J. Povich, The Effect of Oxygen/Temperature Combinations on the Stress Corrosion Susceptibility of Sensitized Type-304 Stainless Steel in High Purity Water; Paper 94, Corrosion '79, NACE, Houston, 1979.
73. T. Kondo, T. Kikuyama, H. Nakajima, M. Shindo, and R. Nagasaki, "Corrosion Fatigue of ASTM 302-B Steel in High Temperature Water; The Simulated Nuclear Reactor Environment," Corrosion Fatigue; NACE-2, O. Devereux, A.J. McIvily, and R.W. Staehle, eds., NACE, Houston, 1972, p. 546.
74. D. Weinstein, BWR Environmental Cracking – Margins for Carbon Steel Piping First Semiannual Progress Report July 1978 to December 1978; NEDC-24625, General Electric, San Jose, California, January 1979.
75. M.O. Speidel and R.M. Magdowski, "Stress Corrosion Cracking of Nuclear Reactor Pressure Vessel and Piping Steels," International Journal of Pressure Vessels and Piping Vol. 34, 1988, p. 119.
76. S. Rahman and M. Ruscak, "Stress Corrosion Cracking of Low Alloy Steels in PWR Environment: Effect of Temperature," Nucleon Vol. 3, 1995, p. 3.
77. W.H. Bamford, D.M. Moon, and L.. Ceschini, "Studies of Statically and Dynamically Loaded Cracks in Simulated Pressurized Water Environment," Paper No. 12, Corrosion '83, NACE, Houston, 1983, p. 12/1.
78. D.A. Hale, "The Effect of BWR Startup Environments on Crack Growth in Structural Alloys," Trans. ASME Journal of Engineering Materials and Technology Vol. 108, 1986, p. 44.
79. T.A. Prater, W.R. Catlin, and L.F. Coffin "Surface Crack Growth Behavior of Structural Metals in High Temperature Water Environments," Trans. ASME Journal of Engineering Materials Vol. 108, 1986, p. 2.
80. E. Lenz, H. Munster, and N. Wieling, "Influence of the Flow Rate on SCC in a Low Alloy Steel," ICCGR Meeting, Erlanger, 1987.

81. Private communication E. Kiss, 1987.
82. D.A. Hale and A.E. Pickett, "Materials Performance in a Startup Environment," Proceedings Second Seminar on Countermeasures for Pipe Cracking in BWRs, Volume 2; NP-3684-SR, EPRI, Palo Alto, 1984.
83. T. Arai, M. Mayuzumi, and J. Ohta, "SCC Maps for Low-Alloy Steels by SSRT Method," Paper No. 140, Corrosion '89, 1989, p. 140/1.
84. S. Ritter and H.P. Seifert, "Strain-Induced Corrosion Cracking of Low-Alloy Reactor Pressure Vessel Steels Under BWR Conditions," Paper No. 02516, Corrosion 2002, NACE, Houston, 2002, p. 02516/1.
85. T. Arai and M. Mayuzumi, "SCC Behavior of Low Alloy Steels in Simulated PWR Secondary Water Environment," Minutes of the 1999 Annual Meeting of the International Cooperative Group on Environmentally Assisted Cracking of Light Water Reactor Materials (ICG-EAC), J. Hickling, ed., 1999, p. 678.
86. L.A. James and W.A. Van Der Sluys, The Effect of Aqueous Environments Upon the Initiation and Propagation of Fatigue Cracks in Low-Alloys Steels; WAPD-T-3078, 1996.
87. G. Nakao, H. Kanasaki, M. Higuichi, K. Ilda, and Y. Asada, "Effects of Temperature and Dissolved Oxygen Content on Fatigue Life of Carbon and Low Alloy Steels in LWR Water Environment," Fatigue and Crack Growth: Environmental Effects, Modeling Studies, and Design Considerations; PVP-Vol. 306, ASME, 1995, p. 123.
88. J. Congleton and T. Shoji, "Slow Strain Rate Testing of RPV Steels in High Temperature Water," Structural Mechanics in Reactor Technology Vol. 2, Lausanne, Switzerland, 1987, p. 265.
89. J. Kuniya, M. Kanno, I. Masaoka, and R. Sasakj, "The Effects of Dissolved Oxygen Concentration and Temperature on the Stress Corrosion Cracking of Low Alloy Steels in High Temperature Water," Boshoku Gijutsu Vol. 32, 1983, p. 649.
90. K. Bohnenkamp, "Caustic Cracking of Mild Steel," Fundamental Aspects of Stress Corrosion Cracking; NACE-1, R.W. Staehle, A.J. Forty and D. van Rooyen, eds., NACE, Houston, 1969, p. 374.
91. X.-C Jiang and R.W. Staehle, "Effects of Stress and Temperature on Stress Corrosion Cracking of Austenitic Stainless Steels in Concentrated Magnesium Chloride Solutions," Corrosion Vol. 53, 1997, p. 448.
92. M.O. Speidel and R.M. Magdowski, "Stress Corrosion Cracking of Nuclear Reactor Pressure Vessel Steel in Water: Crack Initiation Versus Crack Growth," Paper 283, Corrosion '88, NACE, Houston, 1988, p. 283/1.
93. R.N. Parkins, "Environment Sensitive Fracture and its Prevention," British Corrosion Journal Vol. 14, 1979, p. 5.
94. R.N. Parkins and B.S. Greenwell, "The Interface Between Corrosion Fatigue and Stress Corrosion Cracking," Metal Science Vol. 8, 1977, p. 405.
95. G.M. Goodwin and R.K. Nanstad, Effect of Temperature on the Stress-Relaxation Response of a Pressure Vessel Steel; NUREG/CR-3728, ORNL/TM-9149, Oak Ridge National Laboratories, October 1984.

96. S. Ritter and H.P. Seifert, "Strain-Induced Corrosion Cracking of Low Alloy Reactor Pressure Vessel Steels Under BWR Conditions," Paper No. 02516, Corrosion 2002, NACE, Houston, 2000, p. 02516/1.
97. D. Alter, Y. Robin, M. Pichon, A. Teissier, and B. Thomeret, "Stress Corrosion Cracking of Pressurizer Instrumentation Nozzles in the French 1300 Mwe Units," Proceedings of the Fifth International Symposium on Environmental Degradation of Materials in Nuclear Power Systems -Water Reactors, D. Cubicciotti, chair., American Nuclear Society, La Grange Park, Illinois, 1992, p. 661.
98. Private communication with R. Eaker of Duke Power, Charlotte, North Carolina.
99. C.J. Cron, J.H. Payer and R.W. Staehle, "Dissolution Behavior of Fe-Fe3 Structures as a Function of pH, Potential, and Anion - An Electron Microscopic Study," Corrosion Vol. 27, No. 1, 1971, p. 1.
100. J.H. Payer and R.W. Staehle, "Dissolution Behavior of Cr23C6 and TiC Related to the Stainless Steels in Which They Occur," Corrosion Vol. 31, No. 1, January, 1975, p. 30.
101. Personal communication with Brenda Little.
102. F.P. Ford and P.L. Andresen, Corrosion Fatigue of A533B/A508 Pressure Vessel Steels in Water at 288°; NUREG/CP-0112; ANL-90/22, Argonne National Lab., 1990, p. 37.